Quantifying Activity in Nascent Neuronal Networks derived from Embryonic Stem Cells

Natalie Adams

Thesis submitted for the degree of Doctor of Philosophy at Newcastle University

Institute of Neuroscience

School of Chemical Engineering and Advanced Materials

November 2011

Quantifying activity in nascent neuronal networks derived from embryonic stem cells.

Natalie Adams

Thesis submitted for the degree of Doctor of Philosophy at Newcastle University

November 2011

Abstract

The relationship between spatiotemporal patterns of spontaneous activity and functional specialisation in developing neuronal networks is complex and its study is crucial to our understanding of how network communication is initiated. This project quantifies transitions between structural and functional states in embryonic stem cell cultures during differentiation. The work also focussed on the role of γ-aminobutyric acid (GABA), known to be vital for neuronal network development.

The work used many techniques, including carbon nanotube (CNT) -patterned substrates to manipulate network architecture, multi-electrode arrays (MEAs) and calcium imaging to quantify function. An embryonic stem cell line (CC9) was used to generate 'de novo' neuronal networks and these were monitored over 13 – 22 days in vitro (DIV), while network structure forms and stabilizes.

On CNT-patterned arrays, differentiating CC9s migrated and sub-clustered on CNT islands showing that network structure could be manipulated. No spontaneous electrophysiological (unit) activity was found in these cultures. However, intracellular calcium responses were readily induced and seen spontaneously at 13-20 DIV. Activity rate, kinetics and number of active cells increased between 16-18 DIV, correlating with changes in network clustering. Post 17 DIV, activity transformed from near-random to periodic and synchronous. Many events were initiated by 'hubs' and degrees of critical behaviour were observed, moving towards more efficient information processing states with development.

Blockade of $GABA_A$ receptors lead to elevated spontaneous activity and supercritical behaviour, depending on developmental stage. Application of exogenous GABA induced large, slow calcium transients in a developmental stage-dependent manner, suggestive of a mixed excitatory/inhibitory role.

These findings begin to show how activity develops as stem cells differentiate to form neuronal networks. GABA's role in controlling patterns of activity was more complex that previously reported for neuronal networks *in situ*, but GABA clearly played a vital role in shaping population behaviour to optimise information processing properties in early, developing networks.

TABLE OF CONTENTS

LIST OF FIGURES

NOMENCLATURE

aCSF	artificial cerebro-spinal fluid
ADP	after depolarizing potential
AFM	atomic force microscope
AHP	after hyperpolarizing potential
AHPC	adult hippocampal progenitor cells
AMPA	2-amino-3-(5-methyl-3-oxo-1,2-oxazol-4-yl)propanoic acid
AP	action potential
bFGF	basic fibroblast growth factor
cAMP	cyclic adenosine monophosphate
CC9	embryonic stem cell line (controls created for mitochondrial research)
CICR	calcium-induced calcium release
CNT	carbon nanotubes
DIV	days in vitro
DMEM	Dulbecco's modified Eagle medium
DMSO	dimethyl sulfoxide
EB	embryoid body
ESC	embryonic stem cells
EPSP	excitatory post-synaptic potential
eSEM	environmental scanning electron microscope
FRB	fast rhythmic bursting
FS	fast spiking
FWHM	full width half maximum
GABA	γ-aminobutyric acid
GDP	giant depolarising potential
GMEM	Glasgow minimal essential medium
HCN	Hyperpolarization-activated cyclic nucleotide-gated

HCN/GFP	neuronal progenitor stem cell line
IB	intrinsically bursting
ICCR	intracellular calcium release
IPSP	inhibitory post-synaptic potential
ITI	inter-transient interval
ITO	indium tin oxide
LGCC	ligand-gated calcium channel
LIF	leukaemia inhibitory factor
LTS	low threshold spiking
MCS	Multi Channel Systems
MEA	multi-electrode array
MWCNT	multi-walled carbon nanotubes
NMDA	N-Methyl-D-aspartic acid
OGB-1	Oregon Green BAPTA-1
PBS	phosphate buffered saline
PDL	poly-D-lysine
PLO	poly-L-orinthine
PSN	penicillin streptomycin neomycin
ROI	region of interest
RS	regular spiking
SEM	scanning electron microscopy
SWCNT	single-walled carbon nanotubes
TEM	transmission electron microscopy
TTX	tetrodotoxin
VGCC	voltage-gated calcium channel

ACKNOWLEDGEMENTS

I would like to thank Dr Daniel Frankel for introducing me back into the world of research and allowing me the opportunities to work with such a broad spectrum of techniques. I'd also like to thank him for introducing me to Dr Evelyne Sernagor, who was instrumental in helping me to initiate cell culturing in her laboratory, as well as providing collaborations with various groups. A big thank you goes to the Mitochondrial Research Group, a fantastic bunch who welcomed me with enthusiasm and provided me with the tools I needed. I learned a great deal from them about the highs and lows of stem cell culturing, and the support of Prof Bob Lightowlers, Tora Smulders-Srinivasan, Nichola Lax and Marco Nooteboom was invaluable. Likewise, I thank Dr Carla Mellough for the kind donation of neuronal progenitors and taking the time to train me so well in the appropriate techniques. A huge thank you to Dr Yael Hanein and her entire group for all their input throughout my project. It was a great opportunity to be able to visit Dr Hanein's lab and work with such a motivated, friendly set of people. Thank you very much to Dr Andrew Trevelyan for his help and advice with these cultures – it was invaluable. Also, thank you to Dr Jennifer Simonotto and Dr Marcus Kaiser for their good advice on my data analysis.

I'd like to thank Cyril Eleftheriou for his madness in and out of the lab, and a special thank you also goes to Dr Chris Adams for his many words of wisdom. A fantastic chap to whom I wish all the best things. In addition, a special thank you goes to Prof Miles Whittington for everything, and Dr Fiona LeBeau for her kind help and support. On a personal note, I'd like to thank everyone who put up with my general ranting these past years, which includes all the members of the Oscillations Group in the IoN and my parents, who have had to put up with more than their fair share, this year in particular.

CHAPTER 1: GENERAL INTRODUCTION

This chapter is aimed at providing a general overview of the use of stem cells to form nascent neurons and subsequent networks. It deals with the nature of stem cells and progenitors, factors affecting their differentiation, control of network structure and monitoring of function via calcium transients. Specific topics leading to the experiments described in chapters 3 – 6 are introduced within each relevant chapter.

The overall aim of the work in this thesis is to investigate any relationship between structure and function of neuronal networks and how this may occur developmentally. The introduction therefore compares and contrasts the use of embryonic stem cells with progenitor neurons already part-way down the path to differentiation into neurons. Measurement and manipulation of network structure is dealt with in detail, with particular reference to the use of patterned multi-electrode arrays to control basic anatomical structure (*clustering*) of the neuronal elements within nascent networks – the core structural reference measurement used in this thesis. The introduction also reviews work using such multi-electrode arrays to measure network function, along with the alternative method of calcium imaging used extensively in this thesis for methodological reasons (see chapter 3 results and discussion). Finally, it briefly reviews analysis methods for quantifying network function (explained in more detail in chapters 4 & 5) to demonstrate that no single measure can accurately reflect the complexity and sum total of behaviour of active neuronal networks.

1.1 EMBRYONIC STEM CELLS AND NEURAL PROGENITORS

Stem cells have a high potential impact on biomedicine. Regenerative medicine, cell-based therapies, drug discovery, diagnostics and biosensors, developmental biology, functional biological network development; these are all potential beneficiaries of research involving stem cells and progenitors. This section explains the origin of these cells and how they are currently manipulated for use in neuroscience.

Progenitors and stem cells, in essence, are cells with the ability to continually divide in a self-renewing way and differentiate into specific cell types. In the case of lineage-specific

progenitors, the terminal differentiated state can only be of one cell sub-type; but with other types of progenitor or stem cell, the terminal differentiated state could be a variety of cell types.

Stem cells are present from the start of embryonic development and have been shown to exist in multiple locations in the adult mammalian brain. There are many types of cell that show an ability to differentiate into multiple cell types, either with or without an ability to self-renew. Two such types of cell used in this body of work are embryonic stem cells and adult hippocampal progenitor cells (which are neurogenic, but not self-renewing stem cells (Bull and Bartlett, 2005)), an explanation of which is given below. Other such cells of note are produced throughout development and adulthood and have been found throughout the central and peripheral nervous system (Kruger et al., 2002, Morshead et al., 1998) and in other locations such as skin and bone marrow (Morris et al., 2004, Zhang et al., 2003). Stem and progenitor cells have been found, more specifically, in the dentate gyrus and subgranular zones of the hippocampus, the subventricular zone, and the spinal cord (Doetsch et al., 1999, Palmer et al., 1995, Palmer et al., 1997, Sanai et al., 2004, Weiss et al., 1996).

1.1.1 Embryonic stem cells

Embryonic stem cells (ESCs) are present in the inner cell mass of the blastocyst (Martin, 1981, Renoncourt et al., 1998) (Figure 1.1) and can differentiate into the ectoderm (which differentiates into the nervous systems), mesoderm (which forms connective tissues) and endoderm (which differentiates to develop multiple organ systems, including the gastrointestinal and respiratory systems) making them pluripotent cells. The differentiation of these cells *in vivo* is dictated by the secreted factors specific to the location of the cells. It is therefore possible to induce their differentiation *in vitro* by introducing the relevant factors into a defined environment. The *in vitro* culture of these cells has considerably advanced the knowledge of differentiation and migration in the developing embryo.

If the cells come from an immortalized line, the ESCs can proliferate indefinitely in the correct culture conditions under the influence of leukaemia inhibitory factor (LIF). LIF is a cytokine that aids neuronal proliferation and gene expression (Patterson, 1994) and promotes neuronal cell survival by activating the Janus-associated tyrosine kinases (JAK),

which leads to the phosphorylation of the signal transducer and activation of transcription (STAT) pathway (specifically $STAT_3$ for LIF), involved in cell self-renewal (Burdon et al., 2002). The cells can be driven to differentiate into specific cell types by the removal of LIF and the addition of promoting factors to the culture environment. Spontaneous differentiation can also occur, and in such cases the cells differentiate into a variety of cell types that can interact and influence each other. Examples of the results of such spontaneous differentiation have been the development of organized structures resembling aspects of all three germ layers in teratomas triggered by injecting ESCs in mice (Bongso and Richards, 2004).

1.1.1.1 Neuronal Differentiation of Embryonic Stem Cells

Methods of stem cell differentiation involve highly specific, direct or indirect targeting of gene expression. Various methods of differentiating ESCs into neuronal cells in general have been attempted, one of which is the embryoid body method and the application of retinoic acid, demonstrated by Bain (Bain et al., 1995). In this method, ESCs that have been proliferated on an adherent surface are removed from the surface and placed in a non-adherent environment and allowed to proliferate. They form cellular aggregates called embryoid bodies (EBs). The application of retinoic acid into the medium results in cells exhibiting a number of neuron-like properties. Specifically, retinoic acid aids the up-regulation of genes associated with the developing brain, and suppresses genes associated with the development of the mesoderm layer (Bain et al., 1996). Retinoic acid is a key morphogen in embryonic development influencing a number of cell types. Its concentration-dependent action affects differentiation and gene pathways promoting positional identity (Okada et al., 2004).

There are a range of neuron-like cells that can be induced by application of retinoic acid (Finley et al., 1996, Fraichard et al., 1995, Strübing et al., 1995). Morphologically, the cells resemble neurons (Figure 1.2). These cells also test positively for defined neuronal proteins and gene expression. After day 5, voltage-gated currents can be evoked by a stimulating, depolarising voltage. After 10 days, cells are sensitive to kainate, NMDA, GABA and/or glycine. Finley (Finley et al., 1996) demonstrated the ESCs capacity to differentiate into neurons with distinctive axonal and neuritic compartments. This polarity was clarified by GAP-43 (a protein present in growth cones in neuronal axons) and MAP-2 (present in

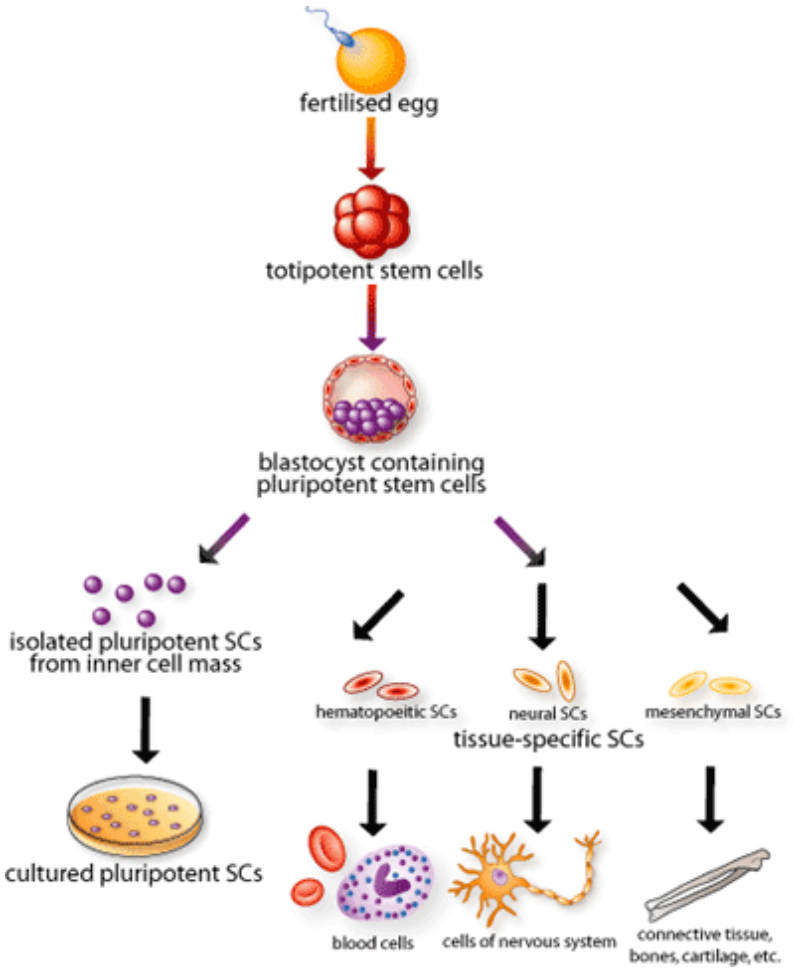

Figure 1.1 Illustration of the origins of cultured ESCs and their potential to differentiate. Once the blastocyst has formed, cells can be removed, destroying the blastocyst, to be cultured *in vitro*. *In vivo*, the cells are pluripotent, with the potential to differentiate into all three germ layers. Many cell types have been differentiated *in vitro*, exploiting this potential. (Image taken from the Science Creative Quarterly, August 2004, www.scq.ubc.ca/stem-cell-bioengineering)

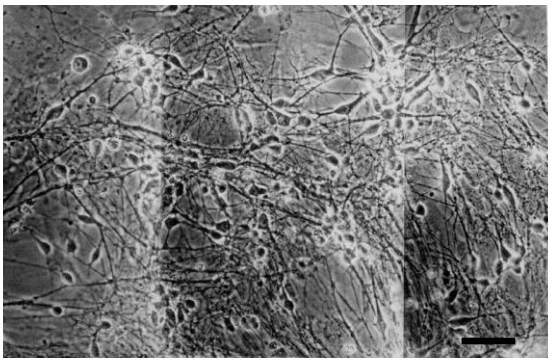

Figure 1.2 EBs plated for 3 days following the retinoic acid differentiation method. Morphologically, these are distinguishable from plated EBs with no retinoic acid treatment. Neuritic branching is clearly evident (Bain et al., 1995). Scalebar = 50µm.

dendrites and active in microtubule assembly) staining, 9 days after plating. The functional synapses observed were mostly excitatory, with a small percentage of inhibitory ones.

Further control of differentiation into specific neuronal subtypes is also possible. Interneuron fate is highly controllable through *Wnt5a*, which specifies GABAergic neuronal

expression in the olfactory bulb, subpallium and cortex (Paina et al., 2011). In addition, neuromodulatory roles for newly differentiated neurons are also controllable by genetic targeting, as has been seen for cholinergic interneurons in the striatum. Here, the *Gbx2* transcription factor is shown to potentially regulate migration patterns of differentiating cholinergic neurons, affecting their gross morphology and placement in the striatum. Precursors expressing *Gbx2* migrated tangentially to become interneurons in the striatum, and precursors lacking in *Gbx2* expression resulted in abnormal neuronal morphology and cell distribution (Chen et al., 2010).

Lineage plasticity of differentiating cells has also been found. It is possible to redirect differentiating stem cells away from a neuronal fate to that of glial cells, as was shown in GAD65- and Dcx-expressing neuronal progenitors in the adult mouse subventricular zone (SVZ). Here, de-myelination of the corpus callosum induced up-regulation of chordin expression and subsequently resulted in cells switching from a neuronal to a glial fate and producing oligodendrocytes, whereas they would have been intended for rostral migration and differentiation into interneurons in the olfactory bulb (Jablonska et al., 2010). This ability to alter neuronal fate once the lineage has been defined has also been shown in other cell types, such as the ability of hemopoietic stem cells to contribute to epithelial cells in the skin, lungs, liver and gastrointestinal tract (Krause et al., 2001). Such plasticities could potentially result from different mechanisms, such as de-differentiation to an earlier progenitor state or transdifferentiation directly across lineages (Jablonska et al., 2010).

In addition to the diversity of cell subtypes that can be derived from stem cells, they also migrate easily on a variety of surfaces to form clusters around more adherent areas, and are therefore very amenable to patterning. Not all progenitor-type cells have the same adhering and migration properties, as can be seen with adult hippocampal progenitor cells (discussed in detail later).

1.1.1.2 CC9 Embryonic Stem Cells and Other Cell Lines

The mouse ESCs used in these studies were a gift from Bob Lightowlers and Doug Turnbull (Mitochondrial Research Group, Newcastle University). These cells are the parentals of transmitochondrial ESC hybrids designed for the study of mitochondrial defects (Kirby et al.,

2009). These 'wild type' cells (CC9.3.1, hereafter CC9) are responsible for the majority of the results generated in the writing of this thesis.

In the past, permanent cell lines have been developed through either the cultivation of cells from tumours and teratocarcinomas (Greene and Tischler, 1976), a form of germ cell tumour, or from the immortalization of a cell line through oncogene expression (Bartlett et al., 1988), but the CC9s have not undergone an immortalization process, so their life-span is limited. Practically speaking, this means the cells will be unable to differentiate effectively after 36 passages (every 2 days).

With any *in vitro* stem cell line it is helpful to understand the developmental process of the cells in order to relate it to the differentiation of neurons *in vivo*. Extremely varied protocols and media formulations developed for each cell line (and even each laboratory) mean the cells are all subject to a unique set of timed factors that affect their developmental process (see above for a few examples). Due to the inability to standardise differentiation protocols, relating the timeline of developmental events (such as synaptogenesis) between research papers can be very difficult and few assumptions can be made about the correlation of development between different cell lines. Nevertheless, many cell lines have been proven to express a multitude of normal developmental features.

In a study in 2009 (Kirby et al., 2009), the CC9 cells were tested alongside other cybrid cell lines created from them and were found to differentiate into various neuronal phenotypes based on both electrophysiological and immunocytochemical data. The cells stained positively for ß-Tubulin III (a neuronal marker) and most were positive for NeuN (a mature neuronal marker) after 16 days of differentiation. A small proportion of the cells expressed GFAP (an astrocytic marker). Some GABA expression was also found. Patch clamp recordings of spontaneous postsynaptic currents inferred network connectivity after 6-7 days post seeding.

A following study in 2010 (Trevelyan et al., 2010) looking at calcium activity in these cells revealed that 0.1Hz pulses of 1mM glutamate induced stable, repeatable calcium transients that could be associated directly with action potential generation observed with simultaneous patch clamping (current clamp). Exposing these cells to combinations of APV (to antagonise NMDA receptors), Ni^{2+}, Cd^{2+} (to block transmembrane calcium conductances)

and NBQX (to antagonise glutamatergic events mediated by AMPA and kainate receptor subtypes) produced reduced responses to the glutamate pulse.

Other cell lines have shown similar results for the presence of neuronal markers and the development of synapses. Bain (Bain et al., 1995), in the paper on which the CC9 protocol is based, showed that cells differentiated from the D3 ESC line had active Na^+, K^+ and Ca^{2+} channels displaying inward and outward currents when stimulated 5 days after plating. After 9-10 days current responses could be elicited in all neuronal cells from the application of kainate, NMDA, GABA and glycine, indicating the expression of a range of functional postsynaptic receptors associated with synapses. In BLC6 and D3 ESC lines, the presence of the presynaptic vesicle protein synaptophysin was also detected after only 5 days of embryoid body formation. Heavy chain neurofilaments and Tau were not present until between 13 and 23 days after the differentiation was initiated (Rohwedel et al., 1998) although light and medium chain neurofilaments are present much earlier (Bain et al., 1995, Rohwedel et al., 1998). The heavy chain neurofilaments are highly specific to neurons, though the lighter chain neurofilaments can also be present in small amounts in undifferentiated cells, are still indicative or neuronal differentiation (Bain et al., 1995). A further study of these particular cells revealed the presence of numerous voltage-gated channels and excitatory and inhibitory responses (Strübing et al., 1995). Similarly, glutamatergic synapses were formed *in vitro* from the differentiation of D3 ESC (Finley et al., 1996), using an almost identical protocol to the one adopted for the CC9 line (Bain et al., 1995, Ying et al., 2003). Polarity was established with MAP-2 and GAP-43 staining for axons and neurites respectively. Synaptophysin and synapsin showed the presence of pre- and post-synaptic junctions respectively. Patch clamping revealed both excitatory and inhibitory spontaneous activity between pairs of cells.

Murine ESCs grown on multi-electrode arrays (MEAs) successfully formed synapses within 7 days, confirmed through synaptophysin staining and FM1-43 fluorescence (which is an active measure of synaptic vesicle formation) (Bieberich and Guiseppi-Elie, 2004). Other methods of differentiation have yielded very positive results for the differentiation of ESC onto micro-electrode arrays (MEAs). Human ESC were grown on MEAs for up to 130 days to follow the network activity development (Heikkilä et al., 2009). This differentiation protocol was a 4-5 week process prior to plating. Spontaneous activity was exhibited by 1 week after

plating and the cultures went on to develop synchronous and asynchronous bursting events. A protocol for producing glutamatergic (65%) and GABAergic (30%) neurons was followed for the BF1/lacZ ESC line. The resulting neuronal cultures could be maintained for 10 weeks. 14 days after differentiation, intracellular recordings showed the cultures were firing spontaneously and after only 1 week of being plated to an MEA, extracellular voltage signals comparable to primary neonatal cultures was reported (although these data were not displayed; only 25 day old data were shown). A similar study using a very similar protocol to that of the CC9 cell line demonstrated ESC ability to be cultured on MEAs for up to 6 weeks, generating increasing levels of activity (Illes et al., 2007) with time. Between 7 and 14 days the first spontaneous spikes were detected. After 3 weeks these spikes appeared as bursts of activity. After 4 weeks there was significant spontaneous bursting activity. GABA and NMDA receptor-mediated activity was found and TTX was successfully used to block action potentials.

In (Kirby et al., 2009) the CC9 cells were maintained in culture for 20 days using Bain's -4/+4 differentiation protocol (Bain et al., 1995), adapted with Ying's plating media (Ying et al., 2003), which are described in detail in the Methods section (Chapter 2). As described earlier, this method involves supplementation of the neuronal differentiation process with retinoic acid to encourage the neural lineage and inhibit mesoderm lineages (Bain et al., 1996), coupled with a short exposure to basic fibroblast growth factor (b-FGF).

The presence of mature neuronal markers is not always a clear indication that ESC derived neural cells will be capable of producing electrical activity. Illes (Illes et al., 2009) compared the development of neural cells differentiated from ESCs using two different protocols: the adherent monolayer protocol and embryoid body protocol. Interestingly, they were unable to show spontaneous synchronous activity in MEA cultures using the adherent monolayer protocol after 24 weeks of culture, unlike the embryoid body protocol, which did reveal positive results for such activity. Thus, while both protocols were able to generate differentiated neurons, only one was associated with these neurons functionally interconnecting to precipitate temporally patterned population events.

1.1.2 Adult Hippocampal Progenitor Cells

Neurogenesis occurs in restricted regions of the adult mammalian brain. One of those regions – the dentate gyrus of the hippocampus – produces adult hippocampal progenitor cells (AHPCs) that are mitotic throughout adult life and are capable of differentiating into both neurons and glia (Palmer et al., 1995). These cells can be isolated and cultured under the influence of b-FGF, which encourages proliferation and inhibits differentiation. The cells can withstand a great number of passages (i.e. continued division) and can be differentiated easily at any stage. Differentiation down the neural lineage occurs through a vast reduction in the levels of b-FGF in the medium (Palmer et al., 1995). More detail on this protocol is provided in Chapter 2.

1.2 CELL/SUBSTRATE INTERACTIONS AND CONTROL OF NETWORK GEOMETRY

Having now established a brief background on the stem cells used in this work and how they can effectively be differentiated into neurons, a description of the environment in which they are grown and maintained is provided. However, it is worth noting that mechanical factors inherent in maintaining cultures of stem cells on patterned structures may also influence differentiation (Bakeine et al., 2000, Curtis and Wilkinson, 1998, Dalby et al., 2002, De Bartolo et al., 2008, Webster et al., 1999). It is therefore not possible to completely separate the subjects of sections 1.1 and 1.2.

The work undertaken here is on stem cells that have been differentiated *in vitro* on 2-dimensional substrates. Such substrates form a highly artificial environment that must be engineered to encourage the cells' survival, differentiation and subsequent network formation. The more the properties of these surfaces can be controlled, the greater the flexibility of network manipulation possible. If the architecture of these networks can be shown to be manipulable, there is great potential for exploring the effects of architecture on patterns of activity. Therefore, not only should the network show the potential to be geometrically patterned, but the surface must be suited to neuronal data gathering techniques.

Creating biocompatible surfaces is usually achieved through chemical modification of a surface, topographical modification, or by making the surface attractive to cells. Micro- and nano-fabrication techniques have opened up the possibilities for patterning cells onto

surfaces by manipulating surface chemistry and topography to encourage or discourage cell adhesion. Such techniques have increased our understanding of the chemistry of cell attachment and its effect on growth, migration and differentiation. In addition, the patterning of cells onto surfaces could have applications in biosensors, tissue engineering and implant technologies. Surface patterning of neuronal cells could potentially mimic some of their lost architecture, either at the cell membrane interface, or more extensively to aid the recovery of tissue structure (Webster et al., 1999). Understanding of how the neuron interacts with its physical and chemical environment and how those interactions give rise to specific functional behaviours is essential to understanding how network form influences the development of network function.

There is a lot of interest in quantifying and defining network activity and in the manipulation of the architecture of networks. Studies of note have focused around understanding neuronal adhesion, differentiation, neurite outgrowth, to name a few. Neurite outgrowth in particular has been extensively studied on patterned surfaces. Examples of chemical and topographical surface modifications used in these studies are detailed in this section, focusing first on chemical modification and then on topography.

Various patterning methods are available to create an array of biocompatible materials for cell adhesion. Advances in nanofabrication have led to the production of various structures and surface chemistries that promote adherence of cells on the nanoscale. *In vivo*, cells adhere to elements of the extracellular matrix (ECM) which have a variety of mechanical and chemical functions. These functions include providing tensile and compressive strength and the activation of chemical signalling pathways, for instance, leading to changes in gene expression in the cell (Chiquet, 1999, Geiger et al., 2001, Larsen et al., 2006).

The interest here is the patterning of neuronal networks. Where *in vivo* studies are not possible, it would be helpful to have an *in vitro* model that can mimic certain properties of the *in vivo* system. When cells are dissociated, their original architecture is broken down. When allowed to attach to a surface, these dissociated neurons initially consist only of their somata, but extend new processes with time to make 'random' 2D networks (Dotti et al., 1988, Walicke et al., 1986). These simplified environments can be used to probe cell physiology, even though the robust, natural architecture of the original system has been lost.

For example, they could be used to gain a fuller understanding of how functional networks form, recover after damage and are affected by environmental changes. The advantages of using *in vitro* networks are that they are relatively cheap and allow an unparalleled deep analysis at both the single cell and network level.

1.2.1 Chemical Patterning

Chemical patterning of surfaces by microcontact printing (Mrksich and Whitesides, 1995) uses standard photolithographic techniques to create a stamp (usually from PDMS), which is then coated with the desired molecules and pressed onto a substrate to transfer the pattern. This technique is commonly used to pattern molecular recognition proteins for biosensor applications (Mrksich and Whitesides, 1995) or to pattern cell adhesion proteins such as laminin, fibronectin and poly-D-lysine (PDL) (Mrksich et al., 1997, Scholl et al., 2000, Zhang et al., 1999).

Gold-coated glass is an example of a good substrate for the transfer of peptides using the stamping method because it requires no chemical modification to bind strongly with specific peptide residues (Mrksich et al., 1996) and so desirable peptides can be transferred directly with the stamp. This particular method was successfully used to direct the structure of mouse hippocampal neurons, directing neurite outgrowth along a patterned grid (Heller et al., 2005).

The resolution of microcontact printing can become limited by the material properties of the elastomer that makes up the stamp. This in turn limits control of cell placement and, more specifically, neurite growth. One study (James et al., 2000) shows a method for improving this by creating a PDMS stamp with 2µm thick lines, spaced 200µm. Primary rat hippocampal neurons were successfully cultured at low density on these patterned surfaces, which were superimposed over an MEA to allow extracellular recording of neuronal activity (James et al., 2004). Another researcher (Jun et al., 2007) implemented a similar strategy to pattern neurons and achieved very low density cultures (200 cells/mm), performing a more in-depth electrophysiological study with pharmacological manipulations to examine the network dynamics.

Patterning surfaces for neuronal attachment that utilize the geometry of MEAs is becoming commonplace and more methods of linking proteins to surfaces for effective and long-term

cell adhesion continue to be developed. Very fine resolution chemical patterning that can be aligned with an MEA for single-cell electrophysiological measurements has also been demonstrated (Nam et al., 2006) (Figure 1.3).

Other unique systems for containing cells are being developed. Quite often, the methods are adapted from micro- and nano-engineering fields and the variety of tools available is making for a varied exploration of architectures for cell culture and analysis. Neuronal progenitors and neuroblasts were cultured, proliferated and differentiated in hydrophilic PDMS microwells and microchannels (Bani-Yaghoub et al., 2005), showing that cost-effective, viable methods for extensive types of cell study can be manufactured simply and cheaply.

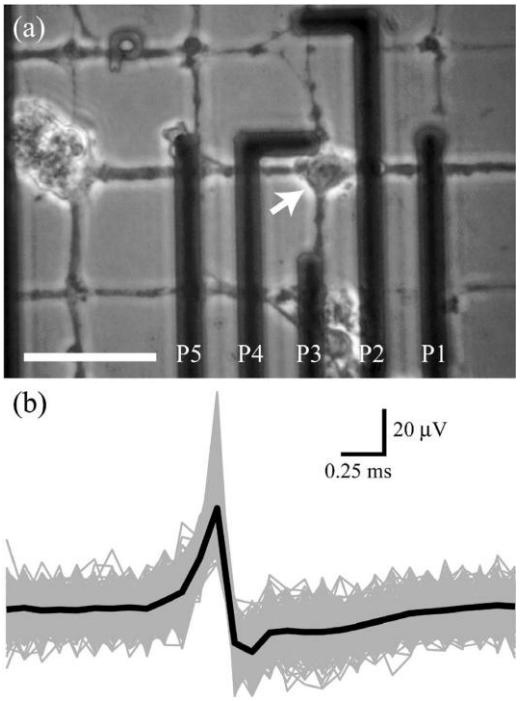

Figure 1.3– Controlling network architecture with patterned substrates. a) A phase contrast image of neuronal cells patterned on a poly-L-lysine grid aligned with an MEA. The arrow is pointing to a cell body. The scale bar is 50µm. b) An averaged spike (black) overlaid on the individual spikes (grey) from electrode P3. (Nam et al., 2006).

Patterning surfaces has also been achieved using a microdrop system (Macis et al., 2007). Poly-L-lysine and laminin solutions were microdropped onto glass and quartz MEA substrates, onto which primary cortical cells were seeded. The cells formed sub-clusters connected by thick neuritic bundles. On the MEA, clusters were positioned on electrodes (Figure 1.4) and spontaneous and evoked electrical activity was observable over 39 days.

Kleinfeld (Kleinfeld et al., 1988), in demonstrating the ability of neurons to grow on chemically patterned lines, showed how the patterning would break down if the distance between the lines was low enough for tensile neurite bridging. Neurons could be patterned

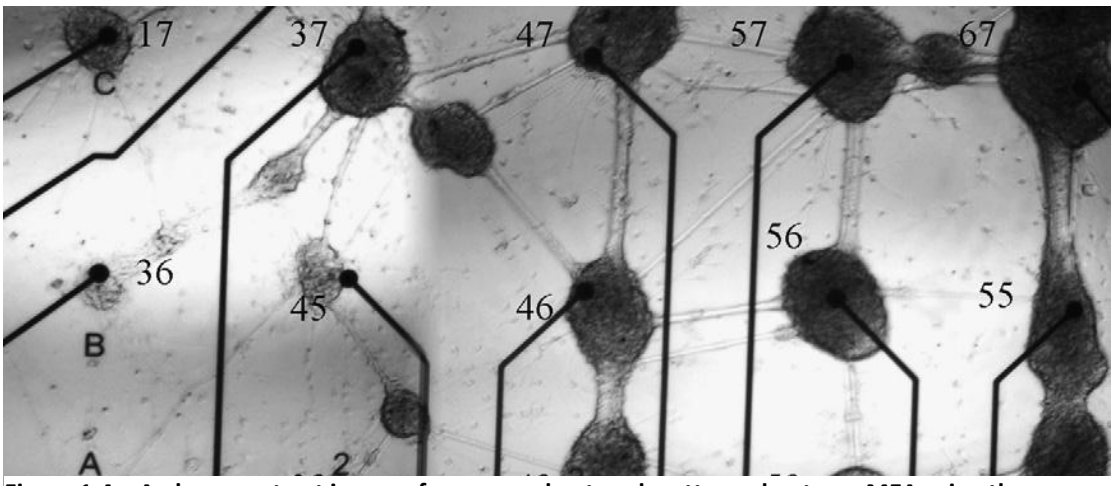

Figure 1.4 – A phase contrast image of a neuronal network patterned onto an MEA using the microdrop system. Cells were cultured for 20days. Note the bundles of neuritic processes between neighbouring cell clusters (dark patches) The scale bar is 100um. (Macis et al., 2007).

to lines as closely distributed as 30µm, but when maintained in cultures, this pattern would deteriorate as neurons bridged the gap over a period of 10 days in vitro (DIV) for lines of this separation or less. A spacing of 50µm between the lines resulted in a pattern that could be maintain for 10 DIV. Clearly, there are limits to the strength of the tensile bridge between cells over non-adherent regions and care must be taken when designing these substrates.

Surface charge can play a significant role in cell adhesion. Carbon negative-ion implantation has also been used for cell patterning, demonstrated with mesenchymal stem cells cultured and differentiated on silicon rubber (Tsuji et al., 2009). Cell adhesion under ion implanted regions is attributed to enhanced hydrophilic functional groups on the surface of the silicon rubber interacting favourable with the cell membrane. Dermal fibroblasts and neuroblastoma cells plated onto a variety of potential carbon-micro-electromechanical system (MEM) materials showed the potential for oxygen-plasma treated surfaces to attract cells preferentially (Teixidor et al., 2008). With no direct chemical patterning, plasma-treated surfaces with pre-patterned carbon electrodes provided an environment conducive to the attachment of ECM components, thus facilitating cell adhesion selectively to the electrode surfaces and not the underlying substrate. Similarly, the chemical properties of carbon nanotubes (CNTs) can be modified quite simply through oxidation to introduce carboxylic and hydroxide groups to the surface. Carboxylic acid (–COOH) groups have been proven to be negative cues for cell surface attachment and neuronal differentiation (Li et al.,

2005a, Li et al., 2005b). CNTs provide interesting substrates due to their unique properties and more information is given about this in Chapter 3 Introduction.

1.2.2 Topographical Patterning

Topographical modifications of surfaces have also been attempted to study their effects on neuronal growth and differentiation. Figure 1.5 shows AHPCs that have been seeded and differentiated on laminin coated microgrooves (Recknor et al., 2006). The cells display normal and varied neuronal morphologies, extending their processes with a strong preference for groove direction (Bakeine et al., 2000, Curtis and Wilkinson, 1998). Particularly, the processes seem to follow the edges of the grooves. When compared to planar substrates, the radial processes of the cells showed no directional preference. When these neurons were seeded onto a layer of astroglia their processes aligned with filamentous structures of the astroglia, which showed a significant degree of aligned with the microgrooves. Actin bundles and microtubules within a cell's cytoskeleton have been shown to align with such groove edges (Oakley et al., 1997). The propensity for neurites to extend along the edges of microgrooves may be related to their affinity for surface curvature and even smaller topographical structures than those designed in the above experiments. The nanotopography of substrates is known to have an impact on cell survival, proliferation and differentiation and a variety of cell types have been shown to react positively to nanotopographic features (with nanotopography referring to surface features scaled between 1-100nm) (Gerecht et al., 2007, Oakley et al., 1997, Recknor et al., 2006, Webster et al., 1999).

This can be clearly demonstrated on gold surfaces. When the gold substrate is manufactured to different levels of roughness, it has varying effects on mouse embryonic stem cells that have been differentiated into neurons. Cell survival was highest on planar gold, rather than on nanotopographically rough gold, however neuronal differentiation favoured the rough gold surfaces, with a greater number of terminally differentiated cells occurring on increasingly rough surfaces (Bakeine et al., 2000). Fibroblasts grown on nanotopographic polymer surfaces showed increased numbers of filopodia on these surfaces than on the planar surfaces, and there was also a broad gene up-regulation (Dalby et al., 2002) linking cell activity with interactions at the cell-substrate interface.

Finally, microfluidics is also a useful tool for neuronal patterning, either onto substrates or onto MEAs with varying degrees of success (Griscom et al., 2002, Martinoia et al., 1999, Morin et al., 2006). Microfluidics refers to systems that can transport liquids in a laminar flow through a network of channels on the microscale. It is an established method for flow cytometry and cell sorting. Fluid flow characteristics are used to direct movement of matter in confined microchannels. Griscom (Griscom et al., 2002) created such a system into which cells can fall and then grow. This microfluidic system was aligned with the electrodes of an MEA and primary cortical cells were seeded between 1 and 10 cells per well. Control of cell placement was not as accurate as with other methods, possible partly due to the thickness of the growth area for the cells. Processes tended to grow along the walls and cell bodies migrated along the channels (Figure 1.6). Also of interest is how microfluidics can be used effectively to control chemical gradients through conjoining laminar flow channels and compartmentalize the soma and processes of neurons cells (Dertinger et al., 2001, Gross et al., 2007, Taylor et al., 2003).

So which is more important: the chemistry or the topography of the surface to which the cells are adhering? Britland (Britland et al., 1997) simultaneously studied the effects of topographical guidance, protein guidance, parallel topographical/protein guidance and orthogonal topographical/protein guidance (Figure 1.7). The heights of the topographical guidance cues were also varied. The primary branches of dorsal root ganglia were found to align preferentially to topographic cues above a certain threshold, whereas terminal neuritic branches were augmented by the chemical patterning and relatively unaffected by topography (Figure 1.8).

Of course, the cell type chosen for the study is a variable in the results seen. Macrophages and fibroblasts were found to react differently to patterned surfaces (Rich and Harris, 1981). Whereas macrophages preferred rough and hydrophobic surfaces, fibroblasts preferred smooth and hydrophilic surfaces. It is clear that different cell types observe different guidance cues to a greater or lesser degree. This could potentially lead to a great flexibility in achievable architectures *in vitro*. It is perhaps also worth noting that with higher densities of culture, and indeed *in vivo*, chemical and topographic cues are presented by neighbouring differentiating cells to each other. Such a mutually influential system has been suggested to play a critical role in shaping the fine structure, and function, of the developing neocortex *in*

situ (Artavanis-Tsakonas et al., 1999, Brunet et al., 2007, Conboy and Rando, 2002, Rakic et al., 1994).

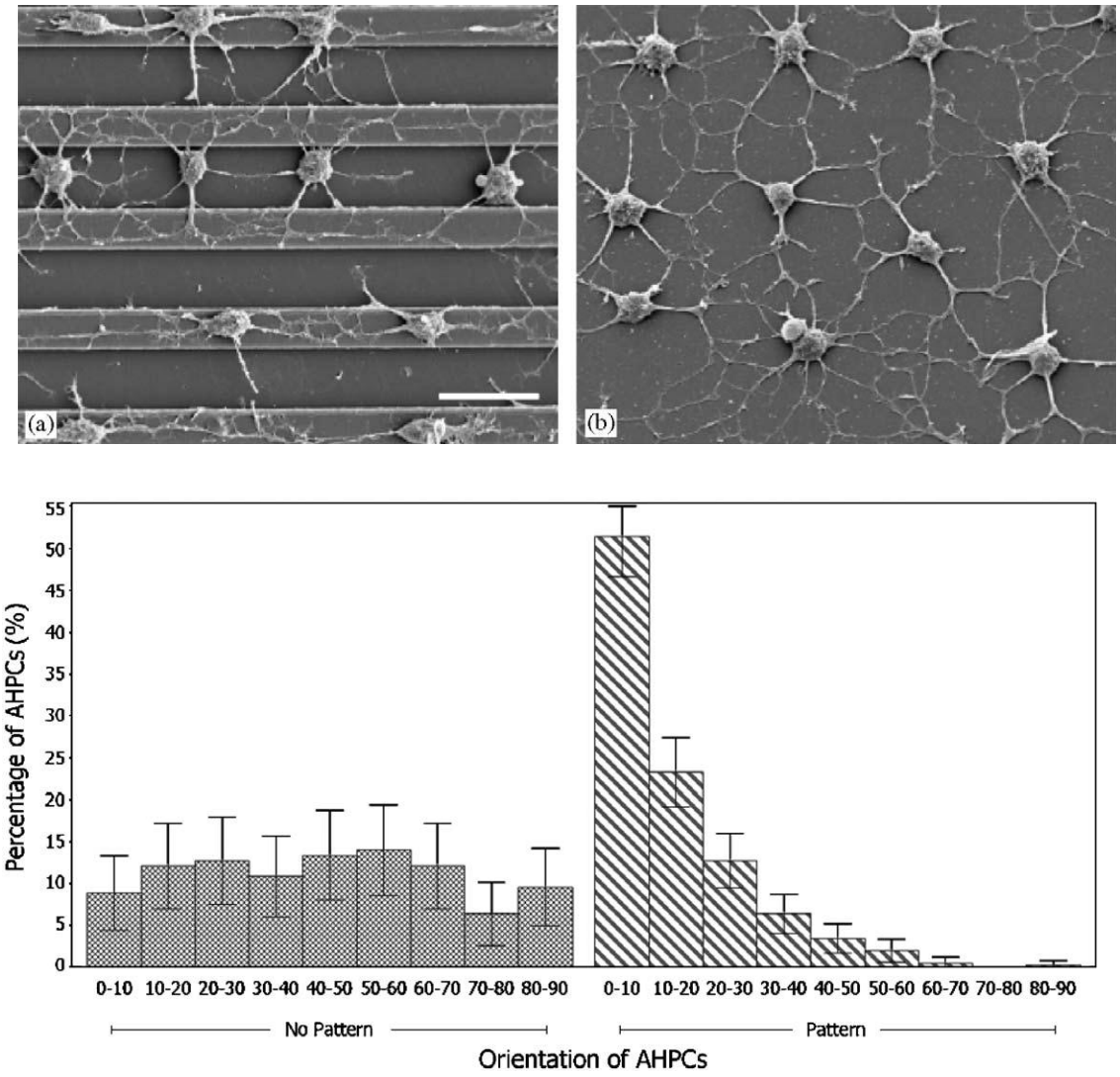

Figure 1.5 Control of AHPCs differentiated on patterned surfaces. a) AHPCs on microgrooves, showing a degree of alignment with the grooves and b) planar substrates showing no alignment preference. The histogram in the lower panel depicts the percentage of AHPCs aligned between 0 and 90 degrees in 10 degree bins for the planar ('no pattern': 'b') and microgrooved ('pattern': 'a') surfaces. (Recknor et al., 2006).

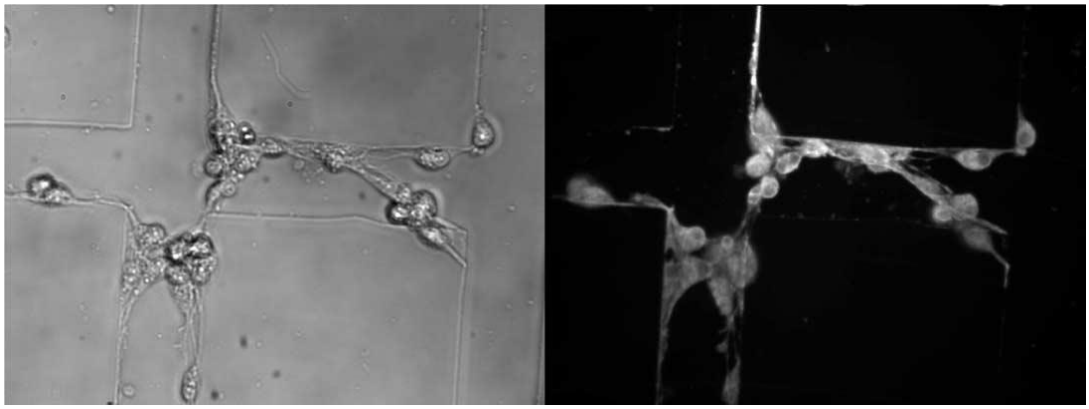

Figure 1.6 – Adhesion preferences for cells in controlled environments. A phase contrast image (left) and a fluorescence image (right) of primary cortical cells cultured in 40µm wide microtunnels. (Griscom et al., 2002). The cells show a preference for the boundary between the patterned walls and the substrate, with processes extending along the edges of the walls.

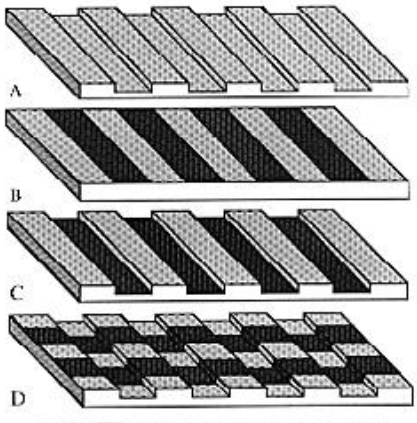

Figure 1.7 – Examples of topographic patterning. A) Topographic patterning with microgrooves, B) Chemical patterning in lines that match the dimensions of the microgrooves in A. C) Parallel topographic and chemical patterning. D) Orthogonal topographic and chemical patterning.

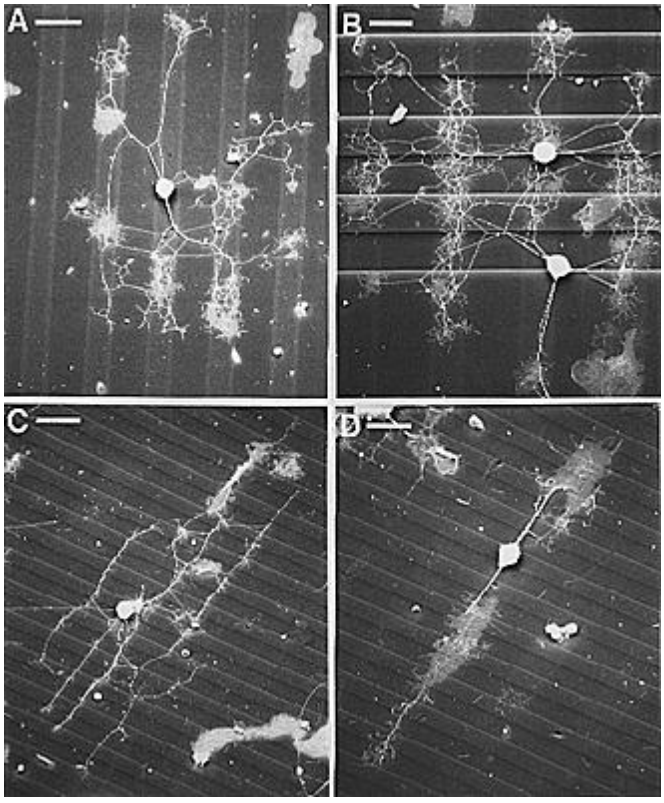

Figure 1.8 – Chemical vs structural influences on neuronal structure. A) SEM of a dorsal root ganglion (DRG) growing on a chemically adhesive substrate with 12um spacing. Scale bar is 16µm. B) DRGs on orthogonally patterned chemical adhesion and microgrooves with 3µm spacing. Scale bar is 10µm. C) Same as in 'B' but with shallower grooves. Scale bar is 25µm. D) Cell aligning preferentially to adhesive rather than topographical cues often had elongated growth cones that spanned a number of topographic periods. Scale bar is 20µm (Britland et al., 1997, Gabay et al., 2005a).

1.4 CALCIUM SIGNALLING IN NEURONS

Calcium is a ubiquitous signalling molecule in cells, involved in many processes. In neuronal systems, free cytosolic calcium concentration changes can be a clear, potent indicator of electrical and metabotropic activity. Various fluorescent probes have been developed for imaging changes in calcium concentration inside cells (Mackenzie et al., 1996, Murphy et al., 1995, Oertner et al., 2002, Yuste et al., 2000) and probes have also been used for imaging activity in entire neuronal networks (Cossart et al., 2005, Pickering et al., 2008, Takahashi et al., 2007, Ukhanov et al., 2011). A brief description of calcium ions in neuronal systems is given here neuronal function on many scales - from looking at single synapses to illustrate it's value as an indicator of neuronal activity and its usefulness in developing our understanding of neuronal function and development.

1.4.1 Calcium Signalling

Calcium ion concentration in cytosol is one of the most potent intracellular messengers available to neurons. Postsynaptic rises in calcium concentration influence mitosis, meiosis and both transcription and translation of nuclear message and are thus vital for cell differentiation (Dumollard et al., 2004, Hepler, 1989, Machaca and Haun, 2000, McKinsey et al., 2002, Poenie et al., 1986) (see section 1.4.3 below). They also change microtubular scaffolds to cause structural changes (such as neurite extension and dendritic spine extension (Lautermilch and Spitzer, 2000, Marcum et al., 1978, Sandoval and Weber, 1978). Cell-cell interactions, including the calcium-dependent Notch signalling pathway, exert a role in, for instance, glial cell fates (Gaiano and Fishell, 2002) and neurite extension (Šestan et al., 1999). In addition they influence the phosphorylation state of ion channels (Kolaj et al., 1994, McDonald and Moss, 1994), metabolic processes and directly activate a number of potassium conductances controlling membrane potential. They influence neuronal excitability (Duchen, 1990, Morita et al., 1982, Smart, 1997), direct electrical connectivity between neurons via gap junctions (Perez-Velazquez et al., 1994, Valiante et al., 1995) and also act to drive co-transporters vital to maintain transmembrane ion gradients (Snyder et al., 1991). It is clear from many of the above effects that calcium ion changes are a vital primary stimulus in controlling synaptic plasticity, and thus the function of neuronal networks (Cavazzini et al.). Finally, when rises in calcium ion concentration are induced by voltage-operated ion channels they can generate very large depolarisations in membrane

potential which dramatically alter neuronal output from single spike to burst behaviour (Grace and Bunney, 1984, Traub, 1979). The latter effect is primarily due to the enormously positive equilibrium potential for calcium ions across the plasma membrane (Henček and Zachar, 1977). The above demonstrate how calcium modulation is critical to neuronal activity in general, not just the electrical domain.

1.4.2 Sources of intracellular calcium and their compartmentalisation

There are different spatial and temporal scales over which changes in intracellular calcium concentration can manifest. Mechanisms of calcium diffusion within the cytosol can rely on the transduction of a range of calcium concentrations, effective over both the nano- and microscale. Calcium binding proteins allow these diffusing calcium signals to be translated into physiological effects through cascade reactions. In addition, specific types of calcium binding protein (E-F hand proteins) (Minami et al., 1987) effectively buffer changes in cytosolic calcium over a range of concentrations and timecourses (e.g. calretinin, calbindin, calmodulin, parvalbumin (Kretsinger, 1976)).

Presynaptically rapid neurotransmitter release is thought to be facilitated by nanodomains of calcium channels where these calcium sensing proteins must be within 50nm of the channel to detect unitary responses (where maybe 1000 calcium ions (Ca^{2+}) will flux through a single channel (Augustine et al., 2003)). In contrast, microdomains of calcium channels allow the detection of more diffuse calcium signals where the calcium sensing proteins may be located within a micrometer of the channels and respond to the summation of signals from the microdomain. Postsynaptically, in dendritic segments, diffuse calcium signals spread 5-500µm. The signals remain concentrated in the heads of dendritic spines due to the distribution of micro- and nano-domains at the head and the thin, restrictive neck of the spine (Augustine et al., 2003).

The primary source of calcium signals in pre-synaptic terminals is voltage-gated calcium channels (VGCC). There are a great many subtypes of VGCC at synapses, and their role in coupling action potentials to exocytosis of neurotransmitter is complex and highly modulatable by neurotransmitter receptors (Parnas and Parnas, 2010). The role they play in shaping presynaptic responses is also highly developmental-state-dependent, with much slower events being associated with earlier developmental periods (Wang et al., 2009). In

general, different fast-acting presynaptic terminals have been implicated in the use of the micro- and nanodomain mechanisms of neurotransmitter release. Slower transmitter release synapses (such as those seen in early development) are related to more diffuse calcium signals.

In post-synaptic terminals, the source of calcium signals can vary greatly, including influx from outside the cell membrane via VGCC and ligand-gated calcium channels (LGCC), as well as release from intracellular stores. There are a number of sources for calcium release from intracellular stores, namely the endoplasmic reticulum (ER), synaptic vesicles, mitochondria and the nuclear envelope (Verkhratsky and Petersen, 1998). Sarco(endo)plasmic reticulum ATP-ase (SERCA) pumps in the ER remove Ca^{2+} from the cytosol (Wu et al., 1995), while calretinin and calbindin proteins aid storage (Baimbridge et al., 1992), and inositol 1,4,5-triphosphate (IP_3) and ryanodine receptors (RyR) provide mechanisms for its release with stimulus from calcium induced calcium release (CICR) or metabotropic receptor activation (Lanner et al., 2010, Taylor and Tovey, 2010). The nature of the homeostatic maintenance of Ca^{2+} stores allows the redistribution of cytosolic Ca^{2+} and potentially the propagation of Ca^{2+} waves to distal compartments in communication and signalling (Mogami et al., 1997).

VGCCs are involved in many cell functions including cell membrane excitability, cell homeostasis and cell development. Post synaptic excitatory responses may involve calcium entry through receptor-coupled ionophores (e.g. NMDA subtype of glutamate receptor and some subtypes of AMPA receptor) and metabotropic receptor-mediated release from intracellular stores (e.g. group 1 metabotropic glutamate receptors and muscarinic cholinergic receptors). Even when subthreshold for postsynaptic cell spiking, these excitatory inputs out on distal dendrites of some neurons can induce additional calcium entry through low threshold-activated (T-type) VGCCs. Above threshold for postsynaptic cell activation sodium channel-dependent rapid conductances underlie action potentials. However, these may also be accompanied by further calcium entry via high-threshold (L-type) VGCCs - contributing to the single action potential calcium signals reported by many researches. In addition, longer L-type channel opening may provide additional depolarisation, generating bursts of action potentials and very large somatic intracellular calcium rises (Jahr and Stevens, 1987, Jonas et al., 1994, Pumain et al., 1987).

The relative permeabilities of these and other calcium ionophores in neuronal membranes differ markedly, as does the net calcium flux through different types of VGCC. Thus a very broad range of local and diffuse magnitudes of calcium ion concentration change in cytosol is possible depending on neuronal subtype, type of synaptic input received and type of output generated. Direct measurement of intracellular calcium concentration is therefore an excellent way to study the diversity of neuronal activity patterns in isolation and in functioning networks.

1.4.3 Calcium signalling and neuronal differentiation

Calcium signalling plays a dominant role in embryonic development, and it is potentially the initial production of fast calcium waves in the early embryo that becomes adapted to the varied functions of calcium signalling as the embryo becomes increasingly complex in both form and function (Webb and Miller, 2000). Subsequently, there is a clear role for calcium signalling in neuronal differentiation and development. Neuronal migration along neurites has been shown to be intimately related to calcium signalling (Komuro and Rakic, 1996). Spinal cord neurons have been found to produce calcium transients that affect their differentiation prior to the development of network activity (Spitzer et al., 1994). The frequency of calcium transients was specifically shown to affect morphology, synapse formation and neurotransmitter expression. Two main forms of calcium transient were recorded from neural-plate stage *Xenopus* neurons; waves and spikes. Waves have been found to affect neurite outgrowth, which ultimately affects synapse formation, general connectivity and signal propagation properties. This was also demonstrated for dendritic growth by Wong (Wong and Ghosh, 2002). Spikes were found to affect the expression of GABA (Gu et al., 1994), which, depending on the stage of development, can impact on excitation or inhibition of the network. During a 7-12hr recording period, 70% of active neurons exhibited calcium spikes, 75% exhibited calcium waves (55% exhibited both). It is noteworthy that the incidence of such activities were very low, ranging up to only 3 spike-like transients per hour and 2 waves per hour in the cell soma.

1.4.4 Characteristics of the calcium transient

Calcium transients correlated to neuronal spikes can most commonly be characterised by their sharp onset and double exponential decay (Figure 1.9). The timecourse of this signal can vary but transients correlating with spontaneously occurring single spikes tend to

extend to around 1 – 2 seconds. Large numbers of summed events at the neuronal cell body correlated with grouped barrages of action potentials (bursts) cause much larger increases in calcium levels in the soma due to the slow kinetics of the calcium activity leading to the summation of individual calcium transients associated with each spike. These large transients have highly variable amplitudes, which can be correlated with the frequency of the spike train (Sasaki et al., 2008). In neurons that have a propensity to generate burst discharges, such as the CC9 ESC-derived cells studied in this thesis, transient pressure ejection of glutamate (to mimic release from immature excitatory synapses) generates bursts of 10's of action potentials over several seconds (Figure 1.10 (Trevelyan et al., 2010)). The calcium transients accompanying these burst discharges were over 10-fold larger than those seen for single spikes (compare data in Figure 1.9 & 1.10). They were also considerably longer, lasting over 10s and importantly, did not peak until 1-2s after glutamate stimulation.

1.4.5 Calcium Indicators

The two main types of calcium indicator currently used experimentally are the genetically encoded type and small-molecule chemical indicators. The chemical variety are commercially available and designed for many different applications. Bright, single wavelength indicators and ratiometric dyes (which allow quantification of calcium levels and avoid problems of uneven loading and bleaching) are both readily available. High affinity indicators can be used to look at cytosolic calcium levels (Ivannikov et al., 2010), while low-affinity indicators are good for use in high concentrations to look at compartmentalisation of calcium within the cell (Echevarria et al., 2003) and the kinetics of calcium transport (Beurg et al., 2009). Loading these indicators into cells usually follows simple, well established protocols but intrinsic problems persist, such as unwanted compartmentalisation of the dye or leakage of the dye out from the cell with time. Probes designed to overcome these issues, such as dextran conjugates, tend to require direct injection to load the cells but can be more effective for long recording times such as over a period of days. Alternatively, Acetoxymethyl (AM) ester dyes can enter the cell from the extracellular medium. They offer a simpler protocol for short-term recordings and the AM ester only breaks down once it has entered the cell, thus ensuring only intracellular calcium changes are seen.

There are other properties to be considered when choosing an appropriate dye. The dissociation constant (K_d) of the indicator can have an effect on the buffering level of the calcium, and if not matched appropriately to the compartment/process being measured, fluorescence signal may be too weak or potentially too slow to react to accurately monitor the physiological signals of interest (linked to $1/K_d$, the decay constant).

If necessary, quantitative measurements of the calcium concentration can be achieved by using ratiometric dyes, which show a change in their emission profile associated with their bound or unbound state. Comparing absolute levels of calcium with these dyes is achieved by dividing the fluorescent intensity signal from the bound- and free-state wavelengths, making it ideal for measuring intracellular calcium for moving cells *in vivo* (as motion artefacts are cancelled out) or for comparing resting potentials (as uneven dye distribution or change with time, such as photobleaching or leakage, are cancelled out) (Kerr et al., 2000, Lohr, 2003). Fluorescence imaging of calcium signals is spatially and temporally limited. Micro- and nanodomains (see 1.4.2 above) test the limit of the resolution of light microscopy and individual dendritic spines can present a considerable challenge. Signals occurring at the level of cell somata, along dendritic segments or larger sets of compartments are much more feasible. The possible limit to temporal resolution on distinguishing signals due to the binding rate has already been mentioned but outside these limits the camera's temporal and spatial resolution is the main limiting factor.

Oregon Green is a high affinity, single excitation/emission dye used for measuring cytosolic levels of calcium and has similar properties to other high affinity dyes also in common use, namely Calcium Green-1 and Fluo-3/4. It has been used successfully for many different types of imaging of live neuronal tissue and individual cells (Behrend et al., 2009, Schwiening and Willoughby, 2002, Bonnefont et al., 2000). It has a high K_d and, as it can be used in lower concentrations, is not as phototoxic. This is the dye chosen for the following experiments.

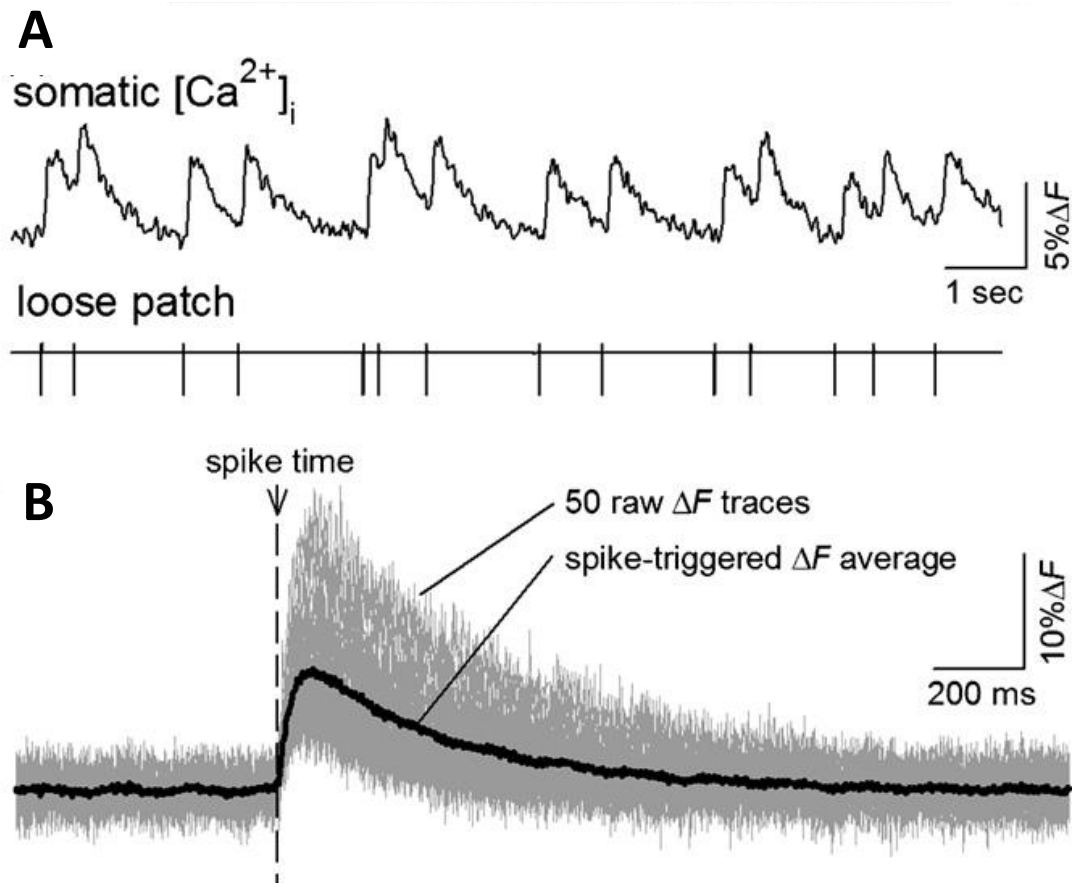

Figure 1.9 - **Examples of typical somatic calcium signals from single hippocampal neurons** (Takahashi et al., 2007). **A)** Discrete (single action potential, evident from the loose patch 'unit' recording) events are associated with small amplitude, but prolonged cytosolic calcium transients. B**)** Mean of 50 action potentials associated calcium transients demonstrating the relatively slow, double-exponential decay.

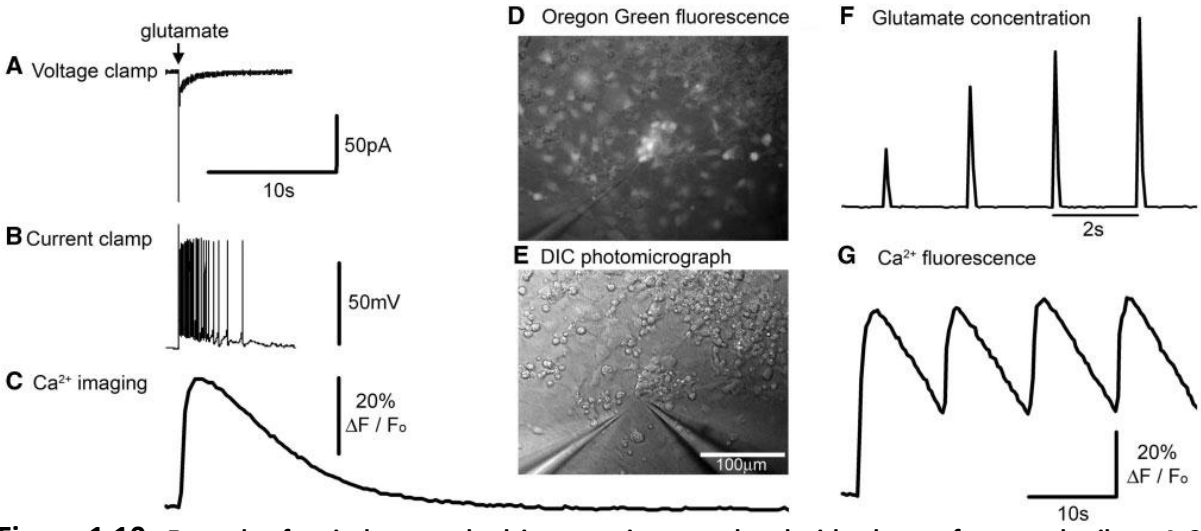

Figure 1.10 - **Example of typical summed calcium transient correlated with a burst of neuronal spikes. A-C) 1mM glutamate delivered 25µm from the cell soma. A)** Cell clamped at -70mV likely displays a break-through action potential. **B)** Current clamp shows a barrage of action potentials. **C)** Full calcium transient response. **D)** Calcium fluorescence image with pipette tip location. **E)** Brightfield image of 'D'. **F)** Representation of glutamate pressure pulses. **G)** Calcium transient responses evoked by 0.1Hz glutamate pulses. (Trevelyan et al., 2010).

1.5 WAYS TO QUANTIFY NETWORK FUNCTION

No single measure can capture the diverse patterns of activity seen in both developing and mature neuronal networks. Developing networks tend to behave in a more stereotyped fashion than mature networks , exhibiting repetitive (though often aperiodic) bursts of activity separated by periods of relative or absolute quiescence. However, how these bursts of activity that propagate through an immature network can be far from stereotyped (Volman et al., 2005). Synchrony, a useful, robust measure of spatiotemporal activity can capture, to some extent, the degree of stereotypy in the output of a network. Firstly, this measure quantifies the number of neurons or clusters of neurons that are temporally co-active. More detailed synchrony measures can reveal something about network behaviour by looking at the magnitude of correlations (a measure of similarity in activity in a number of different areas) across many pairs of regions (Baruchi et al., 2008).

Synchrony is an extreme case in terms of stereotypy in network behaviour. More commonly, bursts of activity are seen to propagate non-simultaneously through networks. By ignoring the absolute path and origin of such behaviour they can be quantified using the concept of 'avalanches'. Briefly, this analytical approach looks for the start of a burst of activity and measures how many neurons or regions are subsequently activated as the activity propagates, along with the duration in time of the process of propagation. Avalanches are often seen as a property of scale-free networks. This method of network analysis is useful in as much as it may in part predict the information processing capacity of a network (Beggs and Plenz, 2003, Paczuski et al., 1996, Pasquale et al., 2008, Zapperi et al., 1995).

Other measures associated with the avalanche approach to network analysis, including the 'coincidence index' and 'branching parameter', reveal more detail about strength of communication within the network and the pattern of propagation (Pasquale et al., 2008). In addition, combining these measures with detailed region-by-region correlation maps can reveal preferred patterns of propagation within a network – termed 'motifs'. The more motifs a network demonstrates the more adaptability it shows to incoming input and thus the more processing power it may have (Haldeman and Beggs, 2005). Finally one can look for common (or most likely) origins of motifs of propagated activity – so called 'hubs'. These can be individual neurons or closely linked clusters of neurons that, on average, are most

likely to seed an autonomously generated avalanche of activity in a network (Bonifazi et al., 2009).

In order to address the main aim of this thesis – whether there are structure/function correlates in artificially created neuronal networks and how they may alter with early development – a combination of all of these measures was used and directly compared to basic measures of network structure. A more detailed review of the use of each measure in given in Chapter 5 and their interaction with structure assessed in the general discussion.

CHAPTER 2: MATERIALS & METHODS

A combination of techniques has been used at each stage of this project and this section aims to provide the key details behind the use of these techniques. Here I describe the methods applicable to the cell lines used, the calcium imaging methods and the data handling and analysis routines. Each results chapter also has specific methods that apply only to findings presented within it.

Two cell lines were used and each is associated with quite different sets of protocols, so sections below detail the protocols used in the maintenance and differentiation of each line separately where possible. Processing of calcium imaging data involved a number of steps with custom-built scripts, and although details of specific measures used in the analysis are given in the appropriate results chapters, the details of the standard processing procedures employed for all the data are given here.

2.1 CC9 EMBRYONIC STEM CELL LINE

Maintenance of the CC9 embryonic stem cell (ESC) line, particularly as they are not an immortalized line, involved freezing protocols to stop the cells aging and spontaneously differentiating. Cell stocks were provided frozen (-80°C). Stocks were then proliferated and re-frozen. Once thawed, the cells had to be maintained and passaged regularly to accommodate their increasing numbers before being differentiated into neurons using the -4/+4 embryoid body technique. The cells could then be maintained for up to 22 days in culture. All cell work up to 10-12 DIV was performed in a class 2 laminar-flow hood. After this the cells were re-located to an incubator next to the calcium imaging equipment and a positive-pressure tissue culture hood in the vicinity was used instead.

2.1.1 Media formulations

2.1.1.1 Growth Medium

Growth medium was used for the growth and maintenance of embryonic stem cells.

Glasgow-minimum essential medium (GMEM) (Invitrogen 21710-025) was used composing (mM):

Calcium Chloride	0.2
Ferric Nitrate • 9H2O	0.0001
Magnesium Sulfate (anhydrous)	0.09767
Potassium Chloride	0.4
Sodium Bicarbonate	—
Sodium Chloride	6.4
Sodium Phosphate Monobasic (anhydrous)	0.1078
Amino Acids	
L-Arginine • HCl	0.042
L-Cystine • 2HCl	0.03129
L-Glutamine	0.292
L-Histidine • HCl • H2O	0.021
L-Isoleucine	0.0524
L-Leucine	0.0524
L-Lysine • HCl	0.0731
L-Methionine	0.015
L-Phenylalanine	0.033
L-Threonine	0.0476
L-Tryptophan	0.008
L-Tyrosine • 2Na • H2O	0.05219
L-Valine	0.0468
Vitamins	
Choline Chloride	0.002
Folic Acid	0.002
myo-Inositol	0.0036
Niacinamide	0.002
D-Pantothenic Acid (hemicalcium)	0.002
Pyridoxal • HCl	0.002

Riboflavin	0.0002
Thiamine • HCl	0.002
Other	
D-Glucose	4.5
Phenol Red • Na	0.016
Sodium Bicarbonate	2.75

The following were also added: 10% fetal calf serum, 1% l-glutamine, 1% nucleosides, 1mM 2-mercaptoethanol, 1mM sodium pyruvate and 1000 units/ml leukaemia inhibitory factor (LIF). Fetal calf serum provide growth factors, l-glutamine is an unstable essential amino acid and provides an energy source for cells (as does sodium pyruvate). It is also a precursor for glutamate. The nucleosides, once phosphorylated, form nucleotides used in DNA and RNA synthesis. 2-mercaptoethanol acts as an antioxidant, scavenging hydroxyl radicals, and aids cell viability and differentiation. LIF promotes proliferation, gene expression and survival.

The same medium, but without LIF, was used from the start of the -4/+4 differentiation protocol (detailed below).

2.1.1.2 Plating Medium

Plating medium was used after the -4/+4 differentiation protocol had been implemented and neuronal cells were being seeded onto substrates for further differentiation and network development.

A 4:1 ratio of Neurobasal (GIBCO 21103) to Dulbecco's modified Eagle's medium (DMEM) (GIBCO 21331).

Neurobasal composed of (mM):

Amino Acids	
Glycine	0.4
L-Alanine	0.0225
L-Arginine hydrochloride	0.398

L-Asparagine-H2O	0.00553
L-Cysteine	0.26
L-Histidine hydrochloride-H2O	0.2
L-Isoleucine	0.802
L-Leucine	0.802
L-Lysine hydrochloride	0.798
L-Methionine	0.201
L-Phenylalanine	0.4
L-Proline	0.0675
L-Serine	0.4
L-Threonine	0.798
L-Tryptophan	0.0784
L-Tyrosine	0.398
L-Valine	0.803
Vitamins	
Choline chloride	0.0286
D-Calcium pantothenate	0.00839
Folic Acid	0.00907
Niacinamide	0.0328
Pyridoxine hydrochloride	0.0196
Riboflavin	0.00106
Thiamine hydrochloride	0.0119
Vitamin B12	0.000005
i-Inositol	0.04
Inorganic Salts	
Calcium Chloride (CaCl2) (anhyd.)	1.8
Ferric Nitrate (Fe(NO3)3"9H2O)	0.000248
Magnesium Chloride (anhydrous)	0.814

Potassium Chloride (KCl)	5.33
Sodium Bicarbonate (NaHCO3)	26.19
Sodium Chloride (NaCl)	51.72
Sodium Phosphate monobasic (NaH2PO4-H2O)	0.906
Zinc sulfate (ZnSO4-7H2O)	0.000674
Other Components	
D-Glucose (Dextrose)	25
HEPES	10.92
Phenol Red	0.0215
Sodium Pyruvate	0.227

And DMEM consisted of (mM):

Amino Acids	
Glycine	0.4
L-Arginine hydrochloride	0.398
L-Cystine 2HCl	0.201
L-Histidine hydrochloride-H2O	0.2
L-Isoleucine	0.802
L-Leucine	0.802
L-Lysine hydrochloride	0.798
L-Methionine	0.201
L-Phenylalanine	0.4
L-Serine	0.4
L-Threonine	0.798
L-Tryptophan	0.0784
L-Tyrosine disodium salt dihydrate	0.398
L-Valine	0.803
Vitamins	

Choline chloride	0.0286
D-Calcium pantothenate	0.00839
Folic Acid	0.00907
Niacinamide	0.0328
Pyridoxine hydrochloride	0.0196
Riboflavin	0.00106
Thiamine hydrochloride	0.0119
i-Inositol	0.04
Inorganic Salts	
Calcium Chloride (CaCl2) (anhyd.)	1.8
Ferric Nitrate (Fe(NO3)3"9H2O)	0.000248
Magnesium Sulfate (MgSO4) (anhyd.)	0.814
Potassium Chloride (KCl)	5.33
Sodium Bicarbonate (NaHCO3)	44.05
Sodium Chloride (NaCl)	110.34
Sodium Phosphate monobasic (NaH2PO4-H2O)	0.906

This formulation was supplemented with 2% B27, 0.2% N-2 and 0.1µg/ml basic fibroblast growth factor (b-FGF). B27 is commonly used Neurobasal media formations for the long-term viability of hippocampal neurons and acts as a substitute in the absence of serum (removed now mainly due to its inhibition on differentiation and encouragement of proliferation). N-2 is a supplement that aids the growth and expression of post-mitotic cells is serum-free environments, specifically for neuronal cells. B-FGF aids the survival, proliferation and differentiation of nascent neuronal cells.

2.1.1.3 Freezing Medium

This was growth medium (see section 2.1.1.1 above), to which 10% Dimethyl Sulfoxide (DMSO) was added, a cryoprotectant that stops cell death during the freezing process through ice formation.

2.1.2 Thawing Protocol

CC9s, stored undifferentiated at -80°C in freezing medium (see 2.1.1.3 above) in 1ml cryovials, were thawed using 10ml of warmed growth medium (diluting the DMSO by 10X) and centrifuging at 1100rpm for 3 minutes to pellet the cells. After aspirating the DMSO-containing medium, the pellet was dispersed by triturating with a fine pipette tip and 1ml of growth medium (as above 2.1.1.1). The cells were then added to a T25 culture flask that had been coated with 0.1% gelatine for 10 minutes before aspirating and adding 9ml of warmed growth medium. The cells were then maintained in an incubator at 37°C in a 5% CO_2 environment for 2 days while the cells proliferated and filled the flask.

2.1.3 Protocol to maintain CC9s in an undifferentiated state

After two days at 37^{o}C in the 5% CO_2 environment (above), the confluence of the cells was checked to ensure the cells had proliferated to fill 70-90% of the flask surface. If the cells were of low confluence, the medium was aspirated and replaced with 10ml warmed growth medium. If the cells were of high confluence they were ready for passage (Figure 2.1).

To passage, the medium was aspirated and the CC9 cells washed with 5ml phosphate buffered saline (PBS) before adding 0.5ml trypsin replacement (TrypLE Express, Invitrogen) and leaving to stand for 2 minutes to lift the cells from the surface of the flask. The trypsin was quenched with 10ml growth medium (which contains serum) and the cells triturated before a percentage (usually 15-20%) were added to a fresh gelatin-coated flask and transferred to the incubator. To increase stock of these cells, each flask can typically be divided as such into around 6 fresh flasks every two days.

2.1.4 Freezing Protocol

If the cells were not to be differentiated soon, they could be frozen by passaging the cells as normal, but centrifuging the cells to remove the trypsin-containing medium and triturated with 5ml freezing medium (see 2.1.1.4 above) (chilled in dry ice) before dividing between 1ml cryovials (also chilled in dry ice) and transferred to a -80°C freezer. If the cells were not to be used within 4-6 months, it was advisable to move them to liquid nitrogen storage.

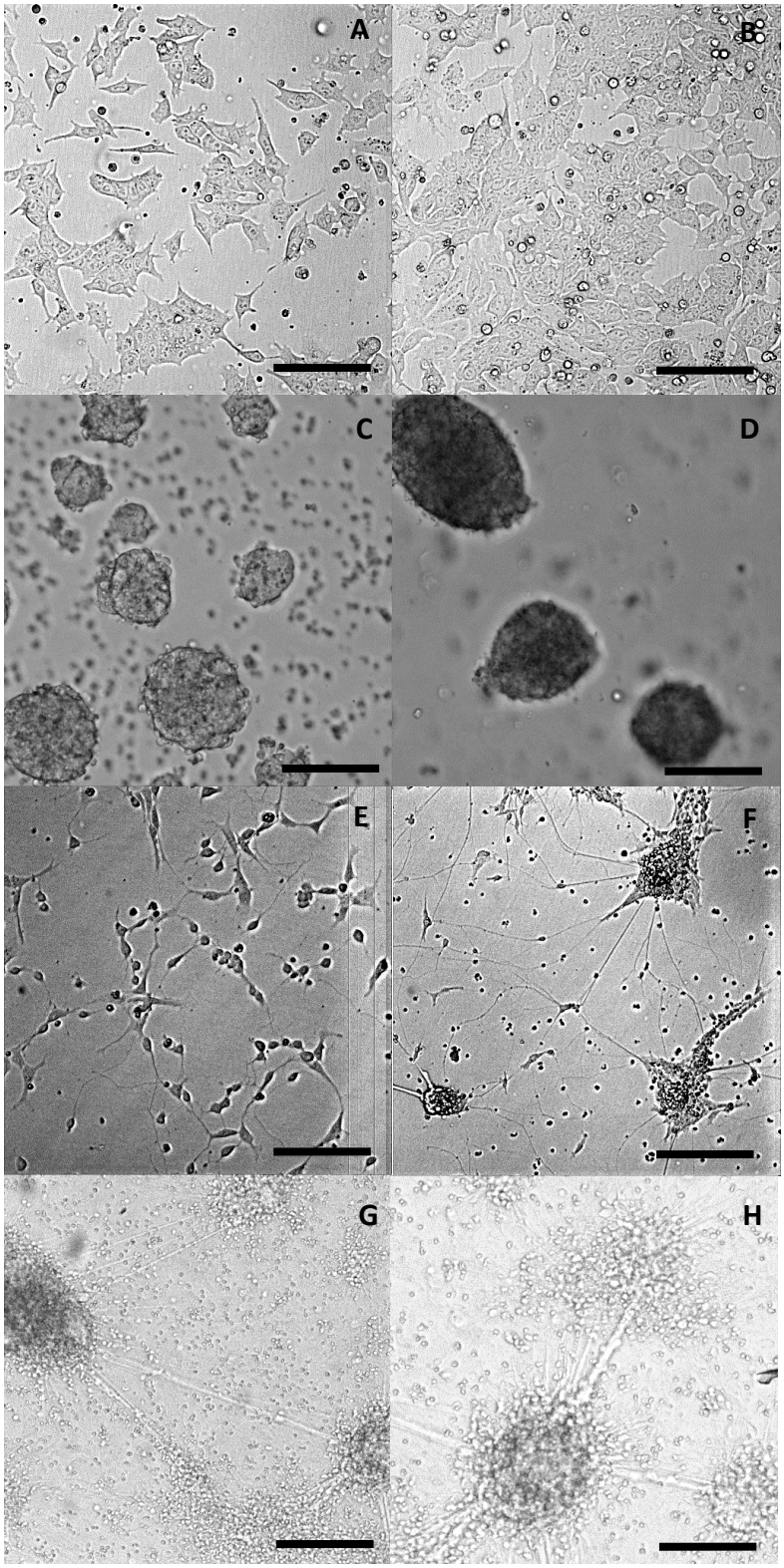

Figure 2.1 – CC9 developmental stages. A) 1 day post thaw, the cells can be seen to be of low confluence, with many gaps between neighbouring cells. These undifferentiated cells have a tendency to cluster, but remain quite flat to the coated substrate. **B)** 2 days post thaw, high confluence of cells (i.e. most of the surface is now covered with cells). **C)** At 2 DIV embryoid bodies are beginning to form. **D)** At 4 DIV embryoid bodies appear larger and denser. **E)** At 10 DIV (2 days after the embryoid bodies are dissociated and the cells seeded to an adherent surface) neuronal processes start extending and neurons migrate across the surface. **F)** At 12 DIV neurons start to cluster and long processes extend between the clusters. **G and H)** 14 days differentiated, clusters have stabilized with thick, fasciculated, neuritic bundles. All images were taken at 20x and the scale bar = 100µm.

2.1.5 -4/+4 Embryoid Body Protocol for neuronal differentiation

If the cells were to be differentiated they were passaged one day beforehand, keeping around 40-50% of the cells. The following day, the confluence of the flask was checked under 10X magnification to ensure the flask was not overpopulated (simply by eye, observing the space between cells still available). The cells were PBS-washed, trypsinized, quenched and centrifuged to remove the trypsin-containing medium. The pellet was dispersed with 1ml growth medium without LIF and topped up with a further 9ml. This was transferred to an uncoated petri-dish and incubated at 37^{o}C in the 5% CO_2 environment. This was taken to be 0 DIV, marking the start of differentiation of the stem cells by removal of LIF.

At 2 DIV the cells, which had now formed clusters of cells called embryoid bodies (EBs), were transferred to a universal tube and allowed time to settle on the bottom. The medium was aspirated and replaced and the EBs transferred to a new petri-dish. This process was repeated at 4 and 6 DIV, with the addition of 0.5µM retinoic acid at both time points to encourage differentiation down the neural lineage and inhibit mesoderm lineages (Bain et al., 1996). At 6 DIV, the EBs were also split into two petri-dishes due to the increased population size (Figure 2.1).

At 8 DIV the EBs were washed in 10ml PBS, incubated for 4 minutes with 1ml trypsin replacement, quenched with 10ml growth medium without LIF and thoroughly triturated to break them up into single cells. The cells were then centrifuged to remove the trypsin replacement and serum-containing medium. The pellet was dispersed using 1ml Neurobasal medium and topped up with a further 9ml. This was centrifuged a second time to ensure the serum was washed from the cells. The pellet was then dispersed with 1ml 4:1/bFGF medium. After the cells had been counted (using a haemocytometer), calculated densities were seeded onto PDL/laminin-coated glass slides in 6-well plates filled with 2ml 4:1/b-FGF medium (coating procedure given below). Here, substrate refers either to glass coverslips, carbon nanotube-patterned quartz chips or multi-electrode arrays.

2.1.6 PDL/laminin coating protocol

The substrate was covered with PDL (1% solution in PBS) for 1 hour and washed three times with PBS. The PDL-coated surface was then covered with laminin (0.2% solution in PBS) and

allowed to stand for 24 hours at room temperature. The coated surface was washed three times with PBS and 2ml plating medium was added before seeding the cells, taking care that the surface did not dry out at any point.

2.1.7 Protocol to maintain CC9s differentiated into neurons

1ml of medium was removed and replaced with 4:1 medium (without b-FGF) every day until the culture was used for an experiment (Figure 2.1).

2.1.8 Development of CC9 cell culture protocols

Culture protocols for the CC9's were based, as previously explained, on Bain's methods (Bain et al., 1995, Bain et al., 1996) and methods from Bob Lightowlers Group (Mitochondrial Research Group, Newcastle University), but these cells are notorious for being delicate and quite difficult to maintain in culture. In order to improve survival of my own cultures, some adaptations to these cited protocols were made.

The seeding density of the cells was found to affect both the cells' survival and differentiation. Very low density cultures were difficult to maintain, perhaps due to the absence or low level of factors secreted by neighbouring cells and the chemical influence of neighbouring cells on each other's development. Larger seeding densities resulted in exponentially larger numbers of cells in the final population on each progressive day. This is because, although the protocol selects cells down the neuronal lineage, the population is still very heterogeneous and a small proportion of cells either remain undifferentiated or differentiated down another lineage. Any lineage is potentially possible from embryonic stem cells, and cells which morphologically did not resemble neuronal phenotypes were regularly spotted in these cultures. It is also expected that there would be a small percentage of glial cells, as has been found before with CC9 cells using these protocols (Kirby et al., 2009). This all adds up to a variety of cells capable of dividing, producing undesirably large populations and reducing the level of control possible over the environment. In addition, high densities of cells increased the chances of cells clumping together into dense clusters that rise above the normal 2D surface structure required. If this occurred it was difficult to distinguish individual neuronal elements in the network under light microscope. More importantly, calcium imaging was severely compromised in raised clusters owing to the spread of cells beyond the focal plane of the optics used. Thus,

optimisation of neuronal density was a problematic but essential part of the methodology used here.

CC9's seeded at less than 300 cells/cm^2 had a low survival rate, forming few processes and floating off the surface a day after seeding, leaving very weakly connected small populations of cells. Above 900 cells/cm^2 the CC9's formed massive cell aggregates that were only weakly bound to the surface. Proliferation continued in these cultures, with far less neuronal cells distinguishable. More dead cells in the culture presumably also increased the secretion of unwanted factors into the medium, reducing the health of the remaining live cells.

In an attempt to improve the health of low density cultures, which were preferable because of the visibility of the network structure and maintenance of 2-D networks, cells were dispersed at low density in the well and an undisturbed ring of cells was carefully placed around the edge of the well to provide the benefits of a larger cell population on the secreted factors in the medium. These cells, however, were still not in contact with the centrally dispersed population, though there was significant migration of the cells and they could impinge on the network if care was not taken.

b-FGF, the factor used to maintain the nascent neurons during days 9-10 of the differentiation, was removed gradually over the two days by replacement of half the medium with a medium not containing b-FGF, instead of the sudden removal of bFGF. The resulting benefits could speculatively have been due to the earlier removal of b-FGF from the environment leading to a more dramatic slowing in proliferation, or potentially the more gradual change in b-FGF concentration causing less disruption to the cell environment.

Also, the concentration of B27, a supplement added to defined media to aid neuronal survival, was increased from 1.6% to 2%, which seemed to impact on the survival of neurons in these low density cultures.

As the lead-time to experiments was quite long from the thawing of each vial of cells an attempt was made to split the cells at day 2 of the -4/+4 protocol and treat half of them as day 0, in order to stagger one differentiation into two consecutive sets (thus allowing experiments to be staggered for this lot of cells). This would mean that one lot of the cells

was allowed to form embryoid bodies for 2 days longer than the standard -4/+4 protocol, before the addition of retinoic acid to select neuronal lineage. Unfortunately, the longer the cells were in embryoid body formations without lineage specification, the more aberrant the differentiations that were seen in the resulting seeded cultures, with many unidentified cell types and very few putative neurons able to form networks. The method may also have brought into question the developmental stage of neuronal differentiation, as although the neuronal lineage is not selected until day 4 of the protocol, differentiation is nevertheless underway spontaneously due to the removal of LIF. Thus, this part of the alternative protocols tried was not successful and could not be implemented.

Finally, there were many problems with bacterial and fungal infections in these cultures. These cells are particularly sensitive to such infections and they take hold quickly and easily, resulting in the inevitable death of the culture. The speed of the spread of infection was also quite phenomenal and in order to maintain an infection-free incubator, any infected cells had to be destroyed immediately to avoid spread throughout the cultures in the incubator, which could take hold within 24 hours. Cloudy media (and string-like substances floating in the media under light microscope) was indicative of fungal infections, and bacterial infections were visible by light microscope as well, in amongst the cells. Infection was most prominently an issue in the non-sterile lab in which the experiments took place and where organotypic cultures were also maintained; thus cultures were stored here only in the last few days leading to experiments. In order to combat the issue, penicillin-streptomycin-neomycin (PSN) was employed in low concentrations (0.05%) after the cells had been plated at 8 DIV. This addition to the media has been shown to combat infection highly effectively in cultures without adverse iatrogenic effects.

2.2 HCN/GFP ADULT HIPPOCAMPAL PROGENITOR CELL LINE PROTOCOLS

The HCN/GFP adult hippocampal progenitor cell (AHPC) line could be maintained more simply than the ESCs. Unlike the ESCs, they are already destined to differentiate into neuronal cells and experimental manipulations required to facilitate this process are therefore greatly simplified.

2.2.1 Growth Medium

Growth medium was used to maintain proliferating AHPCs and contained the following:

Ham’s F12/DME high glucose medium (Irvine Scientific 9052), consisting of (mg/L):

Sodium Chloride	7600
Potassium Chloride	224
Glucose (Dextrose)	1802
L-Alanine	9
L-Arginine HCl	211
L-Asparagine • H2O	15
L-Aspartic Acid	13
L-Cysteine HCl • H2O	35
L-Glutamic Acid	15
Glycine	8
L-Histidine HCl • H2O	21
L-Isoleucine	4
L-Leucine	13
L-Lysine HCl	37
L-Methionine	4
L-Phenylalanine	5
L-Proline	35
L-Serine	11
L-Threonine	12
L-Tryptophan	2
L-Tyrosine 2Na • 2H2O	8
L-Valine	12
Folic Acid	1
Inositol	18
Nicotinic Acid Amide	0.04
Phenol Red, Na salt	1.24
Riboflavin	0.04

Thiamine HCl	0.34
Hypoxanthine, 2 Na salt	5.4
Vitamin B-12	1.4
Pantothenic Acid, Ca salt	0.24
Pyruvic Acid, Na salt	110
Pyridoxine HCl	0.062
Thioctic Acid, D-L	0.206
Putrescine 2HCl	0.161
Thymidine	0.7
Cupric Sulfate	0.002
Ferrous Sulfate	0.8
Zinc Sulfate	0.863
d-Biotin	0.007
Sodium Phosphate, dibasic	142
Calcium Chloride, anhyd.	33.3
Magnesium Chloride, anhyd.	57.14
Choline Chloride	14
Sodium Bicarbonate	1176

with 1% l-glutamine, 0.5% (volume) N-2, 0.1% (volume) PSN and 20ng/ml bFGF (previously described in sections 2.1.1.1 and 2.1.1.2).

Freezing Medium was composed of this growth medium with 10% DMSO, similarly to the medium described in section 2.1.1.4 above for ESCs.

2.2.2 Thawing Protocol

AHPCs, stored at -80°C in 1ml freezing medium (see above in 2.2.1), were thawed by holding the cryovial in a 37°C water bath until 50% thawed. Then 1ml warmed growth medium is added drop-wise into the cryovial to stimulate the cells before being topped up and centrifuged to remove the DMSO-containing medium. The cell pellet is thoroughly

triturated with warmed growth medium and the single-cell dispersion added to a coated T25 culture flask (coating procedure detailed below) and incubated.

2.2.3 Protocol to maintain HCN/GFP cells in undifferentiated state

These AHPCs remained undifferentiated and proliferating, at a far slower rate than the ESCs. Their medium was changed every 2-3 days and it could be between 3 and 5 days before they needed passaging due to reaching a full confluence in the flask.

To passage, the cells were bathed in 2.5% trypsin in growth medium until the cells could be seen to be dislodged from the surface. The trypsin was then removed through two rinses with growth medium and centrifugation (as this is a defined medium with no serum to quench the action of the trypsin). Cells were then added to a coated flask and incubated.

2.2.4 Protocol to differentiate HCN/GFP cells

The cells were allowed to become 50-60% confluent in the flask and then the concentration of b-FGF in the medium was reduced to 0.2ng/ml. The medium was then replaced every 3-4 days. As these are neuronal progenitor cells, their lineage is already defined and no neuronal induction step was required (as in the case of the ESCs).

2.2.5 Poly-L-Orinthine (PLO)/laminin coating protocol

The substrate was covered with PLO (10% solution in sterile DH_2O) for 24 hours and washed three times with sterile DH_2O. The PLO-coated surface was then covered with laminin (0.2% solution in PBS) and incubated at 37°C for 24 hours. The coated surface was washed three times with PBS directly before seeding cells, with the surface never being allowed to dry. Pre-coated substrates could be frozen at -20°C for 3 months until needed. Examples of undifferentiated and differentiated AHPCs are shown in Figure 2.2.

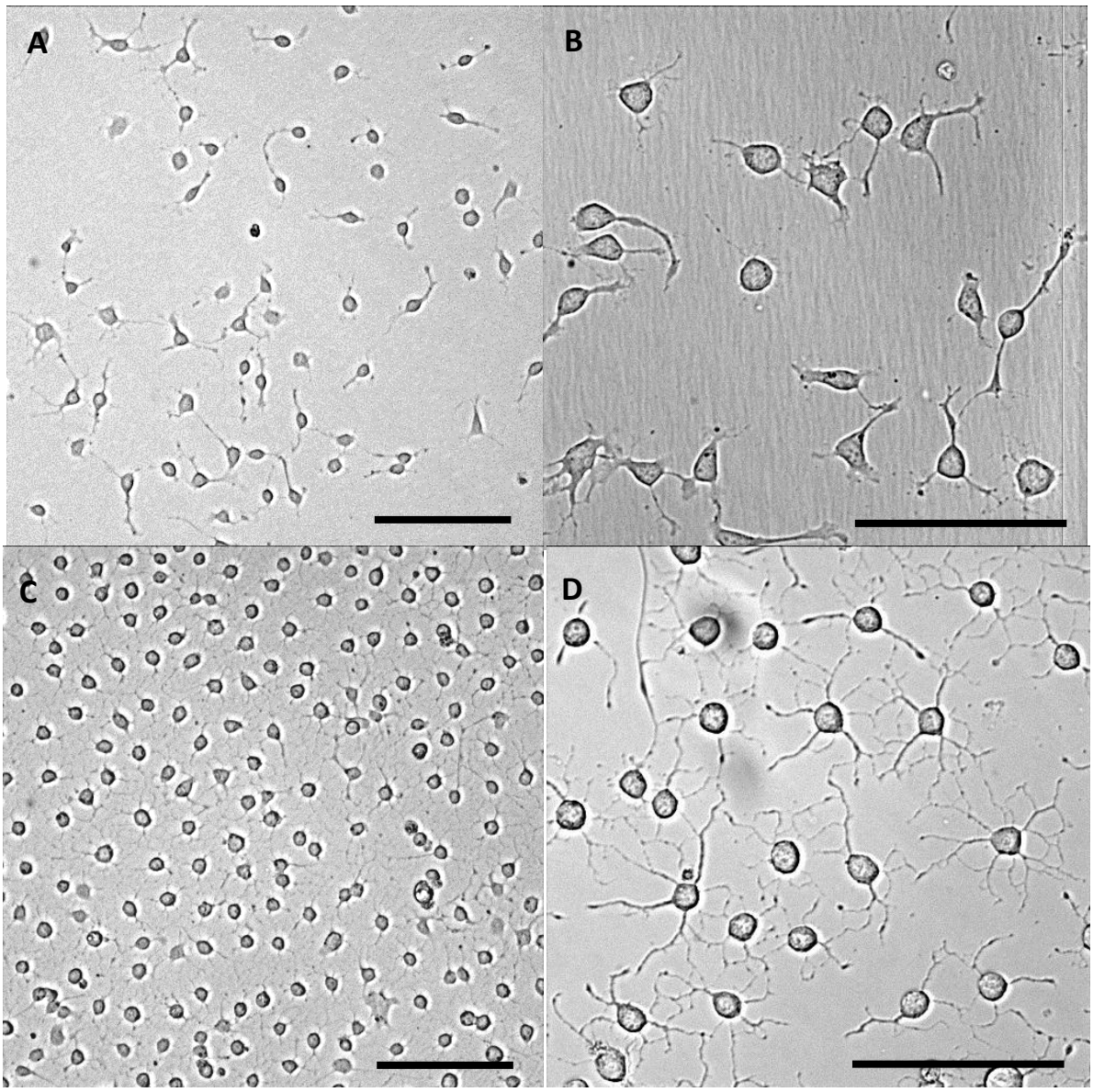

Figure 2.2 – Developmental stages of HCN/GFPs. A and B) Undifferentiated cells at two different magnifications. The spacing of the cells can be seen to be radically different to the CC9s, with cells preferring to space themselves out over the surface (A). Distinct processes can be distinguished at this stage, but they are few and short with a small number of branches (B). **C and D)** In contrast, as early as 2 days differentiated, these cells, remaining well spaced from each other (C), show a rich network of processes that are longer and more branched than for the undifferentiated state (D). Scalebar = 100µm.

2.2.6 ARTIFICIAL CEREBROSPINAL FLUID (ACSF)

For all experiments the cells were perfused with oxygenated (carbogen (95% O_2 and 5% CO_2)) artificial cerebrospinal fluid (aCSF) at a rate of 1.5 ml per minute and a temperature of 32°C pumped through a chamber holding approximately 1ml of aCSF in which the live cell cultures were situated. The following formula was used for aCSF, which has a high calcium content and no magnesium to encourage excitability of the network: 118mM NaCl, 3mM KCl, 1mM NaH_2PO4 x $2H_2O$, 25mM $NaHCO_3$, 10mM glucose and 4mM $CaCl_2$.

2.3 CALCIUM IMAGING PROTOCOLS

2.3.1 Oregon Green BAPTA-1 Protocol

10µg Oregon Green 488 BAPTA-1 (OBB-1) AM (Invitrogen) was dissolved in 2µl DMSO with 0.025% pluronic acid to aid cell permeabilization and reduce compartmentalization. This was added to 2ml of 4:1 differentiation medium and incubated with the differentiated CC9 cells at 37°C, 5% CO_2 for 45 mins until enough dye had entered the cells. The culture was then washed 3 times with 4:1 medium and incubated for a further 10 minutes before placing on the imaging stage. To do this, the coverslip was removed from the 6-well plate and placed into the perfusion cell on the imaging stage, which was heated to 32°C. The cells were perfused with oxygenated aCSF and allowed to settle for 30 minutes. Cells on coverslips were generally on the stage for between 2 and 3 hours during the course of a single experiment.

2.3.2 Equipment for calcium imaging data collection

A monochromator (Optoscan, Cairn Research) was set to provide excitation light at 495nm and a green emission filter (510nm) was used between culture and camera while acquiring data. The fluorescence bandwidth was set to 14nm, above which background fluorescence was high and below which the signal was not so clearly detectable. Image stacks were acquired at 256x256 pixels for 6000 frames at 10 FPS (exposure time of 80ms) using a digital camera (QuantEM 512SC). The acquisition software used was MetaMorph (Molecular Devices). Bright field images were also taken using this camera, though at a higher resolution (512x512 pixels).

For the controlled glutamate stimulation experiment described in Chapter 3, section 3.3.8, an upright Zeiss Axioskop FS microscope with epifluorescence illumination (using standard fluorescein filter block) was used. Images were collected through a Hamamatsu camera, which connected to a computer running IPlab software. In this case, glutamate was applied using a picospritzer pressure application system through patch pipettes ~30µm from the cells with the pressure and timing of the glutamate pulses controlled by a Master 8 Pulse Stimulator (A.M.P.I. Jerusalem, Israel).

2.4 DATA ANALYSIS – CALCIUM IMAGING

2.4.1 Summary

The calcium imaging data was processed initially in ImageJ (National Institutes of Health) to clean up the data and remove background noise. The steps to achieve this are summarized below and explained in detail later:

- Two-stage background subtraction.
- Kalman stack filter and removal of outliers.

This pre-processing stage was followed by a series of processing steps in MATLAB using custom-designed scripts. The stages could be summarized as follows:

- Identify and label active regions (where changes in intracellular calcium above a threshold could be detected).
- Average the fluorescence intensity across a whole region for each frame to create a set of traces for each region showing change in fluorescence intensity with time.
- Eliminate regions with a wandering baseline of activity that do not exhibit calcium transients.
- Locate each peak, with its intensity level, onset time and full width half maximum for each region.

This information was used to form the basis of the analysis, also performed in MATLAB using custom scripts, summarized as follows and explained in detail in the results sections:

- Cell clustering and movement.
- Activity rates, full width half maximums, amplitudes and inter-transient intervals.
- Neuronal avalanche sizes and lifetimes.
- Cross-correlograms and coincidence indices.

Data streams containing population-wide events of synchronous activity were further processed to determine the following:

- The time-course and recruitment profile of each synchronous event .
- The order in which regions were recruited to each synchronous event.
- The probability of each region being a ‘hub’ neuron for the synchronous event.

All figures representing this data were also created in MATLAB. A more detailed description on some more generally applicable aspects of the above methods is now provided, and details of the specific analyses used are given in each results section they are used in (Chapters 3 – 6).

2.4.2 Pre-processing in ImageJ

The pre-processing in ImageJ was implemented as a way to better distinguish active regions from regions that had constant high calcium signal and look at the dynamics of the change in fluorescence of those regions as a measure of activity in the network. It was also important to establish that processing methods did not pick up 'false' positives in calcium changes from non-cellular regions of interest (Figure 2.3). It should be noted that the following data pre-processing and processing steps were taken to increase signal to noise ratio for calcium transients . That relatively rapid, transient changes in calcium represented the activity of a neuron or cluster of neurons in each region of interest is an assumption. This approach and assumption has been effectively used before many times (see general introduction and introduction to chapter 3). However, it is not possible with such data handling to directly relate the absolute amplitude of processed calcium transients to absolute changes in intracellular calcium concentration. Relative comparisons across different regions and different developmental stages in any given culture have still been used.

This was done by subtracting the background from each image individually and then subtracting an average of the initial five images from all following images. A region active in the first 5 frames will therefore be likely to be missed, though this is negligible as this period only accounts for 1 second of the 10 minute recording period. The initial background subtraction removed the effect of an unstable fluctuation of overall light intensity, and possible dye bleaching with repeated light exposure, during data acquisition and allowed all the pixel intensities to be viewed relative to a zero datum to every pixel. Subtracting the initial 5 images from the other images in the stack removed the background fluorescence emitted due to ambient calcium levels in the cells, making it far easier to distinguish active cells in the stack (Figure 2.3). To improve the clarity of this image, improving the signal to noise ratio to better distinguish active cells with lower fluorescence intensities, a Kalman

stack filter was used for each pixel through the length of the stack with the outliers in each image subsequently removed.

There was significant variation in the general fluorescence intensity of each stack, the signal to noise ratio and clarity between cells, even when consistent protocols were adhered to for staining and image acquisition. Image stacks with a weaker signal were more in need of the pre-processing that other stacks, but all stacks underwent the same pre-processing to remain consistent.

The ImageJ code for this entire process is given in the Appendix. The traces in Figure 2.3 show an example of the fluorescence intensity of a region before and after this processing, demonstrating how the information from calcium transients is affected by this method. The traces in Figure 2.4 show examples of a region where there are no cells, and a region where the cell is inactive throughout the recording. In both examples, traces before and after the pre-processing have been shown.

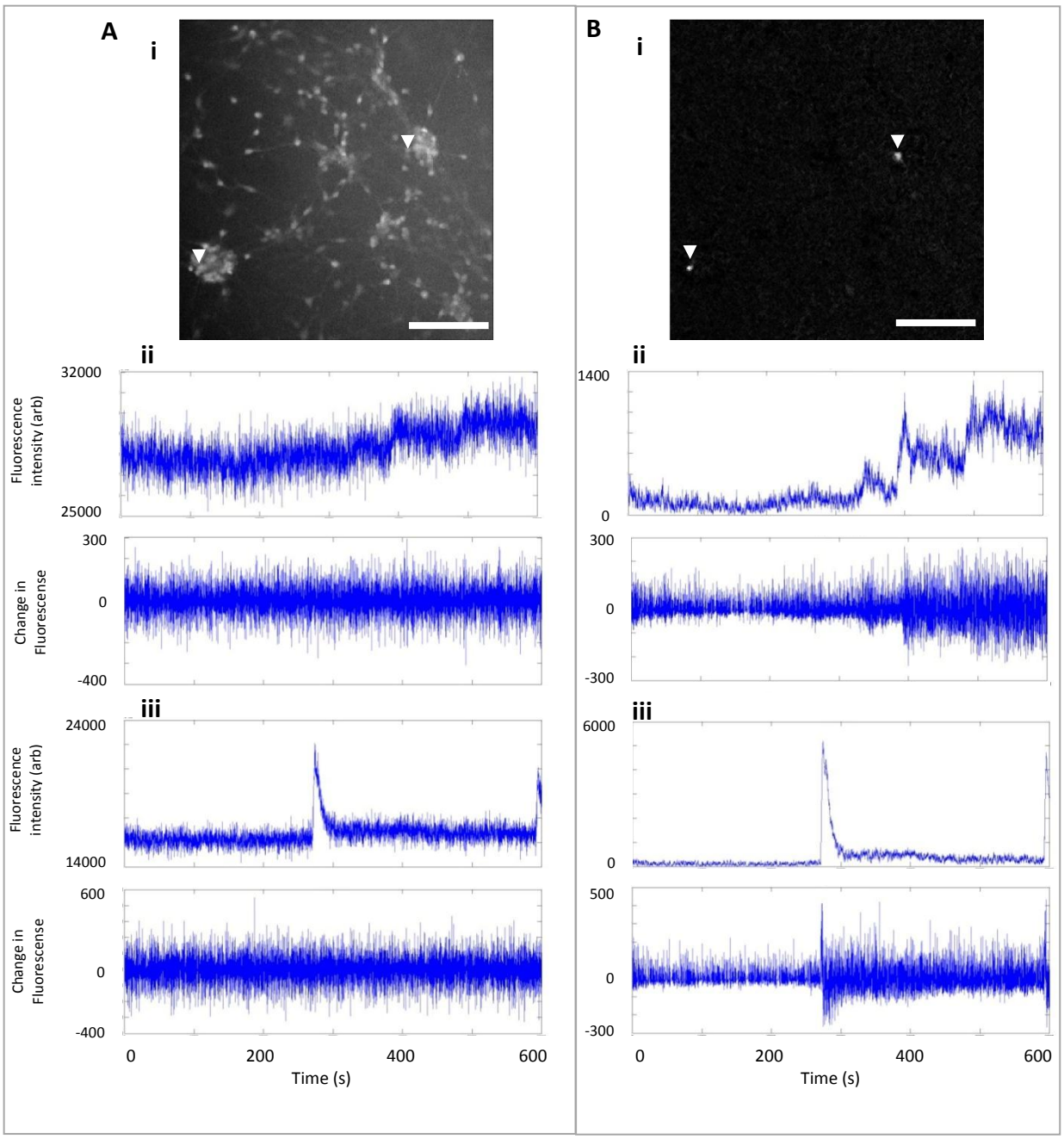

Figure 2.3 – Images and traces demonstrating the effect of pre-processing image stacks in ImageJ. A) i) One frame of the raw intensity data acquired in MetaMorph with the corresponding traces from two selected pixels (shown in 'i' with white arrows) in 'ii' and 'iii'. The upper traces in 'ii and 'iii' show intensity across all frames, and the lower traces in 'ii' and 'iii' show the differentiation of the signal in the upper trace. **B)** i) Once the image has been pre-processed through background subtraction and Kalman stack filtering with the outliers being removed the image is far starker and only shows those regions that display a change in intracellular calcium (i.e. in the single frame displayed here, two cells are active). The same two pixels (again, shown in 'ii' and 'iii' respectively) have a much cleaner signal and higher signal to noise ratio (as in 'A ii and iii', the upper traces show the intensity levels and the lower traces show the differentiation of the upper trace. Scalebar = 100µm.

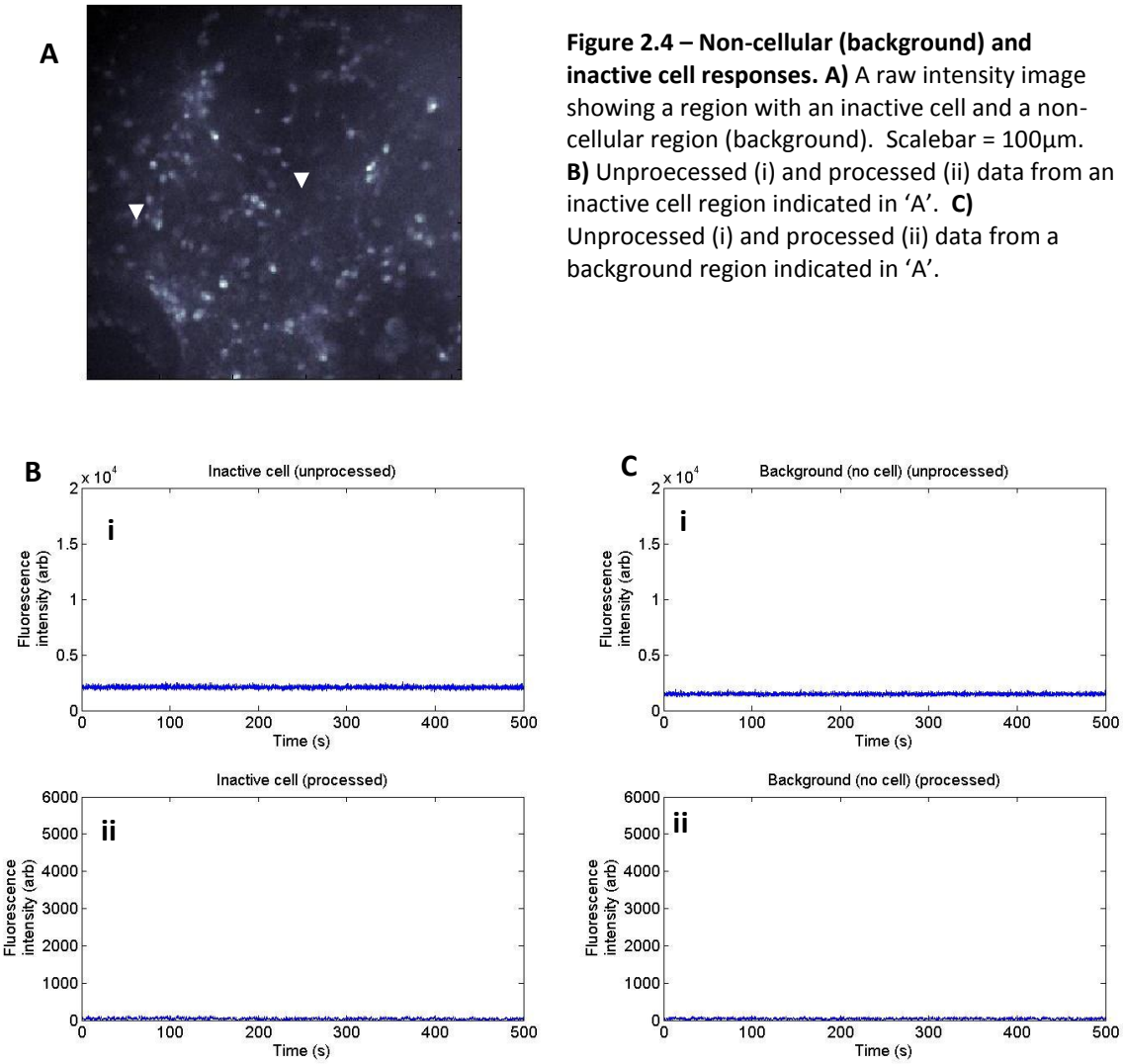

Figure 2.4 – Non-cellular (background) and inactive cell responses. A) A raw intensity image showing a region with an inactive cell and a non-cellular region (background). Scalebar = 100µm. **B)** Unproecessed (i) and processed (ii) data from an inactive cell region indicated in 'A'. **C)** Unprocessed (i) and processed (ii) data from a background region indicated in 'A'.

2.4.3 MATLAB processing

The two main methods tested for identifying regions of interest attempted were through automated thresholding and manual selection. Manually selecting regions was done in ImageJ by selecting the centre of all the active regions in the stack and importing those points into MATLAB. These pixel locations acted as the centroids for active regions and a region map was created with each region measuring three pixels squared – always within the boundary of the fluorescence activity of the cell (Figure 2.5). One of the advantages of this method was that as each specified region had the same area and covered the most active part of the cell's firing area, the intensity amplitude from one region to another could be more directly compared. In contrast, automated thresholding produced regions of various sizes that covered different ranges of the cell's active area, cell to cell. Averaging the intensity over these regions can potentially misrepresent the amplitude of the signal. It

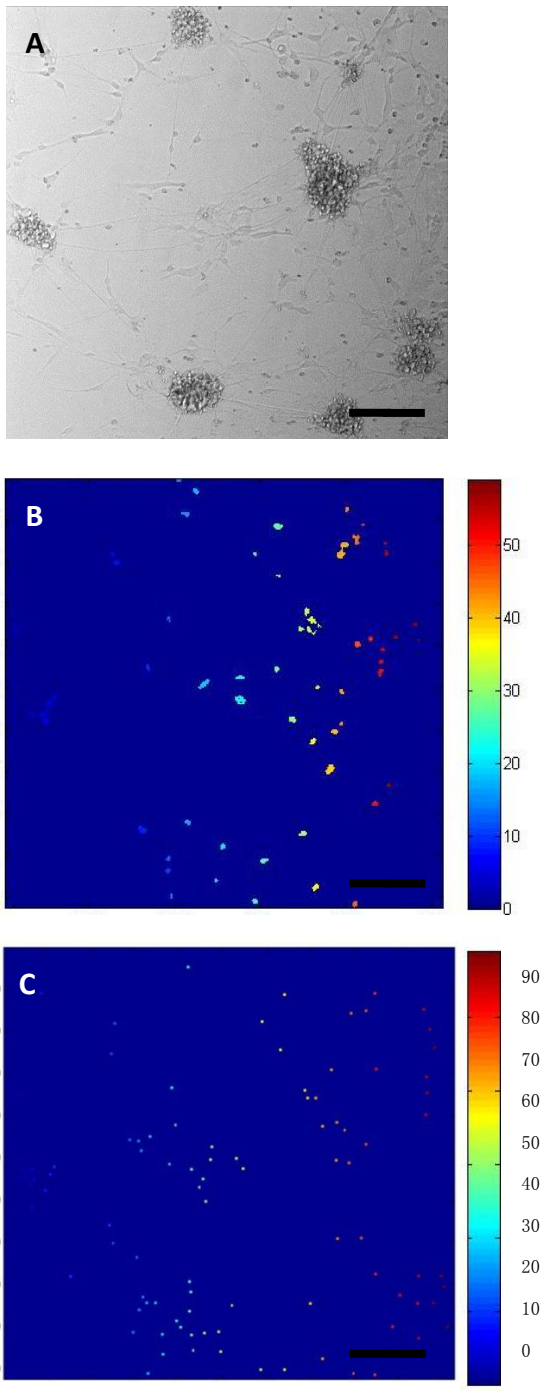

Figure 2.5 Difference between the manual selection of regions and automated thresholding method for specifying regions. **A)** Bright-field image of a network (Scalebar = 100µm) and **B)** the corresponding set of regions determined using a custom script in MATLAB based on thresholding the intensity. **C)** the corresponding set of regions specified manually in ImageJ. There is a large redundancy of regions created when using this laborious manual technique, and most are eliminated when searching for peaks. Also, cell movement from one recording to the next (i.e. over a period of hours) means that regions cannot be recycled in future recordings anyway (a hoped original advantage to this method).

was originally thought that another advantage of the manual method over automated thresholding was that regions could be manually selected over a range of stacks (e.g. before and after bath-application of bicuculline) and compared directly. Interestingly, there was significant movement of the cells during any set of recordings, coupled with the fact that most regions were only active in one recording, leading to many redundant regions.

The second method was thresholding. This was most effective when based on the range of intensity. This was done by finding the range of each pixel across the whole image stack.

The threshold for each stack was selected by hand to optimise the region map created and ensure there that all major active regions were included, and inactive regions, with a lower range of intensity were excluded. In this sense, events were found to be well above the noise level (at minimum, 3*rms). When using thresholding, there was a tendency for close neighbouring regions to clump together, forming one large region covering a group of cells. The blurring together of regions could be altered by hand to a certain extent, reducing the tendency for clumped regions to misrepresent the intensity and rate of activity of cells. The size of the regions produced with this method were equivalent to the approximate size of a single neuron (these cells had typical diameters of 10-20µm), when situated over single cells.

In each stack there are some areas where the baseline fluorescence intensity steadily increased throughout acquisition, or cells that have a wandering base-line of activity with completely different temporal profiles to the expected neuronal calcium transients. When looking at the timeseries data from each pixel, these wandering regions can be eliminated with a highpass filter. A frequency power spectrum of one of these stacks results in a sharp exponential with no significant peaks that can be found repeated across datasets. The calcium transients consist mainly of low frequencies features (less than 2.5Hz, see section 1.4.4). The highpass filter was therefore designed to exclude only the extreme low frequencies present (below 0.05Hz). This highpass filter was applied to the identified regions in order to eliminate those with a wandering base-line. Once this process was complete, each transient for each region could be identified, along with its characteristics. The code for this process is provided in the Appendix, one script for the original method for filtering the entire stack, and the updated method where filtering was effectively employed after initial region identification.

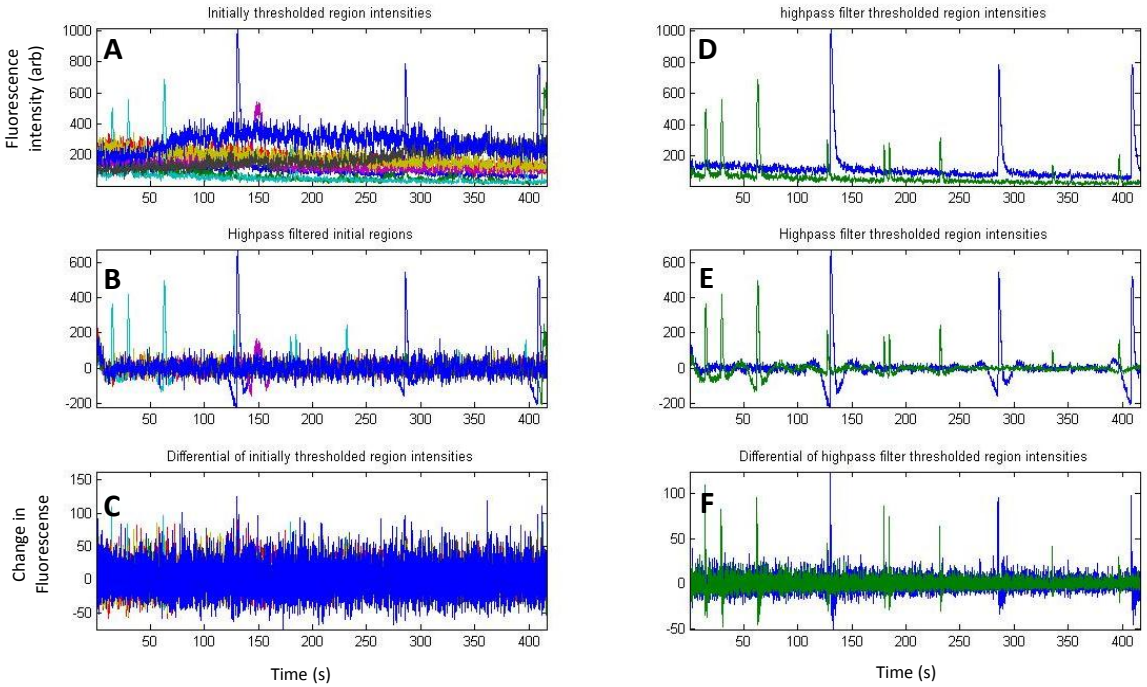

Figure 2.6 – Demonstration of the use of highpass filtering to eliminate wandering regions that remain after the initial thresholding to identify active regions. A) The average intensity of each region from an example 10 minute recording created by intensity thresholding. A number of regions have been identified to exceed the threshold during the recording, but not all display calcium transients. **B)** Highpass filtered version of 'A'. **C)** Differential of 'A'. **D)** The regions remaining after thresholding a second time based on the highpass filtered version. Only two regions remain after eliminating the wandering regions that exhibit clear calcium transients. **E)** Highpass filtered version of D. **F)** Differential of D.

CHAPTER 3: CC9 NETWORK ARCHITECTURE AND EVOKED ACTIVITY

3.1 SUMMARY

The goal of the first stage of this project was to establish the capacity for CNT-patterned substrates to direct the structural organization of nascent neuronal networks (as has been shown to be possible with mature, dissociated cells), and to look at the spatial activation of cells within these patterned nascent networks.

Previously, CC9's have been shown to exhibit normal firing characteristics upon stimulation using patch clamping (Kirby et al., 2009, Trevelyan et al., 2010). Patch clamping was an effective method for exploring in detail the activity of single or small numbers of cells, but in order to examine network characteristics, data must be gathered from a large population of cells simultaneously and multiple techniques were employed to attempt to do this.

Attempts were made to gather extracellular signals from CC9s differentiated into neurons using commercial multi-electrode arrays (MEAs) that are used as standard on neuronal cultures to examine spiking activity and network communication. Alongside this, attempts were made to manipulate the physical architecture of the network using arrays of carbon nanotube islands (CNTs) with the intention of examining the activity output of networks of nascent neurons, using MEAs, whose architecture has been dictated (patterned networks). This was to be compared with self-assembled networks in random configurations determined only by the 'internal' interactions between the nascent neurons arising from the culture (un-patterned networks). The aims of this chapter are outlined below:

To see whether growing CC9s on CNT arrays can determine structural properties of resulting nascent networks and compare any structural patterns in CC9's to those seen using primary neurons (hippocampal progenitor cells).

To see whether CC9's grown on electrode arrays can be activated in a spatially specific manner by the arrays themselves.

The main findings of this chapter were as follows:

- CNT-patterned substrates could be successfully utilised to structurally define the CC9-derived neuronal networks as they migrated and differentiated. The success of such patterning was dependent on the absence of further surface coating.
- HCN/GFP neuronal progenitors did not show the same capacity for patterning using this technique, not displaying the same migratory characteristics as the embryonic stem cells.
- Extracellular electrophysiological signals (units) could not be detected robustly enough for network analysis using MEAs, either spontaneously or through electrical stimulation.
- Stimulation of CC9s did not evoke detectable extracellular signals, but did evoke large, readily quantifiable calcium transients in cells contacting the stimulation electrode. These transients could also be detected up to 138µm from the point of stimulation, initially radiating outwards before producing a seemingly random spatiotemporal pattern of activation.
- Exogenously applied glutamate evoked time-locked calcium transient activity with fast onset and slower decline showing similar characteristics to those previously recorded accompanying action potential burst discharges elicited by glutamate (see Figure 1.10 C in Chapter 1).

Although CC9s could be patterned on CNT arrays, the lack of evidence for detectable unit activity and the opacity of the CNT arrays themselves led to the decision to use self-organized (un-patterned) networks of CC9-derived neurons on glass substrates to examine the development of network activity and phenomena using calcium imaging, due to its success in demonstrating the presence of network activity.

3.2 INTRODUCTION

3.2.1 Network Formation on Carbon Nanotube Patterned Surfaces

3.2.1.1 Neuronal clustering behaviour

The capacity for cells to form clustered networks on pre-defined substrates has already been shown in, for instance, micro-drop patterning studies (Macis et al., 2007). Neurons were shown to bridge non-adhesive gaps with thick bundles of neurites to create sub-clusters of networks that could be aligned with an MEA. CNTs are a good environment for

such patterning because neuronal cells (as explained in detail in the General Introduction) adhere well to CNT surfaces, with neuronal processes extending and latching directly onto the nano-rough surfaces of the CNT electrodes with no further patterning or alignment required. If MEA electrode construction involves such CNTs, the electrodes themselves have been shown to increase signal to noise ratio with time as cells integrate with the CNT arrays (Gabay et al., 2007b, Shoval et al., 2009) .

Dissociated cortical neurons have been shown to self-organise into clustered networks on cell-adhesive islands patterned onto a non-adhesive substrate (Sorkin et al., 2006). The cells settle randomly on the surface when seeded, but gradually migrate, eventually adhering to the islands. As they migrate and neuritic connections are formed between cells, the neurites fasciculate and form thick bundles stretching between the separating islands of cells. The result is that the cell bodies remain on the adhesive islands, leaving the neuritic bundles free of cell bodies. The same behaviour can be observed when the adhesive patches are CNT electrodes on silicon or quartz chips (Gabay et al., 2007a, Gabay et al., 2005a, Gabay et al., 2005b). This method of forming patterned networks, due to the cells' connectivity and migratory behaviour, eliminates the need for high-resolution patterning techniques and has been proven to be effective for neurons cultured from various animal systems (Segev et al., 2003, Shefi et al., 2004).

Sub-clustering of neurons, with the cell bodies attached to the electrodes and neurites bridging the gaps between clusters in pre-defined geometries, may provide insight into any relationship between the physical structure of a network (the spatial location of neurons and the pattern of connectivity between them) and the complex network activity resulting from such specific architectures. To date the subject of structure/function relationships in neuronal networks is contentious and much work needs to be done (Panzeri et al., 2004). Thus far, electrophysiological studies of primary, adult, neuronal network cultures show that they develop spontaneous activity and produce typical extracellular signals (seen as a waveform representing the first derivative of the intracellular action potential lasting ~5ms) (Gabay et al., 2007a).

The mechanisms governing this clustering behaviour, and its effect on network function, are still being elucidated. Undoubtedly this structural patterning behaviour may correspond to

a range of factors including cell-cell adhesion, cell-substrate adhesion, migration, neuritic fasciculation and neuritic tension. Starting with neural adhesion molecules (NCAMs) (Rutishauser et al., 1978), a variety of molecular families have been identified as playing a significant role in mediating neuritic fasciculation.

3.2.1.2 Neuritic tension

Migrating neural cells tend to aggregate into clusters over time, particularly when cell-cell adhesions are favoured over cell-substrate adhesions, as with the migration of neurons along chemical gradients and glial processes (Ayali et al., 2002, Distasi et al., 2002). The tensions along axons and dendrites are powerful enough to overcome the cell-substrate attraction and pull cells towards each other. This leads to an apparent overall structural reduction as the network develops through the fasciculation of neurites as they attract to each other and bind (thus one thick branch is actually a rope of many interwoven neurites). This apparent structural reduction is accompanied by a fall in the neurite production, as demonstrated within locust frontal ganglia. The dissociated cells were cultured on glass and isolated cells were compared with networked cells. The isolated neurons increased neurite formation by 50% over day 2 and 3, which contrasted with the connected neurons, which showed a 50% decrease in the same period (Ayali et al., 2002). Similarly, mechanical forces, such as tensile forces in neurites have been explored for their effect on the development of network geometries (Chada et al., 1997, Shefi et al., 2004, Shefi et al., 2005).

Axonal branching has been shown to be activity dependent (Hua et al., 2005) as has synapse elimination through competition between inputs (Rutishauser and Jessell, 1988, Thompson, 1985). Established mechanical tensions along neurites in a developing network were also correlated with process elimination by Anava (Anava et al., 2009) and consequently affect synaptogenesis and stabilisation of neural networks. Interestingly, the expression of presynaptic proteins was only expressed once the neurite had adhered to the CNT island. In the study performed by Alsina (Alsina et al., 2001), disassembly of synapses preceded the elimination of the branch. The same study also intimated that synapses could feedback to affect the formation of new neuritic arbours.

Finally, the elastic modulus of the substrate has also been shown to affect neural stem cell behaviour (Saha et al., 2008). Adult hippocampal cells cultured and differentiated on coated

hydrogel substrates displayed differing behaviour when the elastic modulus of the hydrogel was modified. Softer (100-500Pa) and harder (1000-10000Pa) hydrogels encouraged neuronal and glial populations respectively. Below 10Pa there was a reduction in cell spreading, proliferation and differentiation. This once again reveals the inherent abilities of cells to detect and react to forces in their environment.

3.2.1.3 Migration and Adhesion

Migration and cell adhesion are intrinsically linked and both are fundamental to the understanding of neural network formation. Many studies are currently trying to elucidate the migration habits of cells and the mechanisms that underlie that migration. *In vivo*, cells migrate along distinct pathways to locate themselves appropriately in the complex architecture of the brain from the development of the embryo through adulthood with the renewal of cells originating in, to name a few, the hippocampus, the olfactory bulb and the SVZ. In addition, a range of chemical cues and target second messenger pathways have been shown to be critical for the normal development of layers in neocortex (Rice and Curran, 2001, Takeuchi et al., 2007). The particular tools utilized by the cells for such migratory behaviour rely on chemical, mechanical and topographical cues provided by the cells' environment (Wong et al., 2004). These cues are numerous and complex and a range of cell types respond differently to them. In addition, glial cells contribute greatly to the migratory behaviour of neural cells *in vitro*. Dissociated chick ciliary ganglia moved randomly unless under the influence of a nearby glial cell, or undergoing migration along neurites (Distasi et al., 2002). In organotypic cultures of mesencephalic structures, longer range axonal outgrowth and migration was critically dependent on astrocytic glial cells (Berglöf et al., 2007).

Cell adhesion is affected by interactions occurring at the external cell surface with its immediate micro- and nano-environment, such as through focal adhesions. Specifically, proteins in the cell membrane, principally transmembrane proteins called integrins, interact with elements of the extracellular matrix (ECM). The cell membrane proteins are attracted to ECM components that have adsorbed to the substrate (Owen et al., 2005), a process that is crucial for neuronal development (Sun et al., 2008). Some of the key components in the ECM that interact with cell membrane proteins contributing to adhesion are laminin, fibronectin, vitronectin, collagen and elastin. Laminin and fibronectin are secreted by

neuronal cells and are readily available in the cells' microenvironment. Integrins in the cell membrane interact, among other things, with the arginine–glycine–aspartic (RGD) moiety found in proteins like laminin, instigating signalling cascades with the cell.

3.2.2 Neuronal Network Activity and Multi-electrode Arrays

The measurement of neuronal activity on a network-wide scale is commonly achieved by using multi-electrode arrays (MEAs). An MEA is essentially a micro-machined chip onto which microelectrodes have been patterned. A variety of materials are commercially available for both the electrodes and the substrate depending on the intended use. Cells have been cultured onto MEAs for *in vitro* (Li et al., 2007, Martinoia et al., 2005, Cohen et al., 2006), and MEAs have been implanted for *in vivo* (Cheung, 2007, Olsson and Wise, 2005) eletrophysiological measurements of both individual neurons and network activity.

3.2.2.1 Spontaneous Network Activity

MEAs are now used commonly in neuroscience for looking at network activity in slice preparations, explants or cultures. Dissociated cultures of cortical neurons have successfully been maintained for months for use in repeated experiments (Ban et al., 2007, Chiappalone et al., 2006, Li et al., 2007). The long-term maintenance of differentiated neurons from embryonic stem cells is more difficult to achieve with some cultures only surviving a matter of weeks (see Chapter 2). Here, an overview of the current understanding of spontaneous activity arising in dissociated and differentiated neuronal cultures on MEAs is given, emphasizing the contrast in activity at different developmental stages.

When seeding mature, dissociated neurons the dissociation process destroys neuronal connections and neuronal processes. Once seeded, although neurites can first be seen after only hours of plating (Banker and Cowan, 1977, Valor et al., 2007), it takes approximately 4 days for the cells to fully extend their new processes and create new functional synaptic connections. It is at this point that the first electrophysiological signals are detectable on the MEA. There is clear path of development in the spiking activity in such networks, as was demonstrated by Chiappolone (Chiappalone et al., 2006, van Pelt et al., 2004) with dissociated rat cortical neurons. After 1 week the activity was sparse and uncorrelated. At 2 weeks the culture was producing widely-spaced spontaneous bursts with almost all electrodes involved in each burst. In the three weeks following this, the burst duration and

interburst distances became gradually smaller and the massive increase in firing rate seen in the first few weeks dropped off considerably. Comparing this pattern of activity development to the connectivity in the network, Muramoto (1993) (Muramoto et al., 1993) found that the number of synapses in these networks increased significantly up to 28 DIV; meanwhile the number of synapses per neuron fell. Also, the number of synapses could be closely correlated to the frequency of synchronous calcium transient activity in the network. Valor (Valor et al., 2007) used primary cultures from the embryonic rat hippocampus to examine gene expression relating to synaptogenesis and integrating that information with MEA activity recordings. At 4 DIV, both presynaptic and postsynaptic markers were clustered together, and the first MEA activity appeared at 4–5 DIV, in line with the assembly of synapses, as visualized with immunostaining. This activity was only over 10% of 59 electrodes. The development profile showed less than 1% of the spike activity seen at 4 DIV (on less than 5 electrodes) compared to that seen at 24DIV. By 20 DIV this activity started to plateau.

Valor's 2007 study (Valor et al., 2007) used dissociated cells from an E18 embryonic hippocampus. Another study using dissociated cortical neurons from an E17 rat embryo demonstrated the same line of development for electrophysiological activity. The culturing of differentiated neurons from embryonic stem cells onto MEAs has also resulted in the generation of spontaneous *synchronized* neuronal spiking when maintained for 5–6 weeks (Illes et al., 2007). Extremely dense networks of cells were used in this study (15000 cell/mm^2), and the appearance of spontaneous activity occurred between 7–14 days after initiation of the differentiation process (although determining a comparative stage of development of these cells is difficult). The activity at this early stage was sparse and non-synchronous and less than 10% of the electrodes were active on average. Synchronous bursting appeared on half of the electrodes by day 28, which increased in frequency to day 41. Two types of burst pattern could be discerned: dispersed, constant-amplitude spiking or a two-phase burst with high-frequency spikes, initially increasing in amplitude, then decreasing in amplitude.

3.2.2.2 Network Stimulation

MEAs are used for both recording and stimulating neuronal systems. Electrical stimulation can be used to induce changes in network firing patterns and increase the responsiveness of neurons (Jimbo et al., 1998, Li et al., 2007, Pizzi et al., 2007).

Local tetanic stimulation was used in dissociated adult rat cortical neurons cultured on MEAs in order to strengthen synchronous firing, demonstrating long-term potentiation through electrical stimulation (Jimbo et al., 1998). Similarly, the activity from dissociated hippocampal neurons of E18 rats developed different spatiotemporal characteristics when influenced by paired stimulation through two adjacent electrodes on the array. Increased activity over a wider area of the network was distinguishable in cultures following the stimulation (Li et al., 2007). Electrode arrays were also used to provide patterned artificial neural network inputs (through multiple electrodes) to real cultures of neuronal cells from human embryos in order to observe the spatiotemporal organisation of activity during and after stimulation. The stimulus was found to permanently modify the output of the network, showing an increase in the information processing capacity of the network (Pizzi et al., 2007).

3.2.2.3 Electrode Materials

A variety of electrode materials is available commercially for use in MEA systems, and new materials are constantly being explored to provide suitable recording and stimulating surfaces for the attachment of cells. The way that cells interact with a substrate, as was discussed in the General Introduction, can be used to exploit selective adhesion and network architecture. Common electrode materials include indium tin oxide (ITO), platinum-black, titanium nitride and gold. Platinum-black is a porous material with a rough nanotopographic surface suited well to extracellular recording as the increased surface area can improve electrical properties of the electrode and the cell contact area. Indium tin oxide electrodes have the advantage of being translucent, to allow clear imaging of the sample at the position of the electrodes. This is particularly useful for fluorescence studies. CNTs, with their unique properties, could provide an interesting substrate both mechanically and electrically.

3.2.2.4 Carbon Nanotubes as a Cell Substrate

In response to the discovery that nanotopography plays a significant role in the reaction of a cell to its environment (Curtis and Wilkinson, 1998), biomaterials research has become

more focussed on finding nanomaterials for tissue engineering constructs, implants and electrode interfaces. One material of particular interest in this area is CNTs. A brief description of this interesting material is given below, followed by a summary of some interesting studies into the effect of CNTs on a variety of cells.

CNTs are of great interest as an emerging biomaterial because of their electrical, thermal and mechanical properties. They are electrically conductive, have a large surface area to volume ratio, are amenable to the attachment of functional groups either along the length or at the ends and they have high tensile strength.

First discovered by Iijima (Iijima, 1991), carbon nanotubes appear as rolled sheets of graphene. The ends can be open or closed by fullerene hemispheres and the tubes have a large length to diameter ratio. These single-walled versions (SWCNTs) can have diameters ranging from 0.7nm – 2nm and can measure millimetres in length (Giugliano et al., 2008). Multiple nanotubes arrange concentrically in what are termed multi-walled carbon nanotubes (MWCNTs). The separation between each concentric tube is 0.34nm, diameters of 2nm – 100nm and lengths measuring tens of microns. Different processing techniques allow for the manufacture of CNTs with quite explicit specifications. By varying the lattice chiral vector (Figure 3.1), the properties of the nanotubes are also altered.

The various effects of CNTs on cells are still being catalogued. CNTs can be used to decrease the activity of astrocytes that cause glial scarring. Astrocytes were cultured on nanofibrous materials where the dimensions of the nanofibres were varied (McKenzie et al., 2004). The astrocytes did not adhere to fibres that had small diameters and high surface energies. Many such studies have looked at how different cell types interact with CNTs (Mwenifumbo et al., 2007). For instance, dissociated hippocampal neurons cultured onto MWCNTs underwent morphological and electrophysiological analysis with immunocytochemistry and patch clamping techniques being utilized (Lovat et al., 2005). After 8 days in culture, neurons on CNT substrates showed a 6-fold increase of spontaneous post synaptic currents and a similar increase is evident when looking at the frequency of action potentials. These cells did not show any morphological differences, or any difference in number of cells or neurites when compared with cells grown on coated glass control substrates. Indeed, these CNTs were

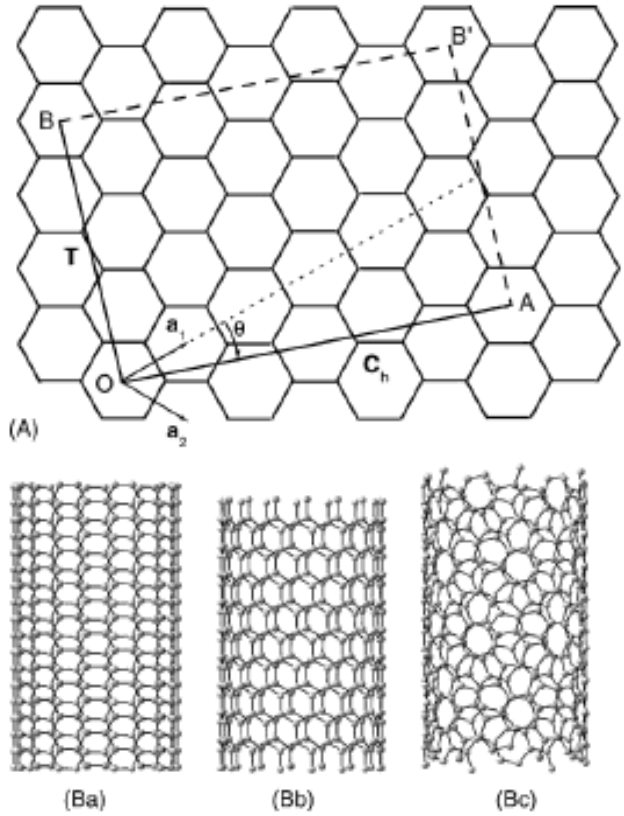

Figure 3.1 - **A schematic of a graphene sheet.** The lattice chiral vector $C_h = na_1 + ma_2$ describes that angle at which the graphene sheet is rolled. B) Illustrated examples of nanotubes with different chiral vectors.

shown in a follow up study to play a role in single cell signalling activity through the back propagation of calcium currents in the dendrites (Cellot et al., 2009). The favoured explanation for this is described in an electrical model that creates an electronic shortcut through the CNT substrate from one area of the dendrite to another (e.g. distal to proximal). This theory is backed up with a transmission electron microscopy (TEM) study that show the intimate contacts that CNTs form with active cell membranes. One unfavourable consequence of this is that 'short circuiting' of the extracellular space across the CNT island may disrupt normal, compartment-specific electrical activity in individual neurons (Branco and Häusser, 2010) detrimentally affecting the ability of these neurons to compute based on synaptic inputs. This brings into question the validity of CNT MEAs as a tool for studying communication between multiple neuronal elements in a network, as it potentially interferes with that communication process in a way that less invasive tools do not (e.g. calcium imaging). However, the use of CNTs does allow manipulation of cell activity and analysis of network-wide consequences.

Additionally, functionalised MWCNTs (where the CNTs have been chemically modified to have peptides or other molecules that will interact with cells coming into contact with them

(Gaillard et al., 2009)) encouraged neurite extension of cultured somatosensory neurons and SEM analysis showed a high level of integration of the neurites with the functionalised CNTs as compared with the non-functionalised CNTs (Xie et al., 2006). These cells are already terminally differentiated. Comparably, the differentiation of embryonic stem cells into neurons on polymer-coated CNTs has also been demonstrated, as has the polymer-coated CNTs propensity to encourage such differentiation (Chao et al., 2009). Poly-acrylic acid (PAA) was chosen for grafting onto CNTs to enhance biomolecular interaction. PAA coated surfaces, on their own, resulted in lower numbers of terminally differentiated neurons than on traditional poly-L-orinthine (PLO). However, a thin film of PAA coated onto CNTs resulted in enhanced levels of terminally differentiated neurons, and cells displayed a more complex network of neurites. This demonstrates the usefulness of CNTs as a scaffold for thin-films that display positive characteristics for cell adhesion in contrast to the bulk-coated alternative. Other polymers have had equal success. Embryonic neural stem cells successfully differentiated into neurons, astrocytes and oligodendrocytes on single-walled CNTs (SWCNTs) coated with poly(ethyleneimine) and their survival was comparable with cells differentiated on PLO (Jan and Kotov, 2007).

Of course, the electrical conductivity of CNTs coupled with their biocompatibility and high contact surface area make them an excellent candidate as an electrode surface for implants and MEAs. Coating traditional electrodes with CNTs and implanting them for recording and stimulation in monkeys and rats showed marked improvement in electrode impedance and an increase in charge transfer (Keefer et al., 2008). Dissociated hippocampal neurons cultured on SWCNTs and characterised electrophysiologically have been used to create models to help understand the interactions of cells coupled to nanomaterial electrodes (Mazzatenta et al., 2007).

3.2.2.6 Rationale behind the experiments performed and described in this chapter.

Previous studies have shown that the CC9 cell line, once differentiated into neuronal cells, exhibits normal electrical activity when stimulated pharmacologically, as determined in patch clamp studies (Trevelyan et al., 2010). No attempt has been made so far to gather extracellular signals, spontaneous or evoked, or to examine network connectivity in these nascent neurons and this was an important hill to surmount in using these cells as a model

of examining network communication, particularly for comparative studies with other cell systems as MEAs are used commonly in the field.

The activity that the network produces will be influenced by an array of factors, including its physical structure, which is, of course, normally stringently controlled *in vivo*. Here, a heterogeneous population of cells is allowed to self-assemble randomly on the surface. By manipulating network architecture using tools that are also suited to gathering electrophysiological signals, this could provide a simple solution for studies focussing on how architecture can affect patterns of activity. There is a wide variety of methods available for influencing the position of cells or even specifying the growth patterns of neurites. CNT patterning is chosen here for its proven success in similar systems, its flexibility as a patterning material and its suitability as an electrode material, giving it a dual purpose. The, admittedly, crude manipulations to be used in these experiments may not resemble any true architecture, but they do provide a very simple and effective way to explore the effects of physical architecture on the development of such nascent networks, with the possibility of near single-cell resolution. It may also provide a starting point for far more complex manipulations, likely combined with other technologies such as those discussed in the Introduction.

Discussed above was the work that has been published on the effectiveness of CNT constructs to organize networks of dissociated adult cortical neurons and allow subsequent monitoring of spiking activity through the CNT electrode array. This has not yet been attempted with developing neurons. With the knowledge that different cell-types react differently to CNTs, it will be interesting to explore the behaviour of differentiating neurons in this environment and be able to compare the formation of such networks with the manipulation of mature neuronal systems already published.

3.3 METHODS

Methods for maintaining and differentiating the stem cells are provided in the previous chapter, though methods specific to this chapter have been given below.

3.3.1 Immunocytochemistry

11 DIV differentiated CC9s were stained for DAPI (for cell nuclei) and β-Tubulin III (specific to cells differentiating down the neuronal lineage). The cells were fixed with 4% paraformaldehyde (PFA) for 20 mins, washed three times with PBS before adding PBS with 30% normal goat serum (NGS) and 0.1% Triton (X100) for 4 mins. This was washed three times with PBS before adding PBS with 10% NGS, 0.1% Triton and mouse IgG_{2b} anti mouse β-tubulin III (1:500) for 1.5 hrs. This was then washed three times with PBS before adding PBS with 10% NGS, 0.1% Triton and goat anti Mouse IgG_{2b} Rhodamine Red-X conjugated (1:200) for 1.5hrs. This was then washed three times with PBS and mounted onto slides with mounting medium containing DAPI. Bright-field images and fluorescence images for the two stains were taken to look at the extent of β-tubulin III expression in these cultures at 11 DIV.

To count the number of β-tubulin III-expressing cells, the DAPI and β-tubulin III-stained images were imported into MATLAB and background subtracted to flatten the intensity images and remove light aberrations. The DAPI intensity image was then used to create a region map of cell locations (Figure 3.2A). The β-tubulin III intensity image (Figure 3.2B) was thresholded (Figure 3.2C & D) and DAPI regions with pixels overlapping the thresholded β-tubulin III pixels were counted as cells staining positive for β-tubulin III.

3.3.2 Carbon Nanotube Island Substrates

The CNT-patterned, quartz substrates used in the following experiments were provided by Dr Y Hanein (Micro and Nano Systems Laboratory, School of Electrical Engineering, Tel Aviv University, Israel), where standard microfabrication techniques were used to create these substrates. Briefly, a thin layer of Nickel is evaporated and used as catalyst for the growth of long CNTs (Gabay et al., 2005a). The result is islands of meshed CNTs (Figure 3.3).

Two geometric configurations were used: 80µm diameter islands spaced 230µm center to center and 20µm islands spaced 500µm center to center. A quartz substrate was used to provide a transparent material for bright-field and fluorescence imaging. The CNTs, however, were opaque, so using an integrated microscope, calcium imaging would only detect signals in between the CNT islands, away from which the cells have migrated and clear of the clusters of somata where calcium transients would be detected.

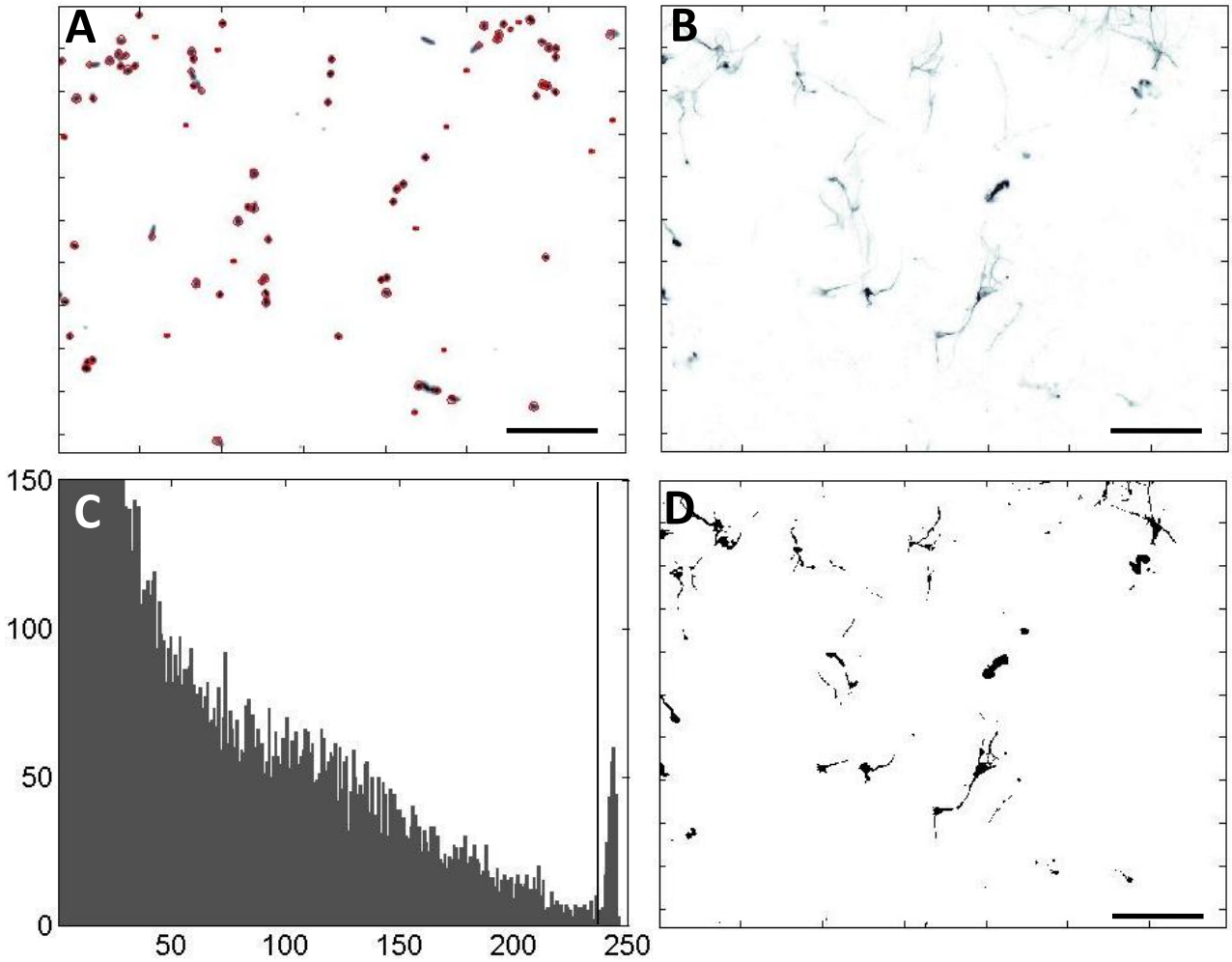

Figure 3.2 – β-tubulin III expressing cells. A) DAPI intensity image with region boundaries overlayed in red. **B)** Background subtracted (flattened) β-Tubulin III instensity image. **C)** Histogram of the intensity values in 'B' showing a secondary peak at the top end of the spectrum. The black vertical line shows the threshold used for creating 'D'. **D)** Thresholded, binary β-Tubulin III image. Scalebar = 100µm.

3.3.3 Atomic Force Microscopy Protocols

An Agilent 5500 AFM/SPM microscope (Agilent Technologies) was used to produce AFM images, using a 90µm scanner (N9521A) and silicon cantilever tips (radius < 9nm) with spring constants (k) of 0.02-0.77Nm^{-1} and 42Nm^{-1}. The liquid cell was heated using a Cryogenic Temperature controller (Model 331, Lakeshore) with 0.025K accuracy.

A liquid-cell with a heated base (set to 32°C) was used to contain the CNT-patterned sample with its cultured cells. This was filled with 4:1 medium. Firstly, a low-k tip was used in contact mode for topographical imaging. This was successful and bundles of neurites were not found to be sensitive to deformation by this tip. The tip was changed for one with a high-k and this was used in AC/tapping mode, which appeared optimal for this kind of imaging, even on this biological sample and in a liquid environment. Magnetic-AC (MAC) - mode was not found to be necessary to produce a stark, detailed image.

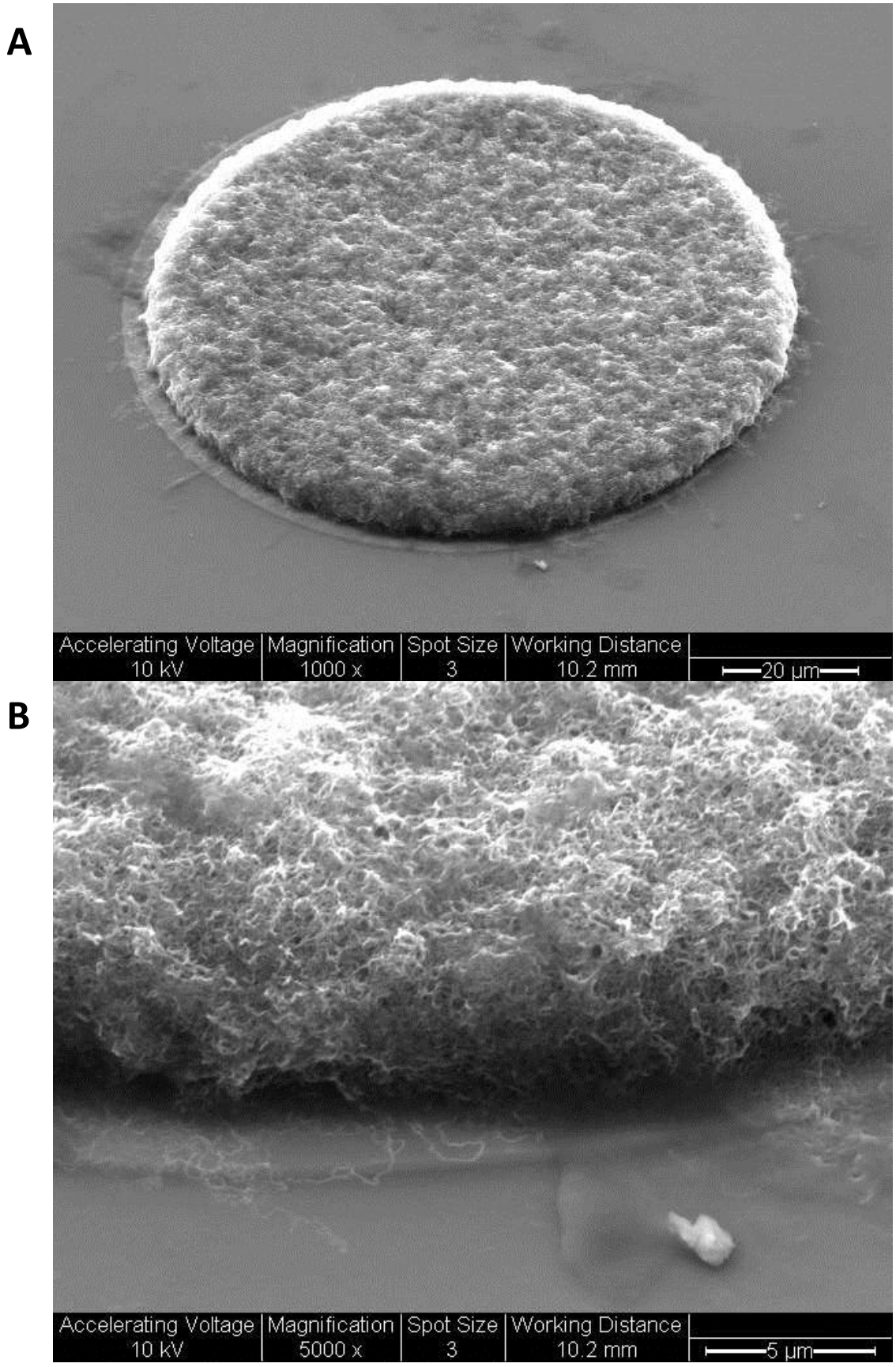

Figure 3.3 – Example of a carbon nanotube (CNT) island patterned onto a quartz substrate, taken with an environmental scanning electron microscope (eSEM). A) Isometric view of a whole island, 80µm across. **B)** Higher magnification image shows the complexity and scale of the meshwork of the CNTs.

3.3.4 Multi-electrode Array system

The Multichannel Systems MEA60 electrode stage and MEA1060 amplifier were used, with data transferred to a PC via the MC_card using the MC_Rack data gathering and analysis software (Multichannel Systems). Stimulation was performed with the STG MC_Stimulus (Multichannel Systems).

3.3.5 Fluorescence Microscopy

An Olympus IX71 inverted research microscope was used to take images of cell cultures on the MEA and for fluorescence imaging. A mercury lamp and an Optoscan monochromator (Cairn Research) were used in fluorescence experiments.

3.3.6 Network Architecture

CNT-patterned quartz surfaces were either left untreated or coated for cell adhesion to examine the structural constraints afforded by the arrays. Surfaces to be seeded with CC9 cells were coated with PDL and laminin and surfaces to be seeded with HCN/GFP cells were coated with PLO and laminin (see the Methods in Chapter 2).

Cells from the CC9 (embryonic stem cells (ESCs)) and HCN/GFP (adult hippocampal progenitor cells (AHPCs)) lines were maintained in culture as described in the methods. At 8 DIV of the differentiation protocol for the CC9 embryonic stem cells the cells were seeded onto a mixture of coated and uncoated CNT-patterned quartz surfaces (described in the Methods in Chapter 2) at a density of between 350 – 1000 cells/cm^2. HCN/GFP adult hippocampal progenitor cells were seeded onto the same surfaces with the same densities and differentiation was fully induced by the reduction of b-FGF according to the differentiation protocol. Half of the medium was replaced every two days.

Bright-field microscopy images of the cells were then taken over 7 days to follow the morphological development of the cells. Environmental scanning electron microscopy (eSEM) images were also taken 3 days after seeding the cells, with no surface treatment prior to putting the samples into the environmental scanning electron microscope (eSEM) (i.e. the cells were neither fixed nor coated).

3.3.7 Electrophysiology

Standard, commercial, microelectrode arrays (with indium tin oxide (ITO) electrodes) were coated according to standard procedures for seeding CC9 cells for electrophysiological measurements. These arrays, which are commonly used for dissociated cell culture, would provide a tried and tested substrate on which to look for extracellular signals. The custom-designed multi-electrode arrays (with CNT electrodes) were of limited availability and their use was reserved for once the production of extracellular activity from these cells had been established.

As in the above procedure, CC9s and HCN/GFP cells were seeded this time onto ITO multi-electrode arrays (Ayanda) that had been coated with either PDL and laminin or PLO and laminin for CC9 and HCN/GFP cells respectively (details of the coating procedure in the Materials and Methods chapter). The electrodes had a diameter of 30µm and 100µm spacing. The same differentiation protocols as above were followed.

The MEAs were transferred to the Multichannel Systems (MCS) stage and perfused with oxygenated aCSF. The stage was heated to 32°C. Bright-field images of the cells on MEA surface were taken prior to data acquisition to keep a record of the distribution of cells over the electrodes. The cells were allowed to settle for 30 minutes. Electrophysiological data were sampled at 10kHz and 5 minute recordings were taken periodically over a period of 2-3 hours. The raw data were logged and exported to MATLAB for filtering, thresholding and spike sorting using the programme Wave_clus.

3.3.8 Electrical Stimulation

Electrical stimulation was used to see if localised extracellular responses could be elicited in CC9 cultures. Calcium imaging was used simultaneously during electrical stimulation experiments. This would provide a global measure of cell excitability to correlate alongside spike activity via calcium influx through VGCCs. The calcium imaging was also more spatially explicit, allowing a clearer examination of the structural properties of the network, as opposed to the ITO MEA, where the cells distribute randomly over the surface and electrodes contact a limited number of cells.

Oregon Green BAPTA-1 (OGB-1) was loaded into the cells (n = 3 MEAs at 15-17 DIV; n = 3 MEAs at 19-20 DIV) according to the protocol provided in the Methods section (Chapter 2)

and the culture was allowed to settle in the perfused experimental chamber for 30 minutes. For the MEAs used in these experiments (n = 4), initial bright-field images were used to select electrodes that had a population of cells adhering both to the electrode and the surrounding area. It was also ensured that the cells had absorbed the OGB-1 dye by visual inspection through the microscope. Areas of highly clumped (and therefore raised) cells were not considered. These electrodes were used to stimulate the cells in the form of a train of current pulses. Biphasic pulses (-/+) between 70-150µA were used for between 60-200µs each phase with a 20µs 'off' period in between each phase (e.g. Figure 3.9). They were delivered as a train of between 3-20 pulses. Electrophysiological data were sampled at 10 kHz and 5 minute recordings were taken periodically over a period of 2-3 hours. The raw data were logged and exported to MATLAB for filtering, thresholding and spike sorting using the programme Wave_clus. Although the calcium data were gathered alongside the MEA data, they were not synchronized. The calcium data were analysed using ImageJ and MATLAB (see the Methods in Chapter 2). Calcium responses that could be detected by eye at the time of stimulation and recording were used to judge whether the cells had responded.

3.3.9 Pharmacological Stimulation

Exogenously applied glutamate was used to excite the CC9s and measure the responses in terms of intracellular calcium changes as a comparison with electrical stimulation. 1mM glutamate was applied exogenously in a train of 10 pulses separated by 2 seconds using a 10ms pulse from a pressure pipette in close proximity to individual 15 DIV cells in the field of view (equipment details provided in Chapter 2). The cells were loaded with OGB-1 (as for electrical stimulation above) and the change in fluorescence intensity was observed.

3.4 RESULTS

3.4.1 β-tubulin III staining

In Figure 3.4 DAPI and β-tubulin III stained images are shown of 11 DIV differentiated CC9s. From these images, it can be seen that a large number of the cells (40, 64 and 55% - see section 3.3.2 for methods) express β-tubulin III, a neuronal marker. A previous study demonstrated that 15-20% of the neuronal cells expressed GABA. Also, a small percentage of glial cells were found in this study (Kirby et al., 2009). It should be noted that a number of the cells in each culture remain undifferentiated and continue to divide, which will contribute to the percentage of unlabelled cells here.

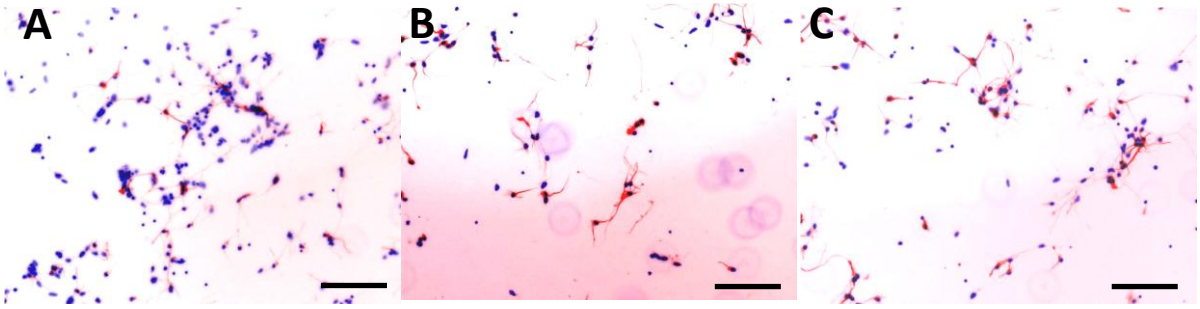

Figure 3.4 – β-tubulin III staining of CC9s differentiated into neurons at 11 DIV. A, B & C) DAPI staining showing cell neuclei in blue and β-tubulin III staining showing neuronal cells in red. In each case, three n's, the percentage of cells labelled with β-tubulin III are 40%, 64% and 55% respectively. Scalebar = 100µm.

3.4.2 Network Architecture

CC9s and HCN/GFPs reacted in different ways to the coated and uncoated CNT-patterned substrates. The effects can be considered in terms of the clustering behaviours of the cells that result from surface treatment, and in terms of the reactions of different cell types to these surfaces. In brief, for both cell types, uncoated surfaces led to more pronounced clustering as cells preferred contact to each other than the non-adherent substrate. The contrasting reactions of the two cell types was that the ESCs were attracted to CNT islands on uncoated surfaces, but neuronal progenitors, which do not normally exhibit migration behaviour as the embryonic stem cells do, were not attracted to the islands.

3.4.2.1 Coated CNT-patterned substrates

On CNT-patterned substrates that were coated to promote cell adhesion, CC9s spread out over the surface, adhering indiscriminately, irrespective of the placement of CNT islands. This can be seen clearly in Figure3.5A where cells adhere flat to the surface of the coated glass, in between the CNT islands. The isometric view shows the morphology of one of the

cells that has differentiated into a neuron, with elongated cell bodies and processes clearly running over the surface. The bright field image in 'B' shows the cells starting to draw together, still flat to the coated surface, again, with no discrimination between coated glass and coated CNT islands. CC9 ESCs typically migrate across surfaces to form clusters of cells, however, HCN/GFPs, which are neuronal progenitors, do not show this behaviour on coated surfaces and instead remain spaced from each other, stationary, and extend processes to form nascent connections. Figure 3.5C demonstrates this behaviour, showing the HCN/GFPs to adhere to the substrate, also regardless of CNT-islands, extending processes across the surface. **These findings show little difference in behaviour of the two neuronal subtypes on coated surfaces**. Both effectively ignore the electrode surface as they develop, failing to become patterned to the MEA they are developing on.

3.4.2.2 Uncoated CNT-patterned substrates

In contrast, a difference in the network structure formed by the two cell types is seen for CNT-patterned substrates that have not been coated for cell adhesion. The eSEM image in Figure 3.6A can be starkly compared with the one in Figure 3.5A, as the cells sit proud of the surface (clearly visible through changing the height of the focal plane), not finding it adhesive, and they have clustered into collections of cells, adhering to each other as opposed to the surface. The CC9-derived cells also show that they are starting to migrate towards the CNT islands with some clusters already sitting on top of them, with thick neuritic bundles stretching off to other cell clusters.

The isometric view illustrates that although these cells are struggling to adhere to the surface, they can still differentiate into cells that display a normal morphology comparable with that seen on normal coated glass surfaces, with the processes stretching over the surface, regardless of the lack of cell-adherent coating. In Figure 3.6B, the clustering habits of these cells are more pronounced than for the coated substrates shown in Figure 3.5B, 'i' with 11 DIV cells showing a preference for the nanotopology of the CNT islands, rather than the uncoated surface. In Figure 3.4B 'ii' the CC9s are further developed at 14 DIV and now show large populations of cells clustered directly over the CNT islands, connected by well defined, spatially constrained, fasciculated bundles of neurites (contrasting with the splayed and seemingly disorganised neurites extending from aggregating cells in 'B i'). The cell aggregates are also very large and dense, containing large numbers of cells (estimates of the

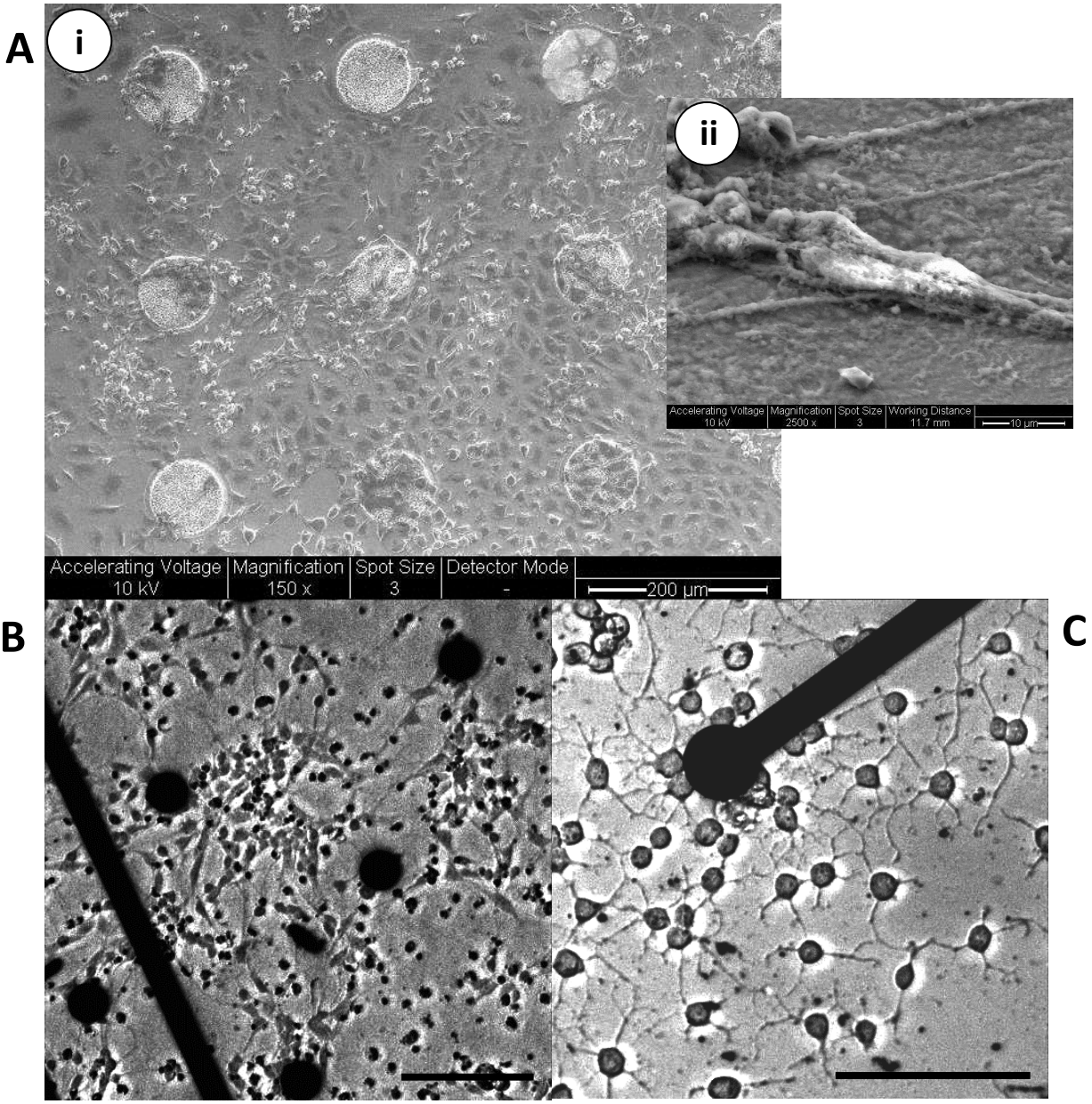

Figure 3.5 – Examples of cell network distribution and surface adherence on CNT-patterned surfaces, also coated with PDL and laminin. A) i) eSEM image of 11 DIV CC9s on 80µm diameter CNT islands. There are still many undifferentiated cells at this stage, and the cells can be seen to adhere all over the surface, regardless of the presence of the CNT islands. ii) Angled view, at 2500x magnification, of a CC9 stem cell that has differentiated (also 11 DIV). **B)** 11 DIV CC9s on 20µm diameter CNT-patterned, coated quartz. The neuronal cells are starting to cluster, and are as adherent to the coated quartz surface as the CNT islands. **C)** i) 7 DIV HCN/GFP cells on 20µm diameter CNT-patterned, coated quartz. These cells also spread over the surface, not showing any preference for the CNTs over the substrate. Scalebar in 'B' and 'C' = 100µm.

number of cells is made impossible due to the tight, 3D clustering).

As there was not an adhesive surface for cells to easily attach to, many cells never adhered to the surface, died and, as they were floating in the medium, were subsequently removed

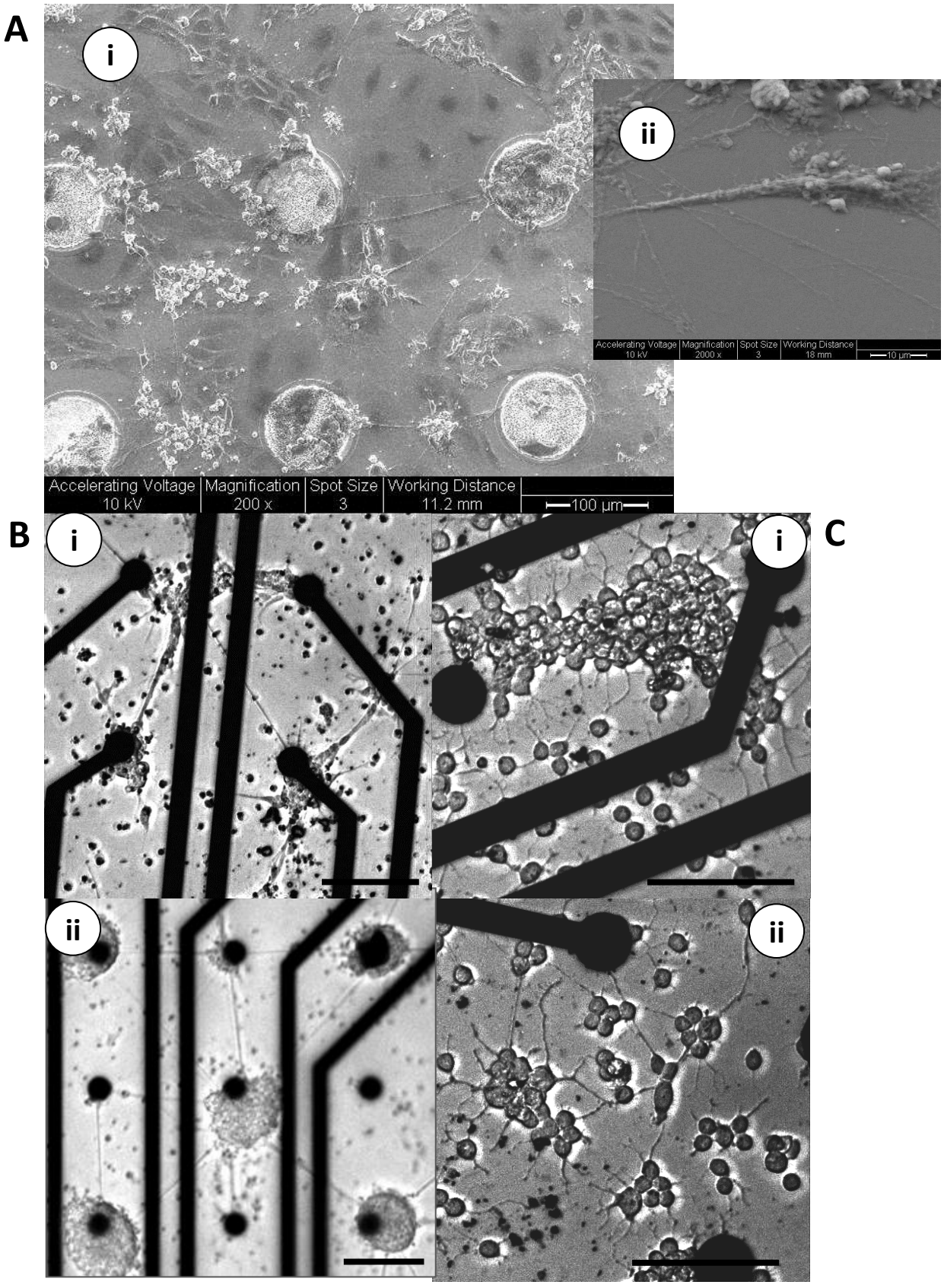

Figure 3.6 – Examples of cell network distribution and surface adherence on *uncoated* CNT-patterned surfaces. **A)** i) eSEM image of 11 DIV CC9s on CNT islands. The cells can be seen to clump together due to the lack of coating on the surface to adhere to. Processes can be seen running between clusters. ii) Angled view, at 2000x magnification, of a CC9 that has differentiated into a neuron (also 11 DIV). **B)** i) 11 DIV CC9s on CNT-patterned, uncoated quartz. The neuronal cells are starting to cluster around the CNT islands. ii) as in 'i' but with 14 DIV CC9s. Clusters of cells have migrated to the CNT islands and away from the non-adherent substrate. **C)** i and ii) 7 DIV HCN/GFP cells on CNT-patterned, coated quartz. These cells also spread over the surface, not showing any preference for the CNTs over the substrate. Scalebar in 'B' and 'C' = 100µm.

with medium changes. This resulted in lower populations of cells on the surface. Seeding densities were increased from 350 cells/cm^2 to 500-1000 cells/cm^2, though the final population size adhering to the surface was unpredictable. In addition, the aggregates of cells, as with embryoid body formations, may encourage cell proliferation and discourage differentiation (see chapter 1), thus resulting in different population sizes as the culture develops. This may also account for the large size of aggregates seen accumulated over the CNT islands in Figure 3.6 'B ii'. In contrast, the HCN/GFPs (Figure 3.6C), while they do show clustering on the non-adhesive surface used, do not show a preference for the CNT islands over the surface.

The apparent structure of cells on CNT-patterned substrates, forming sub-clusters of cells connected by bundles, does not describe the nature of any resulting functional connection between cell clusters. At the light microscopic level and eSEM level it is not possible to see the extent of connectivity between clusters via the bundles. By taking an AFM topographical image of the thick neuritic bundles that connected clusters of cells it was possible to examine qualitatively the extent of neuritic fasciculation (Figure 3.6). The AFM tip was placed directly over a bundle spanning two large cell aggregates (Figure 3.7A) and a rastered image was taken along the top of this bundle (Figure 3.6B). The AFM image, which doesn't quite span across the breadth of the neuritic bundle, shows a complex, dense meshwork of many hundreds of neuritic processes with little apparent parallel directionality and sub-bundles appearing to have sets of parallel neurites.

These data show that CC9-derived neurons can be highly patterned by development on CNT arrays without adherent coatings, much more so than HCN progenitor-derived cells. The specific patterning of clusters, with dense neuritic interconnections between clusters, directly onto the CNT contact points suggests an excellent substrate for examining the function of simple, artificially structured neuronal networks.

3.4.3 Developmental structural changes in the absence of patterned substrates.

Attempting to force structure on nascent networks during development hides any intrinsic ability the neuron population may have to structure itself. Therefore, the results from CC9-derived cultures on coated and uncoated MEAs was compared to that on coated coverslips alone (no patterned MEA substrate). Clustering was seen for CC9 cells on coated MEAs but

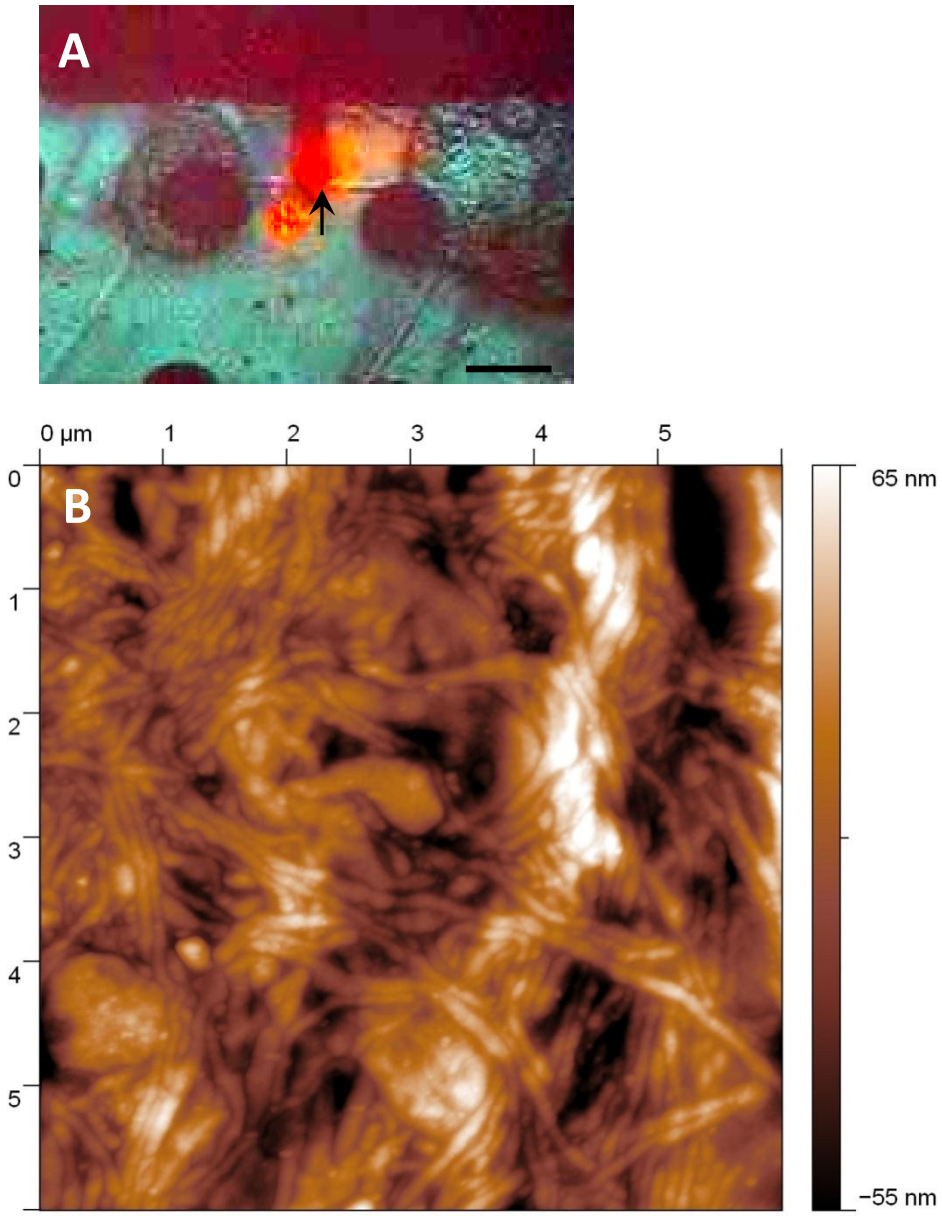

Figure 3.7 – Atomic force microscopy (AFM) topographic image of the surface of a thick, fasciculated bundle of neuritic processes. A) Bright-field image showing the clusters of 13 DIV CC9s around 80µm CNT islands with a large bundle of neurites bridging between. The arrow indicates the location the AFM scan occurred, over a 6µm^2 area on top of the bundle of neurites. Scalebar = 80µm **B)** AFM topographic image of the neuritic bundle shown in 'A' (arrow). Note the lack of uniform trajectory and dense clustering of many individual neurites.

the clusters formed did not correlate with the position of the electrodes themselves (above and Figure 3.5). A similar pattern of clustering was seen when CC9 cells were grown on plain (non-MEA patterned) coverslips (Figure 3.8). These autonomously generated clusters were seen to increasingly form a structural feature of the population of cells from 14 DIV to 19 DIV. By applying a grid to each culture image and quantifying the number of grid-squares occupied by a cluster it was seen that almost no clusters existed at 14 DIV. From that

timepoint on, clustering increased so that from 15 DIV to 19 DIV average clustering effectively doubled from 10% to 20% of the area occupied by the culture (15 vs 19 DIV, $P<0.05$, N = 10 and5 respectively). Clustering then dramatically decreased after 19 DIV to 15 DIV levels by DIV 20 as the cells reached the end of their period of viability in vitro.

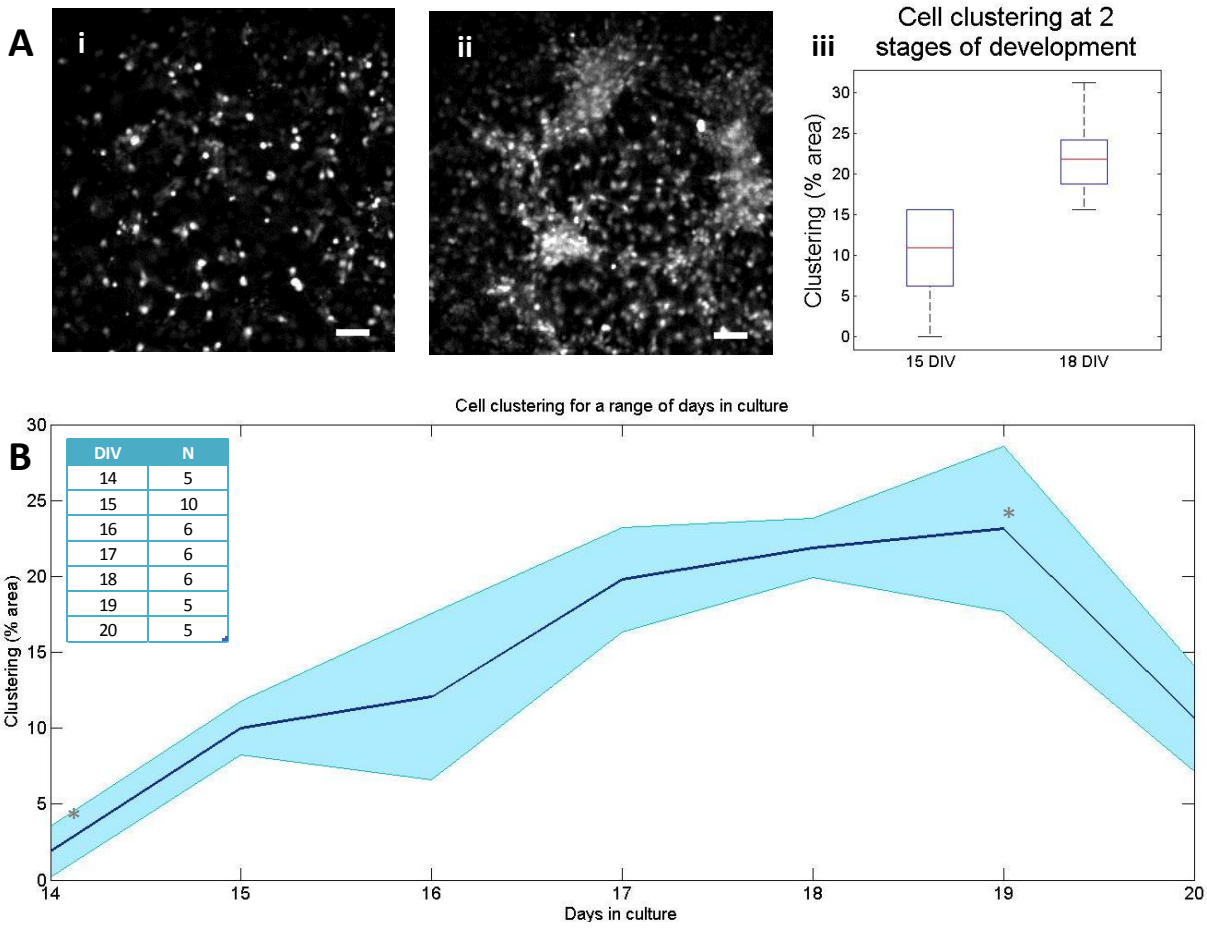

Figure 3.8 – Development of network architecture. A) Example images of a 15 DIV (i) and 18 DIV (ii) culture with resting fluorescence levels, showing the difference in cell distribution across the surface. (iii) a grid was applied to images from different developmental days and grid areas containing clusters were counted. Higher levels of clustering were found in 18 DIV than 15 DIV. **B)** Cell clustering for a range of days in culture found using the grid method. Shaded regions represent the SEM. Very little clustering was seen at 14 DIV, and clustering increased until 19 DIV ($P < 0.05$) before falling at 20 DIV.

3.4.4. Spontaneous and stimulated electrophysiology

Extracellular signals had not been gathered from the CC9 cells line before so commercial arrays commonly used for gathering extracellular signals from dissociated cultures were used here in order to reduce the number of unknown variables and attempt to gather signals in a tried and tested environment (commercial ITO electrodes) before moving to the custom environment (CNT electrodes), which would involve strict directed patterning of the

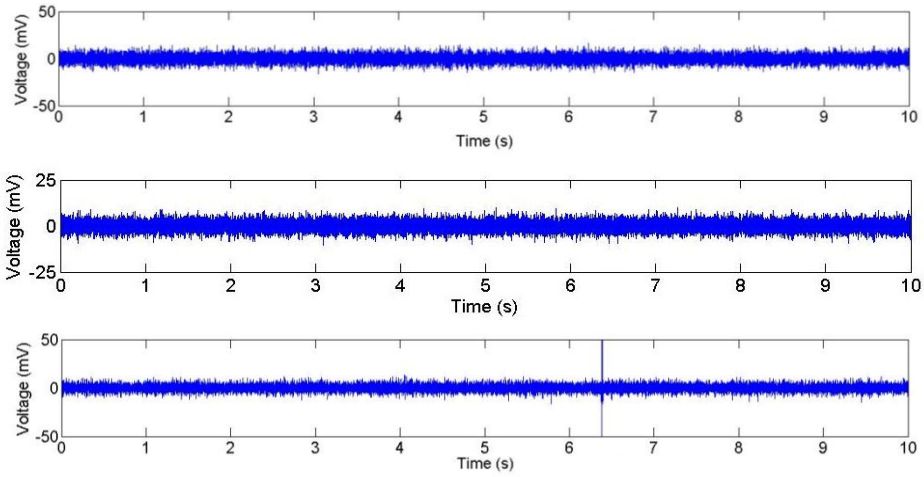

Figure 3.9 – Representative MEA recordings from single electrodes. A) A background noise signal from an electrode on an MEA with no cells seeded, perfused with aCSF as if performing the experiment with CC9s. **B)** The signal from an electrode with 16 DIV CC9 cells seeded ont it. **C)** As in 'B', but with a stimulation (seen as a blue line across the whole Y-axis).

cells. By using ITO electrodes the cells were able to self-organise (i.e. were not patterned) on the surface, irrespective of the electrode locations, able to extend processes freely and remain flat to the substrate with less of a tendency to clump and lift off the surface in 3D aggregates. That surface was made cell adhesive all over to this end, as is performed most commonly in other published work.

At the start of each experiment, the cells (n = 3 MEAs at 15-17 DIV) had healthy morphology and had formed process-rich networks, as expected. The cells could be seen to be dispersed randomly over the MEA and were in contact with large number of electrodes. However, no spontaneous extracellular activity was observed over the 3 hour session (Figure 3.9) as maximums of 10's of spikes could be detected above twice the standard deviation of the background signal (10µV and within the limits stated on Ayanda's website of 20-25µV), with the size of detected spikes never reaching -30µV. In addition, the wave forms of these spikes did not resemble previously reported cell unit activity with these electrodes, not possessing the biphasic voltage deflections typical of healthy neuronal extracellular action potential recordings (Shein et al., 2009), suggesting the detected events were merely the extremes of the noise inherent in the recording system. These experiments were also repeated with cultures where 10µM glutamate was pipetted onto the culture during recording, with the same null result. Having not had any success in measuring extracellular signals from CC9-derived neurons on commercial arrays when allowed to self-organize on

the surface, the experiments were not repeated in the constrained environment of the custom CNT arrays as they were of limited supply. Time constraints added to the decision to concentrate on techniques that did yield results (see below).

3.4.5 Spontaneous and electrical stimulated calcium signals

As no spontaneous activity could be detected I attempted to record activity elicited by exogenous, electrical stimulation using the commercial ITO electrodes. Using current stimulation through a single electrode on an MEA, extracellular units could also not be detected on any electrodes tested (Figure 3.9).

Although this may be because the cells do not generate signals that can be detected with the electrodes, this was addressed as a potentially methodological problem as the cultures looked healthy in general. Thus I switched to using calcium imaging. Although the same electrical stimulation through an electrode on the MEA that failed to reveal unit activity, when using calcium imaging it could be seen that large calcium transients were evoked in cells local to the electrode and evoked further responses in a selection of cells that radiated as far as 138µm from the area of the electrode (Figure 3.10 & Figure 3.12). The responses had a mean amplitude of 782±29 (change in fluorescence in arbitrary units, n = 22 events) The spatiotemporal pattern of activity is illustrated in Figure 3.11 with time-lapse images showing specific frames where different sets of spatially distributed cells are activated at different times following stimulation. The average distance from the electrode of these groupings of cells are shown in Figure 3.11C, and it can be seen that the spatial pattern of activation is only temporally dependent on distance from the electrode for the first 2.3 seconds following stimulation. After this, the average distance from the electrode remains fairly constant, with some activated cells being close to the electrode and other activated cells are at a greater distance from the electrode. There is also no correlation between the amplitude of response and the distance of the cells from the stimulating electrode (Figure 3.12).

3.4.6 Pharmacological stimulation

Having seen the activation of CC9-derived neurons by electrical stimulation, exogenously applied glutamate was used to compare responses. Figure 3.13 shows the response from 10 pulses of 1mM glutamate applied over 20 seconds (in 10ms pulses, separated by 2s). The

pulse was applied within 30µm of two neurons, as judged by looking at the position of the glass pipette. Both cells had a time-locked response to each stimulation pulse and showed marked increases in intracellular calcium that summed with each pulse. The fast rise-time for these pulses was followed, once stimulation had ended, by a slower fall off resulting in temporal summation increasing during the repetitive pulse period. The shape of the transient rise was comparable with that of the electrical stimulation, and the amplitudes had a mean of 1105±117 (change in fluorescence in arbitrary units, n = 14), 41% higher than for the stimulation parameters used for electrical stimulation. It should also be noted that this was a higher magnification image than the electrical stimulation, and this experiment and the stimulation experiments were performed using two different setups, both described in Chapter 2.

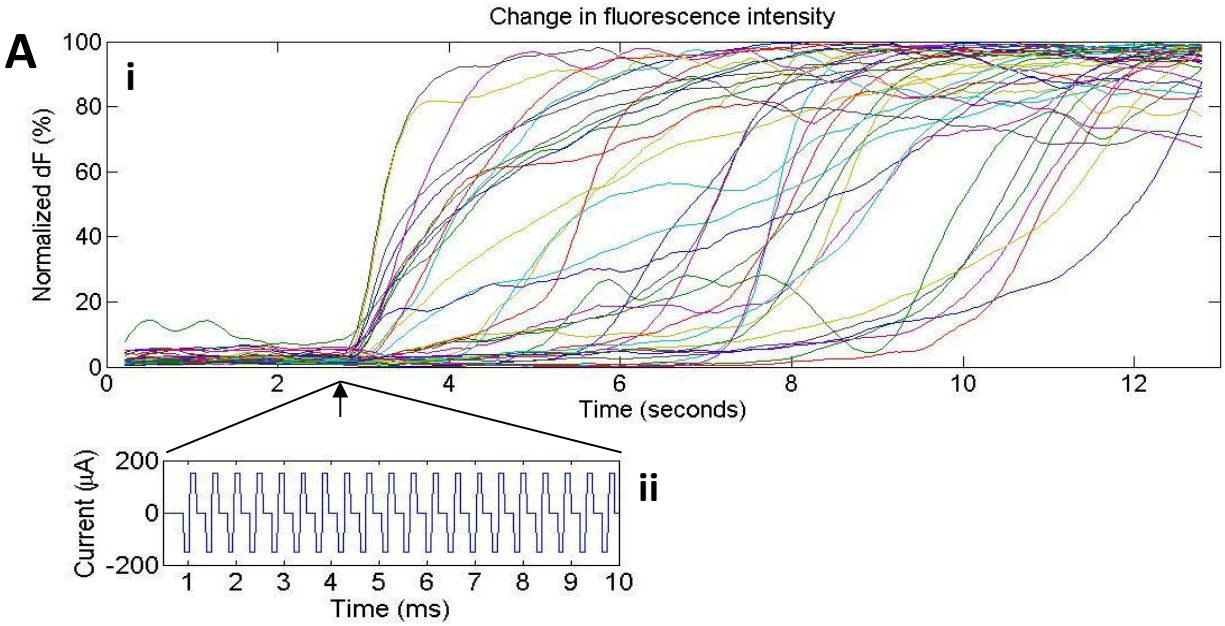

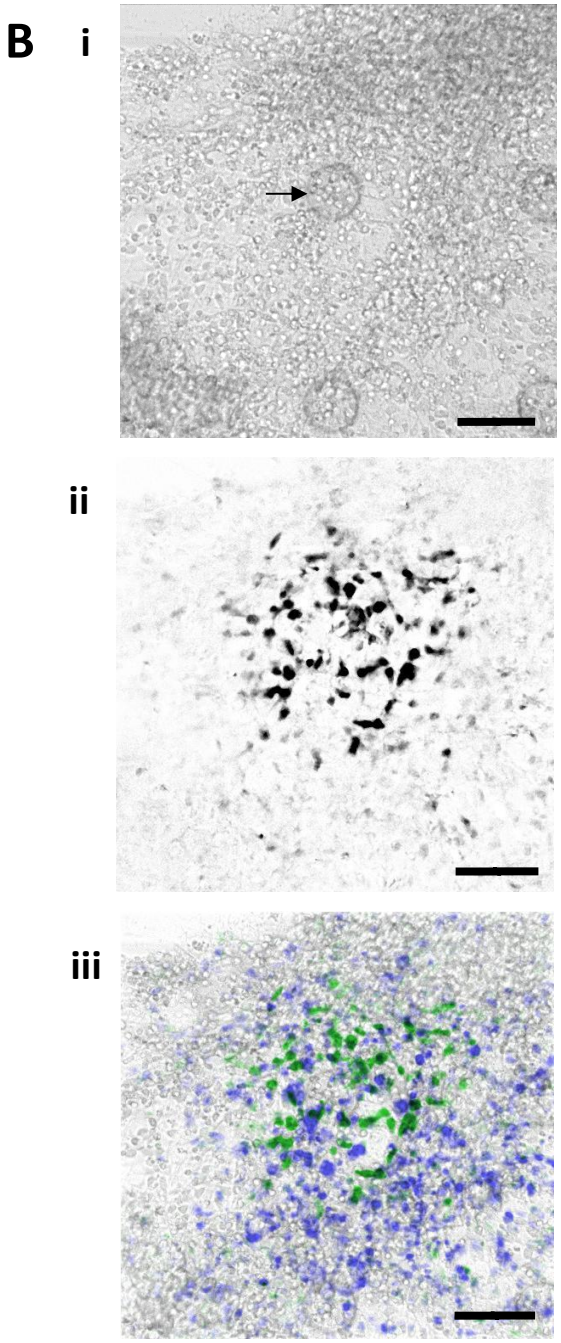

Figure 3.10 – Electrical stimulation evokes changes in intracellular calcium concentration in cells surrounding the stimulation electrode. A) Change in fluorescence intensity for all regions found to be active following electrical stimulation in a 12 second recording (regions shown in 'B ii'). The influx of calcium in most cells starts with the start of the stimulus, but cells are recruited throughout the 12 second recording. A train of 20 biphasic, 150µA, current pulses (depicted in 'ii') which were delivered to the stimulation electrode at the time marked by the arrow in 'I'. **B)** i) Bright field image showing the stimulation electrode (marked by an arrow) and a large population of cells distributed over and around the electrode. ii) Fluorescence image showing the extent of activation of cells surrounding the electrode. This can also be seen in 'iii' where the fluorescence intensity image before (blue) and after (green) stimulation have been overlaid onto the bright field image of the cells. Note that only a small percentage of the cells are activated by the stimulus. Scalebar = 50µm.

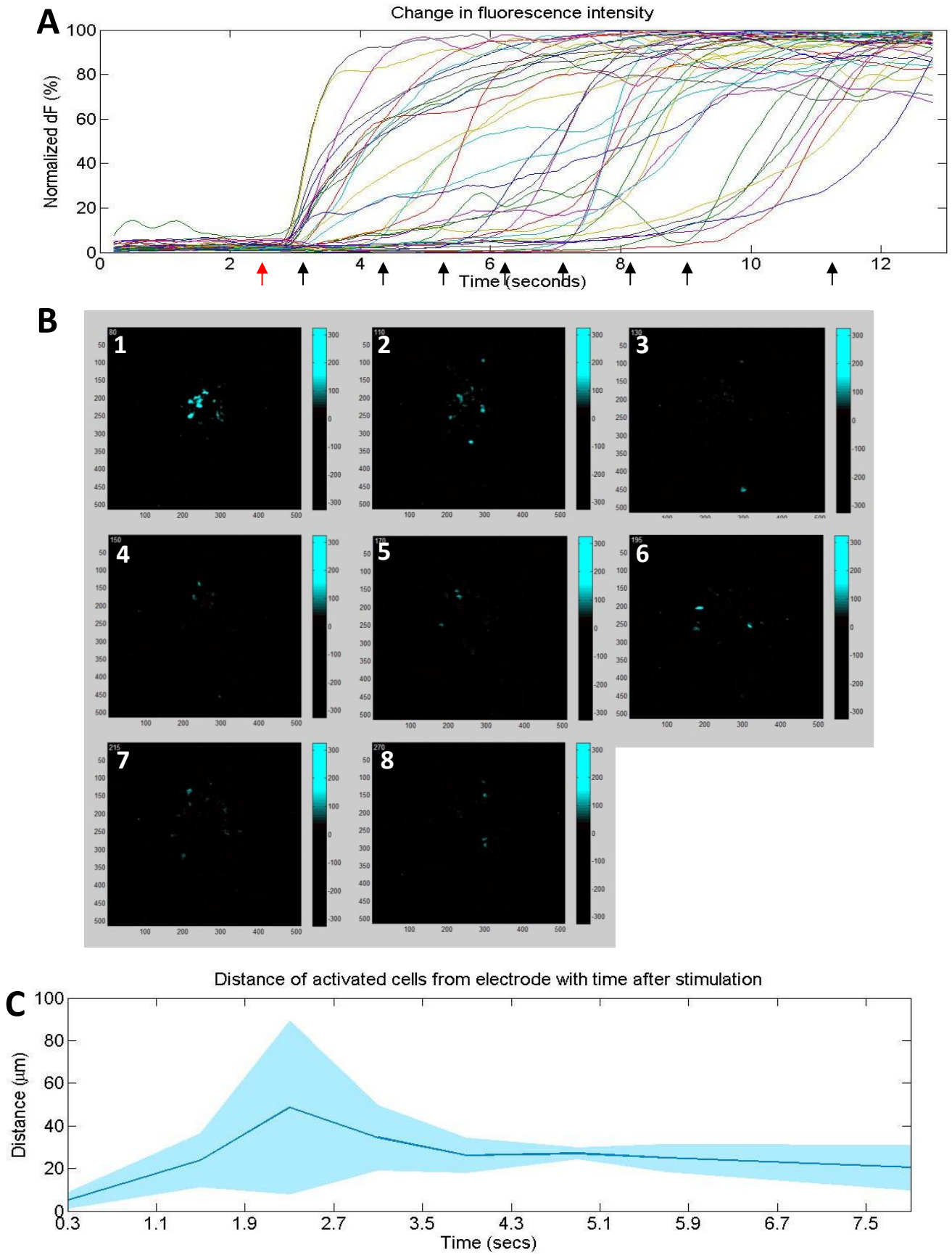

Figure 3.11 – Spatial extent of stimulation with respect to time after stimulation. A) Change in fluorescence intensity with time following electrical stimulation (see Figure 3.9 for details). Red arrow shows time of stimulation pulse. **B)** 1–8) Time-lapse fluorescence images (the times of these images are shown with black arrows in 'A') showing the spatial extend of the reaction to the stimulus over a series of time points following the stimulus. Initially, only cells in close proximity to the electrode are activated ('1'). The activity that follows has spatiotemporal characteristics that are only initially based on distance from the electrode. **C)** The spatial extent of the activity ranged as far at 138.42µm from the periphery of the electrode. The median distances are shown as a function of time (from the frames displayed in 'B') with the shaded area representing the SEM. The spread moves away from the electrode for the first 2.3 seconds following stimulation, but the spatial distribution remains even at a 24.65±2.94µm.

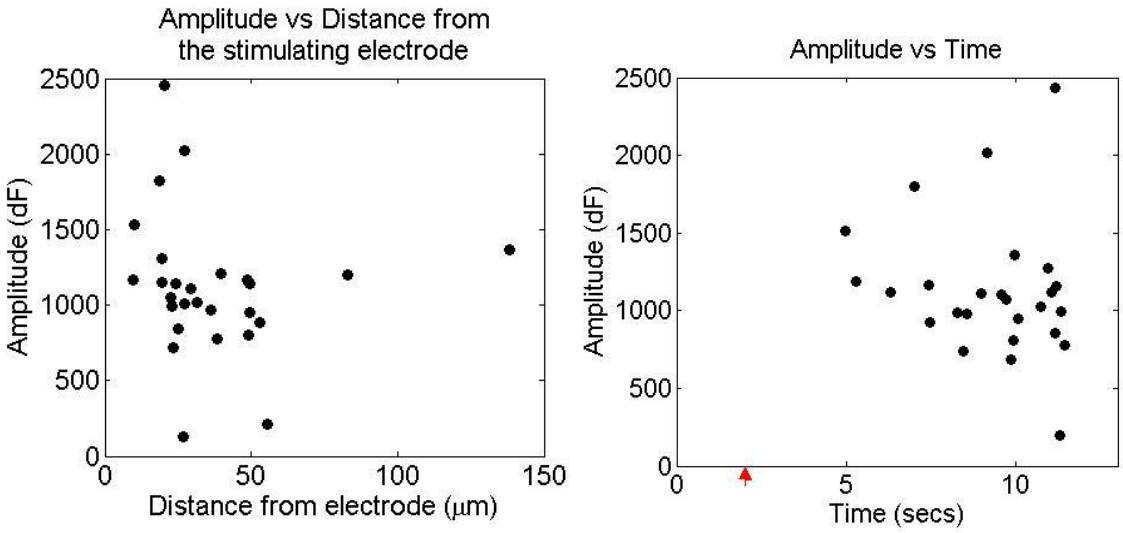

Figure 3.12 – Relationship between amplitude of a cell calcium transient and the distance of the cell from the stimulating electrode. A) No correlation is present between the amplitude of response and the distance of the cell from the stimulating electrode. B) Likewise, no correlation is found between amplitude and time for all active cells, though a far greater variation is amplitudes can be seen with increasing time. The point of stimulus is marked with a red arrow. The amplitudes shown are the maximum amplitudes for each active cell.

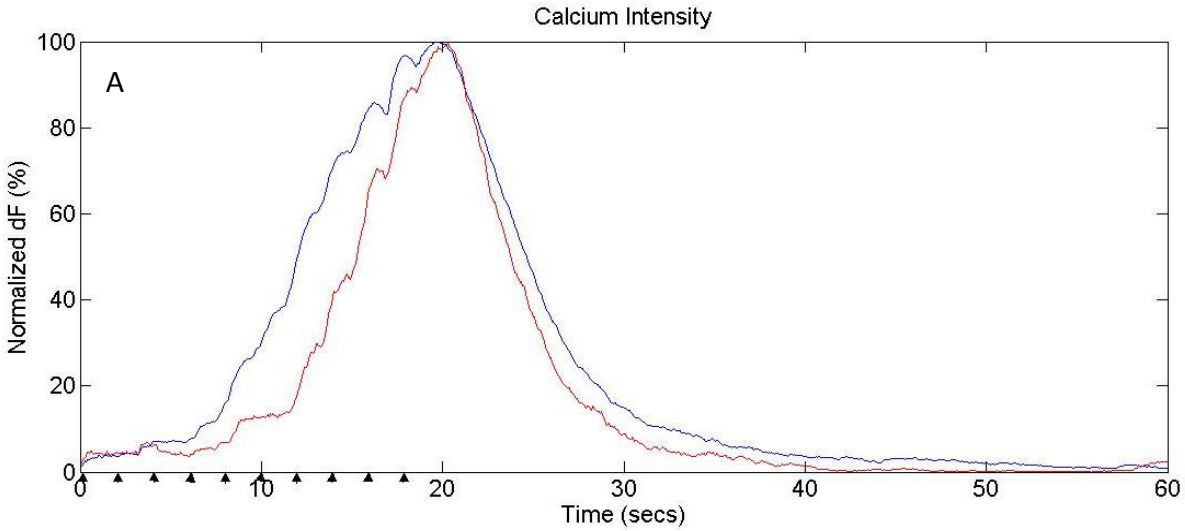

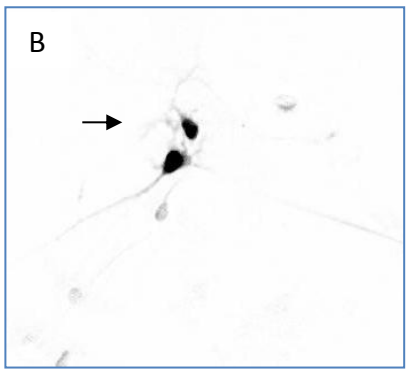

Figure 3.13 – Exogenous glutamate application evokes calcium transients in CC9s. A) Glutamate-evoked calcium transients where 10uM glutamate was applied exogenously using a 10ms pressure pulse in a train of 10 pulses separated by 2 seconds each in close proximity to a cell soma. Here, two cells (shown in **B**) can be seen to be repeatably activated and show a time-locked response with the glutamate application.

3.5 DISCUSSION

3.5.1 Network architecture

During embryonic development *in vivo* the presence of laminin is correlated with phases of neuronal migration. It is found to be specifically involved in the migration of neurons via axonal interaction with radial glial cells (Liesi, 1985). Thus, by coating a surface with laminin, neuronal processes are able to adhere to that surface and cell migration is encouraged. This was seen clearly with the reaction of both ESC and AHPC cells to coated substrates, as they both adhered to the surface and extended processes to create networks of neurons. On uncoated substrates, the cell attachment was severely hindered for both cell types, though the reaction to CNT islands was cell-specific.

Process entanglement was shown to facilitate anchorage of neurites to rough surfaces such as CNTs (Sorkin et al., 2009) and mechanical tension acting on axons during the building of network connections contributed considerably to final network morphology (Anava et al., 2009).

Other chemical cues exist in the environment that aid cell migration and adhesion, such as the ECM (Perris and Perissinotto, 2000), as explained in the General Introduction (Chapter 1). Other than these chemical cues, mechanical cues may also exist. Surface roughness is a factor in aiding cell attachment (Curtis and Wilkinson, 1998, Gerecht et al., 2007) and the nanotopology of CNTs has been postulated to provide cues for neurite extension (Chao et al., 2009). However, CNTs were not found to provide such cues for neurite extension in hippocampal progenitor neurons, nor did cell clustering appear more prevalent around CNT islands for AHPCs. Conversely, ESCs were found to react positively to the CNT islands, migrating towards and clustering over them. Both types of cells are in the process of extending neurites to establish network connections with other neurons and both are in the presence of the same mechanical cues provided by the CNT islands, yet only one cell type (ESC) uses the CNTs as an anchor. The cells are from different developmental stages and thus will be following a separate set of intrinsically activated chemical cues appropriate to that developmental stage. This differing reaction to the same environment therefore suggests that, although CNTs can provide an anchor, the chemical influences produced by the cells may be the overriding factor here in determining migration behaviour. In short,

environmentally nanotopography can be seen to play a role here, as has been seen with mature dissociated neurons and glia seeded onto CNT islands (Anava et al., 2009, Sorkin et al., 2009), though intrinsic chemical cues may be necessary to make use of that environment (summarised in the Table 1). Cell patterning through the use CNTs is therefore dependent on cell type. This correlates with findings in the literature, where different cell types react variously to nanotopographic surfaces (Chao et al., 2009, Gabay et al., 2005a, Mwenifumbo et al., 2007, Xie et al., 2006), and both mechanical and chemical interactions were found to influence process extension and network formation (Alsina et al., 2001, Anava et al., 2009, Ayali et al., 2002, Chada et al., 1997, Distasi et al., 2002, Gabay et al., 2005a, Hua et al., 2005, Saha et al., 2008, Sorkin et al., 2006, Sorkin et al., 2009, Perris and Perissinotto, 2000).

CNTs		
Cell type	**Interaction**	**Reference**
Rat cortical neurons & glial cells	Positive	Gabay et al., 2005a
Locust ganglion cells	Positive	Anava et al., 2009
Human osteoblasts	Negative	Mwenifumbo et al., 2007
Neuronal cells		
Neuronal interaction		**Reference**
Mechanical		Sorkin et al., 2009
Mechanical & biochemical		Saha et al., 2008
Activity-dependent		Hua et al., 2005
Chemical		Perris and Perissinotto 2000

Table 1 – Comparison from the literature of cell interactions with CNTs and the types of interaction influencing neuronal cell development.

CC9-derived neurons that had migrated to form clusters were connected by dense neuritic bundles. Nanoscale imaging of a neuritic bundle revealed highly dense fasciculations of neurites, with many hundreds of processes intertwining in multiple directions and forming ropes where the target of individual connections is lost. The possible presence of connections between neighbouring neurites in the bundle adds to this complexity considerably. As mentioned before, the number of cells in each bundle could not be estimated due to the dense clustering and 3D structure; and the number of neurites in a bundle could not be estimated for the same reasons. The directionality of the connections

could not be determined. What is evident from the entangled neurites and dense cell clustering is that the connectivity between clusters is more complex than the macroscopic morphology indicates. Thus this method of patterning may have implications for intra- and inter-cluster connectivity and consequently the functional output of the networks.

In the absence of a patterned substrate CC9 cells also showed structural changes in terms of clustering during development. From 14 DIV to 19 DIV clustering went from almost non-existent to encompassing 20% of the culture area. The increase in clustering was nearly linear during this developmental stage and, given the inability to match structure with functional measures recorded directly using MEAs (see below), this unpatterned substrate behaviour was used as the comparator for all functional changes quantified in the next 3 chapters.

3.5.2 Spontaneous electrophysiology

There could be a number of reasons for the lack of unit activity detected from the CC9-derived cells on MEAs. Many researchers have recorded from neuronal cultures previously so it was not clear why this could not be the same in the laboratory in Newcastle. Viability of the cells was the first question that arose, though cell viability was confirmed through calcium imaging, so the problem was not with the health of the cells. The cells were examined at different developmental stages and staining has shown that large numbers of cells express β-tubulin III so the problem was also not likely to be due to the cells being in an undifferentiated state, or lacking the generation of spontaneous activity (as will be explored in detail in Chapter 4). Some level of connectivity within the network was demonstrated through calcium imaging (discussed below). The density of the network could affect neurite extension (Banker and Cowan, 1977) and ultimately network output, with lower density cultures displaying sparser, less organised activity (Arnold et al., 2005). The low seeding densities used with CC9 cultures may, therefore, have adversely affected network output. Both neurons and glia produce calcium transient activity (Fanelli et al., 2011, Hirase et al., 2004, Hoogland et al., 2009, Newman and Zahs, 1997), and the cell-type producing the calcium transients seen here were not precisely defined. However, the activity expressed in these cells in this thesis correlated with that of cells of the same line, cultivated using the same protocol, that were previously identified as neurons using immunocytochemistry and patch-clamp studies (see Figure 3.12). To add to this, the complex spatiotemporal patterns

of calcium transient activity seen through electrical stimulation of the cells (Figures 3.10 and 3.11) did not correlate with the typically highly regimented inter-cellular calcium transient wave propagation seen in glia (Hoogland et al., 2009, Newman, 2001, Newman and Zahs, 1997). Further comparisons with glial transients described in the literature are given in Chapter 4 where the temporal aspects of CC9-derived cell calcium transients are described.

The lack of unit activity was thus not likely to be due to the health, network morphology or the lack of a differentiated state (due to clear β-tubulin III staining), though it may potentially have related to the density of the culture or even the phenotypic state of the cell (the latter being examined in Chapter 4). It was also possible that the problem was with the interface between the array and the cells. The array was coated with PDL and laminin, suitable for CC9 cell adhesion (as demonstrated in these results and used in previously published work (Kirby et al., 2009, Trevelyan et al., 2010)) and neuronal differentiation (Luckenbill-Edds, 1997) and cells adhered well to the substrate in an uneven, but well-populated distribution across the electrode array. The coating, commonly used in dissociated cultures of cells, helps the cells remain flat on the surface and extend processes and has thus been proved as a suitable aid to gathering extracellular signals from such systems (Ban et al., 2007, Bieberich and Guiseppi-Elie, 2004, Chiappalone et al., 2006).

Another possible explanation for the lack of measurable unit activity could be the signal to noise ratio. The noise in the system was, however, down at manufacturer-quoted levels, and the threshold for spike detection was set as low as twice the standard deviation of this noise level – a level that spikes are commonly expected to exceed in such systems. So, despite signal to noise ratio being good, still no physiological waveforms were detected above threshold.

Any spikes generated would be from immature neurons, and therefore possibly slower and smaller than spikes normally detected from adult dissociated cultures. This, along with the fact that the cells involved in this study were of ~10µm diameter (smaller than the electrodes, and low density enough to allow leakage of current into the medium from spaces between cells on the electrodes), may have resulted in much smaller spikes than would normally be expected from such systems.

In addition, lack of detected activity on MEAs may have been the result of the cells not producing spikes, despite the precedence for such activity found in previous studies (Kirby et al., 2009, Trevelyan et al., 2010), either because they were potentially not neurons, or they were too young to have fast voltage-gated sodium channels.

Finally, as electrical stimulation also failed to elicit detectable spikes through the MEA electrodes (but generated very clear calcium signals) it may have been that a technical issue with the MEA recording hardware was responsible. At the time of study no comparable additional system was available to test this possibility.

3.5.3 Electrical stimulation electrophysiology and calcium signals

The lack of unit activity detected using the stimulation parameters could be due to factors mentioned in the above section, but may also relate to the particular stimulus parameters chosen. The efficacy of eliciting responses in dissociated E18 rat neocortex cells with current injection was improved by employing a biphasic stimulus rather than a monophasic stimulus, and was improved further when the negative phase preceded the positive phase (Wagenaar et al., 2004). Biphasic pulses with negative leading were used in the case of these CC9 cultures, so optimal phasic properties were employed.

Direct responses were measurable above 80µs (and the number of those responses array-wide increased up to 640µs) for the length of a stimulus phase. As explained earlier, calcium responses that could be detected by eye at the time of stimulation and recording were used to judge whether the cells had responded. 100µs per phase was employed in stimulation of CC9 cultures. Although direct responses are elicited at this duration, this is at the lower end of the scale. However, the entire pulse duration including both phases was 220µs, comfortably within the range where a number of direct responses are elicited. The stimulation provided to the CC9s was also a train of pulses, and thus the likelihood of evoking responses is greatly increased.

The amount of current injected was high, as responses could be elicited in neocortical neurons with only 5 – 20µA (Wagenaar et al., 2004). Similarly, 30µA paired pulses evoked responses in dissociated E18 rat hippocampal cells (Brewer et al., 2009). The possibility cannot be discounted that the 70 – 150µA currents used on CC9 cultures were too great and caused irreparable damage to the cells. Evidence to the contrary comes from the calcium

imaging results, which demonstrate a spatiotemporal propagation of activity in the form of calcium transients (further described below). Stimulation could be repeated to elicit further responses from the same cells, demonstrating the continued viability of these cells following stimulation.

Having used electrical stimulation to evoke calcium responses and having looked at the spatiotemporal patterns of activity produced, speculation can be made about the source of this activity. The electrical stimulus itself is very short (in comparison to time over which responses can be seen following that stimulus) and cells local to the stimulus are activated immediately, though cells at a distance from the electrode are subsequently activated and the strength of this activation is not dependent on distance from the electrode. Firstly, the responses occurring directly after the stimulus are closest to the electrode – indeed are localised to the edges of the electrode. Cells on the centre of the electrode do not respond, either at the point of stimulus or throughout the ~13s recording period. This could imply that cells directly over the electrode are not viable due to some mechanism relating to their interaction with that electrode. Alternatively, it may be owing to stronger field lines present at the edges of the electrode than at the centre, increasing the likelihood of activating cells at the periphery. The distribution of cells on the electrodes was uneven, though a high density could be seen over the stimulating electrode itself. The fact that the propagation of activity is not dependent on distance from the electrode after 2.3s, with the location of activated cells appearing to be 'random', coupled with the fact that the amplitude is also not dependent on distance from the electrode or time from stimulus, together provide strong evidence that detected calcium signals cannot all be the result of neurotransmitter diffusion away from the initial point of stimulation.

The reaction of the cells, however, is a very slow one. Synaptic transmission of single spikes occurs at very fast rates of 0.1–1 ms^{-1} (Kawaguchi and Fukunishi, 1998). Also, postsynaptic responses in new synapses (NMDA-mediated) are very slow (Cathala et al., 2003). If detected activity were from bursts of action potentials propagated via chemical synapses, transmission of activity would result from a bolus of activity in one region building a gradual post-synaptic response through temporal summation, eventually leading to burst firing (see Figure 1.10 in Chapter 1 and Figure 3.12). This would result in the effect that, in the case of non-synchronous behaviour, observed transients could not be related back to the inputs

that create them as they come from a set of much weaker signals from disparate sources. This could explain the apparent slow spread of sporadic activity seen following electrical stimulation.

An alternative source for the spread of activity could be gap junctions, which could propagate calcium activity generated intrinsically (either through membrane properties generating intrinsic bursts, or ICCR generating calcium signals). However, the slow rate of propagation is not consistent with gap junction transmission, where activity spreads away from the point of initiation (through cytosolic diffusion) at speeds of hundreds of microns per second (Yuste et al., 1995). The 'bolus' of activity that builds up from disparate sources at post-synaptic terminals, leading to the generation of events that then cannot be related to their inputs, is not a characteristic of gap junction functionality as they do not possess the phasic mechanisms of synapses and can instead be explained through fairly simplistic voltage/conductance relationships (Vogel and Weingart, 2002).

CC9s-derived neuronal cell cultures are very heterogeneous. The glial population, found as a small percentage of the cells (Kirby et al., 2009), will act to soak up neurotransmitters, terminating their action and lessening any diffusion affects that would be seen ((Barbour et al., 1991, Storck et al., 1992)). This mechanism adds to the argument that the spatiotemporal patterns of activation seen following electrical stimulation are not the result of diffusing neurotransmitters.

3.5.4 Pharmacological stimulation

Upon exogenous application of glutamate, strong, summating calcium transient responses were evoked in cells and this response was time-locked with the application of each pulse of glutamate. This fast-reacting time-locked response is typical of a neuronal response in these cells (Trevelyan et al., 2010). It is also clear from this that glutamate can stimulate as effectively as electrical current stimulations. The glutamate reaction implies that an amino acid receptor-mediated excitatory response is present and active in these cells and the same glutamate activation was shown to produce spike bursts in these cells (Trevelyan et al., 2010), though the lack of detected unit activity throws doubt over this assumption in the present experiments.

3.5.5. Summary

The results in this chapter demonstrate the ability of CC9-derived neuronal networks to be structurally influenced by surface topology, given non-adhesive substrates, far more readily than neuronal progenitor cells (HCN/GFP). Resulting networks showed dense clusters of cells over CNT islands interconnected by dense bundles of neurites. Similar clustering was seen in the absence of patterned (MEA) substrates and changed in a near-linear fashion with developmental stage. However, with the methods used, CC9-derived neurons produced no direct electrophysiological signs of function using the patterning MEA substrates as recording devices. In comparison calcium imaging showed a great many functionally viable cells.

The ability to register unit activity was compromised in these cells and given the resource and time limitations, combined with the precedents showing possible negative influences of electrode islands on cell electrophysiological viability (via extracellular short-circuiting) and the lack of hierarchical structure imposed by patterning, I concentrated on using calcium imaging to quantify activity patterns and their developmental constraints in networks generated by unpatterned conditions: *de novo* differentiated neurons have many mechanisms to influence the structure of resulting networks in an entirely physiological manner (see Chapter 1 and the Introduction to this chapter). The following chapters therefore focus on emergent activity profiles in networks allowed to form naturally, with no exogenous patterning influences.

CHAPTER 4: TEMPORAL PATTERNS OF SPONTANEOUS ACTIVITY IN CC9 NETWORKS

4.1 SUMMARY

In the previous chapter I examined the structural properties of networks of CC9-derived neurons and compared this form of differentiated culture to networks formed from dissociated neurons in culture. The interaction between these cultures and microelectrode arrays was also examined and attempts made to quantify evoked electrophysiological activity patterns in these. In this chapter I specifically focus on spontaneously occurring *temporal* patterns of activity in CC9 differentiated cultures allowed to develop in an unpatterned environment without external structural interference or stimulation. The aims of the work described below were:

To measure the basic properties of spontaneous network activity in developing CC9 cell cultures.

To quantify the change in basic patterns of network activity with structural changes within a short (hours) and long (days) timeframe.

The main findings presented are:

- Discrete, spatially localised calcium transient activity was ubiquitous in networks examined between 13 and 20 DIV.
- Mean patterns of spontaneous activity were stable over a timescale of hours despite overt changes in neuronal somatic location within the network.
- Temporal patterns of activity within active regions were highly variable over time and developmental stage, with a general increase in cell recruitment and transient rate between 16-18 DIV.
- This rate increase correlated with changes in both the kinetics (measured as full-width at half maximum amplitude (FWHM) of individual transients) and a large increase in the relationship between amplitude of fluorescence transients and the inter transient interval.

- This rate increase correlated with measures of structural clustering of neurons within the networks.
- Post 17 DIV elevated activity rates in neurons across the network began to temporally organise and display patterns of synchrony (see chapter 5 for more detailed analysis).

Taken together these data further support spontaneous activity generation as the default mode for developing neurons, now seen in CC9-derived neurons for the first time. Patterns of activity were resilient to small and relatively rapid changes in network structure, but developed – with the network – in a manner dependent on large-scale network topology (structural clustering). These data and their implications are discussed.

4.2 INTRODUCTION

4.2.1 Rationale behind using calcium imaging to study network activity in differentiated cultures.

In the previous chapter, cultures of CC9-derived neurons were grown on multi-electrode arrays (MEAs) in order to try and understand how exerting external influences on network structure affected function. I was unable to obtain an electrophysiological signature of function - extracellular spike activity - using this method. However, if such activity had been successfully measured, MEAs may not have been the most effective way to examine the spatial aspects of nascent activity development (despite their ability to influence network structure, as in the case of CNT MEAs). Firstly, the structural organization of these networks, and the development of that structure over time, cannot be fully appreciated using low density MEAs as they only examine the subset of cells within the network which locate and congregate on and around each electrode placing. Secondly, even grown on electrode arrays, the CC9 networks do not have a uniform structure, and the sparse nature of the networks result in a widely varying distribution of cells across the substrate. This distribution, as shown in the previous chapter, varies with development and the time-dependent manner of this re-structuring occurs on various time-scales, from minutes to days. The quality of this structural change that occurs during an experiment could not be discriminated using a low density MEA (as explained above due to static, localised electrodes as opposed to being able to distinguish the spatial localisation of many cells).

Given that structure and function are closely related in networks (Fan et al., 2011, Sporns et al., 2004), a method that can both spatially and temporally capture both the network activity and the quality of network structure would be favoured.

Calcium imaging provides a partial solution to the above issues as it can simultaneously measure calcium transients from large numbers of cells, often with single cell resolution, irrespective of the cells' relative position in the network. Structural information is quantifiable as there is a baseline fluorescence emitted for each cell. This activity-independent signal can be used as a marker for cell soma position within the network. On top of this baseline, activity-dependent, transient changes in somatic calcium concentration generate fluorescence changes that can be simultaneously used to quantify activity within the growing network. The source of such activity is debatable, particularly at this stage of development when the generation of spontaneous activity has been shown to depend on a variety of mechanisms including intracellular calcium release from stores or chemical or electrical synapses. Nevertheless, calcium imaging can be used to quantify spatiotemporal patterns of activity as the network structure develops making it a useful tool in the scope of this particular study.

4.2.2. Which times and time courses are pertinent to study development of nascent network activity?

In terms of the biological age of experimentally developing neurons it is useful to correlate the number of days that cells are kept in culture with their normal embryonic development to allow for some comparison between different cell lines and the various *in vitro* differentiation protocols. For example, the primary cultures in Valor's synaptogenesis/activity study (Valor et al., 2007) were E18 dissociated cells from the hippocampus. Details of the embryonic stem cells used in the following experiments are given in Chapter 1, but briefly in this context, the origin of the CC9 cells is approximately E6, which puts them developmentally 12 days behind the ones used by Valor in 2007. The CC9s can be maintained in culture for up to 20 days. In Valor's study the cells required 4 days to recover from dissociation before creating functional network connections. Following this, activity increased exponentially for 12 days before starting to plateau. In accordance with this timeline of development, if the activity were expected to correlate with the Valor study, the CC9 cells will not become active until 16 days after the start of differentiation with high

levels of activity expected at around 24 days after the start of differentiation. However, dissociated cells have already expressed a degree of mature endophenotype (depending on the time of dissociation). It is not valid to just assume that development into a 'new' network in culture in these cells follows the same timecourse as that in completely nascent neurons derived from ESCs. Earlier time points therefore need to be studied here.

To expand further on this point, the study of the development of activity in neuronal networks using standard methods such as multi-electrode arrays and calcium imaging has been successfully employed in both dissociated and *in vitro* differentiated cultures (Banker and Cowan, 1977, Chiappalone et al., 2006, Illes et al., 2007). However, in dissociated cultures in particular there is a limit on how early activity can be detected, not least because of the 3-4 days it takes for the soma to extend new processes and re-create connections with other neurons after the destruction of pre-existing connections. *In vitro* differentiated cultures develop in 'random' 2D configurations (as with dissociated cultures), but the development of neuronal processes is not disrupted at any point, unlike the situation with dissociated cultures. This facilitates the study of the development of network activity as the cells themselves develop *de novo* in a manner kept as experimentally close to the physiological situation as possible within such a reduced model system. With mature cells, many initial contributing cellular factors in network formation have already changed as the cells developed outside the culture. With a dissociation and reformation of an already mature, or maturing network there may therefore be a different set of governing factors contributing to the resulting activity patterns seen. *In vitro* differentiated cells, in contrast, have never been subjected to such damage and so the network forms undisturbed from the start in the conditions provided (details in Chapter 2), alongside cell development thus providing a more physiological model of nascent network formation in neuronal tissue.

Concerning electrophysiological measurements of developmental changes, most analyses are suited to data populated by large numbers of extracellular spikes (units) and previous studies have thus explored the behaviour of networks after the onset of significant levels of this kind of activity (Arnold et al., 2005, Heikkilä et al., 2009, Illes et al., 2009, Ito et al., 2010). Early activity (starting before the times explored in the above references), however, may impose an effect on the development of later patterns of activity in the network and early forms of cell activity may govern the network connectivity that follows. Activity is also likely

to be governed by different mechanisms at earlier stages of development due to, for instance, the changes that occur in receptor expression at the cell surface in different cell compartments. Exploring the onset of different hierarchies of activity and determining the temporal landscape of such events is essential to a fuller understanding of the changes and development of functional output in neuronal networks.

A knowledge of the relevant timeframes of molecular mechanisms behind developing network activity is very much a moving frame of reference in cultures where the neurons are still differentiating. This dynamic aspect of the development of activity is a fascinating complexity, the unravelling of which could tell us much about both the stable, adult system behaviours and how the system can be perturbed to achieve the many permutations of this activity.

4.2.3 Factors contributing to development of spontaneous activity in nascent neuronal networks.

Both neurons and glial cells are present in development, and produce various types of spontaneous activity. Radial glial cells are expressed transiently during neuronal development and are precursors for cortical pyramidal neurons. These glia produce spontaneous calcium waves that aid proliferation and possibly structural organization in the cortical ventricular zone. These waves are mediated extracellularly through metabotropic ATP receptors and their propagation is aided through gap-junctions. The half-width of such waves are in the range of 10s of seconds and they propagate outwards from the site of initiation. The dynamics of these waves changes with development, involving more cells and propagating further between E13.5 and E16 (Weissman et al., 2004), though glial calcium transients can be much shorter (Hoogland et al., 2009, Reeves et al., 2011). Spontaneous calcium transients generated by astrocytes differ between regions with transients lasting 10s to 100s of seconds and showing a variety of shapes and frequencies (Aguado et al., 2002). In retinal glial cells, calcium waves dependent on release from intracellular stores could be seen to propagate radially out from the site of initiation with the length of the transient produced by the cell lasting from 10 to many 10s of seconds (Newman, 2001, Newman and Zahs, 1997). Diffusion driven calcium waves that propagated radially from the initiation site (and were reversibly blocked by ATP receptor antagonists) were also seen in Bergmann glia in the rodent cerebellar cortex (Hoogland et al., 2009).

The appearance of astrocytes in development coincides with synaptogenesis in neuronal cells and is thought to play a significant role in the development of synapses (Ullian et al., 2004, Ullian et al., 2001). Calcium transients have been directly associated with neuronal activity, with hippocampal organotypic cultured astrocytic networks displaying calcium waves following neuronal glutamatergic synaptic activity (with latencies of around 2s) (Dani et al., 1992). Astrocytic processes that entangle interneuron processes have been shown to modulate synaptic activity through intracellular calcium release in the astrocyte. Calcium uncaging lead to cascade reactions involving glutamate release that, acting on group II/III metabotropic glutamate receptors (mGluRs), reduced the release of GABA, thus reducing the size of evoked IPSCs (Liu et al., 2004). This caused a decrease in interneuron excitability and thus a decrease in the inhibitory input to CA1 of the hippocampus. Such neuron-glia interactions are further evidenced in the hippocampus. Glutamate from Schaffer collaterals affect calcium elevations in astrocytes via mGluRs. The functional consequences of these calcium elevations are frequency dependent and bidirectional with astrocytes being capable of distinguishing different inputs and integrating their information (Perea and Araque, 2005). Thus glial cells can generate calcium transients alone, influence neuronal activity and be influenced by neuronal activity.

The development of spontaneous activity in nascent neuronal networks has been observed *in vivo* and *in vitro* and can take different forms. Here, somatic activity is described, and this will be followed by a description of dendritic activities. Before synapse formation, early activity seen in embryonic *Xenopus* spinal neurons takes the form of calcium spikes and waves (Gu et al., 1994). The calcium spikes are produced by calcium-dependent action potentials and occur infrequently at 1-10hr^{-1} and propagate through the network via gap-junctions, affecting small clusters of cells. They have a characteristic sharp onset and rise lasting 1s and a biphasic decay lasting 10s. Their function has been linked to neurotransmitter, gap junction and ion channel expression and blocking them impairs neuronal differentiation (Gu et al., 1994). They are intrinsically involved in control of gene expression through cAMP response element (CRE) and its binding protein, along with many calcium-dependent protein kinases (Hardingham et al., 1998). They are also critically important for neurite extension, axogenesis and subsequent synapse formation (Dent et al., 1996, Franze et al., 2009, Lautermilch and Spitzer, 2000). By activating muscarinic

acetylcholine receptors in the developing rat neocortex, calcium waves are seen to propagate at speeds of 50–300µm/s across millimetres of the slice and such activity is only seen up until P6 (Peinado, 2000). Such activity has been associated with both proliferation and differentiation of neuronal progenitors in dissociated cultures of neural stem cells from E11 rats (Zhou et al., 2004).

Propagating calcium signals also occur in dendrites. These smaller signals travel around 50µm at 70µm/s and occur through the release of intracellular calcium from stores (Putney, 2003) following either synaptic activity, metabotropic glutamate receptor (mGluR) activity or back-propagating potentials. Release of calcium from intracellular stores is predominantly through the activation of IP3 receptors (for instance, due to IP3 production from mGluR activation, or directly from Ca^{2+}) on the smooth endoplasmic reticulum (ER), but can also be similarly activated through ryanodine receptors (Augustine et al., 2003). Activation of muscarinic acetylcholine receptors in hippocampal pyramidal neurons by trains of action potentials (or exogenous application of a muscarinic agonist) provides a pathway to the release of calcium from intracellular stores resulting in large calcium transients and increased excitability (Power and Sah, 2002). In individual cells, calcium waves propagate to neighbouring compartments through calcium-induced calcium release (CICR). Regional calcium signals that do not propagate, but extend only a few micrometers at best, are also common (Augustine et al., 2003). In dendritic spines, calcium signals are similarly created through ligand-gated calcium channels (LGCC), voltage-gated calcium channels (VGCC) or release from intracellular stores, however, the Ca^{2+} itself appears to be compartmentalised in the spine and does not flow to the neighbouring dendrite. Other molecules, such as IP3, can still enter the dendrite from the spine.

Spatiotemporal organisation of calcium transients in networks also contributes to the generation of calcium waves. These are produced through calcium-induced calcium release in the growth cones, are of longer duration (~30s) with the same low frequency occurrence ($1\text{-}10hr^{-1}$) and are also associated with neurite extension. This type of activity has also been confirmed in differentiating murine crest cells (Carey and Matsumoto, 1999), where lineage tracing showed that the activity was present in cells that gave rise to clones containing neurons, whereas inactive cells did not and the activity was only present during neurogenesis (7 days in culture).

In the mammalian neocortex, spontaneously occurring calcium transients, synchronous across a small sub-population of cells, can be distinguished in small neuronal domains (~100μm) (Yuste et al., 1995). These events are synchronous across the subpopulation; they propagate through gap-junctions and are initiated at a 'trigger cell', so named as it appears at the initiation of the event (see data and discussion on 'hub' neurons in chapter 5), but the mechanism of activation is not clear (Yuste et al., 1995). Factors that could influence such initiation will be discussed in more depth in the next section. Gap-junctionally connected cells in the embryonic neocortex were found to form into groups of 15-90 cells (Lo Turco and Kriegstein, 1991). These columns of cells form in the ventricular zone, but the number of cells so connected decreases as they migrate from the area. Gap-junctional subunits (Cx26 and Cx43) form adhesive contacts involving internal cytoskeletal elements to aid migration (Elias et al., 2007).

Once chemical synapses have started to form, early network activity appears as synchronous events involving large populations of cells. This can be seen, for example, in developing spinal neuronal networks in the chick embryo (O'Donovan et al., 1998) initially as large depolarizing events that become increasingly complex involving synchronous activity, followed by delayed neuronal discharges (O'Donovan and Landmesser, 1987). Early spontaneous network activity also appears in the developing rat hippocampus as giant depolarizing potentials (GDPs) (Ben-Ari et al., 1989). GDPs involve glutamatergic and GABAergic network interactions and are only present for a short postnatal period (up to postnatal day 7 (P7) in the rat hippocampus). They can be blocked by TTX, NMDA antagonists and bicuculline (GABA antagonist) as GABA is depolarizing at this stage in development (more on GABA in developing neurons in a later section).

It is the interplay between GDPs, GABAergic and glutamatergic connections that result in early network oscillations (ENOs) observed as synchronous, periodic calcium transients in 100's of pyramidal cells and the interneuron network in the rat neonatal hippocampus associated with bursts of action potentials (Garaschuk et al., 1998). They are also seen in a highly laminar-specific fashion in developing neocortex (Dammerman et al., 2000). ENOs occur at a rate of 0.4-2min^{-1} before P5 and far more frequently (up to 15min^{-1}), but with decreasing amplitudes, after P5 (rat hippocampus). Mechanisms for the generation of such spontaneous activity appears to be network driven and involve recurrent, excitatory

connections providing positive feed-back, emphasized by the presence of the excitatory action of GABA early in development. The cellular mechanisms behind the homeostatic maintenance of such activity are described in more detail in the sections below.

The developing retina produces spontaneous activity in the absence of light stimulation. This was first observed as periodic bursts of action potentials in retinal ganglion cells (RGCs) in the neonatal rabbit retina (Masland, 1977). Since then, such activity has been found in a variety of species and following various developmental profiles (Fischer et al., 1998, Grzywacz and Sernagor, 2000, Wong et al., 1993, Sernagor et al., 2003, Sernagor and Grzywacz, 1999). The suggested roles of such activities include the development of retinal receptive fields and retinogeniculate connectivity and the refinement of retinotopic maps (Sernagor and Mehta, 2001, Lee et al., 2002, McLaughlin et al., 2003).

In mammals the development of this spontaneous activity can be split into three stages (Bansal et al., 2000). In stage I, before the onset of synaptogenesis, spontaneous waves of activity propagate via gap-junctions. In mouse, the waves appear at E16 and their generation does not require chemical synapses (Bansal et al., 2000). At P0-P7 they have been seen to propagate from random locations across the retina and result in 25-35s refractory periods during which new waves cannot invade that part of the retina. In the chick retina, these waves can be seen from E8 as calcium transients with fast onset and slow decay (lasting 20 – 30s) with 1 minute inter-event intervals (Catsicas et al., 1998). Appearing before synapse specialization they require voltage-gated sodium channels and rely on calcium intake, rather than release from stores.

At stage II, around P0, starburst amacrine cells start to form nicotinic cholinergic connections (both recurrent and with retinal ganglion cells) (Masland and Tauchi, 1986), and this is how retinal waves are mediated at this stage, although later stage II retinal waves (from around P4-P5) are also mediated by GABAergic and glutamatergic synaptic transmission. Somatic GABA responses at this stage are depolarizing and shift to hyperpolarizing at P6-P7 becoming functionally inhibitory in their modulation of retinal waves (Bansal et al., 2000, Sernagor and Grzywacz, 1999, Sernagor et al., 2003). Cell intrinsic activity is responsible for the initiation of these events, originating in starburst amacrine cells, with strong bursts riding on a large depolarization in these cells during the

propagation of a retinal wave. This is followed by a slow afterhyperpolarizations (AHP) (mediated by a calcium-dependent potassium current) that can last 10s of seconds, with the length of the AHP increased during the large calcium events associated with a retinal wave (as compared with AHPs following cell intrinsic bursts) (Zheng et al., 2006).

Stage III waves appear at ~P11 in mice and are marked by the change from acetylcholine-mediated to glutamate-mediated (Bansal et al., 2000). The profile of this transition varies across species, happening abruptly in chick involving NMDA and AMPA/kainate receptors and with both neurotransmitters necessary almost throughout in turtle and AMPA/kainate constituting most of the glutamate contribution (Sernagor and Grzywacz, 1999, Sernagor et al., 2003, Wong et al., 1998).

In vitro work and computational models dealing with central pattern generation in motor systems have shown that the generation of such network activity can emerge on a network level from modulatory interneuron connections and on a cellular level can be homeostatically controlled by neuromodulatory substances (Marder and Thirumalai, 2002, Weimann and Marder, 1994). Neuromodulation can be intrinsic (Katz and Frost, 1996) (originating from cells within the circuit) or extrinsic (from a source external to the circuit) and many neuromodulators can be in effect at one time. Neuromodulators can dynamically influence the synaptic conductances and the effects of these substances can be seen as changes in the activity patterns produced and in the frequency of those patterns. The influence of a neuromodulatory substance can vary among different neurons and depend on the developmental stage (Fénelon et al., 1999, Marder et al., 2005). For instance, homeostatic control of retinal wave activity is present during development, allowing the network to maintain certain network dynamics with GABA-signalling implicated in these compensatory mechanisms (Hennig et al., 2011).

Neuromodulation of ionic currents can occur through secondary messenger systems such as phosphorylation and dephosphorylation through cyclic aminomonophosphate (cAMP) pathways (Levitan, 1994). In synapse development the fasciculation process, mediated by transmitters such as serotonin, effects the broadness of the presynaptic potentials and increases firing rate and the amount of transmitter released during an action potential (Klein et al., 1986). Calcium is involved ubiquitously in cell signalling processes, and

naturally there is an inherent interaction between neuromodulatory mechanisms and calcium. For instance, the effects due to cAMP on increasing neurotransmitter release and synaptic activity can be antagonized by intracellular calcium to suppress inwardly rectifying K^+ currents and decreases the sensitivity of voltage-gated calcium currents (Kramer and Levitan, 1990). Calcium signalling in astrocytes has been shown to affect glutamate release and subsequently modulate synaptic transmission (Parpura and Haydon, 2000). And modulation of voltage-dependent calcium channels by neurotransmitters such as norepinephrine has been shown to have differing effects in different cell types in rat sympathetic neurons (Chen and Schofield, 1993).

Neurons can be classified according to their firing patterns: regular spiking (RS), fast spiking (FS), intrinsically bursting (IB), fast repetitive bursting (FRB) and low threshold spiking (LTS) (Connors and Gutnick, 1990, Contreras, 2004). They exhibit these behaviours following current stimulation, independently of synaptic input, due to their intrinsic membrane properties. In terms of the resulting effects on calcium dynamics, bursts of action potentials generate large calcium transients owing to the sustained depolarization accompanying them (Chiang and Strowbridge, 2007). In turn, calcium entry feeds back positively onto membrane conductances to further promote bursting (Rubin et al., 2009). These patterns were identified in mature neurons and they provide examples of the diversity of activities that a cell can generate. The potential for the generation of such activity as trains of action potentials, with some cells exhibiting strong spike-frequency adaptation, has already been demonstrated in developing CC9-derived neurons with somatic current injection (Kirby et al., 2009).

4.2.4 Conductances important for organisation of single-cell spontaneous activity into network activity.

Co-ordinated, network activity can be driven by either chemical or electrical synapses; the former providing phasic transmission through a variety of potential excitatory and inhibitory mechanisms, and the latter allowing the transmission of ionic signals between such interconnected cells. The mechanisms of these two means of propagation are here described, with reference to their developmental relevance.

While combinations of opposing conductances can generate spontaneous activity in single cells (Hutcheon and Yarom, 2000), the temporal pattern of such activity is exquisitely sensitive to 'noise'. The noise in neurons within a network usually takes the form of synaptic inputs. A single type of synaptic input can provide diverse postsynaptic effects when interacting with a single intrinsic conductance. For example hyperpolarisation-activated conductance, I_H, can be activated in different ways with contrasting effects (Bender and Baram, 2008). Namely, in adult neurons, during hyperpolarisation induced by GABAergic inputs, I_H results in an increase in conductance that causes a depolarization 'sag' (opposing IPSPs) leading to rebound activity. Conversely, the same mechanism can reduce excitation by reducing membrane resistance to K^+ and Na^+ (i.e. increasing the conductance) during the summation of EPSPs, consequently lowering the summation effect. Its effect is seen when the membrane potential is close to or negative to the resting potential and is mediated by hyperpolarization activated cyclic-nucleotide gated (HCN) channels that are permeable to Na^+ and K^+. This current can either reduce or increase excitability depending on the form of HCN channels present and the particular input; it utilizes both the opposing forces on membrane potential and the membrane conductance to regulate intrinsic excitability.

The involvement of I_H in the regulation of interburst intervals has been demonstrated in the neonatal hippocampus on interictal bursts (Agmon and Wells, 2003). Blocking I_H resulted in an increase in interburst intervals, along with an increase in the distribution of intervals. Interestingly, the developmental profile of HCN channels implies that they have a specific involvement in neuronal differentiation and early network activity (Bender et al., 2005). As already stated, GABAergic inputs generate hyperpolarizations that activate HCN channels. In developing neurons, such GABAergic inputs (often depolarizing) are necessary for GDP generation (see General Introduction). The localized expression of various HCN channels differs dramatically among cell compartments and immature and mature neurons, and their effect on network activity is evidenced in the localisation and timing of GDPs in hippocampal development. HCN1 channels are expressed early in hippocampal development and blockade of these channels significantly reduces GDPs (Bender et al., 2005), demonstrating their presence and role in early activity generation.

In thalamic reticular (RE) neurons (a component in sleep spindle oscillations of the thalamocortical system), both tonic firing and bursting are possible outputs, depending on

the membrane potential and I_T (see previous section). Background synaptic input to these cells (from excitatory afferents and reciprocal connections between RE neurons) modulates their output through a massive increase in membrane voltage fluctuation. This leads to the generation of spindle oscillations and is a demonstration of how activity-dependent synaptic input can generate spontaneous bursting activity in conjunction with intrinsic membrane properties (Fuentealba and Steriade, 2005).

Other methods of maintaining network rhythms come from a combination of network, intrinsic and metabolic mechanisms. In the case of transitions between 'up' and 'down' states in slow-wave oscillations, where the bistability is maintained through recurrent excitation and local inhibition (interacting with the persistent Na^+ current, I_{NaP}), intrinsic metabolic demands of the system were also found to influence the transition from 'up' to 'down' states through metabolic-sensitive ionic currents (Cunningham et al., 2006).

In addition to the development of chemical synaptic machinery, gap-junctions play an important role in the early establishment of cell-cell communication. Conductance through these junctions differs from the phasic action of synapses in that they allow the bidirectional diffusion of ionic species between cells. Although conduction through these channels can depend on the phosphorylation state of channel proteins and also be voltage-sensitive (Moreno et al., 1994, Rozental et al., 1998), gap-junctions do not display the complex interplay between different conductances found in chemical synapses. Gap junctions are present before the development of chemical synapses and this coupling diminishes (but remains present) as neuronal progenitor cells differentiate, as was shown with E18 rat hippocampal progenitor neuroblastomas (Rozental et al., 1998) as cultures treated with bFGF, TGFα and IL-7 (cytokines important in neuronal development) had smaller junctional conductances than untreated cultures. Specific connexins are expressed differentially in development, showing a complex pattern of expression over embryonic and neonatal periods in the rat neocortex (Nadarajah et al., 1997). Between E12 and E19 the expression of Cx43 was up-regulated to E16, followed by a drop in expression at E19. Cx26 followed the same trend, though larger numbers of this connexin were present overall. After birth, Cx43 is strongly up-regulated and Cx32 is introduced, though Cx26 has almost disappeared by P21. Propagation of early neuronal activity through gap junctions was shown in the developing neocortex where gap junctions allowed the synchronization of calcium activity

across subpopulations of neurons (Yuste et al., 1995). This activity can persist in the presence of TTX and is intrinsically generated, thus synaptic equipment is not necessary for the generation or propagation of some forms of early network activity.

From the above it is clear that a great many transmembrane conductances can interact to generate patterns of activity, such as rhythmic bursting, seen in neurons. The developmental sensitivity of so many of these conductances suggests a system which is in fine balance, but with that balance changing with developmental stage. Thus, by observing calcium transients it is possible to focus primarily on one aspect of cellular and network behaviour and follow its genesis and modulation during the establishment and refinement of early networks.

Previous work on CC9s has focussed on patch-clamp experiments and single-cell calcium imaging with few recorded paired events. Therefore, the ability of CC9s to show propagating activity, or any larger scale population activity has yet to be determined. Elucidating aspects of nascent neuronal network activity is made easier by the ability to culture these cells in low density populations on glass coverslips and follow their development over a period of 20 days.

4.3 METHODS

The specific details of the protocols are provided in the Methods section. The following procedures are modification specific to the data in this chapter.

4.3.1 Cultures

Oregon Green BAPTA-1 AM dye was used for all calcium imaging experiments and signals from low-density networks of immature neurons were characterized using ImageJ and custom MATLAB scripts.

CC9 cultures that had undergone the 8-day embryoid body differentiation protocol were maintained for up to 20 days *in vitro* (DIV) on glass coverslips. At 8 DIV the cells are allowed to adhere to the coated glass substrate and at 10 DIV all proliferation factors (known to stifle differentiation) are removed from the medium. Before 13 DIV the cells are highly motile and still migrating over the substrate to form more stable clusters. All results reported here are taken between 13 DIV to 20 DIV.

In the following calcium imaging experiments, the term 'activity' refers to detected calcium transients occurring in individual regions or interest (ROI). These transients, as explained in the introduction, have been shown to correlate best with burst activity in these cells. The degree of pre- and post-processing of the data (to remove baseline drifts and increase signal to noise) precludes the direct comparison between transient signal amplitudes and absolute calcium levels. However, comparison between ROIs within a given culture, and between cultures for each individual experiment, are still valid. In addition, ROIs usually pertain to single cells where significant changes in intracellular calcium were detected. There are occasions when ROIs cover multiple cells due to the high calcium intensity changes overlapping neighbouring cells and high density of cell bodies in structural clusters within the network. Wherever possible, this was corrected manually, but nevertheless, there are some ROI's that unavoidably refer to multiple cells that have adhered to each other. An absence of activity was characterized as no change in fluorescence intensity above the background intensity for that cell.

This activity could be quantified in terms of its rate of occurrence, frequency distribution and an approximation of the kinetics of the transient measured as its full width at half of its amplitude (FWHM). All details of the development of analysis tools have been provided in the Methods (Chapter 2).

4.3.2 Network Organization

Somatic movement was measured using the baseline fluorescence emitted by the cells as a location for the cell soma to create a series of time-lapsed images. Images could be overlaid to allow the direct comparison of soma location between two time-points.

Cell migration over a series of days in development was expected to change the distribution of cells on the surface (the appearance of structural 'clustering') and so the structure of the network. In order to characterize this, two stages of development were chosen (15 and 18 DIV, n = 5 for each day) for comparison. An 8x8 grid was applied to an image of the culture. Cells were counted in each grid square and recorded in order to create a distribution of cell numbers on the surface. Clustering of cells made this process unwieldy, and so a second method was also applied by counting the percentage of grid squares that contained a cell cluster (defined as an area of cells that had clumped to a degree where individual cells could

no longer be distinguished) to create a clustering distribution (used to derive the boxplot in Figure 4.7).

4.4 RESULTS

4.4.1 Appearance of activity and rapid network organization

The quantification of calcium activity in CC9's was examined on two temporal time-scales. The stability of the experimental set-up was confirmed by observing changes over a period of hours, considering environment changes at the start of the experiment and the fact that CC9 network structural changes occur within this time frame. Significant developmental trends were explored by comparing activity over a period of days as the CC9 cultures continue to differentiate and structurally evolve. Though initially, 'activity' needed to be defined in the context of these experiments.

The calcium events detected in the neuronal cells derived from CC9s are all from the cell soma. The baseline activity was highly variable between cultures and over the recording time (usually 160-200 mins), and although a threshold was manually selected for each recording only events exceeding, at minimum, twice the standard deviation were considered. The information content of the variable baseline activity was not assessed and was treated as noise originating either from incompletely resolved, random single spike activity, physiological slow-timecourse changes in baseline cytosolic calcium concentration (see section 4.2.3) and/or methodological issues relating to light source stability and dye behaviour. Nevertheless, discrete calcium transients were readily observed in a proportion of developing neurons in each culture. The number of neurons displaying transients was always less than those with detectable baseline calcium levels (see Figure 4.1B & C), but these transients were of sufficient magnitude to be easily distinguished from both fast and slow 'noise' sources (Figure 4.1D), making their quantification in terms of amplitude and full width half maximum time (FWHM) reasonably straightforward (Figure 4.1E).

The first activity was noticeable as early as 11 DIV and consisted of highly infrequent, discrete, non-synchronous events, where only a single region would be active in any single 600 second recording epoch displaying either a single transient or a train of transients of varying amplitude and interval. These transients were not rigorously characterized, due to their rarity and the difficulty in tracking them, as the cells in cultures younger than 13 DIV

were highly motile. An example of such motility is given in Figure 4.2. The cells' somatic movement was non-linear and they could move more than a cell diameter (~20µm) per minute at some points in the recording period, but become stable for many minutes in others. Movement was always along neurites. It is the somatic compartment of cells that constitute the source of detectable baseline levels of calcium and calcium transients associated with activity. Thus, somatic translocation necessitates a near frame-by-frame registration of regions of interest. The change in speed of somatic translocation with development between 11 – 20 DIV are shown in Figure 4.2, with the highest movement on 11 DIV (7.1±1.0 µmmin^{-1}) and an asymptotic approach to near-zero movement (0.4±0.1 µmmin^{-1}) by 17 DIV ($P < 0.05$).

4.4.2 Activity across a time-scale of hours

During an experiment there was a gradual decrease in activity levels (measured as the occurrence rate of calcium transients) over the first 40 minutes (Figure 4.4) from 16±8 to 7±4 (N = 4) transients per minute. After 40 mins the activity levels remain fairly consistent, though activity fell further to 60 minutes in older cultures At 60 minutes, in recording conditions, the activity was constant at 2±1 and 7±3 transients per minute for younger (<17 DIV) and older (>=17 DIV) cultures respectively. The basis for this choice of grouping over developmental period for the cultures (into young and older) was entirely based on this dramatic increase in transient rate per ROI, and also the equally dramatic increase in number of active ROIs seen per culture (see Figure 4.7C below).

The transient full width half maximums (FWHMs), describing the kinetics of the calcium transient, and thus the underlying bursting behaviour, did not vary significantly over the length of an experiment overall. However, analysis of FWHM over each recording period, pooled for each DIV number, suggested a change in the FWHM measure over these short time periods preferentially at developmental stages below 16 DIV (Figure 4.5A). Above 16 DIV the FWHM property of the transients was remarkably stable over the recording periods used (up to 200 minutes, Figure 4.5A). Pooling data within the earlier (13-16 DIV) and later (17-21 DIV) stages of development also suggested a change in FWHM over a timecourse of ~100 minutes only evident in the later developmental stages (Figure 4.5B). Over 180 minutes in younger cultures FWHM changed from 6.14±0.07 to 6.04±0.02 whereas in older cultures FWHM started at mean lower values and increased over this timecourse (4.74±0.09

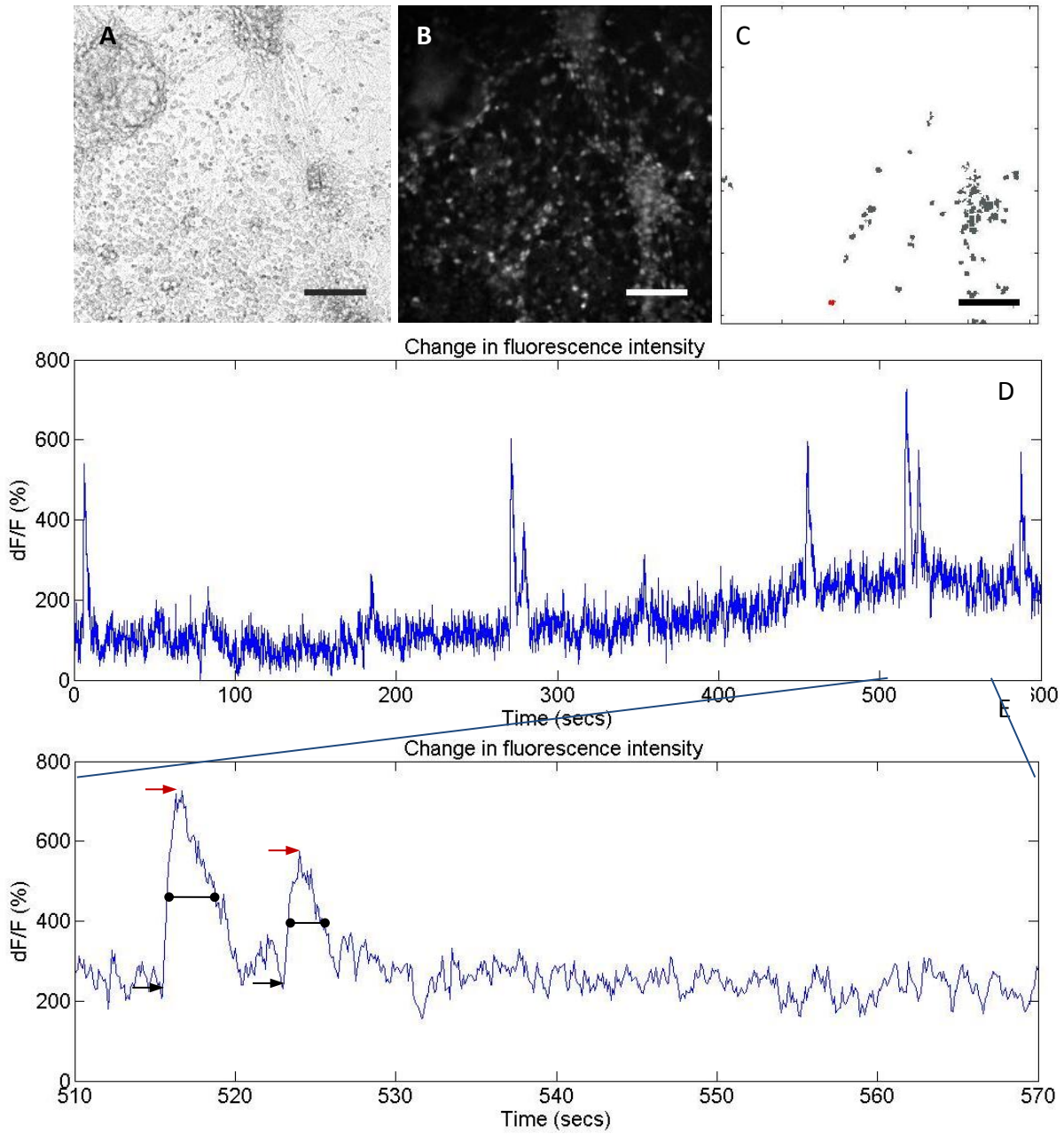

Figure 4.1 – Typical shape of spontaneous calcium transients recorded from a single ROI and the measures used to describe the transients. This example has been taken from an 18 DIV culture. **A)** Bright field image of area of culture over which calcium imaging was performed. **B)** Resting calcium fluorescence intensity in A after staining the cells with OGB-1. **C)** ROI map of active regions during a 600 second recording, determined by finding regions from the fluorescent image where changes in intracellular calcium were observed. Scalebar = 100µm for A-C. **D)** Changes in calcium fluorescence intensity in the region shown in red in B after pre-processing to subtract the background and smooth the signal (the effects of such processing are shown in detail in the methods section). **E)** 60 seconds of D expanded to show the characteristic transient shape and the main measure used to quantify this: the full width half maximum (FWHM) (line). The location of the onset (black arrows) and the peak (red arrows) are also shown.

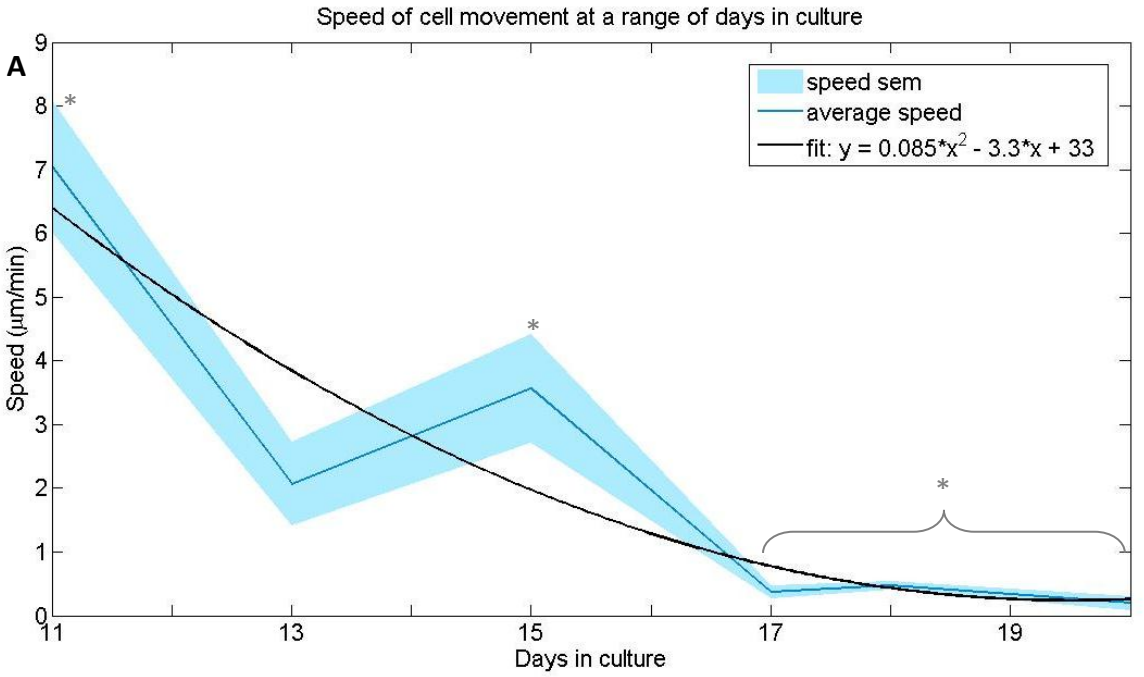

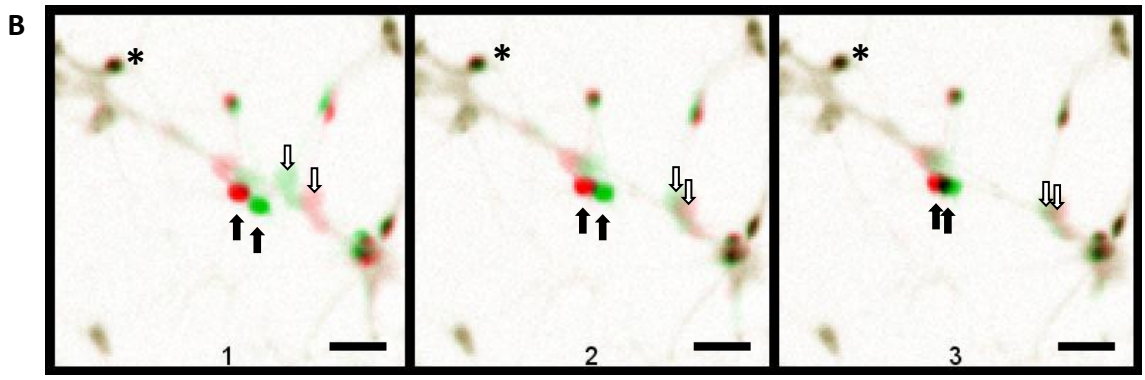

C

Symbol	Cell	Min	Speed (µm/min
⬆	1	1	17
		2	15
		3	9
⇩	2	1	25
		2	11
		3	6

Figure 4.2 – Quantification of the movement artefact seen in cultures during time-lapse recording. A) Mean speed of somatic movement from a selection of moving regions across a range of days in culture (n – 8 for each day). Blue shaded region represents the SEM. Quadratic fit shows an asymptotic approach to zero movement. (*P = 0.05.) **B)** Example of the cell movement in an 11 DIV culture. Each image is an overlay of two fluorescence intensity images from 1) 0 and 1 mins, 2) 1 and 2 mins and 3) 2 and 3 mins that show the start (green) and finish (red) position of the cells for that minute. Hence, superposition of the red and green (before and after) images results in **black when there is no movement** (e.g. cell marked with an asterisk). Cell 1 (filled arrow) and cell 2 (unfilled arrow) can be seen moving in **opposite directions** (with green on the right for one cell and on the left for the other cell (moving along the diagonal neurite) at the speeds given in the table for the 3 consecutive minutes. Speeds were ascertained by calculating the start and finish positions of the centroid of the cell. In 1 minute (6^{th} of a standard recording period) the cell soma can move more than the width of its soma, and its speed is variable. Movement of cells in a particular location usually occurs over a fraction of the recording period, not the entire length. Scale bar = 20µm.

to 6.89±0.15). The amplitude of each transient was far more variable than the FWHM measure in all conditions (Figure 4.6A,B). At individual DIV numbers, mean amplitudes could vary as much as two-fold over the short timecourse of a single recording period (Figure 4.6A). Pooling data into young (13-16 DIV) and older (17-21 DIV) revealed little developmental difference over either short or long epochs (Figure 4.6B). While mean amplitudes appeared smaller and less variable in older cultures there was no statistical difference detected over 160 seconds in the recording rig. Over 160 minutes in younger cultures amplitude changed from 70±8 to 135±18). In older cultures amplitude started and finished at mean similar values over this timecourse (70±8 to 62±10).

4.4.3 Activity development across a time-scale of days

Example traces of all active regions from a selection of recordings have been given in Figure 4.3 to provide a qualitative demonstration of the difference between activities at three stages of development: 14, 15 and 18 DIV cultures. The main changes were a dramatic increase in rate and incidence of transients across the developing network, leading to the establishment of near network-wide, repetitive synchronous events at later developmental times. A quantification of the visibly overt differences seen across a range of developmental days is now given in this section.

The times chosen flanked and encompassed the time period where the largest change in network structure was apparent. In CC9-derived neuronal cultures, clustering of ROIs/cell bodies was evident when comparing pre-17 DIV ages with post 17 DIV ages (Figure 4.7A). In the example illustrated neurons can be seen to change from being near-uniformly distributed across the visible culture area (Figure 4.7Ai) to forming clear clusters of neurons (Figure 4.7Aii). Quantification of this structural reorganisation by counting areas with multiple ROIs (see 4.3.2 above) revealed a near 6-fold increase in clustering. Pooled data from 15 DIV showed 3% (IQR: 0–6%) of areas fulfilled the clustering criteria used. At 18 DIV, pooled data showed 18% (IQR: 15–24%) of areas contained clusters ($P < 0.05$, Figure 4.7Aiii).

The rate of transient occurrence for any region of interest demonstrated an increasing trend from 14 DIV to 20 DIV with 14 DIV and 18 DIV cultures averaging 0.26±0.15 and 0.78±0.22 transients per minute respectively ($P < 0.05$, Figure 4.7B). The number of ROIs/cells found to be active in a 10 minute recording across a range of days in culture increased near 10-fold

up to 18 DIV (Figure 4.7C) with 14 DIV and 18 DIV cultures averaging 2.65±0.5 and 22.02±3.59 transients per minute respectively. After 18 DIV the activity levels were seen to dip, but remained higher than those seen at earlier developmental periods overall. These increases in activity per region and number of active regions were seen over the time periods which were co-incident with network stabilization (a near absence of somatic translocation) and structural organization (clustering) (Figure 4.2 and Figure 4.7A).

These data suggested that high activity levels corresponded to clustered distributions of cells once the clusters had stabilized (i.e. stopped migrating across the substrate).

The FWHMs were averaged over all FWHM data across the time-course of an experiment (see Figure 4.5) for each day to produce overall averages (see Figure 4.7D). The FWHMs were most variable for young cultures (DIVs 13-16) and became marginally briefer over developmental stage, with a mean of 7.1±1.1s for the earlier time period and a mean of 5.8±0.7s for the later time period (17–21 DIV). The lowest FWHM can be seen on 18 DIV at 4.7±0.6s, a significant decrease in transient duration, which temporally corresponded with peak incidence of active ROIs (Figs 4.7C & D). However, the overall shape of the calcium transients (quantified as FWHMs) did not alter to anywhere near the degree seen for the rate and incidence measures (above).

As quantified previously (Figure 4.7D), mean FWHM varied slightly over the developmental period studied. However, a more detailed quantification of this value revealed an apparent peculiar transient developmental signature around 17 & 18 DIV (Figure 4.8). Plotting the overall distribution of FWHM measures for each DIV number confirmed the tightening of the distributions as cultures developed (a trend to more stereotyped calcium transients as network behaviour becomes more organised). At 17 DIV the presence of a plateau of incidences of faster calcium transients can be seen in addition to the robust modal value of 6-7 secs FWHM. At 18 DIV this plateau was seen to be more loosely distributed. In some cases growing a distinct, additional modal peak in FWHM distribution. In these cases, at this developmental time point two distinct types of calcium transient were observed in 4/16 cultures, one with the near-ubiquitous modal peak of 6 secs and a second with a modal peak of 2.8 secs. The possible significance of the transient occurrence of these faster events at this developmental stage was analysed in more detail. Figure 4.8 shows an

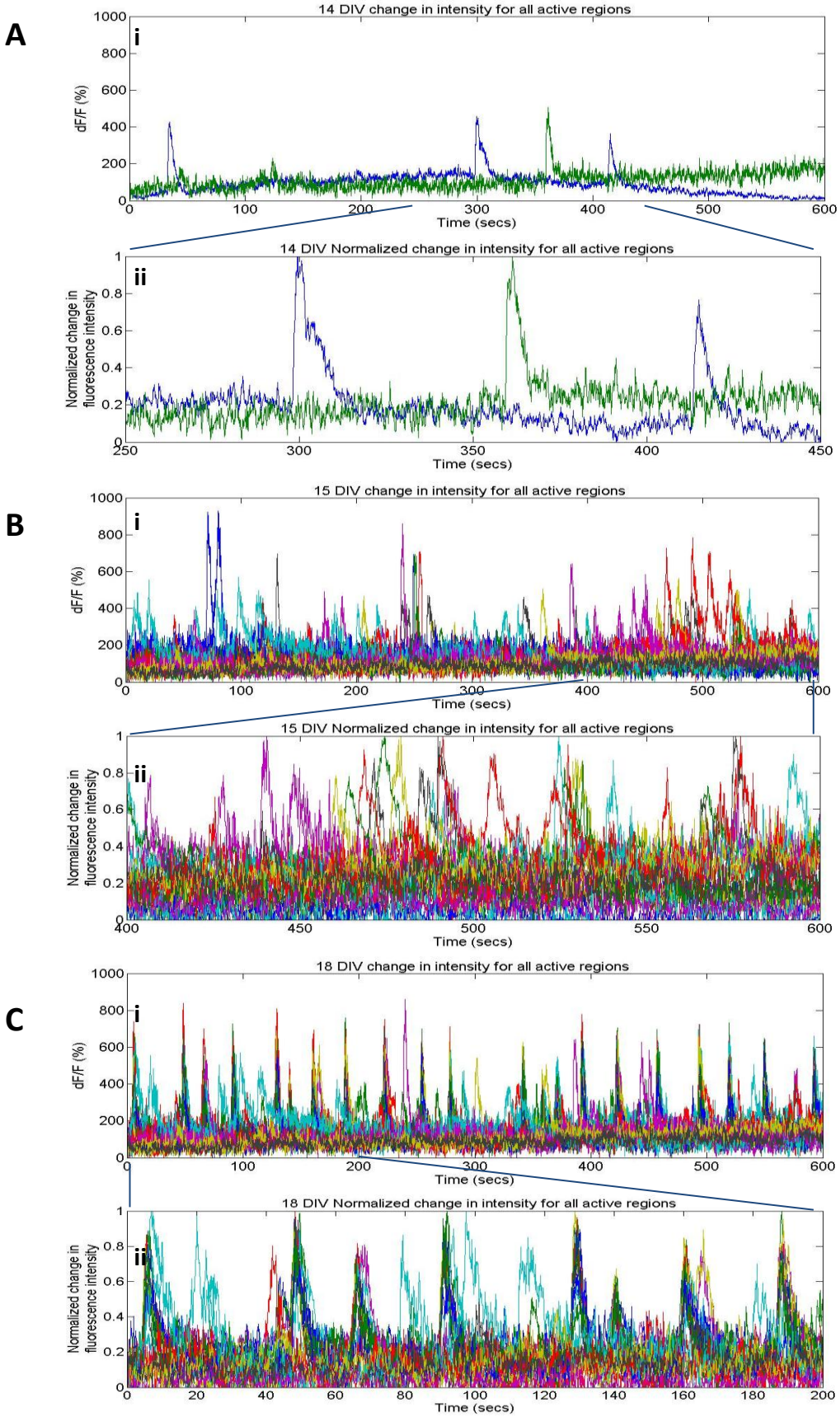

Figure 4.3 – Qualitative development of calcium activity for 14, 15 and 18 DIV. A-C) i) a 10 minute recording showing change in fluorescence intensity in all active regions. ii) an expanded section of 200 seconds from 'i' where each region is normalized to the maximum amplitude for that region. **A)** At 14 DIV there are very low levels of sporadic activity. In this example only 2 regions are active. **B)** At 15 DIV there are high levels of non-synchronous activity where far more regions appear active in 10 minutes than in A. **C)** At 18 DIV synchronous activity can clearly be seen with large numbers of regions recruited. i) The change in fluorescence intensity for all regions that become active in the recording period. ii) The intensity has been normalized for each region to the height of the largest amplitude for that region and the scale of the trace has been expanded to show a period of 200 seconds.

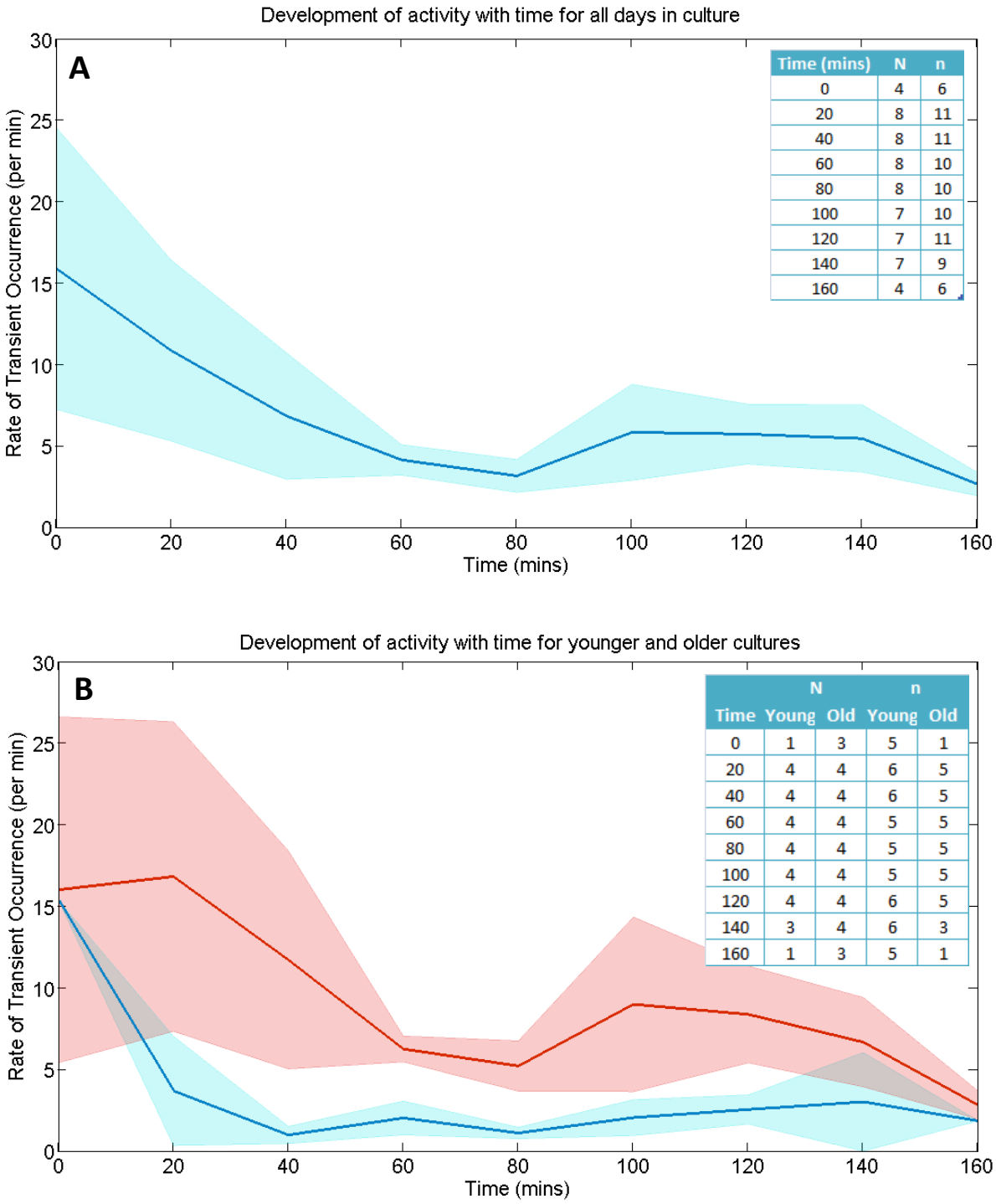

Time (mins)	N	n
0	4	6
20	8	11
40	8	11
60	8	10
80	8	10
100	7	10
120	7	11
140	7	9
160	4	6

	N		n	
Time	Young	Old	Young	Old
0	1	3	5	1
20	4	4	6	5
40	4	4	6	5
60	4	4	5	5
80	4	4	5	5
100	4	4	5	5
120	4	4	6	5
140	3	4	6	3
160	1	3	5	1

Figure 4.4 – Development of activity levels with time on the rig. A) Averaged activity levels over all days shown as a function of time on the rig. Activity is generally higher at the start, and settles to a consistent level after 30 mins. **B)** The same as in A, however, activity has been split into younger (13-16 DIV) and older (17-20 DIV) cultures (blue and red respectively). Both younger and older cultures begin with high levels of activity, but younger cultures display very low levels of activity in comparison to older cultures after the first 30 mins. Overall activity levels over the course of an experiment (see Figure 4.) were used to define the two groupings used here. Inset tables show the data frequencies with 'N' and 'n' referring to the number of cultures and the number of recordings respectively. Shaded areas represent the SEM.

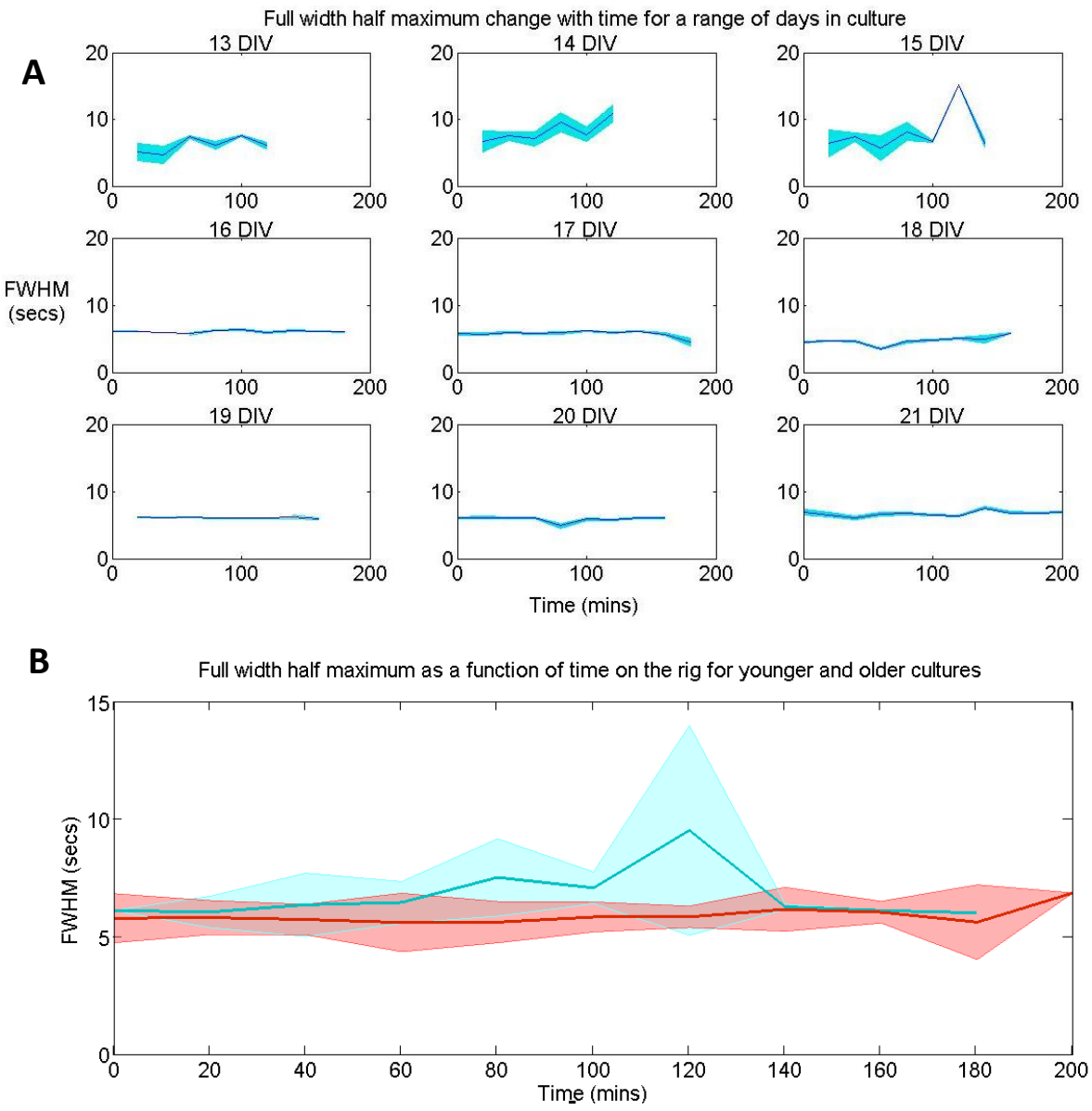

Figure 4.5 – Variation in transient shape, defined by the full width half maximum (FWHM) (see Figure 4.1**), across the time-course of an experiment for a range of days in culture. A)** Each subplot shows the FWHM change over the time course of an experiment for a different DIV number. Shaded regions represent the SEM. FWHMs are most variable in 13-15 DIV cultures, and then can be seen to remain fairly constant in 16 DIV cultures and older. **B)** Averaged FWHM for younger (13-16 DIV) (blue) and older (17-21 DIV) (red) cultures across the timecourse of an experiment (Younger cultures, n = 4, older cultures, n = 5).

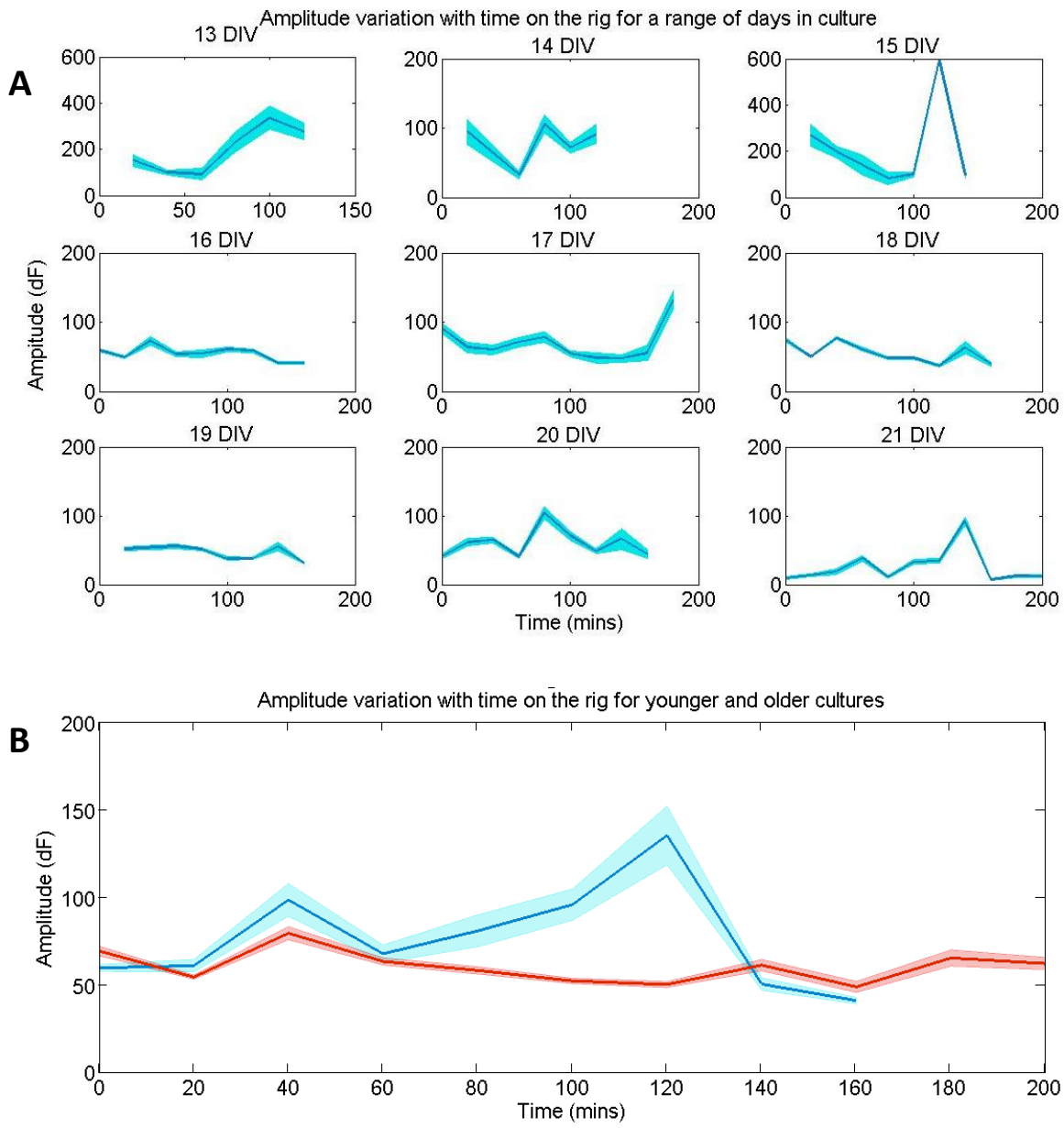

Figure 4.6 – Variation in amplitude of calcium transients across the timecourse of an experiment for a range of days in culture. A) Each subplot shows the amplitude change over the time course of an experiment for a different DIV number. Shaded regions represent the SEM. Amplitudes are largest and most variable in 13-15 DIV cultures. Although the amplitude does vary with time on the rig, there is no trend for it to increase or decrease. **B)** Averaged amplitudes for younger (13-16 DIV) (blue) and older (17-21 DIV) (red) cultures across the timecourse of an experiment. The amplitudes are generally smaller and less variable in older cultures (younger cultures, n = 4, older cultures, n = 5).

example of the overt bimodality in FWHM seen in some cultures at 18 DIV. However, pooling all data and plotting the mean and standard deviation of both kurtosis and skewness, while revealing a small (~25%) decrease in both mean values at this timepoint, did not show a significant change (16 DIV vs 18 DIV, and 18 DIV vs 19 DIV, $P>0.05$, N = 11-16).

Transient amplitudes measured over a range of days in culture showed the opposite trend to rate per ROI and number of ROIs active in any given culture. This decreasing trend with development (Figure 4.9) showed a near halving of calcium transient amplitude with a change in mean fluorescence from 167.25±13.34 to 87.39±0.93 for 13 DIV and 20 DIV cultures respectively ($P < 0.05$). Within this developmental period a brief increase in amplitude was seen on top of the general trend to halving of values at around 17-18 DIV. At 16 DIV and 19 DIV amplitudes were 53±8 and 79±10 respectively. At 17 DIV the amplitude recovered almost to the values recorded at the earliest time point (13 DIV). Along with a number of measures stated above this behaviour suggested, in some cultures, a particular, transient switch in developmental profile at this time point (e.g. see above for FWHM distributions in Figure 4.8). To investigate further, amplitude distributions were compared over days in culture.

These were tightly constrained and unimodal for almost all developmental time points (Figure 4.10A). However, at 17 DIV, at the time when the faster (shorter FWHMs) subset of transients were beginning to manifest in some cultures, the amplitude distribution became very broad. Quantification of the skewness and kurtosis of these amplitude distributions for all pooled data at each DIV number did not show a significant difference at this transient phase in development of calcium transient generation (Figure 4.10B, $P>0.05$, 16-19 DIVs, N = 10-24).

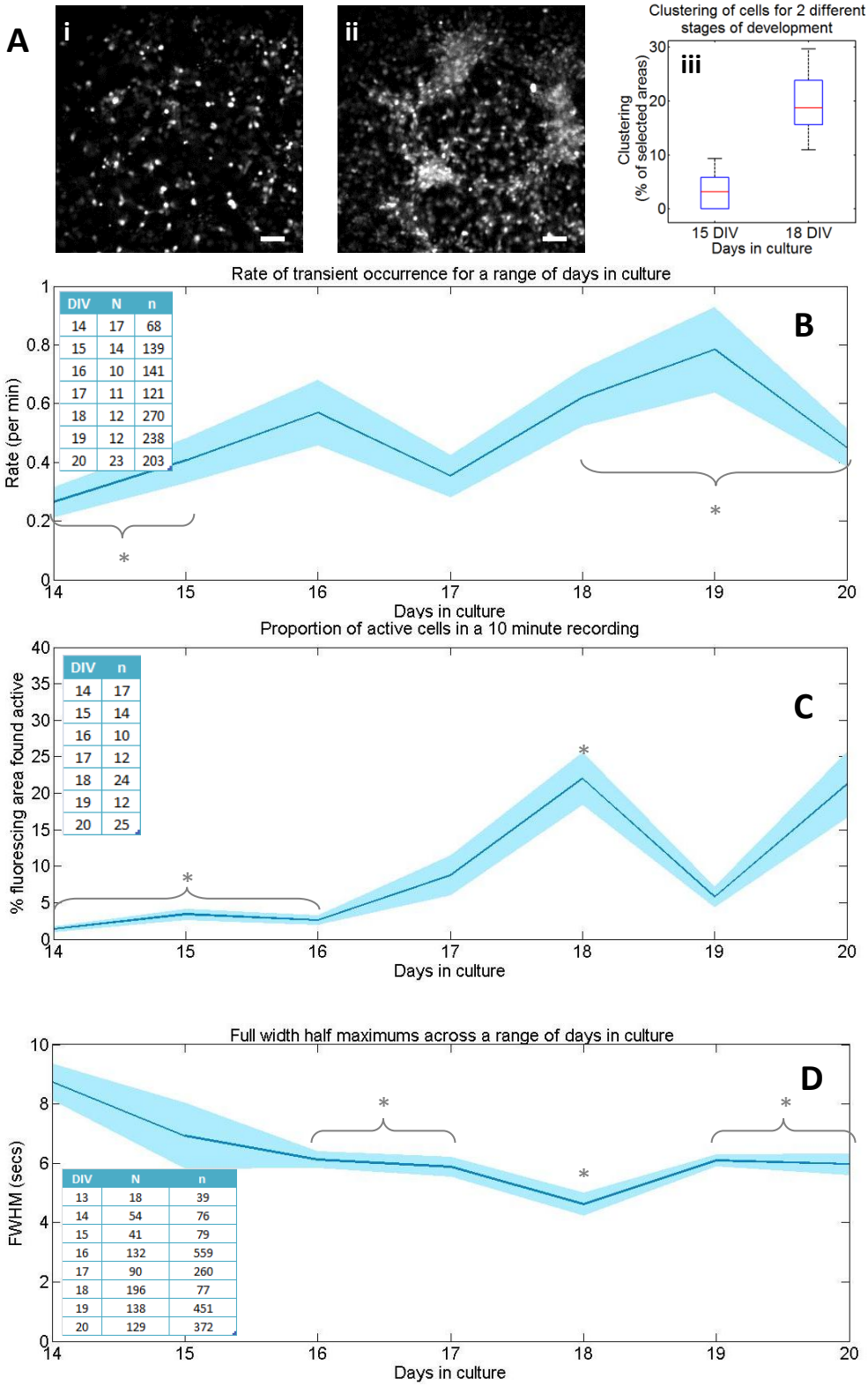

DIV	N	n
14	17	68
15	14	139
16	10	141
17	11	121
18	12	270
19	12	238
20	23	203

DIV	n
14	17
15	14
16	10
17	12
18	24
19	12
20	25

DIV	N	n
13	18	39
14	54	76
15	41	79
16	132	559
17	90	260
18	196	77
19	138	451
20	129	372

Figure 4.7 - Development of activity levels and change in transient shape with days in culture. A) Example images of a 15 DIV (i) and 18 DIV (ii) culture with resting fluorescence levels, showing the difference in cell distribution across the surface. (iii) a grid was applied to images from these two developmental days (n = 5 for each day) and grid areas containing clusters were counted. Higher levels of clustering were found in 18 DIV than 15 DIV (n = 5 for each day). **B)** Activity rates for each region show an increasing trend with DIV number (*P = 0.05), though rates for an individual region remain very low throughout. However, in **C)** the number of cells active in a 10 minute recording can be seen to be very low from 14-16 DIV, leading to a significant increase up to 18 DIV where ~25% of cells are active, as compared with less than 2% of cells in 14 DIV cultures. This is followed by a transient drop at 19 DIV (*P = 0.05). **D)** Full width half maximums (FWHMs) of the transient from 14-20 DIV. Young cultures show larger FWHMs on average, with greater variation and the lowest FWHM value is associated with 18 DIV, correlating with the peak activity levels in C (*P = 0.05). Shaded regions represent the SEM. Tables display the data frequencies with 'N' and 'n' representing the number of regions and events respectively.

To investigate the possibility of an increase in variability of events at the 17-18 DIV timepoints further inter-transient interval (ITI) distributions were studied. ITIs for cultures, summed for all recordings for a range of days in culture in Figure 4.11, varied little in terms of modal values, spread of data (kurtosis) or skewness, with the exception of 17-18 DIV (the times over which structural clustering develops). The change in overall distribution pattern for the ITI measure changed with developmental period in a manner similar to that seen for amplitude (as explained above). Again, at 17-18 DIV the population of recorded values appeared to become more distributed (i.e. there was less kurtosis) and less skewed in favour of lower values in the overall distribution. This phenomenon was most apparent at 18 DIV, with values of 1.53 (kurtosis) and 4.03 (skew) compared with values of 2.12 (kurtosis) and 7.33 (skew) before and 2.44 (kurtosis) and 8.79 (skew) after this transient developmental period. However, plotting means and errors of all ITI distributions at each day in development did not show a significant change at the 17-19 DIV timepoints (Figure 4.11C, $P>0.05$).

In general in dynamic systems the frequency of occurrence of events is inversely correlated with the amplitude of each event – the more frequent the events the smaller they are (e.g. in geophysics where mutual information regarding the appearance of earthquakes (which is based on a relationship between the inter-event interval and the rate of event occurrence) is inversely correlated with the magnitude of the Earthquake and the area of its affect (Omi et al., 2011)). The similarities in the above temporal pattern of changes in mean ITI and calcium transient amplitude (Figure 4.10 & Figure 4.11) suggested a close relationship between these measures in the present system studied here, too. To examine whether the changes in ITI seen here may be causally related to calcium transient amplitude these two measures were directly correlated. Figure 4.12 shows the range of Amplitude/ITI relationships seen for a single region at 18 DIV. While a general trend towards the above relationship was often seen, the correlation coefficients were often weak. To examine this relationship further a cut off correlation statistic of 0.75 was used and datasets falling above this value considered further. Examining these datasets over the developmental period where a sufficient number of events were seen (17-22 DIV) revealed a dramatic,

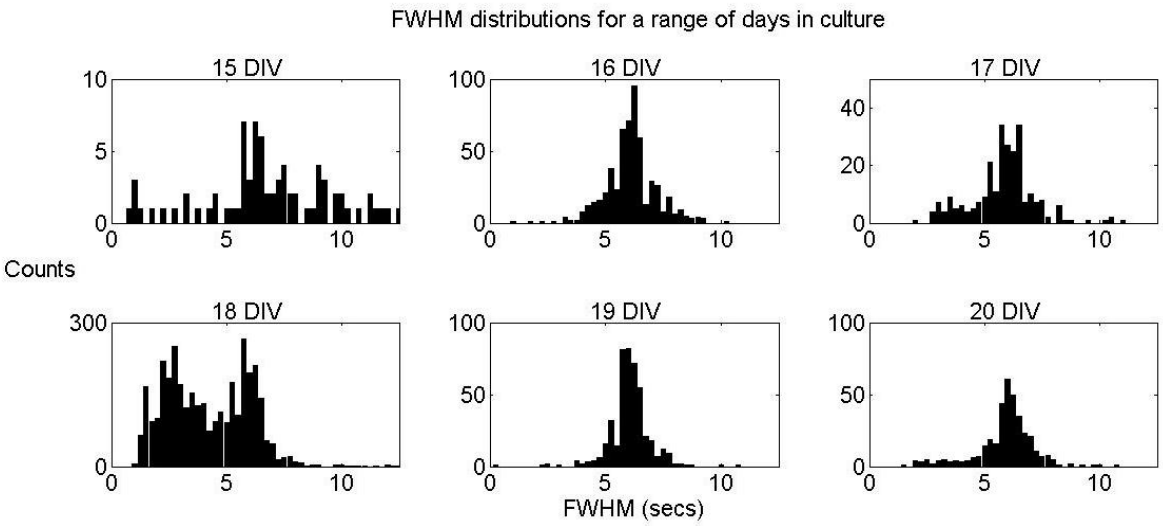

Figure 4.8 - Example summed FWHM distributions for a range of days in culture. Each plot depicts the distribution of FWHMs summed over all 10 minute recordings in a single experiment for particular DIV number. The distributions display a slightly bimodal response, either as a hump secondary to the main peak (16 DIV), or as a distinct second peak (18 DIV).

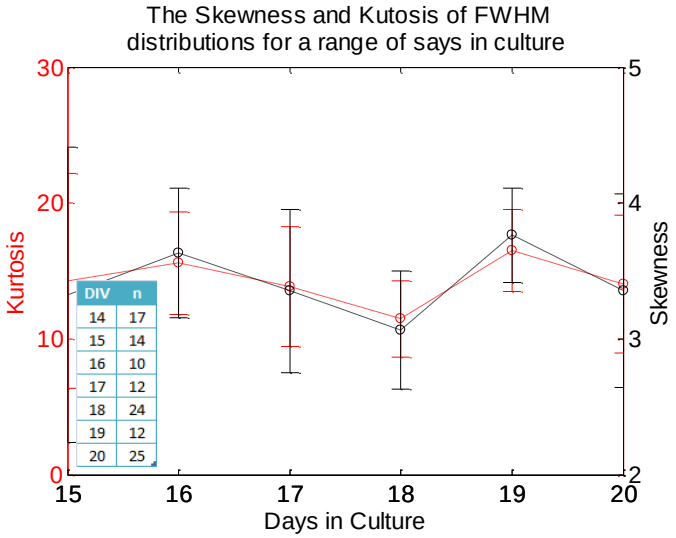

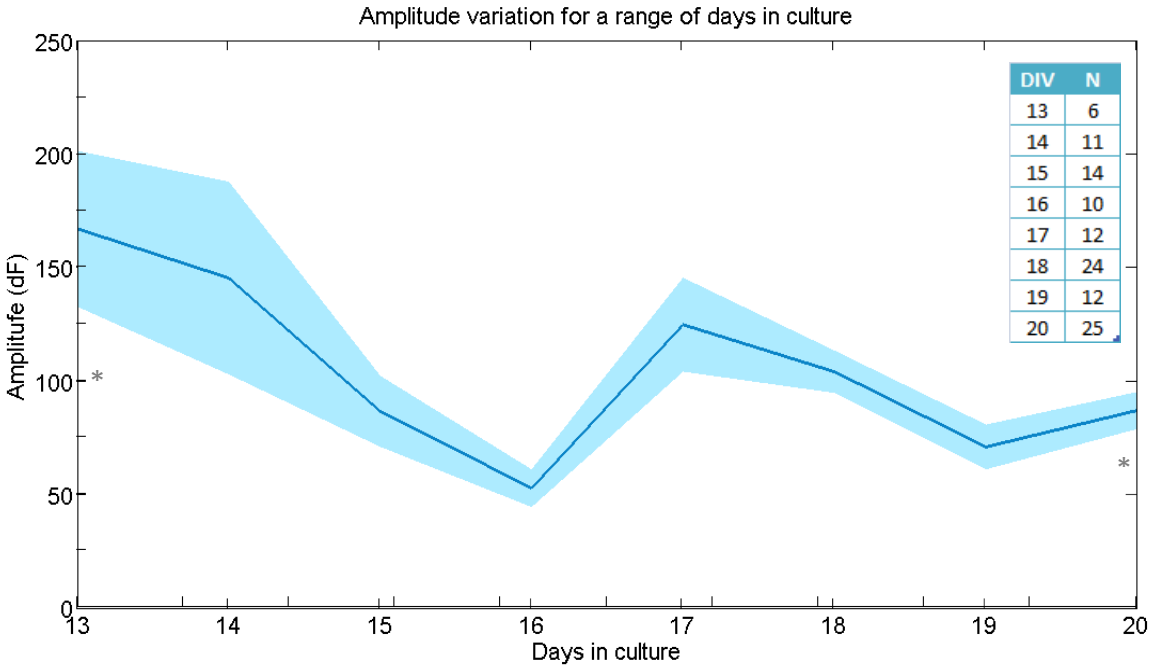

Figure 4.9 – The change in amplitude for a range of days in culture. The amplitude, measured as the change in fluorescence during a transient, is greatest in the youngest (13-14 DIV) cultures and follows a decreasing trend with DIV number with a change in fluorescence of 167.25±13.34 and 87.39±0.93 for 13 DIV and 20 DIV cultures respectively (*P = 0.05).

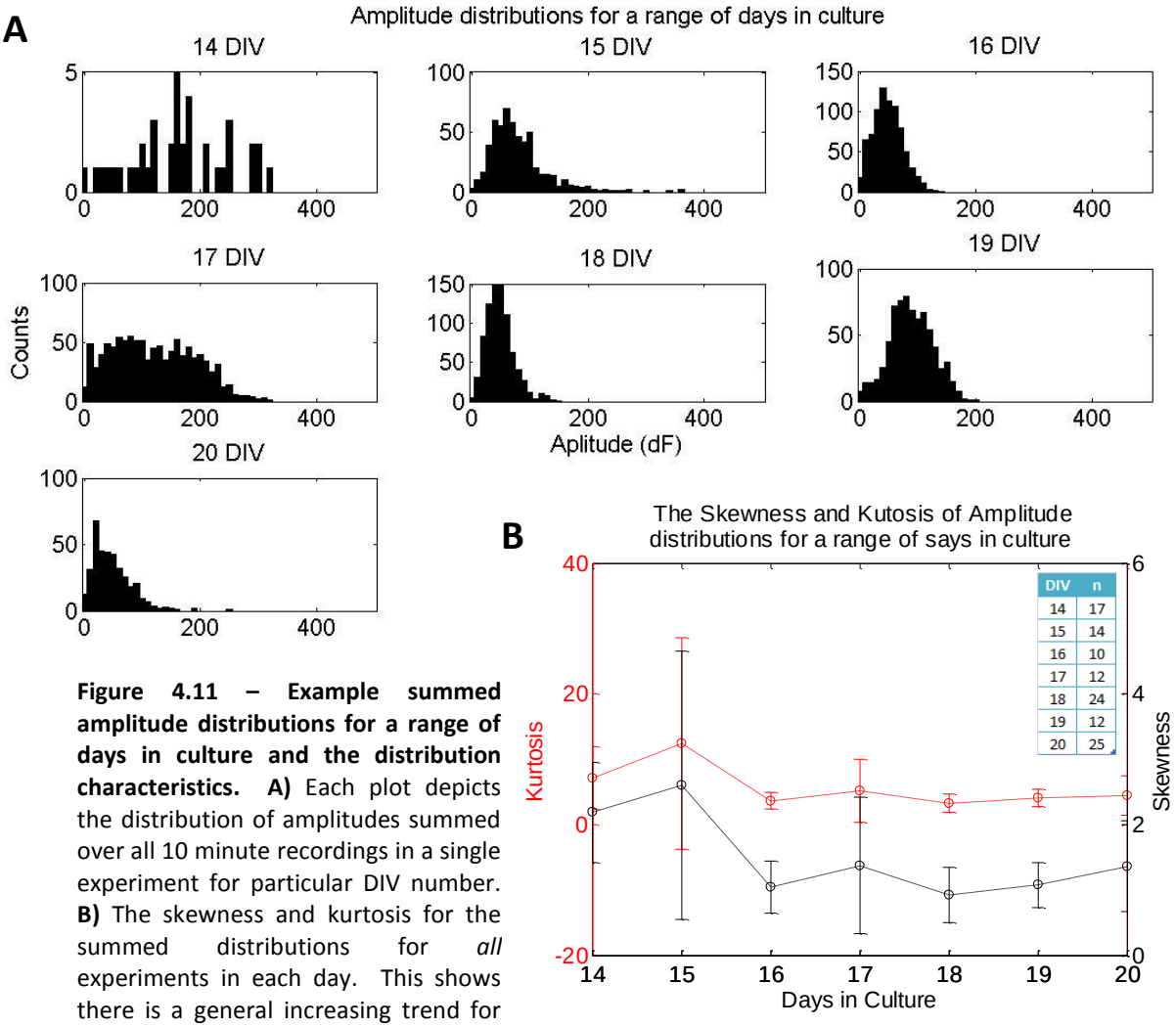

Figure 4.11 – Example summed amplitude distributions for a range of days in culture and the distribution characteristics. A) Each plot depicts the distribution of amplitudes summed over all 10 minute recordings in a single experiment for particular DIV number. **B)** The skewness and kurtosis for the summed distributions for *all* experiments in each day. This shows there is a general increasing trend for both a positive skew and kurtosis for younger (<17 DIV) and older (≥17 DIV) cultures with a sharp dip to a minimum at 17 DIV corresponding to the example distribution shown for 17 DIV in A, depicting a wide, bimodal distribution.

near 5-fold increase in the gradient of the ITI/Amplitude relationship from 17-19 DIV (Figure 4.13). Gradients increased from 0.14 ± 0.20 at 17 DIV up to 0.87±0.16 at 19 DIV ($P<0.05$). These data suggest an overt increase in the influence of transient rate over amplitude in the latter half of the developmental period studied.

At 17-18 DIV, many of the activity measures displayed by cultures were temporally completely different to younger cultures. This change corresponded with the increasing activity levels and the stabilisation of the network structure into clusters of cells on the substrate surface. Areas of the network exhibited highly synchronized events with a high percentage of cells within the field of view (indeed, *all* cells showing any calcium activity)

being involved in the events. The event onset in each region was closely locked (within 1 second) to that of the onset of the other regions. Mention of this change is made here, but the spatio-temporal aspects of this behaviour are characterised in detail in the next results chapter.

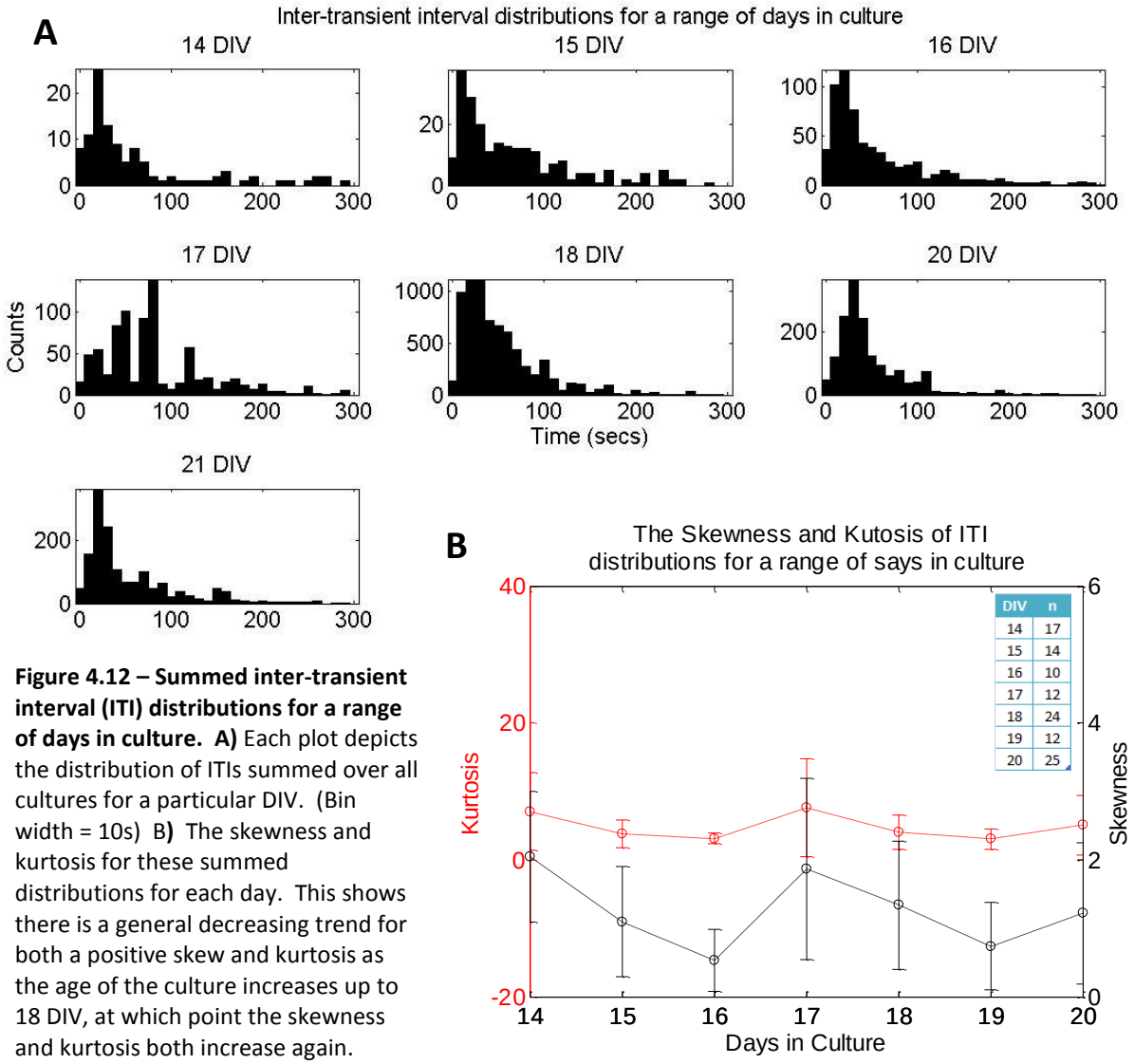

Figure 4.12 – Summed inter-transient interval (ITI) distributions for a range of days in culture. A) Each plot depicts the distribution of ITIs summed over all cultures for a particular DIV. (Bin width = 10s) B**)** The skewness and kurtosis for these summed distributions for each day. This shows there is a general decreasing trend for both a positive skew and kurtosis as the age of the culture increases up to 18 DIV, at which point the skewness and kurtosis both increase again.

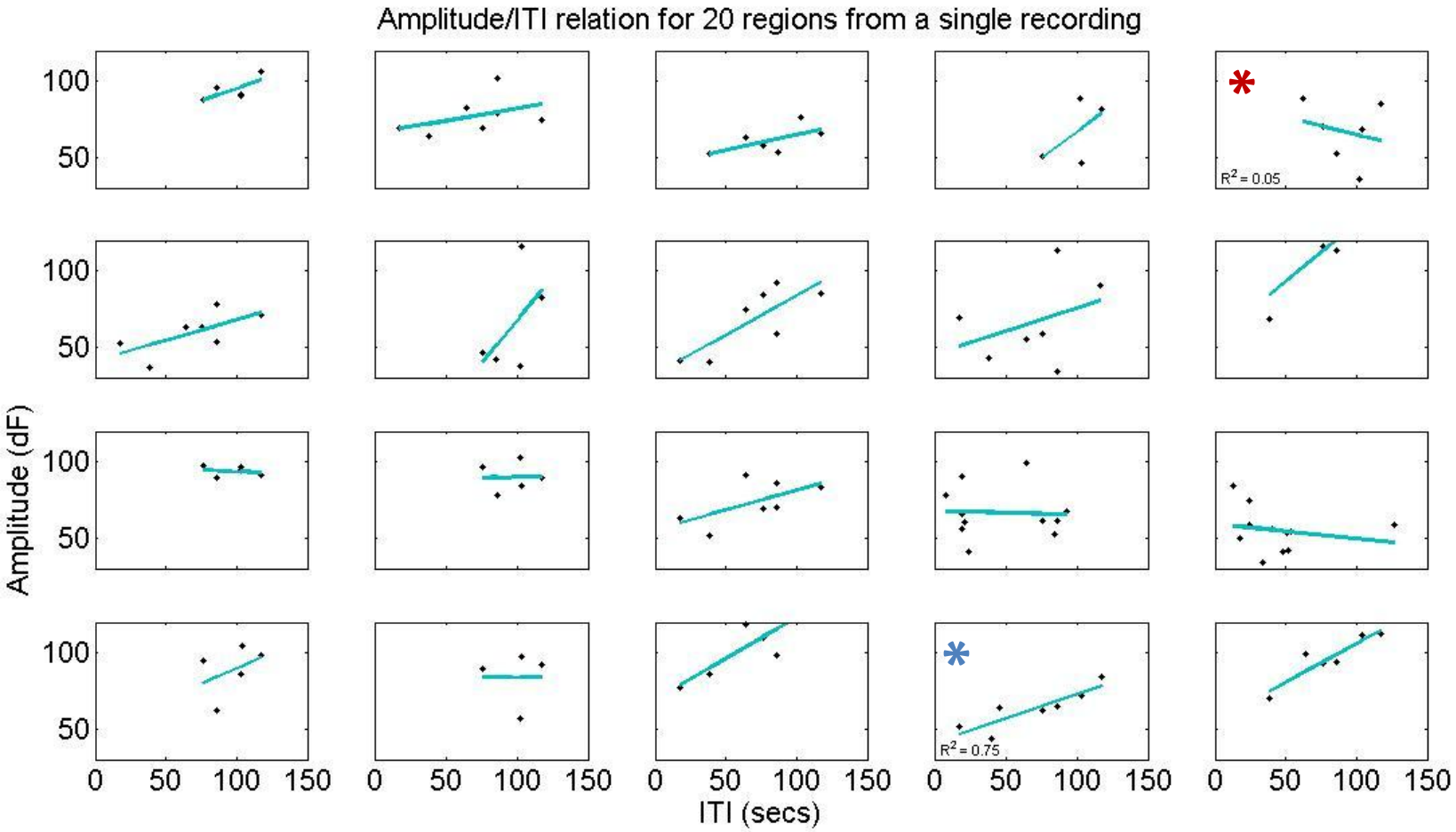

Figure 4.13 – Amplitude/inter-transientinterval (ITI) relationship for an example culture (18 DIV). Each subplot shows the amplitude vsITI for each transient from a single region. This is qualitatively demonstrative of the variation seen within cultures. Some regions show a strong linear (positive) correlation (e.g. blue asterisk), while other regions show a very weak or non-existent correlation (e.g. red asterisk). Strongly correlated regions (quantified in **Figure 4.**) have been used to examine any relationship between the amplitude and the ITI (see **Figure 4.**

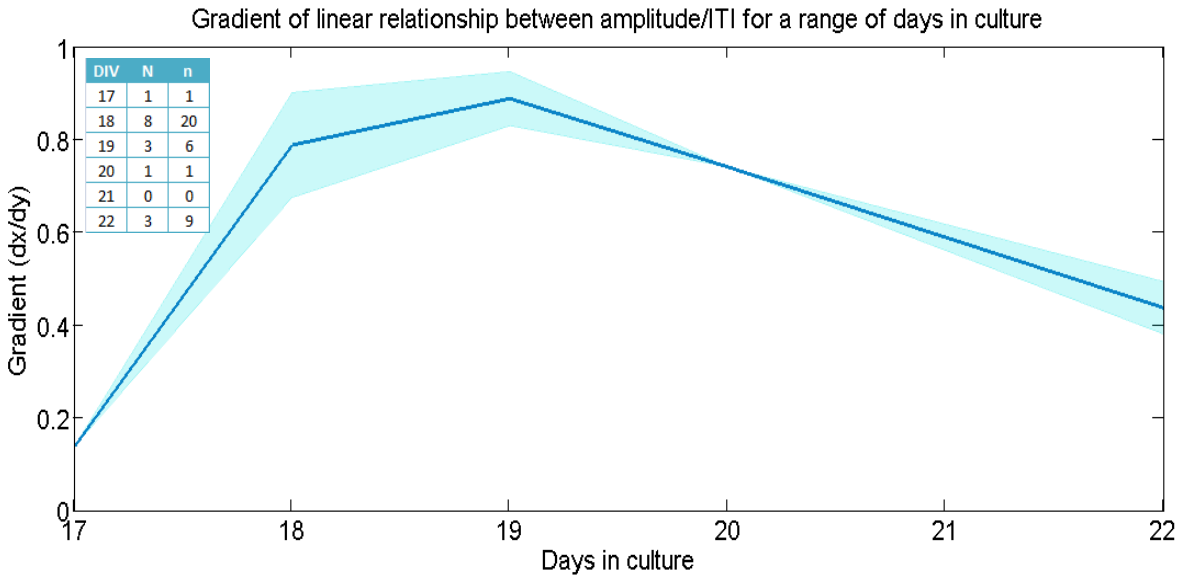

Figure 4.14 – Amplitude/ITI relationship for a range of days in culture. Regions displaying linear correlations with R^2 values greater than 0.75 from all cultures for a particular DIV were used to examine the relationship between amplitude and ITI. The graph shows the mean gradients of the linear regression of amplitude vs ITI with the shaded region representing the SEM. Sample numbers are given in the table, with 'N' and 'n' representing cultures and regions respectively. The gradient rises from 17 – 19 DIV, peaking at 0.89±0.06. This gradient then falls off down to 0.44±0.06 at 22 DIV

4.5 DISCUSSION

4.5.1 Changes in network activity over a time-course of hours.

While observing network activity over the course of an experiment, there was a drop in rates of calcium transient occurrence for the first 40 mins until the culture stabilises. Possible reasons for this observation include:

1) *A change in temperature*. The temperature at which the network is maintained on the stage - 32°C - is lower than the optimal temperature provided by the incubator of 37°C. As the temperature plate was almost directly in contact with the glass coverslip to which the cells adhered with the temperature modulating about the desired level, the temperature was maintained lower than optimal to ensure the cells were not overheated accidentally, which would potentially damage or kill them. However, lower temperatures have been shown to result in lower levels of activity in individual neurons and neuronal systems (Geller et al., 1985). In addition, the temperature of the cells would, however, equilibrate in far less than 40 minutes given the small volumes of solution being used, though the slow equilibration of activity levels may represent an adaptive process in the neurons and

networks themselves. An example of this is a switch to cold aCSF, used to evoke activity in neonatal cortical neurons (Yuste et al., 1995).

2) *A change in ionic composition of media*. The initial environment, with cells maintained in growth medium in the incubator, may have resulted in more network activity than the environment provided by the perfused aCSF during data gathering. One factor that is vital for neuronal excitability levels is the membrane charge screening effects afforded by extracellular concentrations of divalent cations (Hille et al., 1975). The growth medium had a concentration of 2.3 mM divalent cations (Ca^{2+} and Mg^{2+}), whereas the aCSF had 4 mM (all calcium, no magnesium). A switch to media with this increase in charge screening would be expected to decrease neuronal excitability though, conversely, the large increase in calcium ion concentration would be expected to enhance transmitter release at the network level (Matthews and Wickelgren, 1977). The absence of magnesium ions is also likely to be a major determinant of network (rather than single neuronal) excitability. Magnesium ions form an open channel block for current flow through NMDA receptors (Jahr and Stevens, 1990). Thus the aCSF used would be expected to enhance slow ionotropic glutamate neurotransmission between cells in the network.

Extracellular potassium ion concentrations also influence neuronal excitability by modifying conductances vital for the resting membrane potential (Heinemann and Gutnick, 1979). A switch from growth medium to aCSF reduced potassium ion concentration from 5 to 3 mM. Thus a decrease in excitability would be expected as the growth medium was washed out and replaced with aCSF. Finally, pH – as determined by bicarbonate ion concentration, also influences neuronal excitability (Takahashi and Copenhagen, 1996). Bicarbonate concentration was lowered from 32 to 25 mM in switching to aCSF. The small increase in acidity would not be likely, however, to influence activity rates as seen.

These factors suggest that while neuronal excitability may be reduced, activity in the network, via increased presynaptic excitability and postsynaptic excitatory potential increases, should be increased in aCSF, in the case where chemical synapses are active. The slow decrease in activity levels from the initial high values seen in the present experiments suggests however, that adaptive processes take place over a timecourse of tens of minutes and so this may not form the overriding influence on changes in activity rates seen here.

3) *Structural integrity changes*. Another possible source for the reduction in activity over the first 40 minutes on the fluorescence stage is a drop in the structural integrity of the network. This would be due to the sum of disturbances that the cells undergo moving from the incubator to the fluorescence stage, which include moving the coverslip out of growth medium, reorienting the cells and re-covering. Neuronal processes, particularly the finer ones, may break down or retract, reducing connectivity within the network. Thus it is possible that the source of this activity reduction is a network phenomenon induced by environmental disturbance, though all care was taken during the transfer stage to minimise such disruption.

Unlike the rate measures discussed above, measures of transient shape were not altered to such a great degree, if at all, during the course of the experiment. Amplitudes varied across all time-points, showing no significant alterations due to time spent on the stage. FWHMs also demonstrated the same variation in younger cultures (<17 DIV), and in older cultures (≥17 DIV) remaining highly consistent throughout hours on the stage. This was seen despite the potential influence on any synaptic events, as discussed for divalent cation changes on switch to aCSF above. This suggested that the source of the transients was not directly related to strength of synaptic excitation in neurons. This may be due to lack of chemical synaptic contacts in these cultures. The source of transients, however, may be either intrinsic bursting or ICCR (as explained later) regardless of the lack of chemical synapses. Intrinsic burst behaviour is highly stereotyped. It is dependent on voltage-operated calcium channels that are able to compensate for changes in extracellular calcium concentration via binding sites for calcium ions within the pore domains themselves. The very steep voltage dependence of activation also makes currents generated by these channels highly all-or-none in nature (Bahinski et al., 1997). Therefore, as the only measured aspect to be affected by time on the stage was activity rate, it is unlikely that there were intrinsic changes to individual cell properties underlying this. Instead the rate changes measured were likely to be network-based. This would also apply if transients were predominantly internally generated through calcium ICCR from stores.

4.5.2 Developmental Time-course over Days

The main findings from the experiments in this section were that over the first 3 weeks of development the nascent neuronal networks generated more spontaneous activity. A

larger number of ROIs (predominantly single neuronal elements, but see methods) were seen to be spontaneously active and the rate of activity per ROI was seen to increase as the culture developed. Taken alone this would suggest a greater degree of non-spatiotemporally coordinated 'random' activity. However, a large increase in the fluorescence transient amplitude to inter-transient interval ratio was seen. This finding suggested that, while overall activity levels increased, there was a greater temporal constraint on the magnitude of activity. Such a pattern of activity would be expected to favour the establishment of more regular, synchronous activity. This organisation of transients was seen towards the end of the developmental period studied (after 17-18 DIV) and is investigated in more detail in chapter 5.

4.5.2.1 Developmental profile of ESCs in vitro and in vivo

As was explained in the General Introduction (Chapter 1), and briefly again in the introduction in section 4.1 above, following the developmental profile of these ESCs is not trivial. All cells differentiated *in vitro* are subject to the constrictions of their artificial environments and this can have an effect on aspects of their development, for example producing neurons with expected morphological features, but lacking in normal functional activity (Illes et al., 2009). Such observations cannot be disregarded when considering the developmental stages the CC9s go through.

The CC9 cell line was created by removing blastocyst cells from the embryo likely at E6, though the exact day is no longer known (personal communication, Prof Robert Lightowlers, Newcastle University). They were removed before significant development of the mesoderm, endoderm and ectoderm lineages, and thus before any neurulation (and thus neurogenesis) had begun. Environmental step changes in the culture conditions include the following:

- The removal of LIF at 0 DIV with cells suspended in media (rather than adhering to a substrate).
- The introduction of retinoic acid to encourage differentiation and limit proliferation from 4 DIV.
- The provision of an adhesive substrate for neuronal network development through process extension from 8 DIV.

- The removal of bFGF from 10 DIV.

Comparing this with *in vivo* development, LIF expression is seen at E4 (the stage of embryo implantation) and is no longer detectable in post implantation embryos from E8 – E17 (Bhatt et al., 1991). Removal of LIF in the CC9 culture protocol at 0 DIV would therefore coincide with E8, though at this stage, in CC9 cultures, the cells are still fully undifferentiated, unlike in the embryo, where by E8, neurogenesis has already begun. This inconsistency, as described next, is seemingly compensated for in the protocol.

Detectable expression of retinoid binding sites were found as of E8.5 in the neural plate and folds (Dencker et al., 1990) of mouse embryos, 0.5 days after LIF expression has decreased. Two days bridge this gap in the CC9 differentiation protocol, which allows time for differentiation to occur (likely to already have been underway in the embryo). At this point 4 DIV (as opposed to 0 DIV) for CC9 cultures could be argued to coincide with E8.5 *in vivo* as it matches developmentally with a point where neurogenesis will have begun, LIF expression has reduced and retinoic acid has come into play.

B-FGF receptors were found in the early ectoderm clearly detectable at E7.5 (and more specifically in the neural plate and folds by E8) in mouse embryos (Orr-Urtreger et al., 1991). 8 DIV CC9 cultures, if considered equivalent to E12.5 (as observed in line with retinoic acid expression and explained in the previous paragraph) are therefore receiving b-FGF 5 days later than *in vivo*.

From this it is clear that determining the developmental stage of the CC9 cell line as it develops *in vitro* through an analysis of the environmental changes provided by the protocol *cannot be conclusive*. Nevertheless, the above description allows that an approximation can be made at 8 DIV being equivalent to E12.5. Following this, the inclusion of b-FGF at a later stage, along with the lack of normal architectural development or any further changes in environment will undoubtedly alter the development of this CC9 cell line *in vitro* from this point (that is 8 DIV ≡ E12.5) forward. There is therefore an interesting comparison to be made between activity resulting from the development of such nascent networks and that activity found in dissociated cells of a similar developmental time-frame to understand what effect such an artificial environment exerts on the functional development of the network. This bears relevance to any network undergoing development in a culture environment and

the network output properties that result. Comparisons are made below with *in vivo* and dissociated cultures in order to further examine this issue.

4.5.2.2 The onset of spontaneous activity in vivo, as compared with CC9 activity.

The first forms of spontaneous calcium-transient activity observed in the developing embryo are spikes and waves (found in the neural plate and later neural tube of the *Xenopus* embryo) (Gu et al., 1994). The waves, known to affect neurite outgrowth and commonly generated in the dendrites and soma, are not synaptic in origin. Evoked glutamate responses and a comparison of transient characteristics make such waves an unlikely origin of CC9 calcium transients. The other form of activity - spikes - are dependent on ICCR from stores and are affected by blockade of VGCCs by Ni^{2+} and TTX, and appear to be activated by low threshold calcium currents (LVAs). They can be seen to fire synchronously in small groups (i.e. not population responses) and function to modulate the expression of potassium channels and GABA (Desarmenien and Spitzer, 1991). Co-existence of spikes and waves in the soma also point to a mechanism for spontaneous spike generation through depolarisation from the waves activating LVAs, then producing spikes. In other words, individual developing neurons can be spontaneously, and rhythmically active without synaptic input from neighbours.

This spontaneous activity is present in CC9s before the development of spontaneous synchronous activity (see next chapter and compare Figures 4.3B & C). The discrete transients that appear earlier, while network spatial structuring is still in progress, show a wide distribution of ITI with no overt temporal organisation. Their presence in the developmental stages when neuronal migration is still in force suggests that these discrete calcium transients are generated intrinsically (above) and contribute to structural aspects of network formation, which appear to be a dominant function of spontaneous activity generation during migration in embryonic development.

Transients from glial cells, as described in the literature, display a large range of widths from 10s of seconds to 100s of seconds (though just under 10 seconds has also been reported) (Fanelli et al., 2011, Hirase et al., 2004, Hoogland et al., 2009, Newman, 2001, Newman and Zahs, 1997, Weissman et al., 2004). In contrast, the transient widths described here are relatively very short at around only 6 seconds. The spatial propagation of glial transients is

compared with CC9 transient propagation in Chapter 5, which deals with the spatiotemporal patterns of activity. As stated earlier, a small percentage of these cells were previously found to be glia (Kirby et al., 2009) and the presence of a large proportion of cells differentiated along the neuronal lineage is also confirmed with β-tubulin III staining (see figure 3.3). These data suggest that the calcium transients recorded here are of neuronal origin. However, it is possible that functional neuron-glia interactions play a role in the activity seen in CC9-derived cultures, with calcium transients being generated in astrocytes following neuronal synaptic activity (Dani et al., 1992, Liu et al., 2004, Perea and Araque, 2005, Ullian et al., 2004, Ullian et al., 2001). This will be discussed again in Chapter 6 when looking at the role of GABA in these developing cultures.

Early action potentials in the neural crest and developing spinal cord (still undergoing lateral migration) are calcium-dependent at first, switching gradually to sodium-dependent spikes (Spitzer and Lamborghini, 1976) during development. Spike activity dictates migration pathways and increases in these early calcium spikes encourage the phenotypic expression of inhibitory neurons in neighbouring cells. Conversely, decreases in calcium spikes encourage the expression of excitatory neurons (Spitzer, 2006, Spitzer et al., 2004). The balance of inhibition and excitation in neuronal networks can thus begin to be established very early on, showing how network properties are defined even before more mature network communication mechanisms are in place. The presence of GABA-ergic and glutamatergic neurons is already known in CC9 cultures, and so this phenotypic differentiation process is evidently underway as the network structure develops in these nascent CC9 networks. It is thus natural to speculate that the sporadic activity noted in early CC9 cultures may have such a functional bearing on the development of specific network properties that shape later more rhythmic, synchronous population events.

Speculation about the physiological basis for the early activity seen in CC9s leads again to the previous patch clamp study (Trevelyan et al., 2010, Kirby et al., 2009), which show glutamate-evoked spike bursts juxtaposed with calcium transients with similar characteristics to those detected in the results in this thesis. CC9 calcium transient activity was reduced by the blockade of VGCCs, NMDA, glutamate and AMPA receptors (Trevelyan et al., 2010), signifying their involvement in the functional activity produced by the network at this stage of development, similarly to that seen in the examples of early network activity

given above. There is therefore a possibility that the transients here are similarly the result of spike bursts within the cell (see above). The lack of spatiotemporal relation between cells in the network could be the result of not detecting the sources of individual spikes that sum to produce bursts.

Alternatively, the structural immaturity may rule out integral synaptic machinery; in which case disparate bursting events would be intrinsically generated, based on ICCR, and VGCC influences. In other words, when activity first appears it is generated at the single cell level, the resulting uncorrelated activity guides network formation until sufficient influence of neighbouring neurons on each other provides a shift to network-wide, population (synchronous) events. Such correlated activity may then be the result of either electrical or chemical synaptic effects. While the presence of gap junctions has not been confirmed, they may also play a role in early network activity. They are highly likely to be present as gap-junctions typically develop very early, before chemical synaptic transmission, allowing for functional electrical and, later, chemical communication between neighbouring cells (Charles et al., 1996, Jorgensen et al., 1997, Yuste et al., 1995). Gap junctions have been shown to be involved in the propagation of calcium activity across subpopulations of cells (Yuste et al., 1995) and thus is a candidate for the activities seen here.

4.5.2.3 Comparison of CC9s to dissociated cultures of developing neurons

The primary cultures in Valor's synaptogenesis/activity study (Valor et al., 2007) were E17 dissociated cells from the hippocampus. In this study the cells required 4 days to recover from dissociation as they created functional network connections. Following this, activity increased exponentially for 12 days before starting to plateau. In accordance with this timeline of development and in line with the above estimate for CC9 cell development, if the activity were expected to correlate with the Valor study, the CC9 cells will not become active until 17 days after the start of differentiation with high levels of activity expected at around 29 – 33 DIV (though CC9 cultures did not survive past 22 DIV). Taking into consideration the 4 days the cells require to extend processes and make connections in dissociated cultures, initial activity levels may be underestimated and thus activity may appear later in these dissociated cultures than would be expected *in vivo*, or indeed in CC9 cultures, where connecting processes have never been disturbed.

The advantage of the CC9 cultures used in this study is that the *de novo* cultures develop *in vitro* and there is no disruption to this process through dissociation at any point. As such, the onset of activity would be expected to be in line with their development, rather than their re-construction after dissociation. The timing of the appearance of such activity is therefore significant as a developmental comparison between *de novo*, dissociated and *in vivo* networks. The natural developmental profile has been compromised, as explained above, by the protocols used. However, the CC9-derived neurons form a bridge between neurons in their natural environment and the contrived environments of dissociated cultures. Interestingly, activity is measured from at least 4 days before activity is seen in the Valor study where cultures required 4 days to re-connect with neighbours. Significant increases in activity in CC9 cultures are seen at 17 – 18 DIV, which is consistent and equates developmentally with the onset of measurable activity in the Valor study.

The onset of activity and its rise in both the primary neonatal hippocampal cultures and the ESC-derived neuronal cultures, although not coinciding in terms of developmental stage, coincide in terms of their relative time in culture, indicating that this particular pattern of activity development is dependent on the level of connectivity in the network; i.e. both differentiating neurons (extending processes to create connections for the first time) and dissociated neurons (extending processes to re-create connections after they have been lost) follow the same activity-level developmental profile. This denotes the similarity between wiring dynamics in these distinct systems.

4.5.2.4 Calcium transient sources in development

There are two possible sources of the calcium transient activity described in these results. It may be from ICCR from stores, in which case the activity could resemble the calcium-dependent action potentials involving N-, L- and T-currents that subsequently evoke the ICCR seen in developing spinal neurons (Gu et al., 1994, Holliday et al., 1991). The FWHMs of CC9-derived neurons (across all developmental days examined) fall within expected values of the duration of such ICCR-mediated spikes (1–10s) (Spitzer et al., 1994). The rate of occurrence of these spikes (1–10hr^{-1}) is consistent with younger CC9-derived cultures. Such calcium-dependent spikes could propagate through a cell network via gap-junctions, and this may be the source of the synchronized behaviour seen in older cultures. As gap junction connectivity is expected to fall with neuronal development (Rozental et al., 1998)

(and indeed, calcium activity propagated by dendro-dendritic gap junctions in the developing neocortex exist transiently in development (Yuste et al., 1995)) it is interesting to note that CC9-derived neurons have a transient dip at 19 DIV in the number of active cells. This is explored in more detail in Chapter 5, where spatiotemporal aspects of activity are explored. CICR is not the only source of ICCR from stores; spontaneous ryanodine-mediated ICCR has been observed in adult hypothalamic neurons due to membrane depolarisation (in the absence of extracellular Ca^{2+}) (De Crescenzo et al., 2004).

The second source of the calcium transient activity could be from spike bursting within the cell, either entirely intrinsically or secondary to synaptic input. If the bursts are produced entirely intrinsically as synaptic junctions have yet to coalesce, again, gap junctions could be the source of activity propagation. A range of amino-acid-based synaptic receptors have been shown to be functionally active in CC9 cultures, though whether these receptors have migrated to synaptic junctions has not been determined. If calcium transient activity were due to chemical synapses, this would imply that the activity measured is a hierarchy above the unit activity measured in, for instance, the Valor study discussed above. A further study with primary cultures of E17 dissociated hippocampal cells (MacLaren et al., 2011) demonstrated that less than 10% of all detected spikes are involved in burst activity at 4–5 DIV and this percentage increases gradually to hit ~80% by 11–12 DIV. With the possibility that bursting activity is measured in CC9 cultures, it would follow that the levels of activity seen reflect that proportion of activity only involved in bursts in the developmental profile shown in the Valor 2007 study. From neocortical neurons dissociated from E16 rats (Opitz et al., 2002), spontaneous bursts from 16 DIV cultures showed a positive correlation between burst length and burst interval, as with CC9-derived neuronal cultures (Figure 4.12 and Figure 4.13).

The speed and direction of propagation of GDPs, a form of population-wide synchronous activity seen at P0 – P7 (Garaschuk et al., 1998), are highly dependent on the network architecture (Bolea et al., 2006), with typical activity rates recorded at $0.05–2s^{-1}$ (Leinekugel et al., 1997) (equating to $3–120min^{-1}$). In contrast, CC9 cultures activity rates for single ROIs were less than $1min^{-1}$. As architecture plays a role here, the possibility should not be discounted that the structure and population sizes in CC9 cultures result in far lower rates of activity. The type of activity described above, however, involves synchronized populations

of neurons. Such activity was produced in CC9 cultures (≥17 DIV) and further details of this are given in Chapter 5, so will not discussed further here.

Overall population activity rates could be directed by metabolic or network properties. Both have been shown to act together to govern transitions between activity states in slow wave oscillations (SWOs) in the adult rat entorhinal cortex (Cunningham et al., 2006), which oscillate between 0.1 – 0.5Hz and even slower with lowered temperature and reduced glucose concentration. The switch to the 'down' state in SWO was found to depend on the metabolic-sensitive potassium channels (i.e. a reduction in the ATP:ADP ratio led to a switch to the 'up' state). Even slower rhythms (0.05 – 0.5Hz) have been found in brainstem and respiratory system neurons (Lambertz and Langhorst, 1998). Calcium transients evoked by low levels of glutamate receptor activation in immature neocortical neurons have been reported at even lower rates still – approximating to the variable, slow frequencies seen in the results described here (Yuste and Katz, 1991).

Morphological development, gap junctional connectivity, level of ICCR activation and synaptic strength are all potential candidates for changes seen in amplitude of calcium transient with development in CC9-derived neurons, as is now explained. The presence of calcium channels in CC9 cultures is highly likely, as although ICCR from stores (Kirby et al., 2009) is a source for calcium transients, VGCCs are present very early in embryonic development *in vivo*. Calcium channels were shown to be fully developed in rat superior cervical ganglion (SCG) neurons by E14.5. Although the waveforms remained unchanged as the embryo developed, the current density decreased as the cell size increased with development (Nerbonne and Gurney, 1989), perhaps reflecting the decreases in mean transient amplitude seen in this thesis (Figure 4.7 & Figure 4.9), though this fall is interrupted by a transient rise in amplitude at 16 DIV. Conversely, the decreasing amplitude could reflect a reduction in the strength of gap junctional connectivity as the neurons develop, although this would contradict the increases in activity seen (and also spatiotemporal aspects described in Chapter 5) and again, does not account for the two-step change seen at around 16 DIV. A fall in amplitude may also be seen if there is a decrease in ICCR activation with development, and may be independent of the input resulting in ICCR from stores. Finally, there is a stark inverse relationship between the rate of network activity and the amplitude of responses, which appears to be mirrored for each

day in development. This would be consistent with the concept of reduced calcium responses with increasing synaptic activation.

Calcium entry also has down-stream effects on many other conductances controlling neuronal excitability. Thus further developmental factors relating to calcium dynamics need to be considered For example, a calcium-dependent, fast, outward potassium current, I_A, was not yet present in E14.5 SCG neurons, but developed over 2–5 DIV. A different, slow activating, potassium current, I_K, therefore forms the predominant outward current seen in neurons this young. This current is not noticeably different between E14.5 and E20 (Nerbonne and Gurney, 1989). This implies that CC9 neurons, existing at the same developmental stage, are likely to be functioning with I_K, and I_A may still have yet to fully develop, perhaps going some way to accounting for the very slow transient rates seen. In addition, the presence of a calcium-dependent K^+ current can act to truncate bursts, reducing the number of spikes in each burst and increasing the clustering ratio (Chiang and Strowbridge, 2007). In CC9 cultures, voltage-dependent K^+ currents are more likely to dominate, as calcium-dependent currents are slower to develop (above). The potential development of these currents in CC9 cultures with time *in vitro* may in part explain the transient shortening (lower FWHM) and less activity in between transients seen at later developmental stages here. Decreases in amplitude and FWHM may be indicative of precisely this, especially as activity in general becomes more temporally organised and regimented after 17 DIV.

At 17–18 DIV the FWHM distributions become transiently bimodal in some instances during the period when activity levels significantly increase and temporal organisation of that activity is initiated. Indeed, only those cultures displaying synchronous activity display the bimodal response, and only within the 17–18 DIV developmental window. This will be dealt with again in Chapter 5, but bears mentioning here from a physiological perspective. Further statistical analysis did not show a significant change in either skewness and kurtosis for the distributions from each 'n'. In addition, this bimodality was not reflected in ITI distributions, implying that either the bursting behaviour of cells recruited into synchronous events may be governed by two distinct physiological mechanisms, though one of these mechanisms is only transiently active; or no single abrupt change in any of the measured

parameters was responsible, alone, for the establishment of synchronous discharges (see chapter 7 for further discussion).

4.5.2.5 Structural and functional features of CC9 networks, contrasted with in vivo development.

Two interrelated factors in terms of network structure are important when considering any correlation between structure and function: the number (density) of neurons across each culture, and the pattern and rate of connectivity between neurons. These are dealt with below and compared and contrasted to in vivo developmental issues.

1) *Neuronal density*. The increase in activity seen with increasing days in culture may simply be related to the rise in the number of neuronal cells present. Previously underdeveloped cells at early developmental periods tested will continue to differentiate into functional neurons. Proliferation seems to continue to an extent in cultures, even after the removal of bFGF at 10 DIV (notable by eye in the density of mature cultures, e.g. Figure 4.7 A).

CC9 cultures appear to be quite heterogeneous. The number of active regions in any recording or the percentage of the population recruited into synchronous bursts, as compared with the number of calcium-fluorescent cells, therefore does not directly reflect the number of neuronal cells, nor demonstrate the percentage of active neuronal cells in each culture. However, a sharp, near-exponential increase in the number of active regions up to 18 DIV correlated at least superficially with the overall density of ROIs visible with baseline calcium signal.

2) *Network connectivity rates and patterning (structural clustering)*. The extent of the network and the interconnectivity in that network are increasingly difficult to estimate due to the heterogeneous nature of the population and self-organisation into clusters separated by dense bundles of neurites. Regardless of this, the timing of re-organization is clearly juxtaposed with changes in activity development, as cell migration comes to a halt at the same developmental point that an accelerated increase in the amount of activity and distinct changes in the temporal organisation of that activity are observed.

The process of cluster formation appeared to be related to patterns of somatic translocation. Somatic translocations can occur along leading processes that are either axonal or dendritic

(Kawaji et al., 2004), so somata may be migrating towards retrograde signals from active synapses, or be moving away from that target, or neither. A variety of forces act on migrating neurons, including extracellular current flow generated by transmembrane potential changes (Gabi et al., 2010), neurotransmitter receptors and ion channels (Komuro and Rakic, 1998) or mechanical and molecular forces induced by the environment (Lauffenburger and Horwitz, 1996, Liesi, 1985, Lom and Hockberger, 1997). Migration processes are dependent on f-actin and myosin, which are intracellular calcium-dependent (He et al., 2010b). Cell density also has an effect on cell clustering behaviour. Small populations of neuronal cells distributed themselves uniformly across the surface, but large populations formed tight clusters connected by neuritic bundles (point 1 above). The drop in somatic translocation corresponded well with the emergence of clustering in this current study (compare figures 4.7Aiii and 4.2). These clusters appeared in the absence of glia and when electrical activity was blocked with TTX (Segev et al., 2003). CC9 neuronal clustering appears in the same way as the cells described in the Ben Jacob 2003 study and so glia and electrical activity are evidently not necessary for the structural organisation of the network. This further supports the idea that these differentiating neuronal cells develop functional activity as a self-organised network structure emerges that does not depend on that activity, but ultimately will influence it (as will be further described in Chapter 5). Physical distance between neurons is one of the predominant factors determining rate of connectivity. For projection neurons (those designed to target distal neurons) there is a dramatic drop off in probability of functional connectivity over a few 100 microns from source (Thomson and Deuchars, 1994). This is also true for interneurons (usually GABA containing inhibitory cells) very dense connections are seen within 100's of microns of each cell soma. Gap-junction connectivity can be seen to extend nearly 400µm from the soma (Fukuda et al., 2006). Thus, the emergence of clusters of tightly packed neurons, with dimensions of this order, would be expected to increase functional connectivity enormously. The rate increases for calcium transients per ROI with development may therefore, at least in part, represent an increase in excitatory synaptic inputs to active regions as clusters develop.

It is also interesting to note that termination of somatic translocation, and formation of clusters, appears to reach maturity at the time (17-18 DIV) when significant interruptions in the general trend in many activity measures (above section) are seen. It is interesting to

speculate that the apparent 2-stage developmental profiles seen may represent two very different modes of population activity: an early state where sparse, irregular calcium transients are mainly intrinsically generated (i.e. network independent) – driving maturation of each cell and, more importantly, driving network formation; a later stage where the reverse occurs – the network formed by the early state becomes a functional unit in itself, with sufficient connectivity and neuronal density present to drive individual neuronal calcium transients indirectly through either electrical or chemical synaptic intercommunication.

A number of correlates of the structural and functional developmental profile quantified here can be seen *in vivo. In vivo*, populations of differentiating neurons create synaptic connections with ingrowing axons, recruiting AMPARs into glutamatergic synapses even before chloride gradients have caused GABA to switch from depolarising to hyperpolarising (see chapter 6). They do this through the generation of spontaneous activity (unlike the mechanisms of experience-dependent plasticity in mature neurons) (Voigt et al., 2005). Examples of the generation of this activity were given in the introduction, but briefly, they take the form of (sub)population-wide calcium oscillations, dependent on either early excitatory GABA-ergic and/or glutamatergic synapses (Bacci et al., 1999, Dravid and Murray, 2004, Garaschuk et al., 1998, Murphy et al., 1995), or on gap-junctions (Charles et al., 1996, Yuste et al., 1995). This stage of activity development is therefore oriented to producing a structurally defined network that can propagate and process information, allowing the progression to a more mature activity. This also supports the notion presented in the above paragraph.

In addition, it is likely that network properties exerted an influence on activity rates. These cultures are very low density initially, but as they differentiate and mature, migrating over the surface, the density of connections with neighbours is increased. An apparent simplification of this structuring is seen as the cells form clusters, connected by bundles of neurites; but as was described in the previous chapter, this apparent reduction in complexity is not evident on a the nano-scale, and an estimation of the extent of intra- and inter-cluster connectivity is not morphologically possible. Estimates of connectivity can therefore be best achieved by looking at functional network properties. The increases in activity (for individual neurons and the number of neurons activated in the network) and

eventual regimentation of the temporal patterns of such activity seen throughout development of CC9s could point to increasing connectivity, and eventually over-connectivity. This is expanded on further in Chapter 5, where properties of spatiotemporal organisation of network activity are more closely examined.

4.5.3 Summary

The many possible explanations for developmental changes seen in the activity of CC9 networks could not be adequately elucidated with quantification of the simple properties of calcium transients presented in this chapter. In particular, changes in the rate and extent of activity may have been due to intrinsic cellular or network properties or, indeed, both. In the next chapter I consider a more detailed analysis of network properties during development, focussing on spatiotemporal factors with the aim of further characterising the nature of the development of outputs from de novo neuronal networks.

CHAPTER 5 – SPATIOTEMPORAL PATTERNS OF ACTIVITY IN CC9 NETWORKS

5.1 SUMMARY

In the previous chapter I examined temporal aspects of CC9-derived neuronal network activity and used calcium imaging to quantify the changes in basic patterns of activity over the time scales of hours and days. In this chapter, the *spatial* element of network activity is introduced, and spatiotemporal phenomena are examined. The aims of the work described below were:

To examine spatiotemporal properties of activity as the network develops periodic, synchronous behaviour during maturation.

To compare CC9 network properties with known information processing metrics.

The main findings presented here are as follows:

- Cultures began to display periodic, synchronous activity at 17 DIV and these events were present as large populations of neurons recruited rapidly within a 2 second period.
- Synchronous events displayed a degree of stereotypy, with consecutive events showing a similar temporal distribution for the initiation of individual regions.
- Hub cells were present for the initiation of such synchronous events and activity propagated out into the network involving all sub-clusters of cells simultaneously.
- Signal propagation in the network, analysed within the conceptual framework of neuronal avalanche size but not lifetime, was found to transition from subcritical to supercritical, showing a switch from highly damped activity to over-activation of the network.

The results suggest a move towards a dynamic structure of activity as the network develops until, lacking appropriate external inputs, it produces activity indicative of over-connectivity within itself. The spatiotemporal equivalence between discrete population events points to

a degree of organized connectivity where a subset of 'hub' cells orchestrate the specific neuronal dynamics of more developed cultures.

5.2 INTRODUCTION

5.2.1 Brief recap on spontaneous activity generation in development

Much explanation of the generation of spontaneous activity in development was given in the Introduction in Chapter 4. This chapter deals with the spatio-temporal organization of that activity. As detailed in Chapter 4, patterns of synchronous activity first appear in development after a period of sparse, apparently disorganized activity (Garaschuk et al., 2000, Heikkilä et al., 2009, Spitzer and Gu, 1997). The progression to this new form of synchronized activity reflects changes in network architecture and the intrinsic properties of the neurons within the network (Chiappalone et al., 2006, Nerbonne and Gurney, 1989, O'Dowd et al., 1988). This has also been demonstrated in neural network models and is the default mode for activity generation after synapse formation in developing networks of neurons with sufficient levels of connectivity (Hosaka et al., 2008, Reyes, 2003).

Emerging functional network properties at this stage exact a move from network formation (during phenotypic differentiation, architectural formation and synaptic development) to a more flexible information processing state. The functional relevance of synchronous activity may be the need for temporally discrete integration of information and the need for a precise timing to that processing (Baker et al., 1999, Sanchez-Vives and McCormick, 2000).

Retinal waves were also described in the Chapter 4 introduction and are an example of how spatiotemporal information is encoded in such spontaneous activity. These developmental temporal and spatial patterns of activity have been postulated to provide competitive inputs for the structural development of connectivity in the retina. This was demonstrated in new-born ferret retinas where altered inputs were provided from each retina by altering the frequency of retinal waves differentially and observing the structural developmental consequences of this in the lateral geniculate nucleus (Stellwagen and Shatz, 2002). Topographical maps created during development require this spontaneously generated activity to allow refinement of the maps, with retinal ganglion cell axons forming focal termination zones. This was demonstrated in mice lacking the β2 subunit of the neuronal

nicotinic acetylcholine receptors and were thus unable to generate retinal waves (though were able to generate far less correlated activity) (McLaughlin et al., 2003).

5.2.2 Network topology and structure/function relationships

As discussed extensively in Chapter 4, synchrony (a new functional output) appears as the structure of the network solidifies. Structure/function relationships in neuronal networks can be explored through the use of graph theory (which looks at network structure) and complex system dynamics (which looks at function) (Feldt et al., 2011). This has provided insights into how network topology can affect information processing. Some neuronal systems display scale-free topologies (He et al., 2010a), where the connectedness of neurons follows a power law distribution, with high numbers of neurons having few connections, with a very small percentage of highly connected neurons. In accordance with this concept, by creating power law distributions of neuronal connectivity in live, functioning networks it has been possible to demonstrate the existence of 'hub' neurons in the neonatal hippocampus that are actively involved in GDP generation (Bonifazi et al., 2009). These are GABA-ergic neurons that display high functional and effective connectivity (functional connectivity being the probabilistic causal connections assumed between neurons based on the timing of their firing in relation to each other; and effective connectivity relating to the activation of other neurons following stimulation). Stimulation of hubs affected GDP frequency, where stimulation of low-connectivity neurons had no effect of GDP activity, and hubs exhibited action potentials that preceded spontaneous GDPs (by ~200ms). Interestingly, highly connected neurons could also be pyramidal cells, though stimulation of these neurons did not produce the same effects on network activity (as stimulation of GABAergic interneurons) and so they did not act as hubs. Interneuron hubs thus form an architecturally specific, temporal stereotypic, functional element of neuronal activity patterns. *Structural* stereotypy is a clear aspect of neuronal development (Silberberg et al., 2002), and the extent of *functional* stereotypy that results from this is still being explored.

In the developing neocortex, where early calcium activity generated through ICCR is propagated through gap junctions (and thus the mechanisms of activation and propagation are both very different), a trigger cell activates neighbouring gap junctionally connected cells in a radial fashion, showing how cells with extensive connectivity can affect activity

propagation in a developing network (Yuste et al., 1995) (and this is similarly seen in rat osteoblastic cells (Jorgensen et al., 1997)).

5.2.3 Spatio-temporal aspects of activity propagation

Spatio-temporal stereotypy is observed *in vivo* in the mouse olfactory bulb using calcium imaging, and different activation dynamics were seen for different odour stimuli (Spors and Grinvald, 2002). This ability for networks to display a variety of temporally distinct activity patterns is also demonstrated by looking at spontaneous activity in dissociated cultures of P1 rat cortical neurons on MEAs, where correlations between electrodes reveal subgroups (activity attractors) of bursting events that exhibit their own, non-uniform, temporal sequence (Volman et al., 2005). This behaviour can be modelled with overlapping sub-networks of neurons (that share a small selection of inter-cluster connections) and different spatio-temporal patterns could then be regulated through a fluctuating background current, showing the potential for neuronal networks to vary activity patterns based on neuromodulatory inputs. Such activity motifs were found to exist in real networks of dissociated E18 rat cortical neurons (Raichman and Ben-Jacob, 2008).

Further to this, coupled sub-networks of comparative size such as those mentioned above move towards a state of mutual synchronization (by activating each other) and over time this coupled activity can develop two distinct types of asymmetry: 1) activity propagation asymmetry where activity is preferentially initiated in one specific sub-network and 2) sub-networks develop different correlation (functional) patterns (Baruchi et al., 2008). These two asymmetries can be regulated separately because the *propagation* asymmetry is governed by inter-cluster connectivity and the *functional* asymmetry is governed by intra-cluster connectivity. There is a strong propensity for the development of asymmetry *in vivo*, both structurally and functionally (Nowicka et al., 1996, Pujol et al., 2002, Schlaug et al., 1995) and the above work on connected sub-clusters of neurons indicates network-level mechanisms that could lead to, for example, the lateralisation of functions and directionality of information flow seen *in vivo*.

Neuronal avalanches are another observable property of scale-free networks, where the distribution of numbers of neurons involved in discrete cascades of activity, and the length of such cascades also have power law relations. This property looks at the way information

is propagated through a network by examining the hierarchical patterns of how far that information propagates by comparing discrete events (Beggs and Plenz, 2003, Paczuski et al., 1996, Pasquale et al., 2008, Zapperi et al., 1995). Examining the spatio-temporal organization of activity in this way has made it possible to assess self-organizing networks as they approach optimal levels of information processing – known as self-organized criticality. A slope of -1 on log-log distributions of these power law relations indicates a theoretically ideal state for information processing in a network, as activity is neither dampened down too quickly (stopping propagation) nor spread so freely that most sites become active, reducing the flexibility to allow the appearance, for example, of discrete motifs of activity. Such activities have been seen in mature (21–42 DIV) networks of dissociated E18 rat cortical neurons, which developed a variety of critical behaviours. Not all reached a state of optimal processing and cultures varied between subcritical, critical and supercritical (Pasquale et al., 2008), though a characteristic exponent of -1.5 was nevertheless found for cortical cultures (Beggs and Plenz, 2003). Pharmacological manipulations of neuronal networks can alter these dynamics away from criticality (Pasquale et al., 2008).

Further measures, such as the coincidence index and the branching parameter, were correlated with the state of criticality. The coincidence index (the ratio of direct, cross-correlation to the integral of the cross-correlation over all time lags) was found to be smaller for subcritical than supercritical behaviours. i.e. Higher levels of synchrony are seen for critical than sub-critical behaviours, though synchrony continues to increase when the network moves towards supercriticality (Pasquale et al., 2008). The branching parameter (which examines the number of neurons activated by each previously triggered neuron in activity cascades) is 1 for optimal information processing and higher and lower values pertain to super- and sub-critical behaviours respectively. The branching parameter provides insight into network connectivity as it is influenced by the level of 'fanning' of input and output connections (Beggs and Plenz, 2003). An optimal branching parameter maximizes the number of attractor states into which a neuronal network can be drawn and so increases the processing power of the network by propagating more activity motifs (Haldeman and Beggs, 2005).

Multiple, specific spatio-temporal patterns of activation have been confirmed when gathering unit activity from organotypic cultures of P0–2 rat cortical slices (Beggs and Plenz, 2004). These patterns were distributed over the range of avalanche sizes and were sifted out as families of avalanches that had similar spatial activation and repeated more often than would be expected by chance. There was no local area in the network from which activity preferentially propagated, i.e. motif initiation was spatially distributed.

Dynamic properties of neuronal networks, analysed using the tools described above, reveal much about the influence of structure (network topology) on the functional output of the system. The work described below uses this context to further understand the functional output that CC9-derived neuronal cultures develop, through their uninterrupted differentiation and self-organization into *de novo* networks.

5.3 METHODS

5.3.1 Recruitment profiles

As this chapter deals with the recruitment of many cells into synchronous events, the profile of these recruitments has been examined. This section describes the process used to create the results seen in Figure 5.4.

In cultures showing synchronous activity (such as the one shown in Figure 5.1A), regions do not all fire exactly simultaneously in each event; regions are instead recruited into the event over ~1–2 seconds. Examples of such recruitments can be seen cumulatively in Figure 5.1B. The recruitment rates for each event are calculated based on the point of maximum cell recruitment into the event. This is shown in 'C' as the steepest slope on the cumulative recruitment profile for that event, quantified in 'D' as the maximum peak on the differential of the cumulative profile shown in 'C'. The means of these profiles, shown in 'E', can be calculated once the 'zero' time point has been taken as the point of the maximum recruitment rate. This mean then corresponds to a mean recruitment rate for events in that recording.

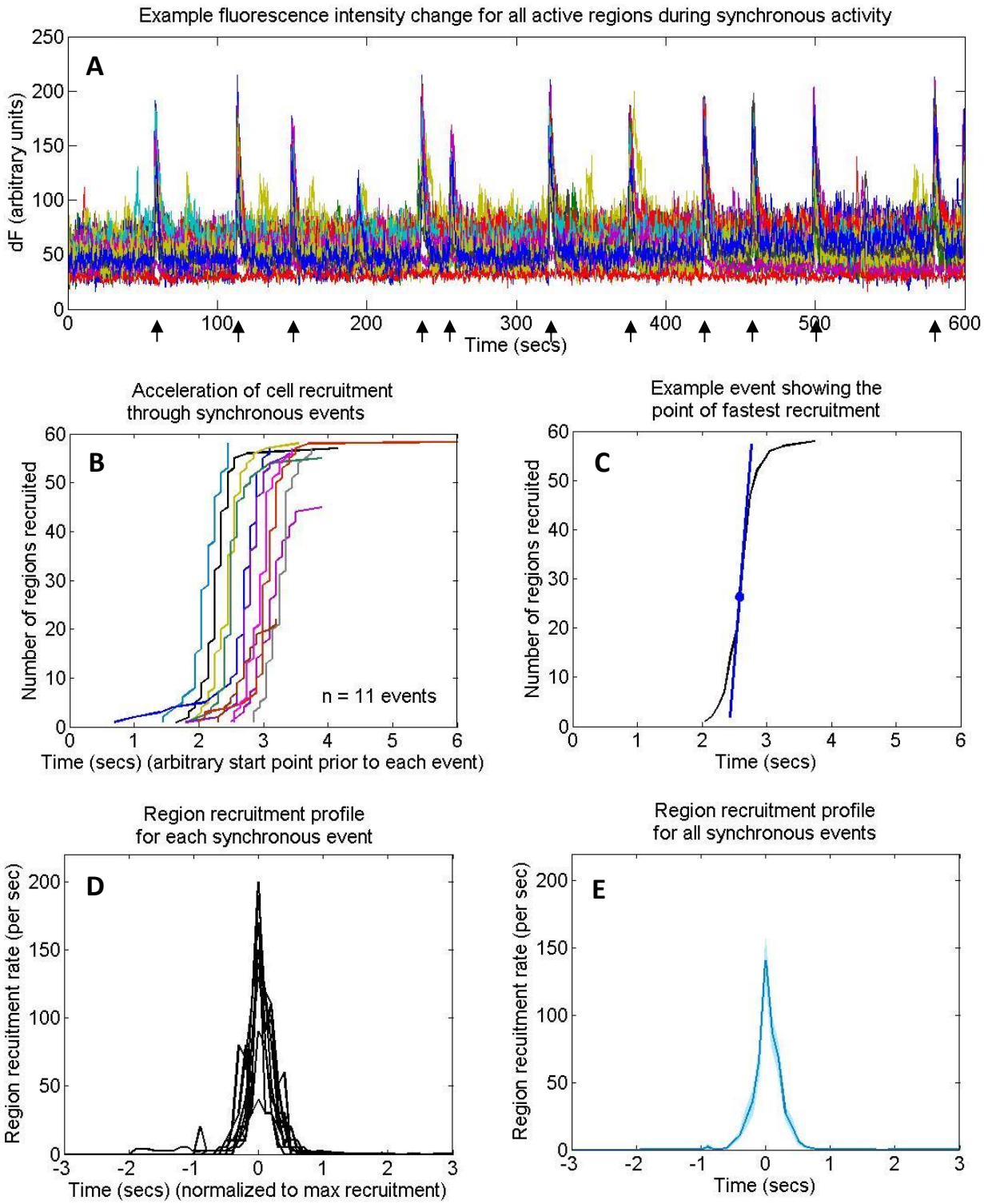

Figure 5.1 – Explanation of how region recruitment profiles during synchronous events were created. A) An example 10 minute recording from an 18 DIV culture displaying synchronous activity (with each synchronous event marked with an arrow). **B)** Cumulative recruitment profile for each of the 11 synchronous events marked with an arrow in 'A'. **C)** An example event chosen from 'B' with a smoothed curve, showing the point of the fastest region recruitment in the event (i.e. the steepest slope). This point is defined as the maximum peak on the differential of the event, shown for each event in '**D**' (i.e. the recruitment rate for each time point throughout the event). The 'zero' time point has been defined as this peak recruitment rate point. **E)** The mean recruitment rate for all events in the recording (n = 11 in this case), with the SEM shown as a blue shaded area.

5.3.2 Z-testing

Stereotypy and 'hub' probabilities were tested for significance by using a z-test based on a null hypothesis. The null hypothesis assumed that there was no special temporal placement of regions within the burst. Z values greater than 2 indicated those regions that were significantly different from the null hypothesis.

$$z = \frac{observed - expected}{standard\ deviation}$$

This was adapted from the standard z-test, which uses the standard error (SEM) (which uses the standard deviation, accounting for the sample size), as opposed to the standard deviation (Freedman et al., 1998). When using the SEM, due to a large sample size and a non-Gaussian distribution, a false impression of significance appeared due to the weight of values skewed from the norm. Ignoring the size of the sample by reducing the denominator to the standard deviation, probabilities were only significant at far larger values that exceeded the bulk of the skew putting significance into the extreme tail of the distribution.

5.3.3 Coincidence index

The coincidence index (CI), used to look at correlated activity across all active regions in a culture, was calculated as the ratio between the correlation coefficient (with zero time lag) (*Cxy(0)*) across all regions and the integral of the cross-correlation across time lag $-T$ to T (with T being the length of the recording) (*Cxy(T)*).

$$CI = \frac{Cxy(0)}{\Sigma Cxy(\mathrm{T})}$$

5.3.4 Neuronal avalanches

Neuronal avalanches describe cascades of activity that spread across a network of neuronal cells and their significance is expounded on in the introduction above. In the following results, the size of the avalanche refers to the sum of the collective network activity occurring in a specific temporal window. The start and end of each temporal window are defined as the frames which contain no activity across the whole network. The length of this temporal window refers to the avalanche lifetime.

5.4 RESULTS

5.4.1 Synchronous Activity

Synchronous events, as described in the previous chapter, start appearing at 17 DIV. Prior to this, activity is seemingly random, non-synchronous, discrete events with fewer than 3 regions active in any 2 second period (Figure 5.2A). In contrast, cultures displaying synchronous activity contain events where at least 10 times as many regions are recruitment in a 2 second period. Unlike the local, discrete events commonly seen in younger cultures, these are population-wide events where the majority of regions found active in a 10 minute recording, spatially distributed over the whole field of view, are recruited into the event. In some cultures, synchronous activity was interspersed with non-synchronous activity, and in other instances only synchronous activity was found (Figure 5.2B & C). On some occasions it was apparent that another hierarchy of ordering is present, as can be seen in Figure 5.2C, where population-wide events were grouped, with subsequent events in each groups recruiting fewer regions into the event. Each grouping was followed by a quiescent period in which no regions fired. A wider spacing between events resulted in a longer grouping before a silent period.

Synchronization had a measureable effect on the basic temporal properties of transient activity, as is shown in Figure 5.3. All three key measures (FWHM, amplitude and ITI) showed marked changes when moving to synchronous activity, with the FWHM showing a change over the transition period only, and amplitude and ITI simply displaying a difference between synchronous and non-synchronous activity overall. At 18 DIV there were no cultures displaying non-synchronous activity. The FWHMs split into a bimodal distribution for 17 – 18 DIV when synchronous activity begins to emerge and only appears in those cultures displaying synchronous activity. The secondary peak shows cultures at this stage to exhibit shorter FWHMs at 3.2 seconds, as well as a peak at 6.2 seconds, seen in younger cultures. This peak disappears in cultures older than 18 DIV, leaving only the original peak at 6.2 seconds (Figure 5.3A). The transient, 3.2s, peak was considerably more pronounced than the 6.2s peak (consistently present throughout development) in 17 DIV cultures, although in 18 DIV cultures both peaks were comparable in height.

This bimodal distribution was not seen in the amplitude or ITI distributions, although increases in both were seen in cultures displaying synchronous activity. Over all cultures from 17–19 DIV, amplitudes increased from 60-70 to 100-110, and ITIs increased from 20-30s to 30-40s (Figure 5.4B & C), showing that transients involved in synchronous bursts were higher in amplitude with longer times between subsequent transients. The peak in the distribution of ITIs for 17 DIV cultures displaying synchronous activity was markedly higher (at 90-100s) than for non-synchronous activity at the same developmental stage (20-30s). At other developmental stages, this difference was only marginal, showing a move in the peak from 20-30s to 30-40s.

The recruitment profile for synchronous events was very consistent within a single recording (Figure 5.4A). At all developmental stages the recruitment profile showed a fast onset up to a sharp peak before falling rapidly off to zero. However, recruitment rates at the peak varied between developmental stages. They were lowest at 17 DIV (9±2), increase sharply for 18 DIV to 73±8, then show a transient decline for 19 DIV before recovering up to a maximum at 20 DIV (85±12). This maximum has declined to 56±13 by 21 DIV (Figure 5.4B). This recruitment shown as a ratio of the maximum region recruitment to the total number of active regions shows the same developmental pattern, with a rise to 17DIV, a transitory dip at 19 DIV and a rise again at 20 DIV (Figure 5.4C).

5.4.2 Stereotypy

Within synchronous events, the spatial aspects of region recruitment showed a degree of stereotypy; i.e. regions recruited in specific temporal windows throughout an event can be seen to consistently appear in that temporal window in consecutive events. An example of this is shown in Figure 5.5A where four events from one 10 minute recording are depicted in 0.2 second frames showing the regions active within that temporal window. In this example, it can be seen that although the same regions are not always activated in the same window (e.g. each of the first 0.2s frames in this example displays quite a different set of neurons primarily activated with only 1 region showing any repetition of activation at all), there are occasions when same region activation is clear (such as 0.6s into the burst). Even when the same region is not activated in the same temporal window of a subsequent event, regions neighbouring the expected active region can become active instead, showing a spatial activation relationship that spreads beyond individual region activation.

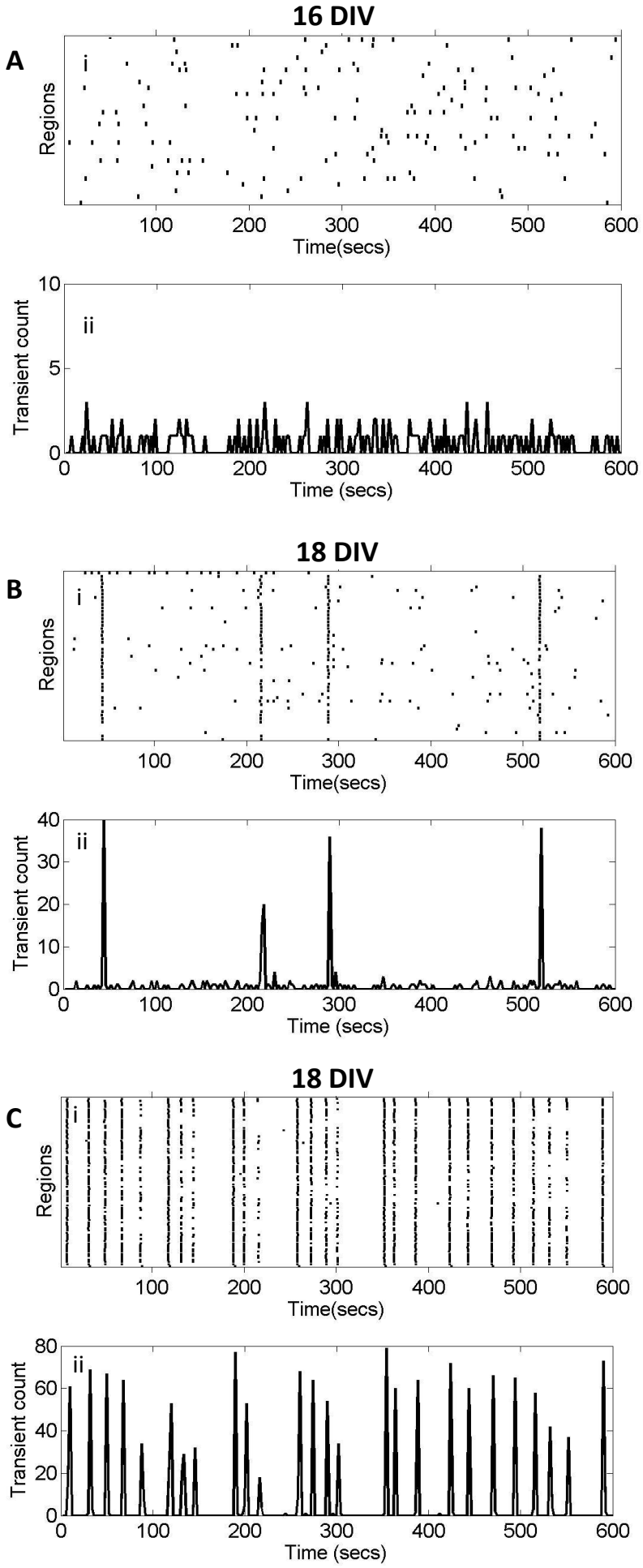

Figure 5.2 – Example raster and instant frequency plots showing non-synchronous and synchronous behaviour. A) A 16 DIV culture displaying non-synchronous activity (i) where no more than 3 regions are active in any 2 second period (ii). **B)** An 18 DIV culture displaying widely spaced synchronous activity with non-synchronous activity present between the synchronous events (i). Synchronous events can be seen to recruit at least 10 times as many regions within a 2 second period than non-synchronous events in the culture (ii). **C)** An 18 DIV culture displaying synchronous activity with no non-synchronous activity occurring between these events.

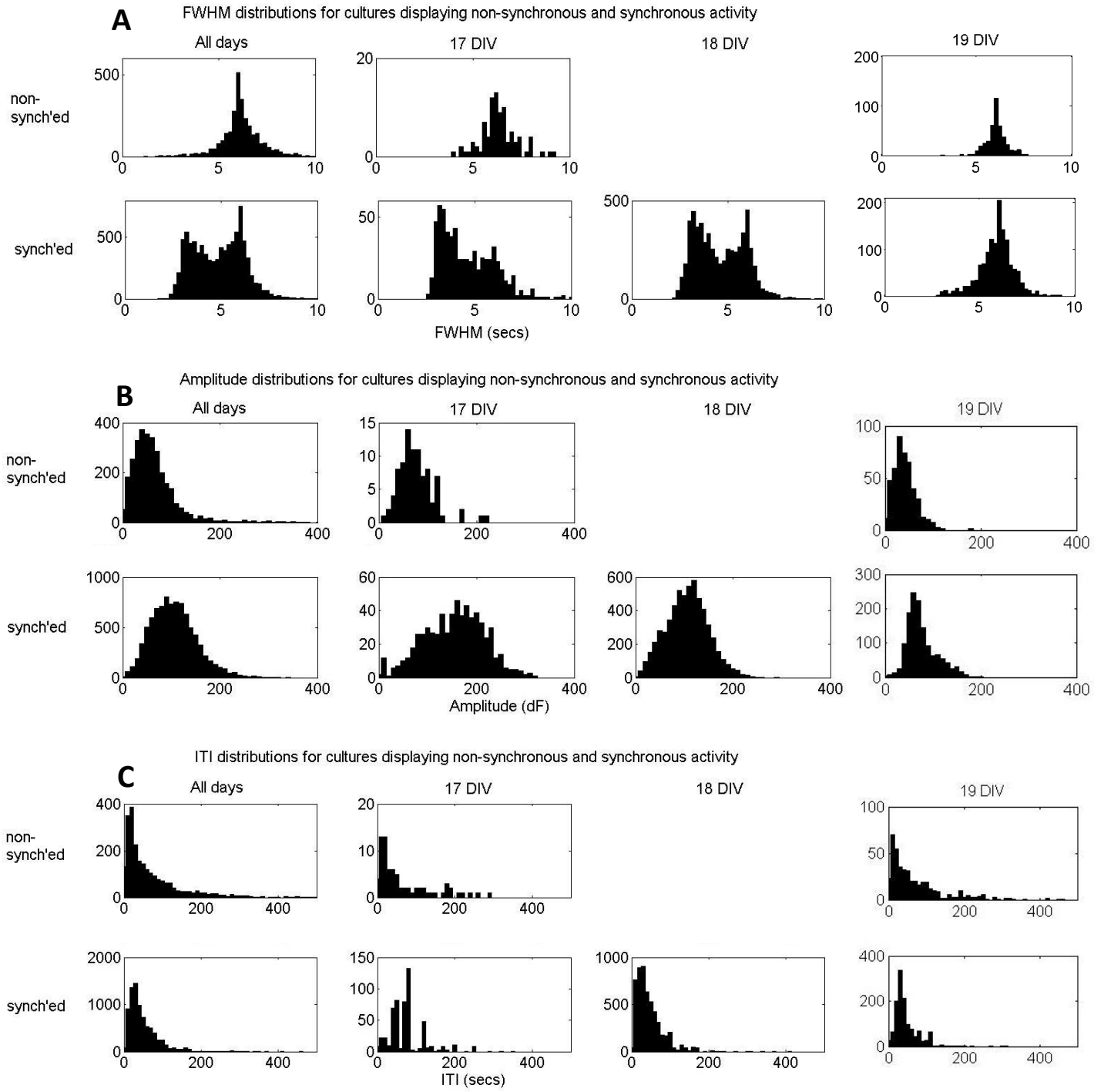

Figure 5.3 – Distributions of FWHMs, amplitudes and ITIs for non-synchronous and synchronous behaviours and the change of these distributions with DIV number. Note: no non-synchronous activity was seen at 18 DIV. 'Non-synch'ed' = pooled data for cultures displaying non-synchronous activity and 'synch'ed' = pooled data for cultures displaying synchronous activity. Also note the variation in limits for the y-axes. **A)** FWHM distributions for all cultures summed together show a unimodal response with a peak at 6.2 secs for cultures exhibiting non-synchronous behaviour and a bimodal response with peaks at 6.2 secs and 3.2 secs for cultures exhibiting synchronous behaviour. The bimodal response can be seen to be attributed to at specific developmental stage with 17-18 DIV synchronous cultures showing a bimodal response and synchronous cultures older than 18 DIV showing a unimodal response. The Peak at 3.2 secs only appears in 17 – 18 DIV cultures exhibiting synchronous behaviour. **B – C)** Amplitude and ITI distributions show no clear bimodal responses for cultures exhibiting synchronous behaviour as seen in the FWHM distributions. However, amplitudes are greater for synchronous than non-synchronous activity at 106.7±0.4 and 59.6±0.7 respectively; as are the ITIs at 82.4±1.7 and 59.2±0.5 respectively (errors given as SEM).

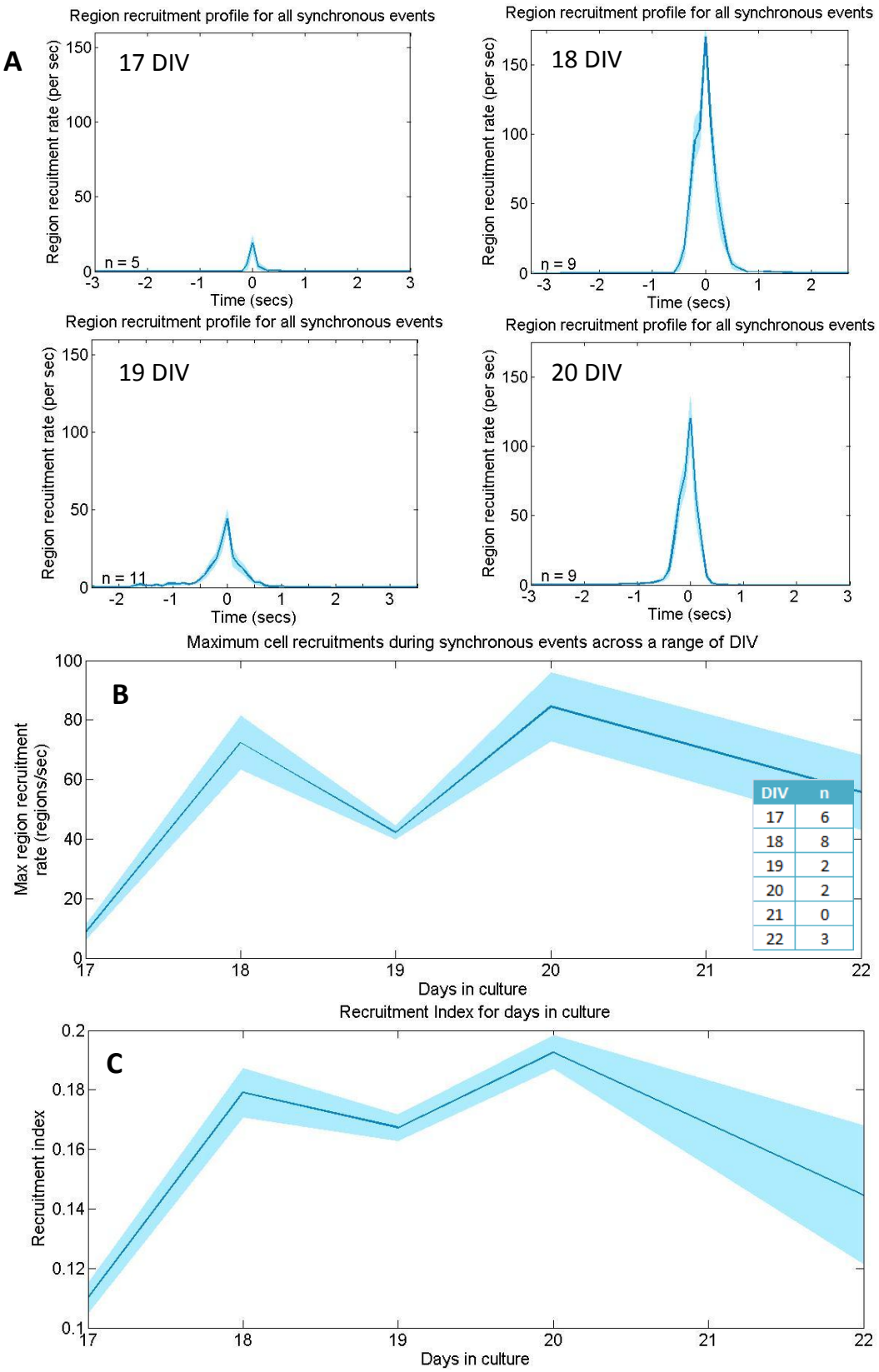

Figure 5.4 – Cell recruitment profiles and rates for a range of days in culture. A) Example average recruitment profiles for all synchronous events in a single 10 minute recording period for a selection of DIVs show very similar shapes. Peak values vary among cultures and days and averaged 76.5±9.27 regions per second. The recruitment period was consistent regardless of the number of regions recruited at an average of 1.42±0.04 seconds. **B)** The average peak values for region recruitment for all cultures for a range of DIVs displaying synchronous activity showing an increasing trend with day in culture with a peak of 84.5±11.5 regions per second at 20 DIV and a minimum at 17 DIV of 8.62±2.32 regions per second when synchronous activity first appears. **C)** The recruitment index (maximum recruitment rate/total number of active regions) for a range of days in culture, which follows a very similar profile to 'B'.

A distribution of the probabilities of each region appearing in a specific temporal window over all recordings is also shown in Figure 5.5B, showing the majority of regions to have low probabilities (0.1) of appearing in the same temporal window in other events, and there is a fast fall off in higher probabilities from this. However, 8% of regions displayed a significantly higher probability of appearing within a specific temporal window that precluded chance (i.e. more than twice the standard deviation of the probability of a region appearing in a temporal window due to chance). This was determined using a z-test based on a null hypothesis (see Methods Section 5.3.2 above). Only the highest probabilities for each region were included; i.e. a region with 90% probability of appearing in the first temporal window may be accompanied by a 10% probability of appearing in the second temporal window, but only the higher probability is included, rejecting repetitions of the same regions at lower probabilities. It should therefore be noted that if there are multiple spatio-temporal patterns of activation, only one of these is considered for each neuron.

A coincidence index (described in the Methods, section 5.3.3) was used to look at correlated activity for a range of days in culture (Figure 5.6A) and shows a gradual rise over developmental stages, with an increase from 1.71×10^{-3} at 14 DIV to a peak of 1.97×10^{-3} at 22 DIV. This is interrupted by a transient increase in correlated activity above the steady rise at 17–18 DIV (with a value of 1.96×10^{-3} reached at 18 DIV).

Cross-correlograms showing the correlations between all active regions for example recordings from 17, 18, 19 and 22 DIV cultures are shown in Figure 5.6B 'i–iv' respectively. The ordering of the regions by their average, relative times of activation within all synchronous events reveals the presence of temporally organized activity motifs. These can be made out as characteristic 'checkerboard' patterns where all regions are correlated to a degree but the temporal ordering is different for subsets of neurons. Motifs do not appear as clearly defined in 18 DIV cultures as in 19 and 20 DIV cultures as the 18 DIV example 'B ii' demonstrates. Neighbouring regions of high correlation (ordered by temporal activation) are interrupted by regions of low general correlation. This gives a false impression of sub-clusters of temporally correlated regions where there are none. Instead, there is an overall high correlation across most regions; i.e. any individual activity motifs have become mutually synchronous into one massive motif, transitorily, at this stage in development.

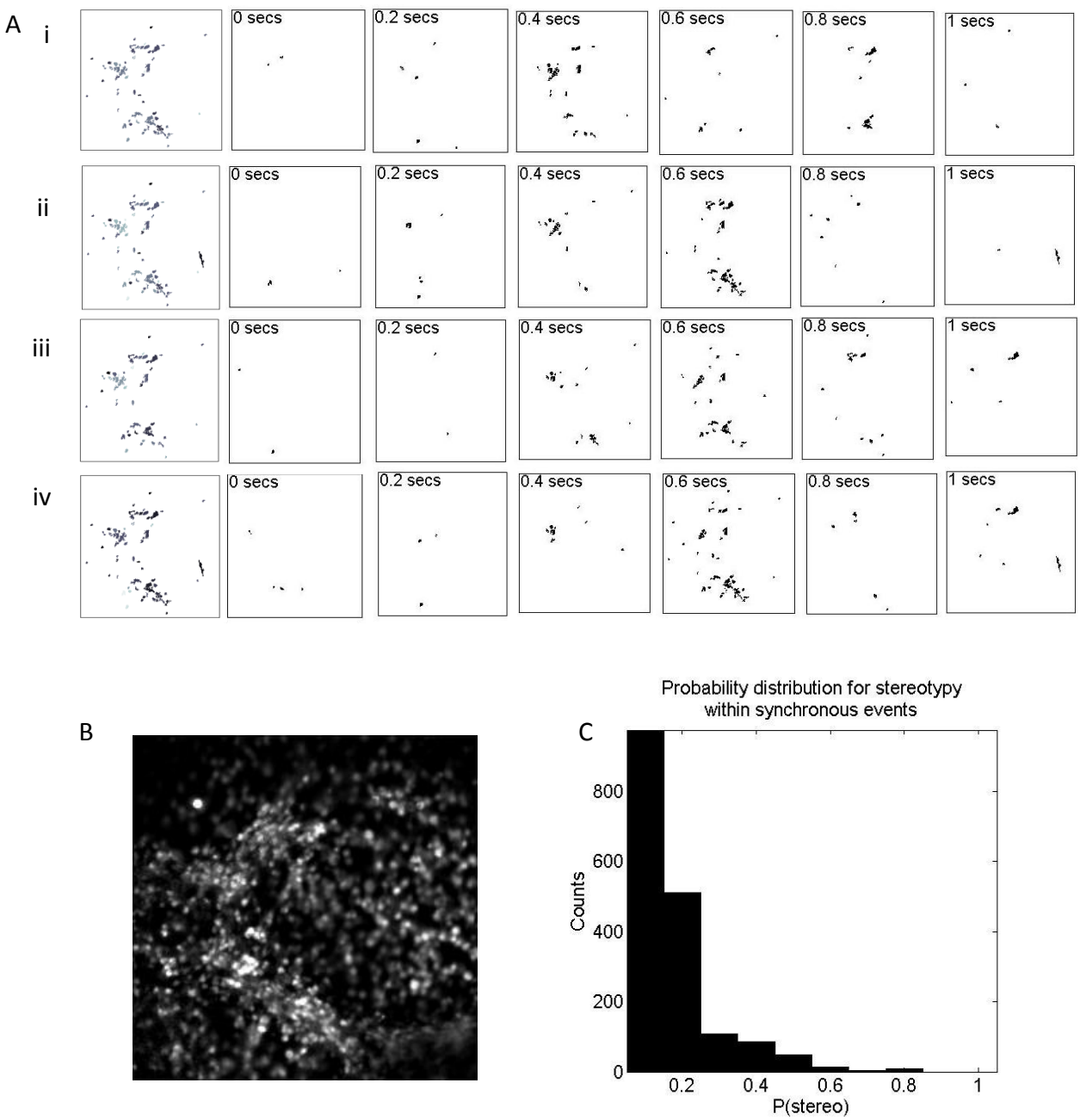

Figure 5.5 – An example of stereotypy in the spatiotemporal pattern of region recruitment during repeated synchronous events from a single culture. A) 'i – iv' Four example synchronous events from a single 10 minute recording that have been segmented into 0.2 second windows, with each frame showing the regions recruited in that window for that event. The first image shows all regions active in the event. **B)** Fluorescence image showing all cells stained in that culture. C) A probability distribution showing the spread of probabilities that any one region appears in a specific 0.2s time window during a synchronous event over all recordings where >5 events occurred in the recording and >10 regions were involved in that event. A z-test shows that 8% of these probabilities are significantly high enough to preclude chance.

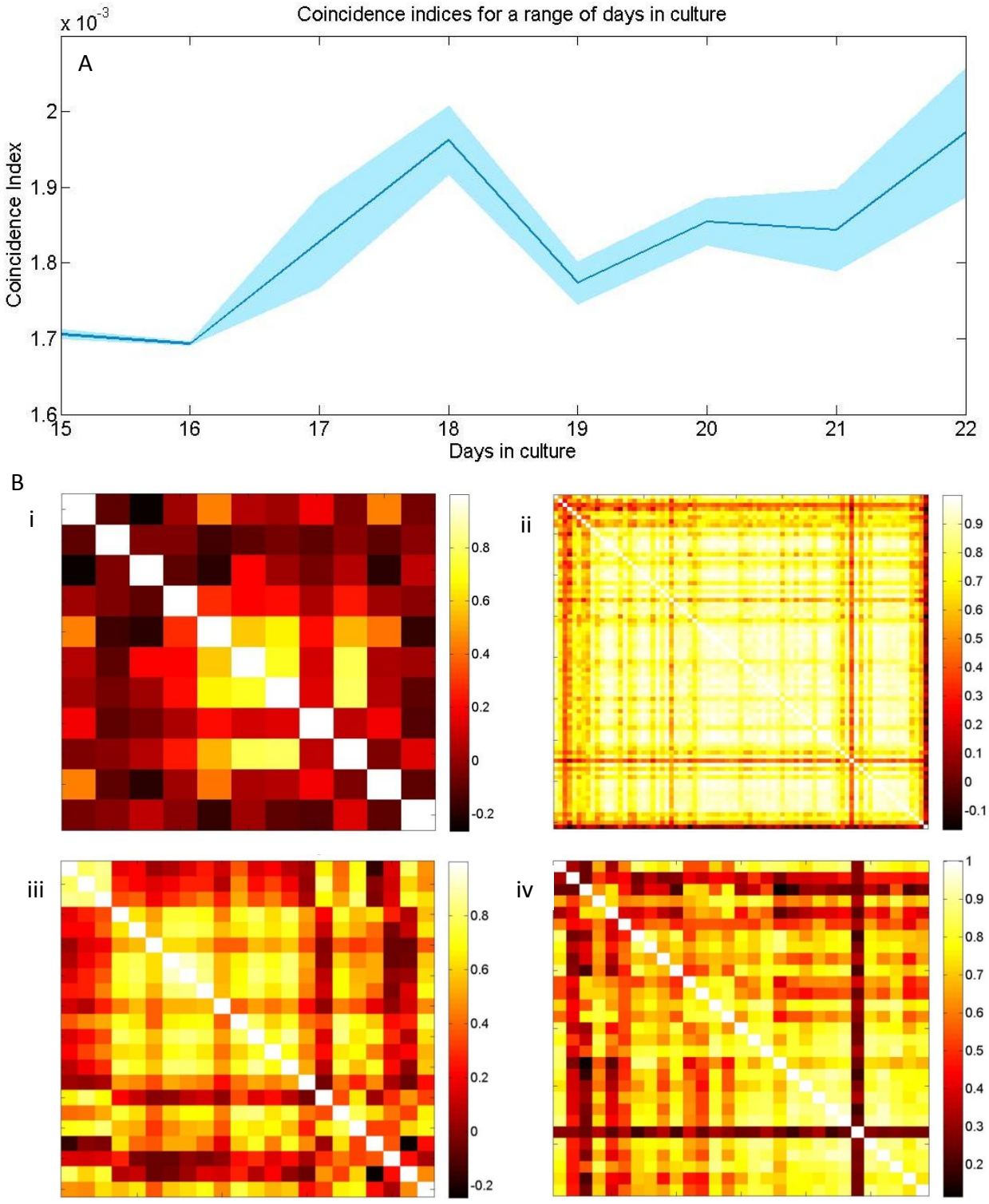

Figure 5.6 – Region correlations for different developmental stages. A) The coincidence index (explained in the text) for a range of days in culture shows an increasing trend with development, with a rise from 1.71×10^{-3} at 14 DIV to 1.96×10^{-3} at 18 DIV, followed by a dip at 19 DIV to 1.77×10^{-3}, then increasing gradually to 1.97×10^{-3} at 22 DIV. **B)** Cross-correlograms showing the correlations between all active regions for representative individual recordings from 17, 18, 19 and 22 DIV cultures ('i–iv' respectively). The regions are ordered by their average, relative times of activation within all synchronous events in the recording. The presence of activity motifs can be made out as characteristic 'checkerboard' patterns as all regions are correlated to a degree, but the temporal locality of that correlation is different for subsets of neurons. Motifs do not appear as clearly defined in 18 DIV cultures as in 19 and 20 DIV cultures ('B iii & iv'), as the 18 DIV example is 'B ii' demonstrates where temporally neighbouring correlated regions are interrupted by regions of low general correlation, giving a false impression of sub-clusters.

Furthermore, there was evidence for the existence of 'hubs' that are consistently active at the start of synchronous events. Three examples of this are provided in Figure 5.7 from 18, 19 and 20 DIV cultures. Regions active at the initiation of the synchronous event are shown for 4 example events for each of the three days (Figure 5.7C) with red arrows indicating the hub region(s) for that event. The inset shows the cumulative recruitment profile for that event, with a line to mark the initiation of that event. The red regions (also marked with red arrows) confirm that, although more than one region may be activated at this time point, the same 'hub' region is also consistently activated at the start of these events, prior to the rapid recruitment of the rest of the population. Occasional instances of dual recruitment profiles were found, and one example of such a dual recruitment can be seen in Figure 5.7 in the 19 DIV example 'C, iv'. There is an initial, slower recruitment before the 'hub' neuron (seen in the previous 3 examples from this recording) is activated. At this point the population recruitment accelerates with a profile similar to that seen in 19 DIV 'C, ii and iii'. The entire population of active regions for all events in a single epoch (shown in Figure 5.7A) are not activated for every event (as shown in the raster in Figure 5.2), though the majority are.

A distribution of 'hub' probabilities was created based only on those cultures displaying more than 5 synchronous events in a 10 minute period with more than 10 active regions in each event (Figure 5.8A). The shape of the distribution mirrored the one for stereotypy. Using the z-test method described in Methods Section 5.3.2, 10% of regions displayed a significantly high probability of being a hub neuron – i.e. high enough to preclude chance.

Correlation coefficients were calculated separately for all regions with significantly high probabilities of acting as a hub and for all other regions (Figure 5.8B). Far higher correlations were found for hubs, which had a median value of 0.6±0.31 (n = 1183), as compared with the median correlation coefficient of 0.03±0.34 for all other regions (n = 8836). The spread of activity through spatially distributed clusters of cells can be seen in Figure 5.9A–C, with 'C' showing the propagation of activity according to distance from the 'hub' neuron for a selection of synchronous events. 'A' shows a culture with two large, distinct clusters and 'B' shows a culture with a large number of clusters. The activity can be seen for both of these examples to propagate throughout all clusters concurrently

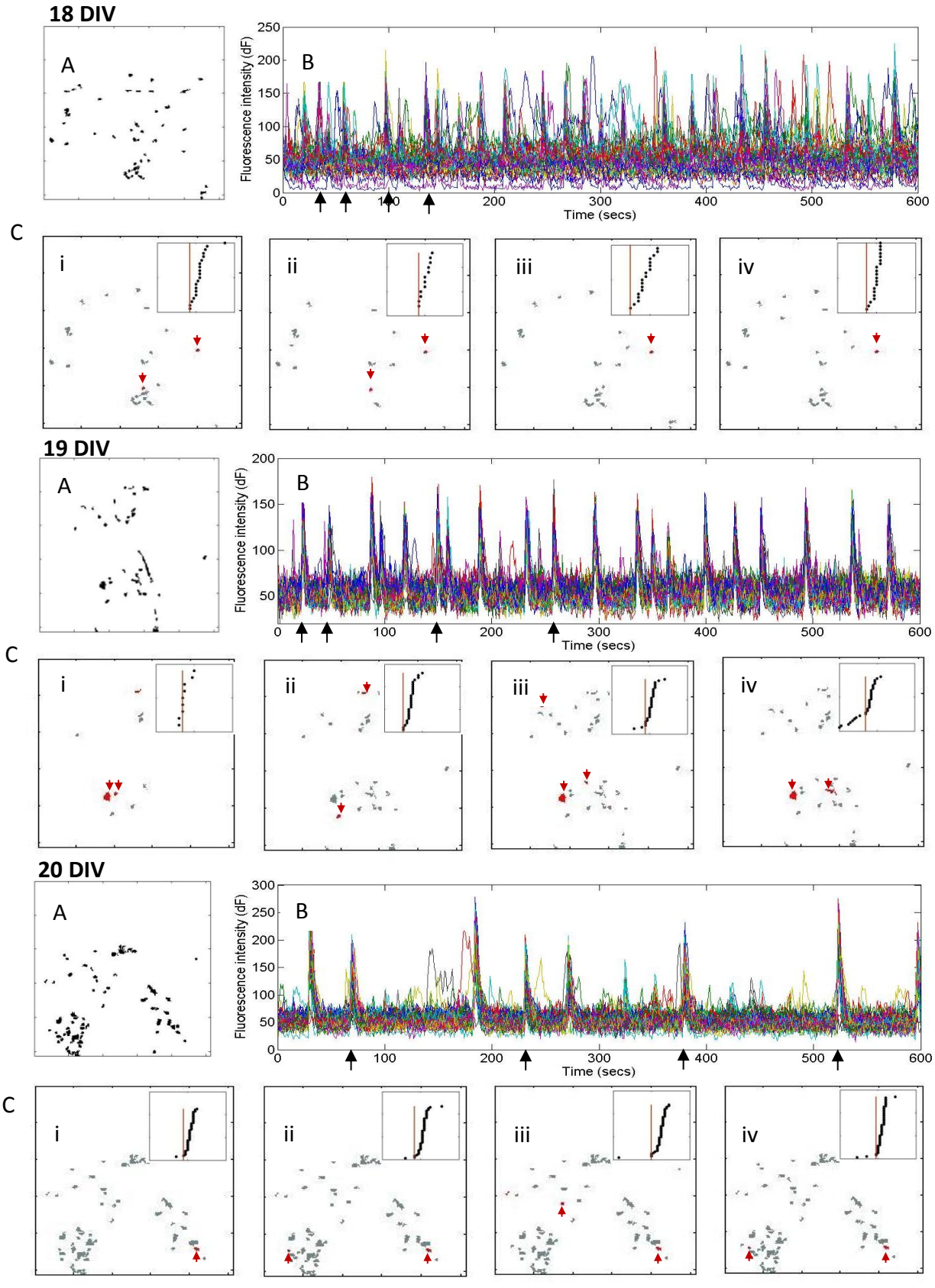

Figure 5.7 – Demonstration of the existence of hub neurons from example 18, 19 and 20 DIV cultures. For 18, 19 and 20 DIV: **A)** Binary image of all regions found to be active during a 10 minute recording with the traces from all these reasons shown in '**B**'. **C)** i – iv) The image shows the regions that become active in a single synchronous event. The 'hub' region(s) for that event are marked in red with an arrow. The inset shows the recruitment profile for that event with black dots showing the cumulative recruitment of regions into the event and the red line marking the location of the 'hub' region(s) for that event. Each event shown in i – iv is marked in 'B' with an arrow.

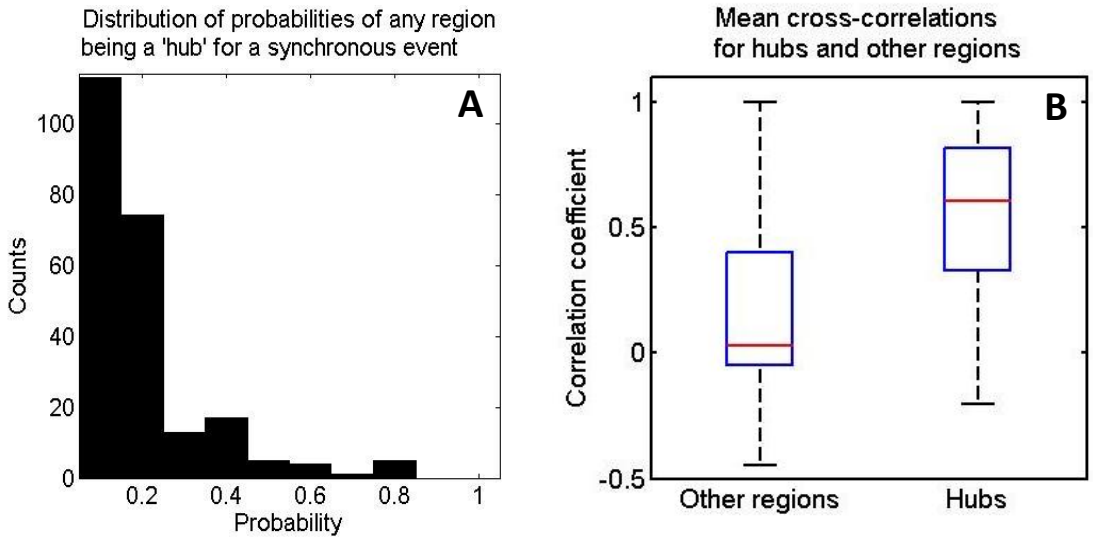

Figure 5.8 – 'Hub' probabilities and their correlation coefficients. A) Distribution of probabilities for a region to act as a 'hub' region for a synchronous event across all cultures showing synchronous activity with more than 5 synchronous events in the 10 min recording with more than 10 active regions. A z-test shows that 8% of these probabilities are significantly high enough to preclude chance. **B)** The median correlation coefficient of 0.6±0.31 was found for regions exhibiting a significant probability of being a hub (n = 1183), as compared with the median correlation coefficient of 0.03±0.34 for all other regions (n = 8836).

(shown in 'C'). There is no discrimination between clusters for the propagation of activity. As the regions are arranged (for each cluster) in order of distance from the hub, it is interesting to note that some regions show a clear spatio-temporal pattern of propagation (e.g. 'C a' third plot and 'C b' last plot), where regions are activated in order of distance from the hub.

5.4.3 Criticality

Neuronal avalanches (explained in Methods above) in CC9-derived neuronal cultures display negative power law distributions for both their size and lifetime (Figure 5.10). For cultures which display non-synchronous activity, avalanches show a power law relation with slopes of -1.96 for size and -6.17 for lifetime, demonstrating subcritical behaviour. In contrast, in cultures displaying synchronous activity, avalanches show a power law relation with slopes of -0.58 for size and -4.06 for lifetime. Though the lifetime distribution is still subcritical, the size distribution has moved from sub- to super-critical.

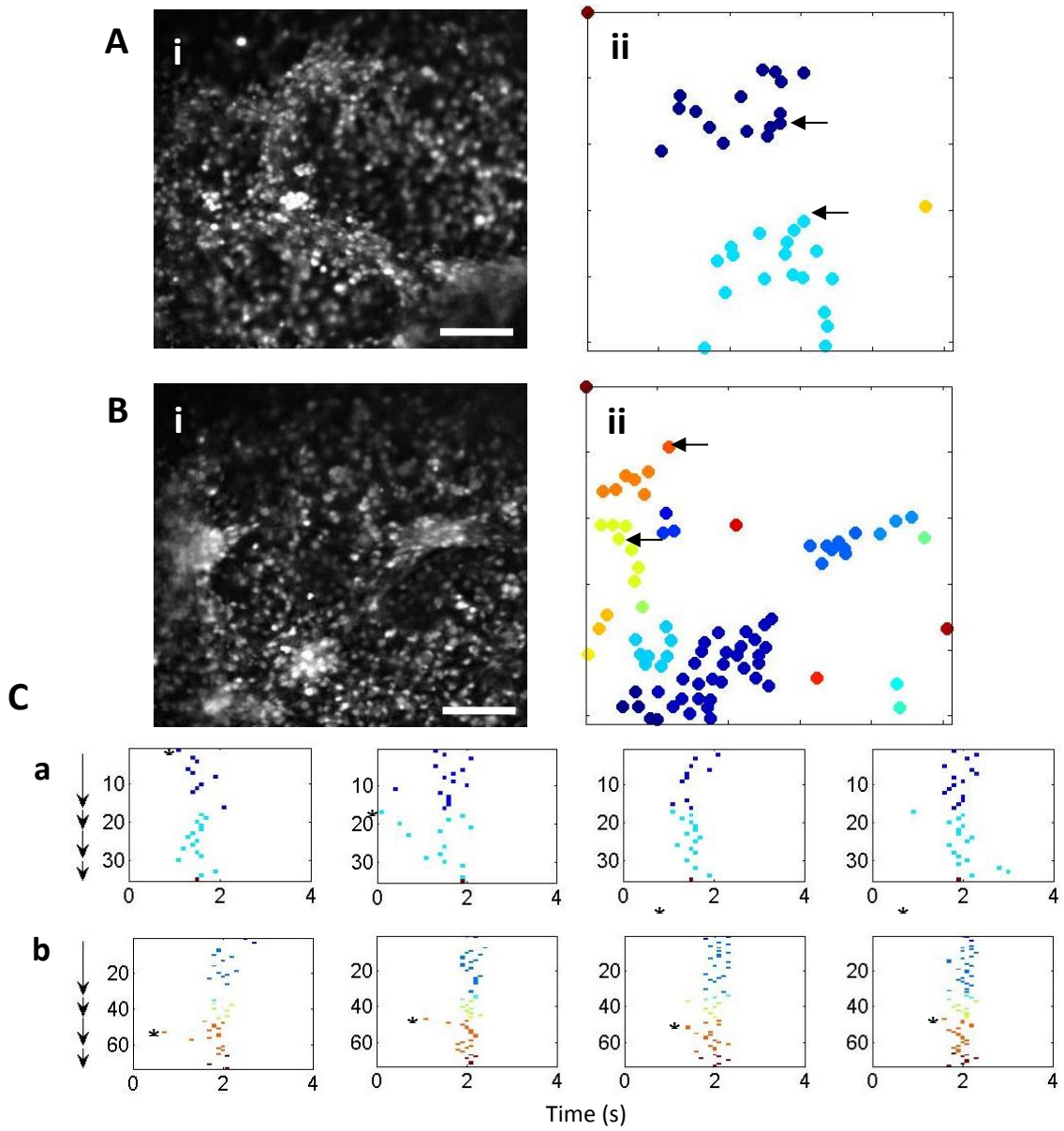

Figure 5.9 – Examples showing qualitatively the spread of activity through sub-clusters of regions during synchronous events. A – B) Active regions in the culture were split into sub-clusters based on spatial distribution to look at the spread of activity following synchronous event initiation. The resting fluorescence intensity image is provided for reference (i) (Scalebar = 100µm) and the sub-clusters are shown in 'ii'. The 'hub' regions are shown with arrows. The spread of activity in 4 example synchronous events from these cultures is then shown in '**C**' as a raster plot with 'a' and 'b' corresponding to 'A' and 'B' respectively. The regions are displayed in order of clusters and then distance from the 'hub' region for that event.

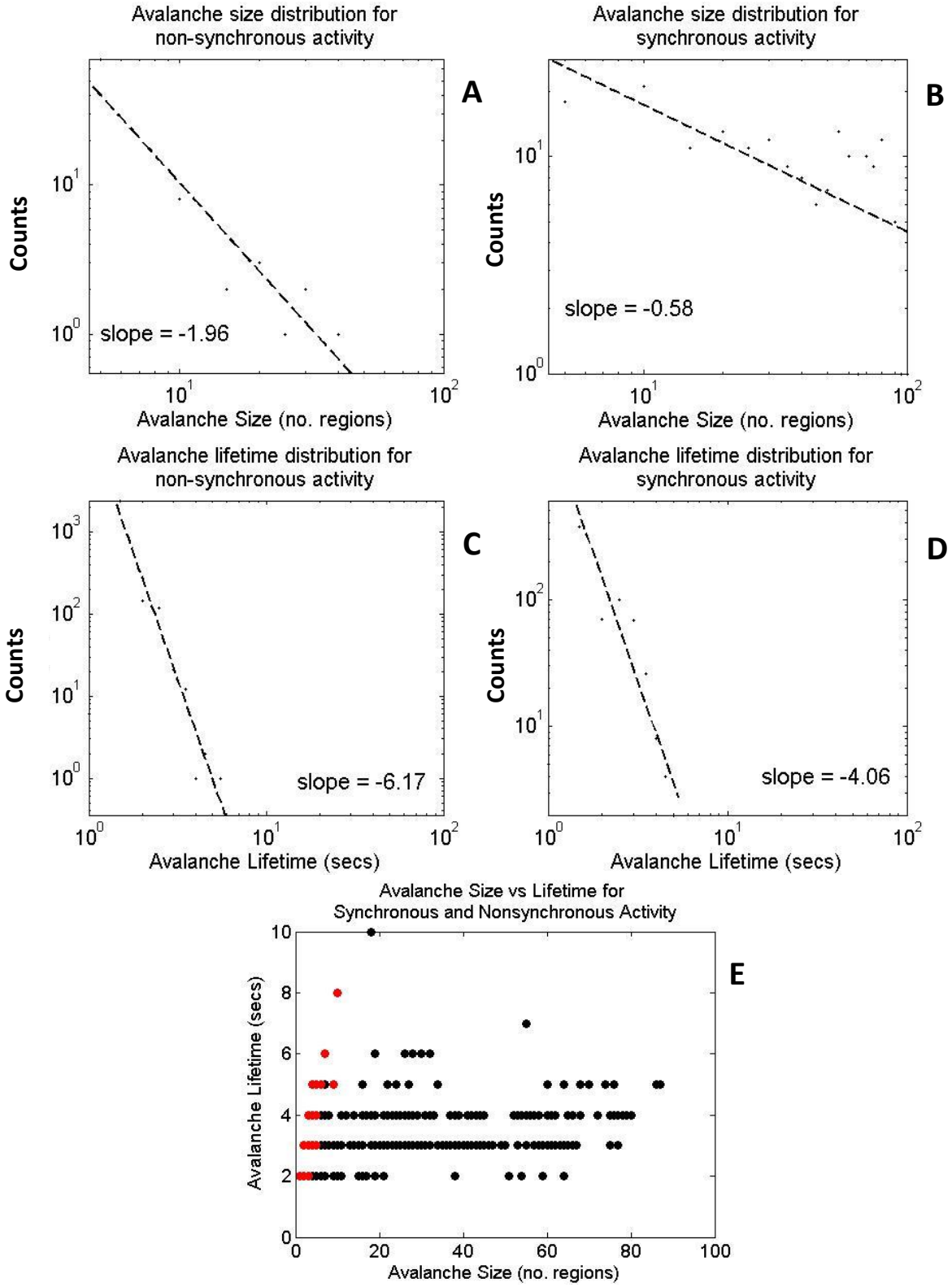

Figure 5.10 – Neuronal avalanche size and lifetime distributions for non-synchronous and synchronous activity. An avalanche is defined as the collective activity occurring in a culture in a temporal window, the edges of which are defined by the absence of all activity in the culture. Avalanche sizes are taken to be the number of regions that become active in an avalanche and the avalanche lifetime is the length of the temporal window in which the avalanche occurs. **A)** Avalanche size distribution for non-synchronous activity has a power law relation with a slope of -1.96, showing the culture activity is in a subcritical state. **B)** Avalanche size distribution for synchronous activity has a power law relation with a slope of -0.58, showing the culture activity is in a supercritical state. **C)** Avalanche lifetime distribution for non-synchronous activity has a power law relation with a slope of -6.17. **D)** Avalanche lifetime distribution for synchronous activity has a power law relation with a slope of -4.06. **E)** The size vs lifetime of avalanches for both synchronously (black) and non-synchronously (red) active cultures. Although lifetimes remain consistent between the two types of activity, the number of regions involved in avalanches includes a much larger spread with synchronous acitivity.

5.5 DISCUSSION

5.5.1 Synchronous activity

Synchronous activity appears spontaneously in CC9 cultures as they develop (17 DIV) after a period of apparently 'random' spatio-temporally dispersed activity. This onset is accompanied by increases in the levels of activity and coincides with the termination of migration processes (see Figure 4.2 – somatic translocation falls to near zero by 17 DIV) and the structural organisation of the network (see Figure 3.8 – clustering of neurons within the network reached maximum at 17-19 DIV). The appearance of spontaneous, synchronous activity have been shown in dissociated cultures (Ban et al., 2007, Chiappalone et al., 2006, Heikkilä et al., 2009, Opitz et al., 2002), slice preparations (Ben-Ari et al., 1989, Garaschuk et al., 1998, Yuste et al., 1995) and in vivo (Leinekugel et al., 2002), and similarly such highly correlated activity has also been found in the retina and spinal cord (Sernagor et al., 2003, Tabak et al., 2001). In development, such activity has been associated with large calcium transient fluxes and the sources of these activities can be synaptic or gap-junction-mediated (Ben-Ari et al., 1989, Garaschuk et al., 1998, Leinekugel et al., 1997, Yuste et al., 1995) (as was discussed in the Introduction in Chapter 4). It is useful to note what CC9 activity has in common with these established forms of spontaneous synchronous activity in order to understand the possible mechanisms behind it, in terms of the developmental stage of CC9 cells and the effect of environment on them.

Spontaneous patterns of calcium activity have been shown in glial cells. In these, the spread of calcium activity between cells occurs in a slow, wave-like manner, propagating away from the initiation site (Hoogland et al., 2009, Newman, 2001, Newman and Zahs, 1997, Weissman et al., 2004). In contrast, the activity propagations shown in this chapter (e.g. Figures 5.5 and 5.9), follow complex spatiotemporal patterns that do not have a distinct linear relationship between activation time and distance from activation source. This is also shown in Chapter 3, Figure 3.9 with electrical stimulation of the cells.

Spontaneous synchronous activity in the developing neocortex can be activated through trigger cells and propagated, non-synaptically, through gap junctions (Yuste et al., 1995). The calcium spread has been attributed to release from stores (via IP_3) and the presence of these gap junctions coincides with the period of development prior to and overlapping

synaptogenesis (Kandler and Katz, 1995). The size of domain recruited in such synchronous events is around 100µm^2, limited by gap-junctional connections, and has a far smaller spatial extent than for the synchronous activity seen in CC9 cultures. The speed of propagation of this activity was estimated at ~100µm/s and trigger cells appeared centrally to the domain, with activity radiating outwards. Recruitment of regions from CC9 cultures in ~500µm^2 occurred over 1-2s, the full spatial extent of the event could not be determined due to the restriction of the field of view and 'hub' neurons could not be placed relative to the extent of the activation (though they frequently lay on the outskirts of the field of view). Sub-clusters of cells, larger than the gap-junctionally connected domains of the neocortex, were also bridged for the generation of these synchronous events, though this does not rule out gap-junctional connectivity as these connections have been seen to extend up to 500µm from the cell soma in other systems. Also, these 2D configurations, coupled with a lack of normal afferent inputs, may result in more extensive or widely distributed gap junctional connections in CC9 networks than seen in the developing neocortex.

However, there is a distinct difference in the spatiotemporal activation of cells in CC9 cultures when compared with the gap junctional propagation described in the developing neocortex. In neocortical slices activity propagates radially out from a central source (Yuste et al., 1995). In contrast, in CC9 cultures the propagation does not follow such a linear time/distance spread and multiple sub clusters of cells are activated within the same temporal frame, regardless of distance from the site of activation. This is not consistent with gap-junctional transmission, as explained in Chapter 4.

Spontaneous, synchronous giant depolarising potentials (GDPs) that correlate with intracellular calcium influx in whole populations of cells from P3 – P5 rat hippocampal slices co-activate $GABA_A$ and NMDA receptors in the generation of spike bursting activity (Ben-Ari et al., 1989). They are themselves generated through the action of ATP and glutamate (via AMPA receptors) (Bolea et al., 1999, Safiulina et al., 2005). As is described in the next chapter, in CC9-derived cultures GABA is an excitatory force at 17 DIV (though this effect decreases and has almost entirely lost its excitatory effect by 21 DIV). NMDA and AMPA receptors are functionally present (Trevelyan et al., 2010) and the excitatory action of glutamate was demonstrated in Chapter 3 (see Figure 3.11), although the presence of

synaptic activity has not been confirmed here. Propagation of activity via chemical synapses is nevertheless discussed, due to the possibility of their existence.

The speed and direction of propagation of GDP activity is highly dependent on the network architecture (Bolea et al., 2006) and had activity rates of 0.05–2s^{-1} (Leinekugel et al., 1997). Well delineated architecture is not, however, necessary for patterned, synchronous network discharges to occur. Random wiring, as may be present in 2D cultures of differentiating neurons, can lead to such activity generation (Traub et al., 1984). Although the rates of activity are greater than seen in CC9 cultures, this could well be dependent on the architecture and cell density of the network (Arnold et al., 2005, Bolea et al., 2006). Spontaneous early network oscillations (ENOs) appear as regular calcium depolarisations and occur in P0 – P6 rat hippocampus slices at rates of 0.4–2min^{-1} (blocked by TTX and are associated with high frequency burst activity that is predominantly GABA-mediated) (Garaschuk et al., 1998). Inter-burst intervals (IBIs) *in vivo* in the rat neonatal hippocampus showed a prevalence for 0.33Hz and 0.1Hz rhythms with a wide distribution of IBIs between 0–40s (Leinekugel et al., 2002), and in the developing spinal cord also exhibits a broad range of inter-event intervals (Tabak et al., 2001) confirming that such oscillations can occur at a large range of low frequencies. In the developing retina, very low frequency oscillations (ITIs of 50s) occur transiently during structural development (Wong et al., 1993). Spontaneous periodic oscillations have also been observed in dissociated cultures of neurons (Ban et al., 2007, Chiappalone et al., 2006, Feller, 1999, Heikkilä et al., 2009), including developing cortical neurons where GABA is still depolarizing (Opitz et al., 2002) and homogeneous cultures of excitatory neurons (Robinson et al., 1993). Cultures of ESC-derived neurons have also been shown to develop spontaneous synchronous activity, however, these studies show such activity alongside hyperpolarizing GABA (Heikkilä et al., 2009, Illes et al., 2007) and so the source of this activity generation is different and pertains to more developmentally mature mechanisms. In contrast, the ESC CC9-derived neurons cultured for short periods (allowing the examination of activity development at the earliest stages of network formation) display such activity as seen in *primary* cultures of embryonic neuronal cells (Ban et al., 2007, Chiappalone et al., 2006), and contains many of the features of such activity seen in slice preparations and *in vivo* (Ben-Ari et al., 1989, Garaschuk et al., 1998) (as explained above).

The development of spontaneous synchronous activity in cultures of neocortical neurons dissociated from E16 rats (Opitz et al., 2002) demonstrates how such activity arises as the number of active cells increases, with synchronous activity appearing after 9 DIV (~P4), and all cells being involved in it by 15 DIV. This is mirrored in CC9 cultures with an increase in activity levels and number of regions recruited before synchronous activity appears at 17 DIV (potentially equivalent to a few days post-natal).

In these CC9-derived cultures 18 DIV sees the pinnacle of the production of synchronous activity before a subsequent fall off. This rise and fall during network developmental changes could be relevant to other *in vitro* studies, and the development of mature activity processes (both intrinsic and Hebbian) *in vivo*. Correlograms and coincidence index measures were used to look at the connectivity at different stages of development for the cortical neurons (Chiappalone et al., 2006), showing that 21 DIV cultures (dissociated from E18 rat cortices) tended to have higher levels of connectivity than younger, and indeed older cultures. The two-stage process of increasing and then decreasing correlated activity can be related to the changes in global connectivity. Long-range connections dominate initially, and from 14 – 21 DIV, a fall off in long-range connections is accompanied by an increase in short-range connections. This is during the period of observed increased functional connectivity. This peak in functional connectivity then falls off with further development in culture. Such a decrease could be related to a drop in the density of synapses per unit volume (as seen in dissociated E18 cortical neurons, maintained in culture for 35 days (Ichikawa et al., 1993)). Activity dependent processes, a move to the balance of excitation and inhibition and homeostatic maintenance (Turrigiano, 1999) are all mechanistic aspects of network dynamics that are under change in this developmental period. As will be explained in Chapter 6, the mature processes of excitation and inhibition decrease asymptotically throughout CC9 development and are fully in force at 20 DIV. CC9 cultures demonstrated coincident settling in structural organization alongside increased network output and temporal organisation of activity. It is intriguing to note that the structural changes move from fairly uniform distributions of cells across the surface, to tight clusters of cells bridged by neurites across hundreds of microns. This is suggestive of an environment that would favour short-range connectivity and the pruning of long-distance connections across bundles of neurites.

It cannot be discounted, however, that the reduction in activity levels and drop in synchronous activity patterns after 18 DIV may be related to the decreasing health of the cultures (and thus number of cells/synapses involved in activity generation and propagation), as they did not generally survive passed 22 DIV.

The transient bimodal response seen for FWHMs in some CC9-derived neuronal cultures at 17 DIV is a phenomenon noted in cells dissociated and cultured, long-term, from E18 rat neocortices as part of a rich repertoire of activity patterns cultures are capable of producing when maintained under the same conditions at variable cell densities (Wagenaar et al., 2006). The bimodal response was noted mainly in a small proportion of dense cultures for ~6 days between 12–27 DIV. This may reduce its significance in this particular context, both because it is demonstrative of the variability seen in cultures, and its appearance at a variety of points in culture development (all likely to be later than the developmental stage observed in CC9 cultures.

Nevertheless, there must be an underlying mechanism generating this response, and it seems striking that this transient response should appear in CC9 cultures at precisely the time that other developmental changes are noted across the board (such as termination of migration, structural organisation, increases in activity and the appearance of temporal organisation of activity). As explored in the previous discussion, intrinsic neuronal properties *in vitro* and *in vivo* during such upheavals are still developing (such as the migration of amino-acid receptors to synaptic junctions, changing the balance of their action, and the switch in balance of Ca^{2+} and Na^{+} channels during action potential generation, the shift in chloride gradient altering the effects of tonic or phasic GABA on network activity and so are responsible for many changes in network output. The structural changes, as discussed above, may be correlated with expected changes in wiring characteristics of the network, ultimately affecting network output. The mode of network communication is not directly determined in these experiments, though sub-clustering of cells will result in a higher likelihood of increased local connections, regardless of their type. Such state changes in dynamic systems can be accompanied by fluctuations in measured parameters across 'phase transitions' from one stable system attractor to another, and there can also be multistability/multifunctionality, where more than one attractor state exists simultaneously (Schoner and Kelso, 1988).

5.5.2 Synchronous event recruitment profile

The shape of the recruitment profile with a characteristic fast onset, sharp peak, and fast decay of region recruitment is comparable to the profile found in rat hippocampal slices when looking at calcium signals during GDP generation (Bonifazi et al., 2009). The speed of cell recruitment into synchronous events is a variable feature in the development of older (≥17 DIV) CC9-derived neuronal cultures. This recruitment speed is not a function of the number of cells recruited into the event; there are fewer active cells at 19 DIV as compared with the days either side, but the recruitment index, which looks at propagation speed of a synchronous event as a ratio with the number of active regions in the culture, confirms that the recruitment rate changes observed across these developmental stages are not affected by the change in the number of active cells. This means that there was both a drop in the number of active regions *and* the speed of cell recruitment into synchronous events at 19 DIV as compared with developmental stages just before and after it. Speed of cell recruitment in CC9 cultures was similar to that seen in thalamic reticular nucleus neurons during depolarising GABA-mediated rhythms of 25–150 cells/s (Bazhenov et al., 1999). Speed of propagation of activity is increased by a larger number of connections, and thus a larger immediate network of connected components, but the speed is also changed by alterations in depolarising $GABA_A$ conductances (Bazhenov et al., 1999), which was shown to increase with development in cerebellar granule cells (Brickley et al., 1996).

5.5.3 Stereotypy

As explained in the Introduction (Section 5.2.3), a degree of stereotypy is observed in networks that have reached a state of self-organized criticality and this stereotypy is realised as spatio-temporal patterns of activity embedded in neuronal avalanches (cascades of activity of varying length and size following a power law distribution) (Raichman and Ben-Jacob, 2008, Volman et al., 2005). This stereotypy allows for the propagation of multiple activity motifs (meta-stable attractors states of the system) to maximize information processing within networks and models show that the expression of these states appear in the case of sub-clustered network architectures and can be influenced by modulating background currents (Haldeman and Beggs, 2005).

CC9-derived neuronal cultures show a similar, possibly higher, degree of stereotypy to that found in P0–2 rat cortical slices (Beggs and Plenz, 2004) embedded in the synchronous

activity of older cultures (≥17 DIV). In cortical slices, 30±14 motifs were found to be significantly repeatable (i.e. with a similar spatial activation of regions) above the level of chance appearance in 4736±2769 activity cascades (Beggs and Plenz, 2004). In comparison, 10% of regions in CC9 cultures could be repeatedly temporally placed within activity cascades (significantly above the level of chance appearance) (Figure 5.5). As the appearance of motifs in neuronal cascades is associated with a network architecture characterized by connected sub-networks of neurons, it is meaningful that such stereotypy should become evident in CC9 cultures at the point of structural consolidation of sub-clusters of neurons, adding weight to the argument that the overt morphological changes observed are accompanied by an underlying network topology change.

Furthermore, in CC9-derived neuronal cultures the increasing network correlations are the result of a general rise in network connectivity with developmental stage. What is most interesting here is that this increase is interrupted by an exaggerated transitory rise in overall network correlations at 17–18 DIV and this increase is marked by a qualitative difference in local temporal correlations, pictorially represented in cross-correlograms in Figure 5.6B. The appearance of temporally distinct subgroups of activated neurons forming activity motifs can be found in synchronously active CC9-derived cultures at a range of developmental stages, similarly to motifs found in cultures of dissociated rat cortical neurons and modelled overlapping sub-networks of neurons (Baruchi et al., 2008). The highly correlated activity at 18 DIV, however, denotes a change from groups of motifs to one giant synchronous group. Network wiring changes from long-range dominance to short-range dominance, postulated to occur in CC9 cultures over this stage of development (see above), may result in network property changes that influence network output; as is mirrored in the fleeting marked increase in bursting seen at 21 DIV in dissociated E18 rat cortical neurons, cultured over a period of weeks where such changes in functional re-wiring occur (Chiappalone et al., 2006).

The mechanism underlying the appearance and regulation of spatiotemporal patterns of activity described here may be either due to chemical synapses or gap junctional connections. The non-phasic nature of gap junction transmission favours highly correlated activity, whereas chemical synapses are likely to promote the appearance of temporally distinct motifs of activity through the complex interplay between excitatory and inhibitory

mechanisms. This could indicate that both modes of communication are present concurrently in CC9-derived networks and the changes in correlated activity noted through their development (based the structural and functional organization) may reflect a changes in the balance of forces between them.

The presence of 'hub' neurons, (the concept of which was introduced in section 5.2.2), was also confirmed in CC9-derived cultures (Figure 5.7 & Figure 5.8) with 8% of active regions possessing a significant probability (above chance) of initiating synchronous events, showing the potential for a scale-free topology (known to underlie neuronal activity *in vitro* and *in vivo*) with only a very small fraction of neurons exhibiting this behaviour, associated with high levels of connectivity (more on the scale-free properties of CC9 networks in section 5.5.4 below). *In vivo*, such hubs are restricted to a phenotypic subset of neurons, and although other neuronal types show high levels of connectivity, only aspiny stellate interneurons could be classed as hubs based on their effective connectivity (observed through stimulation). These hubs were identified in developing neurons where in general GABA is depolarizing, though not all hub neurons had an excitatory effect on GDP generation; some inhibited GDP occurrence (Bonifazi et al., 2009) (presumably owing to an uneven distribution of chloride gradients throughout the interneuron population during the flux in GABA potentials at this developmental stage). The method of hub identification used in the results in this chapter was based on their placement at the initiation of events (rather than initial discovery through a functional connectivity analysis to identify highly connected neurons, as used in the Bonifazi study (Bonifazi et al., 2009)), so the presence of highly connected neurons that inhibit activity were not discovered as a consequence of the method used here.

These particular features of network activity (stereotyped spatio-temporal organization, activity motifs and hubs), here witnessed in ESC-derived neuronal cultures, show the capacity for cultures of self-organized, differentiating neurons to form a network architecture that is organized to allow the propagation of a variety of spatio-temporally organized signals from the earliest onset of network communication. What is more, the developed activity produced by the uninterrupted self-organization of these *de novo* networks resembles that of neocortical slice preparations (Beggs and Plenz, 2004, Bonifazi et al., 2009) regardless of the lack of developed architecture.

5.5.4 Criticality

Neuronal avalanches appearing in CC9 cultures were analysed as a way to understand the underlying dynamics of this system as different activity regimes evolve. CC9 cultures are scale-free in nature throughout activity development with both non-synchronous and synchronous activity regimes displaying power law relations for both size and lifetime distributions. Avalanche size measures differed markedly when comparing non-synchronous vs. synchronous activity. The former suggested sub-critical activity – i.e. activity that was highly damped within the system. The latter demonstrated super-critical activity – i.e. activity that was 'overly organised', reducing the ability of the network to process information. This indicates that even during the early development of different activity regimes, the system gravitates towards a form of critical behaviour. The fact that it overshoots a more optimal critical state during development may represent a pathological condition brought about by the absence of patterned external inputs as would be expected for a neuronal network in a full, developing organism (see below).

It is this distribution of avalanche dynamics that is necessary for the propagation of multiple meta-stable states (manifested as temporal and spatial motifs) (Paczuski et al., 1996). The slope of these distributions varied between the two activity regimes, with non-synchronous activity residing below the expected value for optimal processing of -1.5 (Beggs and Plenz, 2003), and synchronous activity overshooting this value, becoming supercritical. This implies that although both states are created through self-organization to scale-free percolations of activity, non-synchronous CC9 cultures result in the truncation of information transfer and synchronous CC9 cultures are too ordered to provide the flexible substrate necessary for information processing. Such an extreme level of organization is clearly witnessed at 18 DIV in CC9 cultures, as compared with developmental states before and after it. This backs the supposition that 18 DIV cultures (as illustrated in Figure 5.6B and discussed in section 5.5.3 above) do not support the percolation of activity motifs. It then follows that this activity either fleetingly appears as the result of the transition from one network state (prior to 17 DIV) to another (after 20 DIV), and/or it is necessary for that transformation and is innate to the functional development of the network. Alternatively, the network hits a pathological state of over-connectivity (this possibility was discussed in the Chapter 4) at 18 DIV. As motifs can be seen to re-appear in older cultures and the level

of overall correlated activity in the network decreases after 18 DIV, this would suggest that the network compensates for the over-regimentation, adapting back towards a state of criticality.

These criticality measurements need to be considered with a number of caveats however. The system studied was small compared to in vivo or ex vivo 'real' brain networks. In addition, only a relatively small number of samples were analysed owing to the proximity in time between establishment of synchronous activity and the end of the viable period of the cultures used. In particular the failure of this analysis method to show any change in avalanche lifetime when comparing the two types of activity (synchronous and non-synchronous) suggested that the system was too simple and contained too few active elements for estimates of criticality to be an accurate measure of the information processing capability of the nascent neuronal networks studied.

5.5.5 Summary

Networks of CC9-derived neurons have been shown here to self-organize into various spatiotemporally ordered states. The genesis of new activity regimes is correlated with structural consolidation of the network and a variety of activity measures indicating changes in intrinsic network properties (see Chapter 4). These measures converged to provide evidence of a system where a small number of highly active regions (hubs) were able to precipitate predominantly stereotyped patterns of propagation of activity in a near-synchronous manner across the network. Sufficient numbers of hub regions, and degree of interconnectivity between regions, existed to confer a number of activity motifs upon even the simple, nascent system studied. Avalanche size measures suggested the switch to the generation of these spatiotemporally ordered activity patterns may represent an increase in information processing ability. However, a number of factors (above) cast uncertainty over the use of this analysis tool in this particular situation.

The final results chapter to follow (Chapter 6) will examine the effects of pharmacological perturbations of the network, focussing on the unique development of GABAergic influence on activity output.

CHAPTER 6 – THE ROLE OF γ-AMINOBUTYRIC ACID IN THE MODULATION OF CC9 NETWORK ACTIVITY

6.1 SUMMARY

The previous chapter brought together spatial and temporal aspects of activity coordination in these nascent networks. Data demonstrated the network's developmental drive towards criticality and subsequent supercritical behaviour where activity generation explodes into regimented, population-wide events with little room for variable signal propagation or perturbation. This was finally followed by a return to a state that favours the propagation of activity motifs.

γ-aminobutyric acid (GABA) has been found to play a significant role in neuronal development in a great many model systems and human and animal studies. This chapter will explore how this neurotransmitter affects activity patterns across these developmental stages in the CC9-derived neuronal networks in light of the findings of the previous chapters. The aim of this chapter is as follows:

To assess any dependence of developmental changes in spontaneous network and single neuronal activity on GABAergic neurotransmission.

The main findings presented are:

- Blockade of $GABA_A$ receptors with bicuculline had no significant effect on the kinetics of calcium transients at any stage in development examined.
- Blockade of $GABA_A$ receptors significantly elevated activity rates and the amplitude of responses across networks in an age-dependent manner.
- Propagation of activity was not spatially altered by blockade of GABA receptors and the continued presence of 'hub' neurons was confirmed, along with simultaneous propagation of activity through spatially distinct subpopulations of neurons.
- Blockade of $GABA_A$ receptors moved the self-organized culture towards supercriticality, demonstrating an inhibitory role for GABA, dampening signal transmission in the network.

- Application of exogenous GABA robustly induced large, dose-dependent, slow calcium transients.
- There was a quiescent period after recovery from the excitatory effect of exogenous GABA application, and this was followed by a slow re-establishment of activity.
- The excitatory effect of GABA on these cells decreased with development and had almost completely vanished by 20 DIV, suggesting the gradual positive shift in chloride gradient with development towards hyperpolarization.

These findings, complement those from the previous two chapters, giving evidence that GABA is playing a complex, dynamic and important role throughout these stages of development. Characteristic responses are manifest which imply both excitatory and inhibitory roles and these are discussed. Together, the overall effect lends itself to establishing a network capable of self-organising and migrating towards a level of functional criticality. Factors that could be responsible for the dichotomy of behaviours GABA provides in development will also follow in the discussion, drawing from the conclusions of the previous results chapters and precedents in the literature.

6.2 INTRODUCTION

6.2.1 GABA in development

$GABA_A$ receptors appear early in neuronal development and have been found in immature neurons in many brain structures (Brickley et al., 1996, Ganguly et al., 2001, Garaschuk et al., 2000, Kandler and Katz, 1995, Mienville, 1998, Sipilä et al., 2005, Sernagor et al., 2003). At the earliest stages of development, due to the Cl^- concentration in immature neurons being much higher than in mature neurons, activation of $GABA_A$ receptors is depolarizing (rather than hyperpolarizing, as is common in mature neurons). Thus, in many systems in early development, GABA acts like glutamate as an excitatory neurotransmitter because in both cases the reversal potential for the ionophores is more positive than the sodium spike threshold.

In embryonic rat cortical slices, application of GABA and glutamate elicited voltage and current responses from E15, before other receptor agonists could be seen to have any effect (such as glycine or NMDA) (LoTurco et al., 1995). In cultures of hypothalamic neurons,

dissociated from E15 embryos, GABA was found to be depolarizing for the first 7 DIV, exceeding the threshold for action potential generation and increasing neuronal activity (Chen et al., 1996). The GABA reversal potential (E_{GABA}) was found to decrease during development. After 20 DIV E_{GABA} had become hyperpolarizing. Interestingly, in the first week *in vitro* while GABA is found to be depolarizing its effects can be either excitatory or inhibitory: excitation occurs through the activation of EPSCs with spikes often appearing on the decay phase of the EPSC. In contrast with the above described excitatory effects, inhibition was seen as a result of a shunting effect on membrane resistance that comes into play close to the peak of the EPSC. In such a case, increased chloride conductances are thought to inhibit the effect of glutamate-induced conductances, and so inhibit excitation (Staley and Mody, 1992). This can be explained through the latency between GABA- and glutamate-evoked postsynaptic responses, showing that GABA has a simultaneously active opposing influence on glutamatergic synaptic transmission. This said, the role of GABA in this early developmental stage, with its depolarizing effect, is primarily excitatory (Chen et al., 1996). GABA-induced depolarisations also reduce the Mg^{2+} block on NMDA receptors, fulfilling a similar role to glutamate-induced depolarisations in more mature cells, but during the phase when glutamate receptors are absent/silent.

Activations of $GABA_A$ receptors results in the flux of chloride across the cell membrane. The chloride concentration in neuronal cells is governed primarily by the chloride co-transporters NKCC1 and KCC2. High expression of the inward chloride transporter, NKCC1, in immature neurons results in high intracellular chloride concentrations, while the KCC2 transporter develops later and is the cause of the overall shift in intracellular chloride (Delpire, 2000, Rohrbough and Spitzer, 1996).

The timing of the switch from excitatory to inhibitory GABA responses has been shown to occur in the second postnatal week in the rat hippocampus, and 20% of cells could still produce an excitatory GABA response at P7–10 (Garaschuk et al., 1998), though it varies between species, sex and neuronal type (Kyrozis et al., 2006). This switch is regulated by GABA itself, as chronic blockade and activation of $GABA_A$ receptors resulted in delaying and accelerating the switch respectively (Ganguly et al., 2001, Leitch et al., 2005). There is also a huge transient drop in the GABA potential around the point of birth, inducing a temporary

shift to an inhibitory GABA effect, though this neuroprotective action is induced by the release of oxytocin by the mother and is not produced intrinsically (Tyzio et al., 2006).

Before the development of mature, functional synapses, GABA release acting on GABA receptors has a trophic action, influencing many developmental processes, in sometimes contradictory ways such as reducing DNA synthesis in striatal slices (LoTurco et al., 1995), yet increasing proliferation in granule cells precursors (Fiszman et al., 1999). GABA influences neuronal migratory processes and a bimodal dose-dependent change in migration of E18 rat cortical neurons was found for a range of GABA concentrations (femto- to micro-molar) (Behar et al., 1998). The low GABA concentration responses were chemotactic as directed migration was induced by the presence of a GABA concentration gradient, whereas high GABA concentration responses were chemokinetic, showing no directionality (Behar et al., 1996). The GABA-induced chemotaxis of immature neurons is related to the effect of GABA on VGCC and fluxes in intracellular calcium are required for migration (as inhibition of these calcium currents reduces migration (Behar et al., 1996, Komuro and Rakic, 1996). Further early trophic effects of GABA include the facilitation of dendrite outgrowth in a variety of neuronal systems such as the embryonic rat and chick cortex and immature E18 rat hippocampal neurons and cerebellar neurons (Barbin et al., 1993, Sernagor et al., 2010) and increased morphological complexity in more developed P6–8 rat cerebellar granule cells (Borodinsky et al., 2003). GABA currents are active before the development of vesicle release mechanisms associated with mature, functional synapses. In rat hippocampal slices, these are large currents that can be seconds in duration (longer than synaptic GABA currents) and can be evoked in immature neurons by electrical stimulus or pharmacologically with GABA. These currents were most prominent at E18–P6, and reduced and disappeared in the second postnatal week.

The development of functional GABAergic synapses precedes that of glutamatergic synapses and the maturation of both types of synapse occurs over a period between 17–21 DIV in E18 rat hippocampal dissociated cultures (Anderson et al., 2004). Initially, clustering of glutamatergic and GABAergic pre- and post-synaptic proteins is heavily mismatched, with mixtures of both appearing at the same developing junctions. Activation of both types of receptor progresses the stabilization of GABAergic synapses, though NMDA activation appears to encourage the mismatch of pre- and post-synaptic proteins in general.

GABAergic synapses are seen to strengthen at 17 DIV, but glutamatergic synapses do not stabilize until 21 DIV.

While $GABA_A$ receptors are ligand-gated chloride channels (sensitive to bicuculline), $GABA_B$ receptors are not sensitive to bicuculline and are metabotropic receptors that affect (via G-protein activation) the potassium channels responsible for the later phase of inhibitory post-synaptic potentials. They also inhibit VGCC and so inhibit neurotransmitter release (Mintz and Bean, 1993). While both $GABA_A$ and $GABA_B$ receptor activation in general have an inhibitory effect in mature neuronal systems, during development, $GABA_B$ receptors have an inhibitory role in the excitation of $GABA_A$ receptors (Kirmse and Kirischuk, 2006). This is mediated by a tonic curtailing of intracellular calcium rises, as was shown in dissociated cultures of E18 rat hypothalamus cells, taking effect before synapse formation (Obrietan and van den Pol, 1998).

6.2.2 The role of GABAergic signalling in generating and controlling spontaneous activity in developing networks.

In the developing retina, GABA is involved in the modulation of retinal waves. In turtles, GABA's influence becomes apparent at S25 (while it is still depolarizing) slowing waves down (Sernagor et al., 2003). The application of low concentrations of bicuculline (1-5µM) stopped wave activity at this stage, whereas higher concentrations (20µM) allow fast propagation of waves. It was suggested that these two contrasting responses may be due to the overall balance between the excitatory effect of GABA at this stage and shunting inhibition, or perhaps is due to the differential effect of bicuculline on synaptic and extrasynaptic $GABA_A$ receptors. Puffs of GABA resulted in large, slow waves of excitation. It was suggested that this effect is not due to spiking activity but instead is due to calcium activity; i.e. it could be explained through K^+ efflux following the opening of voltage-gated calcium channels after a GABA-evoked depolarizations. As GABA becomes inhibitory, the waves become patchy and stationary and shortly after disappear and thus GABA is suggested to play a significant role in both the modulation of retinal waves and their disappearance with development (Ganguly et al., 2001).

It was shown in *Xenopus* spinal neurons that spontaneous spiking activity, generated through VGCC activation and ICCR from stores, is necessary for the expression of the

neurotransmitter GABA itself (Spitzer et al., 1993) and a blockade of these spikes resulted in no GABA immunoreactivity (Spitzer et al., 1993). Thus, in this study, not only is spontaneous activity not reliant on the early excitatory action of GABA, it is a necessary precursor for the development of neurons into those that synthesise and release GABA.

Spontaneous oscillatory activity in developing neuronal systems, such as GDPs, was described in detail in the previous results chapters. The sources of these activities vary and, in contrast to the Xenopus study above, GABA often plays a crucial role in the development and cessation of these activities with development. The source of action potential generation in GDPs is intrinsically bursting pyramidal cells, yet the rhythmicity is set by the *tonic* action of GABA, upon which GDPs rely along with a degree of GABAergic synaptic activity (Sipilä et al., 2005, Ben-Ari et al., 1989). It is also through the synergistic action of GABA and NMDA in early development that these oscillations are propagated, owing to the way GABA reduces the Mg^{2+} block on NMDA receptors as detailed in Section 6.2.1 (Leinekugel et al., 1997).

These two contrasting lines of evidence for a role for GABA in early activity may be due to region-specificity. For example, ENOs generated in the hippocampus and the neocortex react differently to bicuculline (a GABA antagonist); 20µM bicuculline completely blocked ENOs in hippocampal slices, but only partially blocked ENOs in the neocortical slices. Also, even though the calcium transient rate was reduced, amplitudes of the transients in the neocortex increased in the presence of bicuculline (Garaschuk et al., 1998, Garaschuk et al., 2000). Even within hippocampus, where most evidence for early excitation from GABAergic interneurons in the brain is derived, hub-like neurons (see previous chapter) can be seen to have both excitatory and inhibitory effects on GDP generation, potentially showing the effect of interneuronal maturation (and lowering of the chloride gradient) on cessation of GDP generation with development (Bonifazi et al., 2009).

Furthermore, even considering the ubiquitous impact of depolarizing GABA in early development, not all early oscillations rely on GABA. In the intact P0–3 mouse cerebral cortex 11–14 Hz oscillations involved in functional network formation depended on a complex combination of gap-junctions, glutamatergic synaptic transmission and

metabotropic glutamate activation, but were completely unaffected by GABA blockade (Wagner and Luhmann, 2006).

Owing to the complex interactions between excitatory and inhibitory neurons in the CNS, the action of GABA is not always intuitive. Large depolarizations induced in pyramidal neurons were shown to be a consequence of increased high-frequency activation of the interneuron population (associated primarily with inhibition) in adult rats during induced epileptiform activity. This could be facilitated by the application of the GABA uptake inhibitor, tiagabine (Jackson et al., 1999). Such $GABA_A$-induced depolarizations are the result of sudden, large accumulations of GABA that break down the ionic balances. Initially, large, hyperpolarizing chloride fluxes break down the ionic balance of bicarbonate and chloride, reducing chloride flow and increasing bicarbonate flow. This secondary flux induces a depolarisation. The upshot of this, in the adult CNS, is to reduce the Mg^{2+} block on NMDA receptors and thus modulate NMDA synaptic activity in an interneuron activity frequency-dependent manner (Staley et al., 1995).

Other studies have demonstrated biphasic effects of GABA application on mature neuronal tissue in the absence of an NMDA receptor mediated effect (Alger and Nicoll, 1979). More recent, detailed studies have demonstrated that initial hyperpolarising responses rapidly switch to depolarising responses owing to the continued presence of GABA (Jedlicka et al., 2010). In model studies this could be attributed to the accumulation of chloride intracellularly. This effect was most marked in smaller volume cell compartments like distal dendrites and even axons (Traub et al., 2003) and strongly suggested a frequency-dependent component to depolarising GABA expression; i.e. low frequency synaptic stimulation would elicit repeated hyperpolarising events whereas faster frequencies would facilitate chloride accumulation and thus depolarising responses. All this is mostly due to potassium accumulation in the extracellular space during intense activity, which leads to KCC2 channels reversing their direction of action.

These above examples are from mature neuronal systems, though a further example of non-intuitive GABA responses comes from the neonatal hippocampus, where GABA is found to be depolarizing, yet the interneuron population has an inhibitory action on pyramidal activity. Application of muscimol (a $GABA_A$ agonist) depolarized pyramidal cells (an effect

countered by bicuculline), transiently increasing spiking activity before silencing spike output; while bicuculline increased spiking activity (Lamsa et al., 2000). It has been speculated that the inhibitory effect of muscimol application could relate to inhibition through GABA conductances (shunting inhibition (Staley and Mody, 1992)), or it may be due to massive calcium influxes interfering with gap-junction coupling, reducing signal propagation (Lamsa et al., 2000, Staley et al., 1995, Staley and Mody, 1992, Strata et al., 1997).

In summary, evidence for a depolarising, excitatory action of GABA in developing networks, and even in mature networks, is strong. However, the effects of this key neurotransmitter were always complex, with both inhibition and excitation coexisting, even in the same neuron. In addition, region-specificity of depolarising responses is evident throughout the literature. As it is impossible to known the putative ultimate fate of spontaneously developing CC9-derived networks (i.e. are they developing towards neocortical networks, hippocampal, cerebellar or subcortical structures?) it is important to understand how their activity patterns relate to the GABAergic system.

6.3 METHODS

Detailed methods are provided in Chapter 2, and the procedure for calcium imaging was expanded on in the methods section of Chapter 4. The only methods specific to this chapter are therefore the use of a GABA agonist and antagonist. For blockade of $GABA_A$ receptors, cultures were perfused for 30-60 mins with 50µM (+)-bicuculline in aCSF. For activation of $GABA_A$ receptors, GABA was manually pipetted directly onto the culture in 10 and 20µM (1 and 2µL) concentrations once recording had started.

6.4 RESULTS

6.4.1 Blockade of GABA receptors with (+)-bicuculline: temporal properties

Bath application of 50µM (+)-bicuculline produced an increase in mean measures of excitability of the network at all observed days (13 – 20 DIV), with the number of active regions and number of transients observed by each active region increasing at most developmental time points studied (Figure 6.1). The number of cells active in a 10 minute

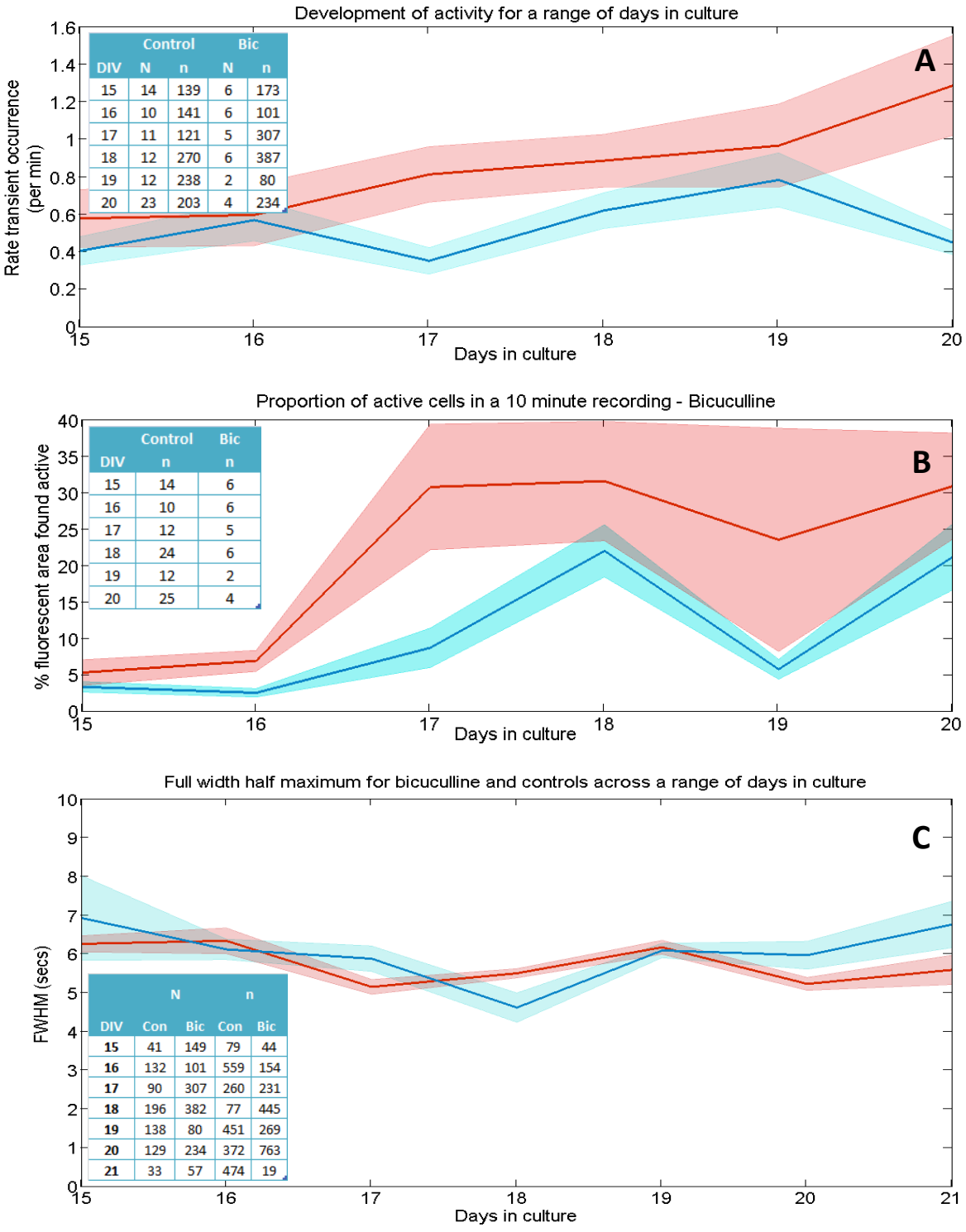

Figure 6.1 –Development of activity levels and change in transient shape with days in culture for cultures perfused with 50µM (+)-bicuculline for 30-60 mins. Shaded regions represent the SEM. **A)** Mean rate of transient occurrence for individual regions for bicuculline perfused cultures (red) were higher than for controls for all DIV numbers (P = 0.05, pairing across like days except 16 DIV). For bicuculline-perfused cultures, levels of activity for individual regions increased with DIV number (P = 0.05, pairing across all days except 19 DIV). ('N' refers to number of cultures; 'n' refers to number of regions.) **B)** Due to the tendency for active regions to join together, particularly as cell clustering increases, a ratio of the surface area of active regions to the total fluorescent surface area was used to estimate the proportion of active cells. The mean number of active cells in bicuculline-perfused preparations (red) can be seen to increase up to 17 DIV, with more than 30% of fluorescent cells being active at 17-18 DIV. Initially, ~5% of cells are active (compared to 3% in controls), and the variation in number of active cells is greater in bicuculline-perfused preparations than in controls. ('n' refers to number of cultures) **C)** The FWHMs are not significantly different for bicuculline-perfused cultures than controls, and little variation is noted across all DIV numbers. 'N' refers to number of regions, 'n' to number of events.

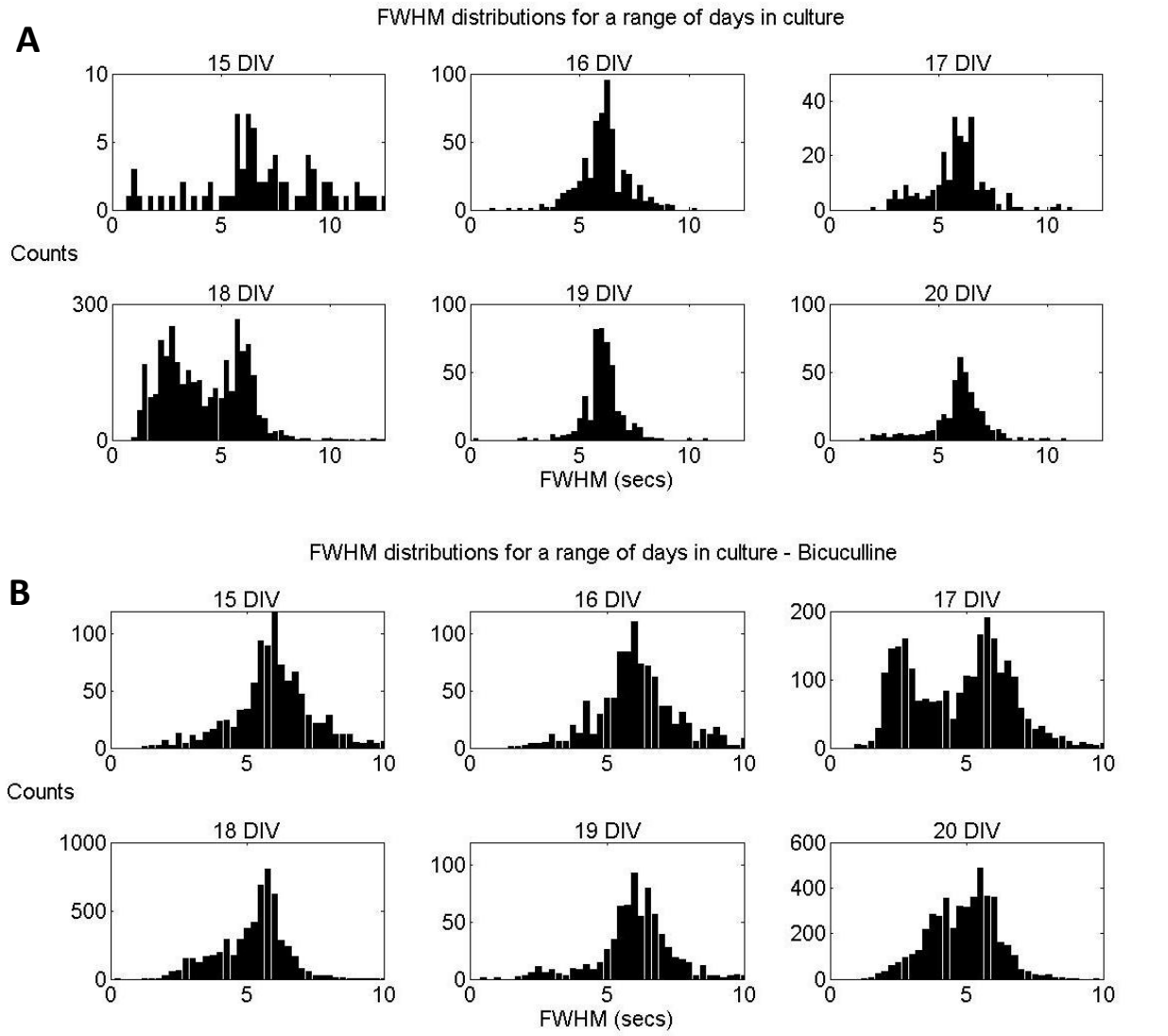

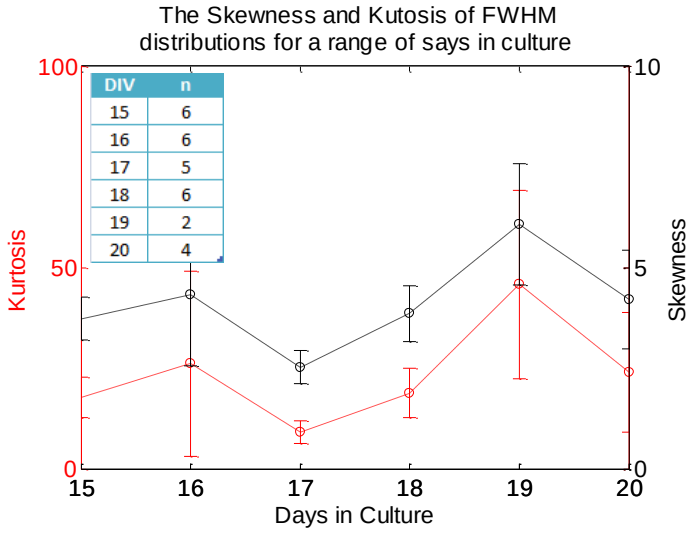

Figure 6.2 – Example summed FWHM distributions for cultures perfused with 50µM (+)-bicuculline for 30-60 mins for a range of days in culture. A) Reproduced from Chapter 4 for reference. **B)** Each plot depicts the distribution of FWHMs summed over all 10 minute recordings in a single experiment for particular DIV number. The distributions display a slightly bimodal response, either as a hump secondary to the main peak (18 DIV), or as a distinct second peak (17 DIV).

recording in any given culture could be seen to increase steadily across DIV numbers, from 5±2% to 31±7% for 15 DIV and 20 DIV respectively ($P< 0.05$ across all days except 16 DIV) (Figure 6.1B).

The mean rate of transient occurrence for each region was also found to be consistently higher for all developmental days (Figure 6.1A) and the increase in proportion of active cells became suddenly more pronounced at 17 DIV, remaining high. Younger (<17 DIV) and older (≥17 DIV) cultures averaged 6±1 and 30±2 transients per minute respectively in the presence of bicuculline, whereas transient rate per cell changes less in controls (values 2±1 for younger, and 14±4 for older cultures ($P < 0.05$)) (Figure 6.1A).

The FWHMs did not show a changing trend from the controls for bicuculline application across the developmental period studied (Figure 6.1C). However, some suggestion of a change in sensitivity to $GABA_A$ receptor blockade with developmental profile was seen: A significant dip ($P < 0.05$) in the FWHM was seen for 17 DIV instead of at 18 DIV as seen for controls. This effect, while small, was compounded by an observed change in the developmental time bimodal peaks in FWHM distributions was seen (Figure 6.2). Although the peak values were the same as for controls (6 and 2.8s), the bimodal distribution seen for 18 DIV for controls was seen most strongly in 17 DIV. However, further quantification, by examining mean and variance of the skewness and kurtosis of these distributions, as with the control data, did not reveal any significant changes over the developmental period ($P>0.05$) or when compared at each timepoint with controls ($P>0.05$, see Figure 4.8).

Calcium transient mean amplitudes were seen to be lower for cultures perfused with 20μM (+)-bicuculline across all days in culture ($P < 0.05$). This effect was large and developmental time point-dependent. At the earliest time studied (15 DIV) amplitudes in the presence of $GABA_A$ receptor blockade were reduced by almost 85% from controls (control 87±15 dF, bicuculline 14±14 dF). In contrast, at the latest time point of 20 DIV this reduction in transient amplitude with bicuculline had decreased to only 55% of controls (control 87±8 dF, bicuculline 49±29 dF). However, the pattern of amplitude changes seen during development displayed a similar trend as controls with an increase from 16 – 17 DIV (at values of 10.6±15.9 and 55.4±36.6 respectively) and a drop to 19 DIV down to 8.2±17.8 ($P < 0.05$) (Figure 6.3). The amplitude distributions appeared widest at 17 DIV, correlating with

the bimodal response seen for the FWHM at 17 DIV, however, statistical analysis of skewness and kurtosis revealed no significant differences in the dataset overall during development (P>0.05) (see Figure 4.10).

Figure 6.4'A' provides ITI distributions from all recordings with bath application of bicuculline for a range of days in culture. The distributions show a peak at 20-30s for all days except 17 DIV. At 17 DIV the peak is shifted to 50s. The peak also drifts a little above 18 DIV, to 30-40s. The skew and kurtosis measures remained unchanged except at 19 DIV, where they both drop. This positive skewness and kurtosis are slightly larger for bicuculline-perfused cultures than for controls suggesting a moderately altered distribution pattern of ITIs (reference Figure 4.11 for controls) (Figure 6.4B).

As both amplitude and ITI profiles changed sensitivity to bicuculline with development, it was interesting to see whether the effects were additive or cancelling in terms of amplitude/ITI relationship. The amplitude and ITI relationship gradients, shown in controls to have a positive correlation that rises from 17 DIV to 19 DIV with a peak at 0.89±0.06 before falling off again to 0.44±0.06 at 22 DIV, showed a different developmental profile for bicuculline perfused cultures (P = 0.05 for cross comparison with all DIV numbers). Instead of a skewed, inverted 'U' shaped relationship a gradual, near linear rise from 0.52±0.18 at 17 DIV to 0.87 at 21 DIV was seen (Figure 6.5). This latter comparison suggested a marked change in the dynamics of network behaviour with developmental period in the absence of active $GABA_A$ receptors. It was therefore necessary to look at spatiotemporal properties of CC9-derived networks.

6.4.2 Blockade of GABA receptors with (+)-bicuculline: spatiotemporal properties

For cultures that displayed synchronous activity after 17 DIV, the overall level of region recruitment per synchronous event was significantly higher for bicuculline-perfused cultures that showed a peak at 131±35 regions per second, as opposed to controls, which peaked at 84±12 regions per second. Median values across all days for controls and bicuculline were 76 and 128 respectively (Figure 6.6).

It is also interesting to note that the developmental time point at which maximal recruitment was seen changed. Peak recruitment rates were seen at 20 DIV (following a

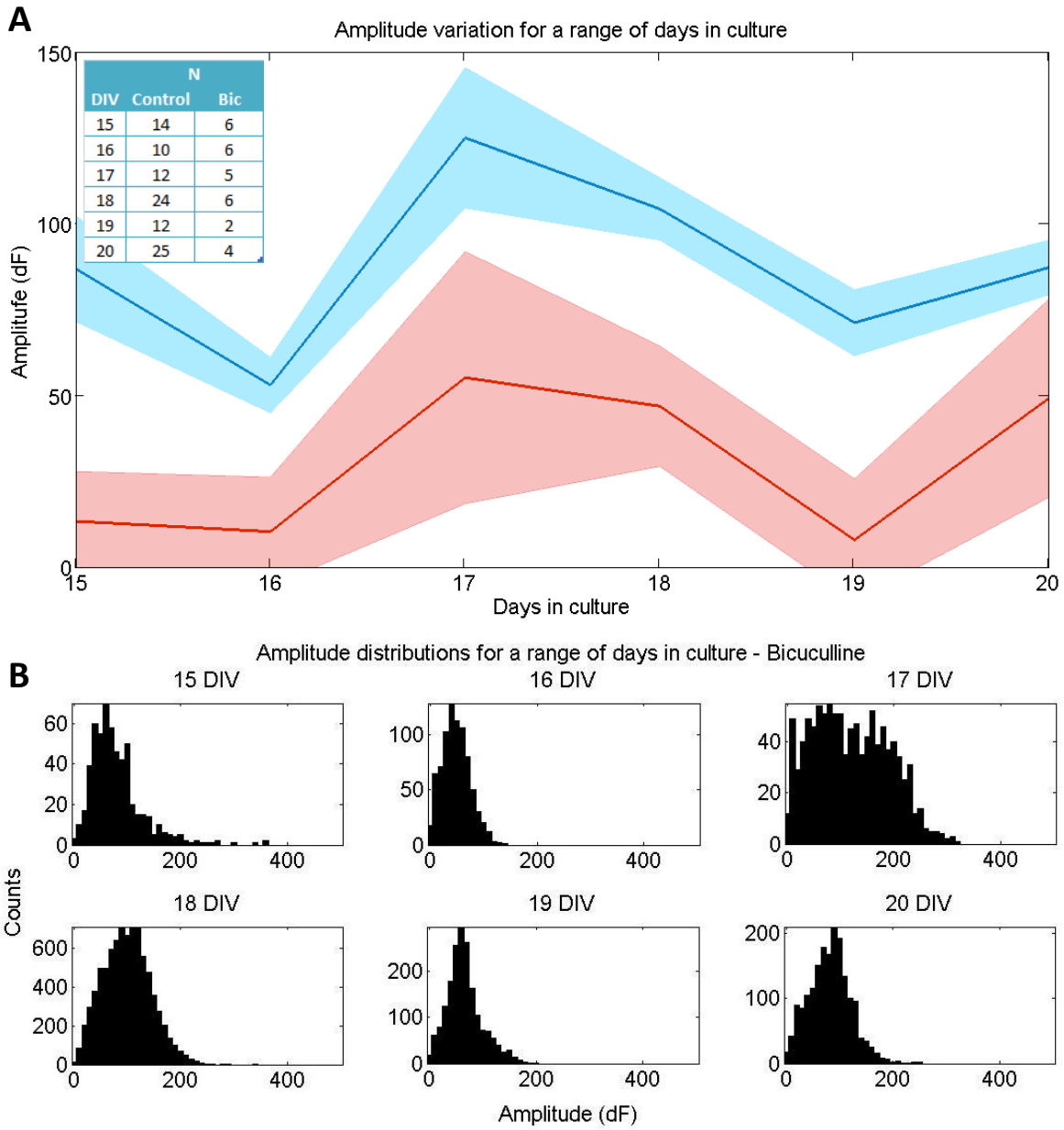

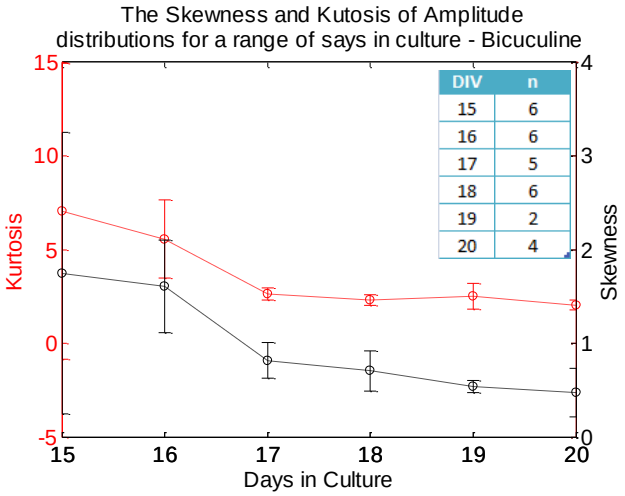

Figure 6.3 – Change in amplitude with day in culture for cultures perfused with 50µM (+)-bicuculline for 30-60 mins. A) The amplitude for bicuculline-perfused cultures (red) was consistently lower than for controls (blue) for all DIV numbers. The greatest amplitudes are seen on 17 DIV, as for controls, and the lowest amplitudes for 15-16 DIV cultures. **B)** Amplitude distributions summed for all recording from a range of days in culture with bicuculline. A wide range of amplitudes is evident for 17 DIV, when a bimodal response in FWHM is evident (see Figure 6.2 B).

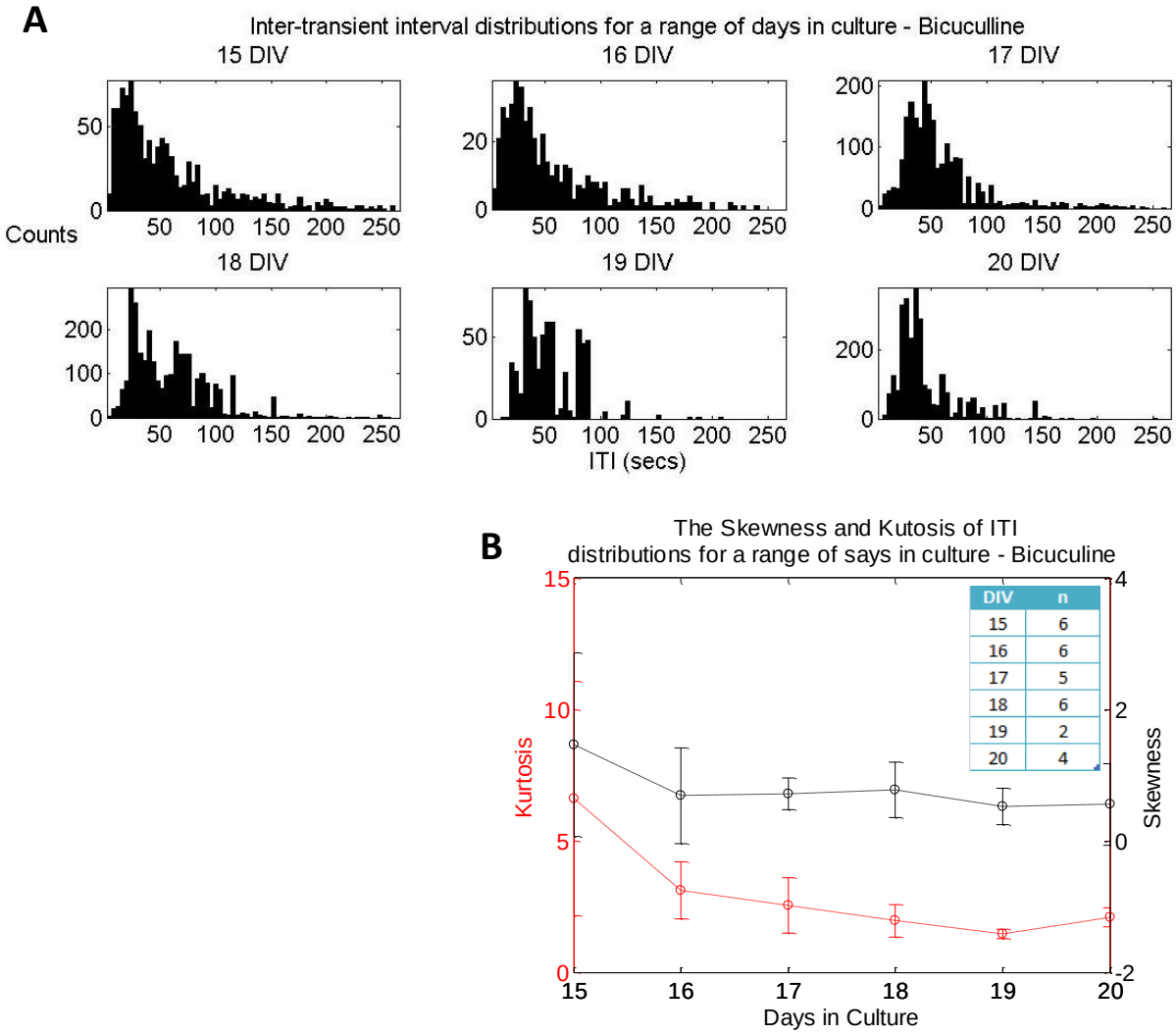

Figure 6.4 - Inter-transient interval (ITI) distributions from cultures perfused with 50µM (+)-bicuculline for a range of days in culture, summed over all recording for that day. A) Each plot depicts the distribution of ITIs summed over all 10 minute recordings for particular DIV number. The distributions for all recordings and all experiments for a given day were summed. Over all experiments, there is a much lower variation in ITI than for controls. A peak of 20-30s is seen in all days except 17 DIV, where the peak is shifted to 50s. The peak becomes broader after 18 DIV. **B)** The skewness and kurtosis for these summed distributions for each day. This shows there is a slight increase in kurtosis with the age of culture, but no change is seen for skew across the DIV numbers (excepting 19 DIV) (see Figure 5.13 for comparison with controls).

transient peak at 18 DIV) in controls. In contrast, mean peak recruitment rate was seen at a time corresponding to the dip between control maxima at 19 DIV in the presence of bicuculline – though a note of caution should be expressed in interpreting this result as only one 'n' was captured at 19 DIV with bicuculline in this study. As with measures of individual region calcium transient amplitude, the trend in this measure of synchrony was largest at earlier developmental time points.

Many of the synchronous events, as with controls, were initiated by 'hub' neurons with 26% (n = 19) of regions with a significant probability of acting as a hub (significantly higher than appearance by chance – see Methods in Chapter 5) (Figure 6.7A). This is very much higher than for controls, where only 8% of regions had a significant probability of being a hub (This significance shown using a z-test – see methods section 5.3.2). The coincidence indices for these hubs was far higher on average (0.59±0.07, n = 14) than any other regions (0.19±0.43, n = 6232) (Figure 6.7B). However, these values were comparable to equivalent correlation coefficients for hubs and non-hub regions in control (see Figure 5.8 B) suggesting the underlying network properties that defined a hub were the same with or without $GABA_A$ receptor blockade. Activity spread through spatially distributed sub-clusters of cells within the network in the same spatial fashion as for controls (Figure 6.7C & D), with all sub-clusters affected by the spread of activity within the same temporal window, and no difference in the spread of activation times for cells within one region compared to across regions.

These increases in the number of hub neurons and recruitment rates within synchronous events were compounded by the observation that the coincidence index across networks in older cultures was larger in bicuculline-perfused cultures than for controls (Figure 6.8A).

A mean of 1.9×10^{-3} for controls and 2.2×10^{-3} for bicuculline-perfused cultures was seen above 17 DIV. Representative cross-correlograms from 17– 20DIV show overall a very high level of synchronization between regions and no temporal motifs appeared at any stage.

This is in stark contrast to controls, where only cultures from 18 DIV behaved in this manner, with motifs appearing at later developmental time points following this initial establishment of synchrony (see Figure 5.6).

In terms of the networks' capacity to process information, analysis of neuronal avalanches was used again to look at self-organized criticality. As shown in the previous chapter, the power law relation for non-synchronous activity indicated subcritical behaviour – a failure of activity originating at a single source to propagate through the network, and synchronous activity showed supercritical behaviour – activity spreading comprehensively throughout the network. For these older bicuculline-perfused cultures, only highly synchronous activity, arising from many more hubs and recruiting more regions than controls (above) could be

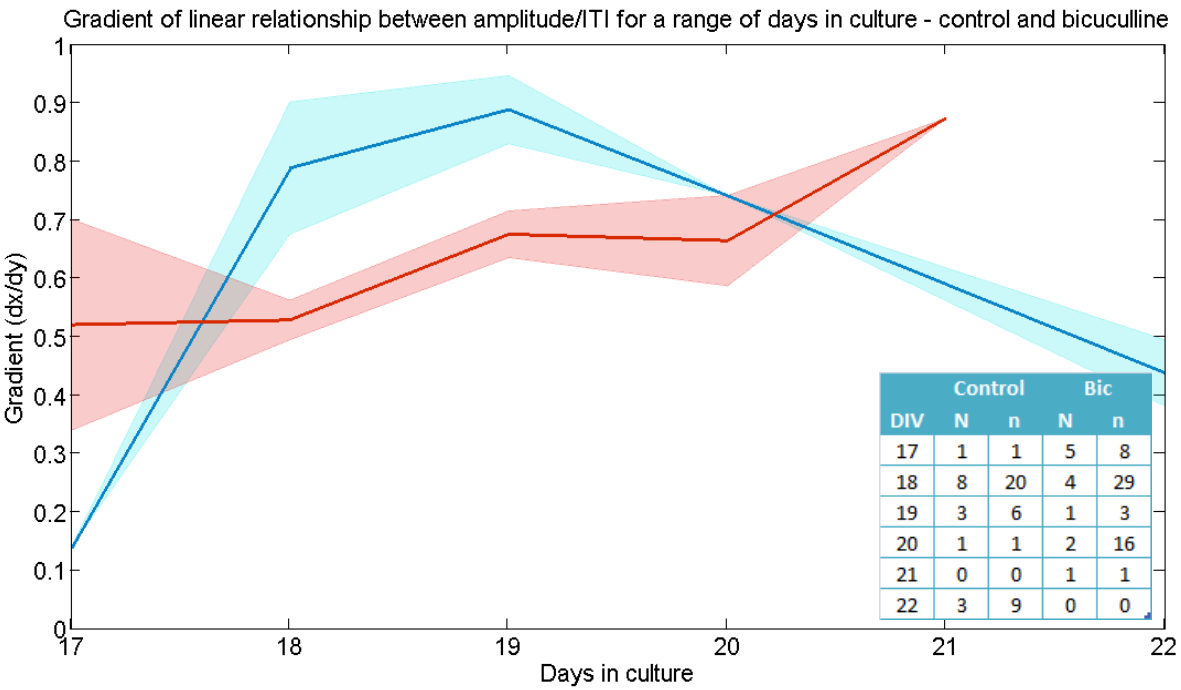

Figure 6.5 – Amplitude/ITI relationship for a range of days in culture for cultures perfused with bicuculline compared with controls. Regions displaying significant linear amplitude/ITI correlations (i.e. with R^2 values greater than 0.75) from all cultures for a particular DIV were used to examine the relationship between amplitude and ITI. The graph shows the mean gradients of the linear regression of amplitude vs. ITI with the shaded region representing the SEM. Blue and red represent controls and bicuculline respectively. Sample numbers are given in the table, with 'N' and 'n' representing cultures and regions respectively. Bicuculline-perfused cultures show a rise in gradient from 17 – 21 DIV from 0.52±0.18 to 0.87, as compared with the controls, which rise from 17 – 19 DIV, peaking at 0.89±0.06. This gradient then falls off down to 0.44±0.06 at 22 DIV. The difference in the developmental trend with Bicuculline is stark, with cultures at 17 and 18 DIV being affected in opposing ways.

observed. The result was a power law relation indicative of highly supercritical behaviour with a slope of -0.29. This is a shallower slope than seen for synchronous activity in controls, which had a slope of -0.58 (Figure 6.9A, compared with Figure 5.10 B), although the avalanche lifetime still exhibited subcritical behaviour with a slope of -3.08, although this moved closer to criticality than controls (Figure 6.9B).

6.4.3 Activation of GABA receptors with GABA

The application of GABA directly onto the culture resulted in a sudden synchronous increase in intracellular calcium levels across cells, followed by a more gradual decline. This was followed by a quiescent period in which prior spontaneous activity either was absent or very much reduced (Figure 6.10). The example images in Figure 6.10 give a qualitative representation of how the number of cells responding to exogenous GABA application decreased with development, as did the amplitude of that response. In cultures displaying

synchronous activity, such as in 17 DIV, activity returned gradually, with increasing amplitudes and number of cells with time after GABA application. It is interesting to note the apparent inverse correlation with incidence of synchronous, spontaneous behaviour and calcium transient amplitude and rate induced by exogenous GABA.

The proportion of cells active in a 10 minute recording showed an increasing number of cells to become active from 16 – 18 DIV, followed by a decreasing trend from 18 – 22 DIV, with the peak proportion of cells active (47±4%) at 18 DIV and the minimum (16±0%) at 22 DIV (Figure 6.11A). The FWHM were also much greater than seen for spontaneously produced

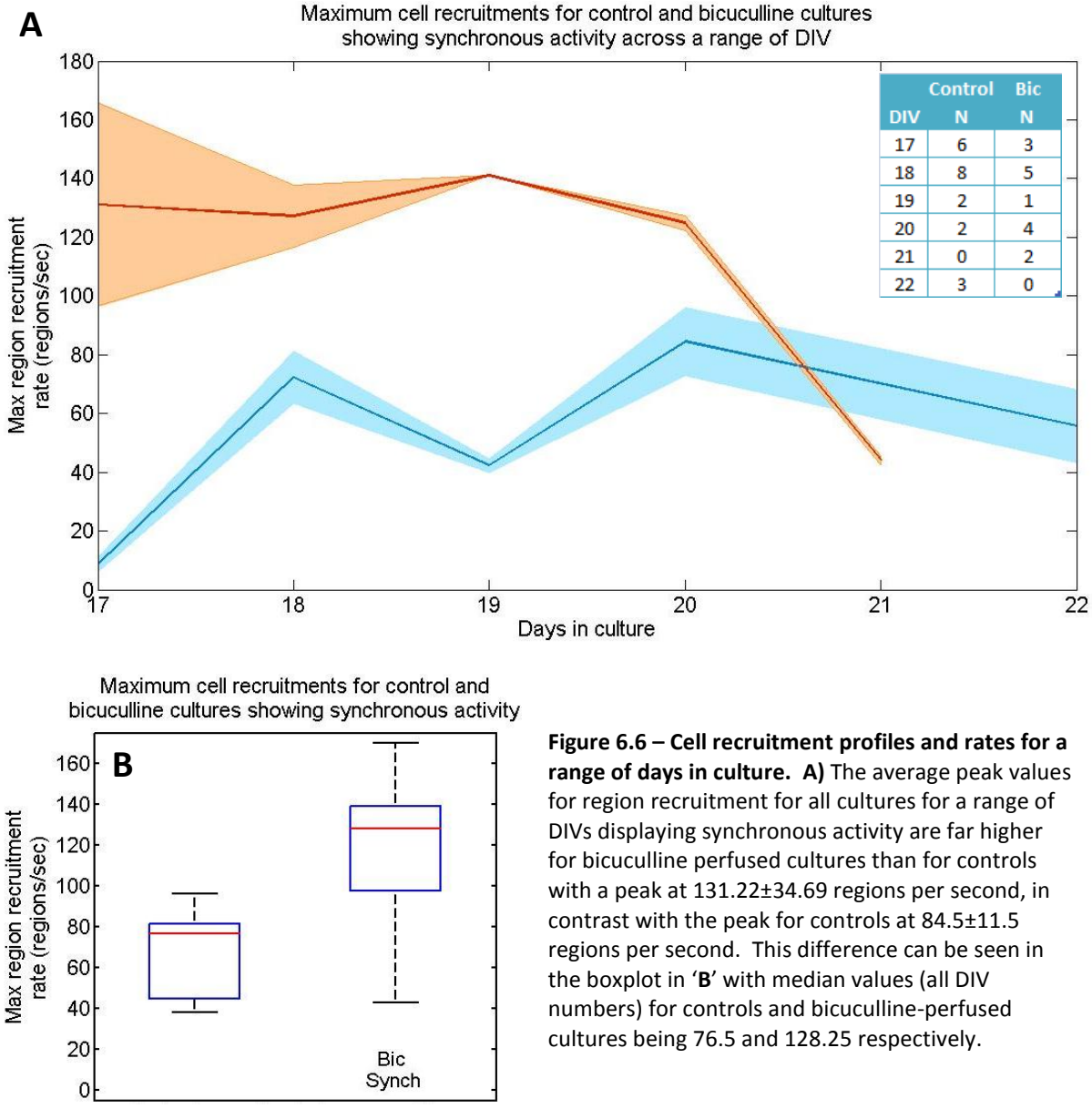

Figure 6.6 – Cell recruitment profiles and rates for a range of days in culture. A) The average peak values for region recruitment for all cultures for a range of DIVs displaying synchronous activity are far higher for bicuculline perfused cultures than for controls with a peak at 131.22±34.69 regions per second, in contrast with the peak for controls at 84.5±11.5 regions per second. This difference can be seen in the boxplot in '**B**' with median values (all DIV numbers) for controls and bicuculline-perfused cultures being 76.5 and 128.25 respectively.

calcium transients (Figure 6.11B), averaging 16.73±5.07 seconds as compared with 6.05±0.75 seconds for spontaneous transients (see Figure 4.7 D). There was an increase in length from 15 DIV to 17 DIV, followed by a steady decrease from 18 DIV onwards. The amplitudes of the transients evoked were considerably larger than for spontaneously occurring transients across all days in culture at 275.6±43.26, as compared with 94.85±20.81 for spontaneous transients (see Figure 4.9). There was a weakly negative linear relation between amplitude and day in culture (R^2 = 0.22) (Figure 6.11C). A rise is seen from 16 – 17 DIV (P = 0.05), correlating with the shift from entirely non-synchronous activity to the start of synchronous activity generation. There is a significant dip at 18 DIV (P = 0.05) correlating with the developmental stage showing the peak in the proportion of active cells and the size of FWHMs.

Evoked responses with 20µM and 40µM GABA application eliciting 152 and 262 amplitude responses respectively from the cells (Figure 6.12A). A clear summary of the GABA response effect immediately after the application of GABA can be seen in Figure 6.12B with an asymptotic decrease in both amplitude and FWHM of evoked calcium transient with DIV. The FWHM and amplitude fall from 16.2s (FWHM) and 348 (amplitude) at 17 DIV to 7.6±0.8s (FWHM) and 58±4 (amplitude) at 22 DIV, with 20 DIV cultures responding similarly to 22 DIV cultures.

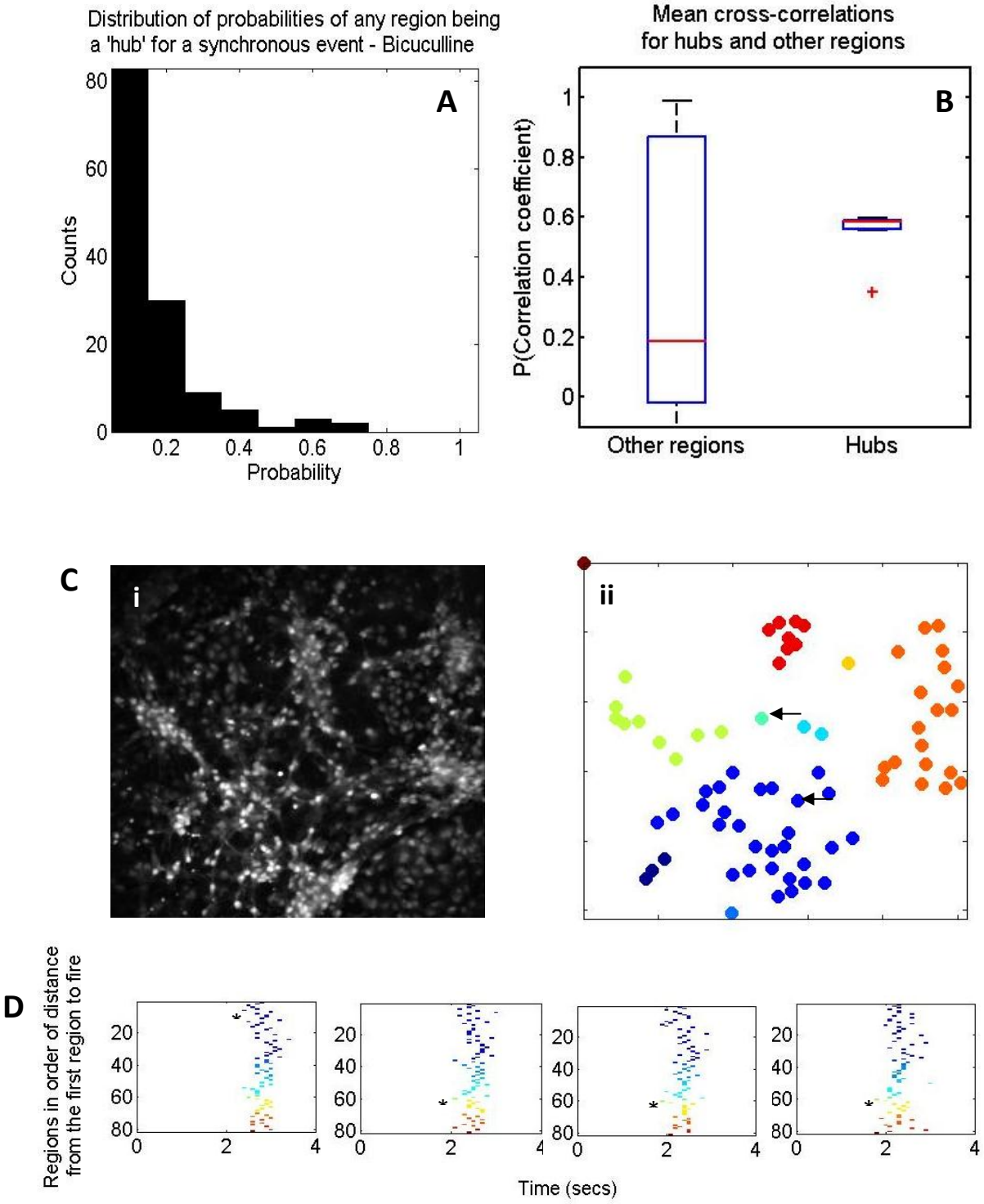

Figure 6.7 - 'Hub' probabilities and examples showing qualitatively the spread of activity through sub-clusters of regions during synchronous events. A) Distribution of probabilities for a region to act as a 'hub' region for a synchronous event across all cultures showing synchronous activity with more than 5 synchronous events in the 10 min recording with more than 10 active regions. **B)** The coincidence indices for hub regions was significantly higher on average (0.59±0.07, n = 14) than any other regions (0.19±0.43, n = 6232). **C)** Active regions in the culture were split into sub-clusters based on spatial distribution to look at the spread of activity following synchronous event initiation. The resting fluorescence intensity image is provided for reference (i) and the sub-clusters are shown in 'ii'. The 'hub' regions are shown with arrows. The spread of activity in 4 example synchronous events from these cultures is then shown in '**C**' as a raster plot. The regions are displayed in order of clusters and then distance from the 'hub' region for that event. (See Figure 5.9 for comparison with controls).

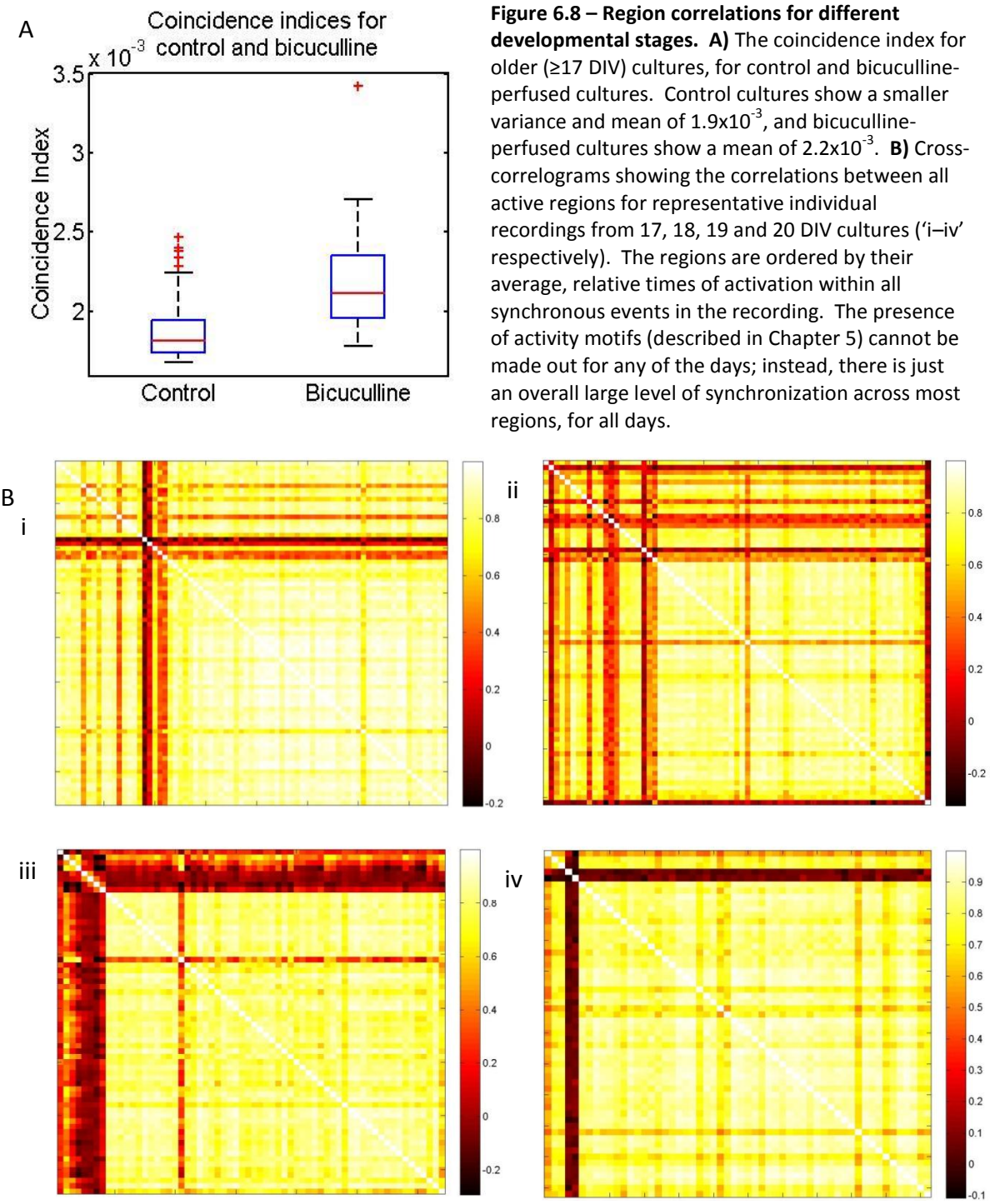

Figure 6.8 – Region correlations for different developmental stages. A) The coincidence index for older (≥17 DIV) cultures, for control and bicuculline-perfused cultures. Control cultures show a smaller variance and mean of 1.9×10^{-3}, and bicuculline-perfused cultures show a mean of 2.2×10^{-3}. **B)** Cross-correlograms showing the correlations between all active regions for representative individual recordings from 17, 18, 19 and 20 DIV cultures ('i–iv' respectively). The regions are ordered by their average, relative times of activation within all synchronous events in the recording. The presence of activity motifs (described in Chapter 5) cannot be made out for any of the days; instead, there is just an overall large level of synchronization across most regions, for all days.

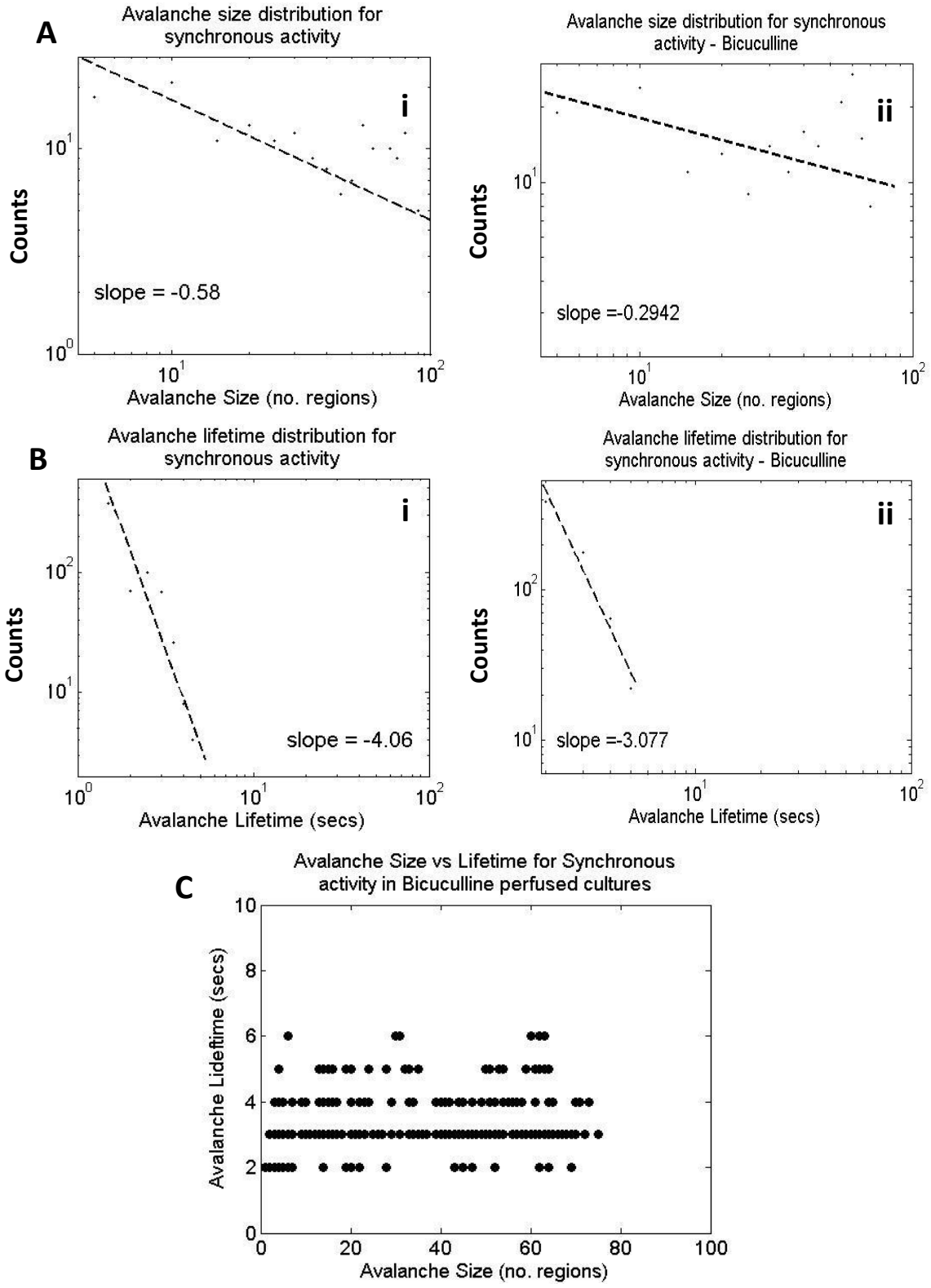

Figure 6.9 - Neuronal avalanche size and lifetime distributions for non-synchronous and synchronous activity. An avalanche is defined as the collective activity occurring in a culture in a temporal window, the edges of which are defined by the absence of all activity in the culture. Avalanche sizes are taken to be the number of regions that become active in an avalanche and the avalanche lifetime is the length of the temporal window in which the avalanche occurs. **A)** i) Avalanche size distribution for synchronous activity in controls (reproduced from Figure 5.10) has a slope of -0.58. ii) In comparison, bicuculline-perfused cultures show a slope of -0.29, showing the culture activity is in a more supercritical state. **B)** Avalanche lifetime distribution for synchronous activity in bicuculline-perfused cultures has a power law relation with a slope of -3.08 (ii)., as compared with the controls at -4.06 (i). **C)** The size vs lifetime of avalanches for bicuculline perfused, synchronously active cultures.

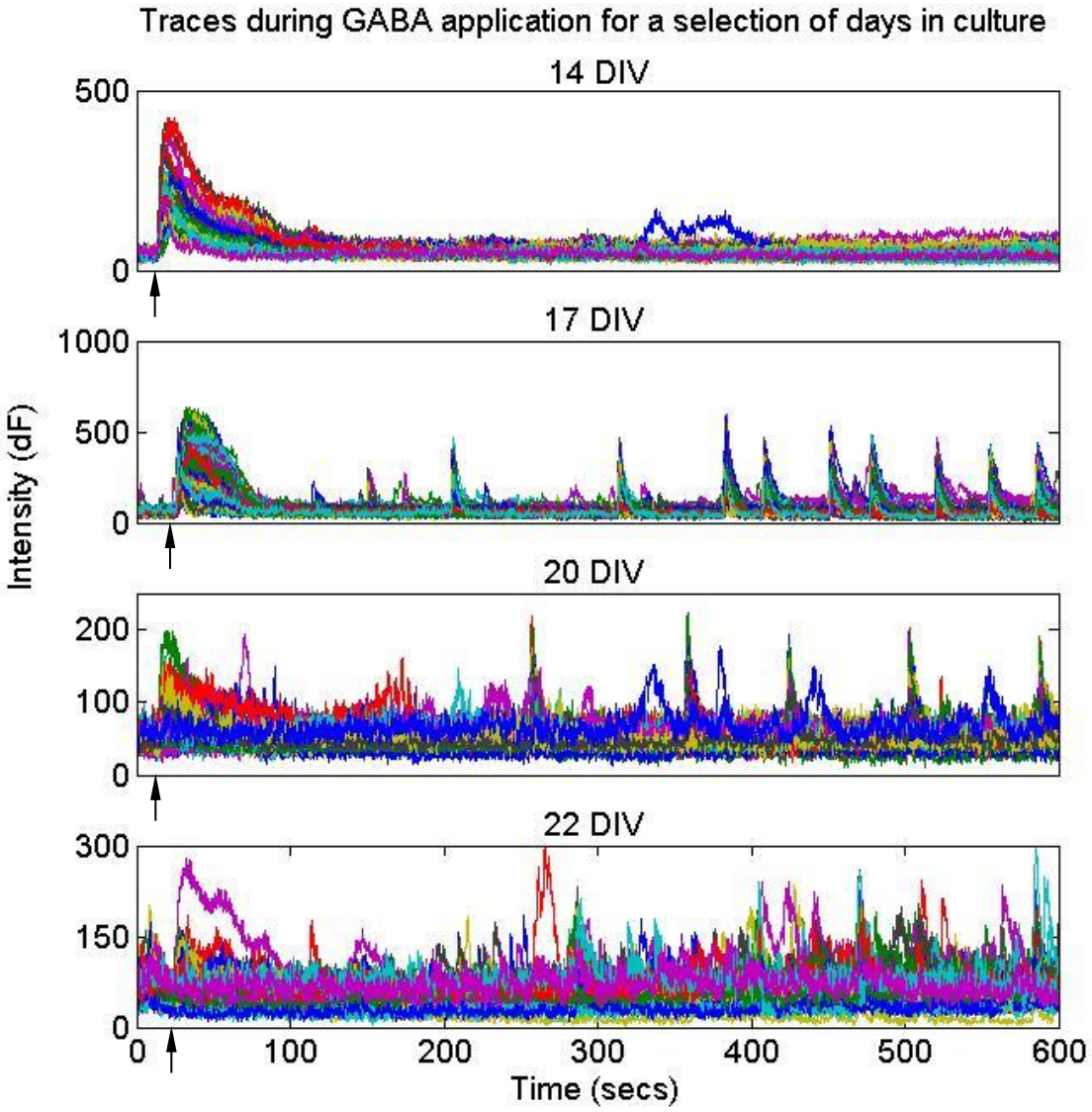

Figure 6.10 – Example traces of all active regions from a 10 minute recording for a selection of days in culture during an evoked GABA response. 20µM GABA was applied directly onto the culture by pipette after recording had started. Arrows indicate the time point at which GABA was pipetted onto the culture. Each of the 4 graphs shows the region intensity data for all regions that became active during the 10 minute recording over the full 10 minutes. The initial GABA evoked response appears as a depolarization in a large population of cells simultaneously, although this response decreases in size and the number of cells recruited with the day in culture. Cultures exhibiting synchronous activity show a quiescent period after the depolarization where the synchronous events are either absent or reduced (see **Figure 6.**).

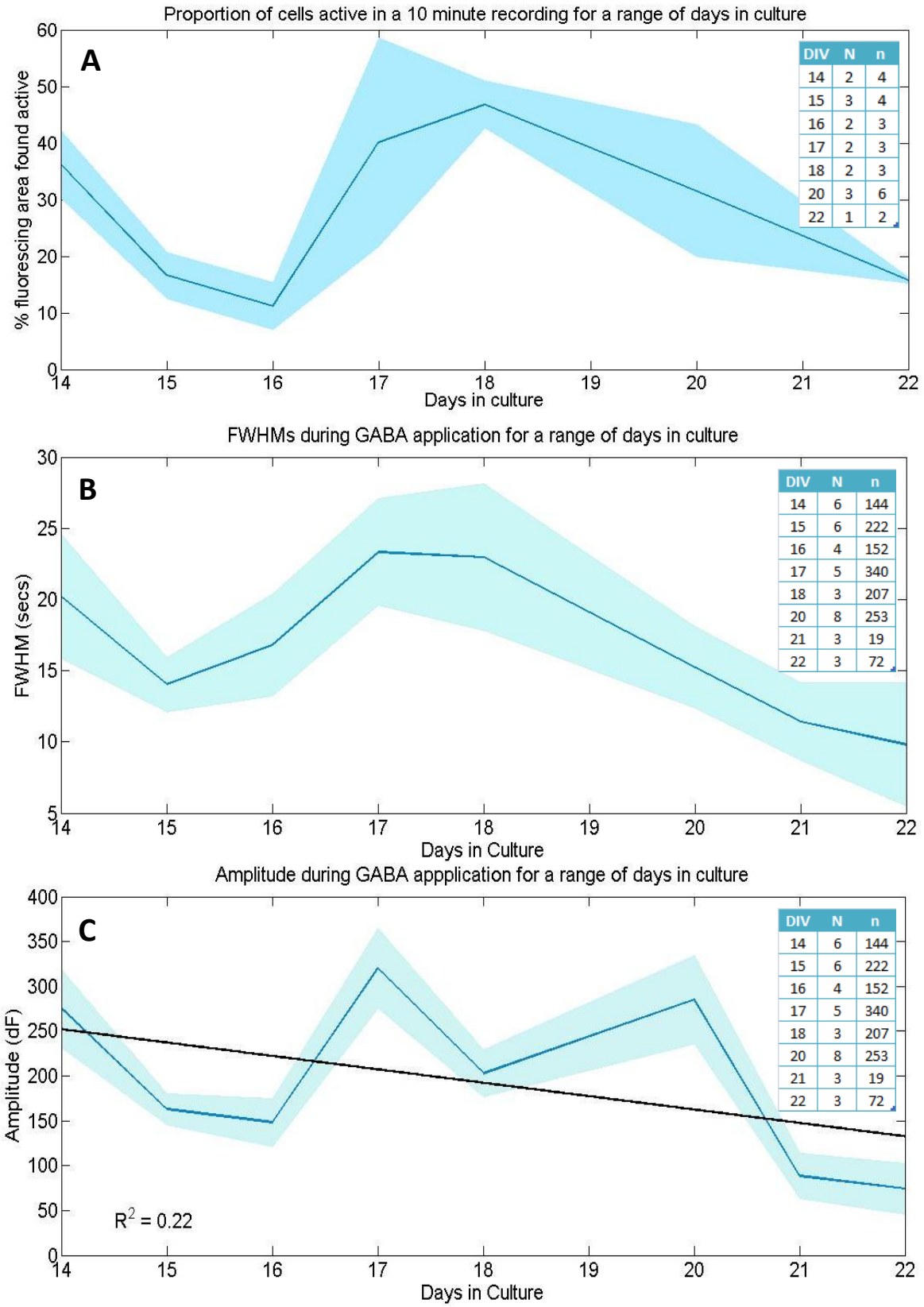

Figure 6.11 – Activity levels and transient kinetics during an evoked GABA response following GABA application for a range of days in culture. A) The proportion of cells active in a 10 minute recording for a range of days in culture. An increasing number of cells are active from 16 – 18 DIV, followed by a decreasing trend from 18 – 22 DIV, with the peak proportion of cells active (46.86±4.15%) at 18 DIV and the minimum (15.75±0.49%) at 22 DIV. **B)** The FWHMs show an increase in length from 15 DIV to 17 DIV, followed by a steady decrease from 18 DIV onwards. The FWHMs are considerably larger than the controls, with 14 and 22 DIV cultures averaging 20.22±4.35 and 9.81±4.33 respectively (P = 0.05). **C)** The mean amplitude across all recordings for each day in culture, showing a weakly-negative linear fit (R2 = 0.22). 14 and 22 DIV cultures average amplitudes of 275.6±43.26 and 9.81±4.33 respectively (P = 0.05).

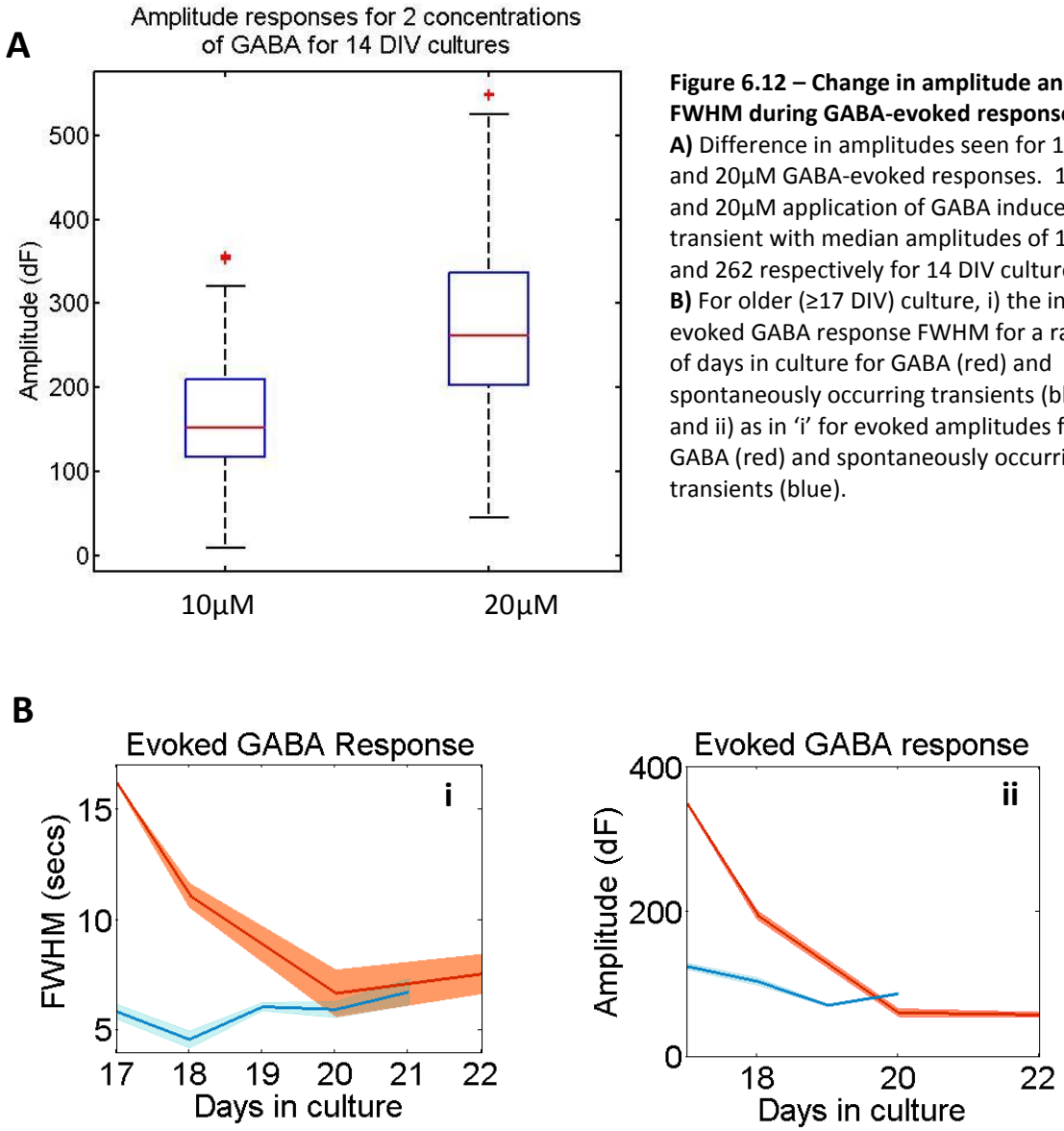

Figure 6.12 – Change in amplitude and FWHM during GABA-evoked responses. **A)** Difference in amplitudes seen for 10µM and 20µM GABA-evoked responses. 10µM and 20µM application of GABA induced transient with median amplitudes of 152 and 262 respectively for 14 DIV cultures. **B)** For older (≥17 DIV) culture, i) the initial evoked GABA response FWHM for a range of days in culture for GABA (red) and spontaneously occurring transients (blue), and ii) as in 'i' for evoked amplitudes for GABA (red) and spontaneously occurring transients (blue).

6.5 DISCUSSION

6.5.1 The role of GABA in CC9-derived neuronal networks

As explained in the Introduction, GABA is a significant and complex driving force during the development of early neuronal networks. Usually associated with an excitatory action due to the inverted chloride gradient in immature neurons (Anderson et al., 2004, Bolea et al., 1999, Bonifazi et al., 2009, Leinekugel et al., 1997, Chen et al., 1996), GABA is also known to exert trophic effects, influencing a variety of developmental processes (Barbin et al., 1993, Borodinsky et al., 2003, Fiszman et al., 1999, Represa and Ben-Ari, 2005). Two findings directly suggest the existence of a depolarising $GABA_A$ component to network communication in CC9-derived networks during the developmental stages considered here.

Firstly, there is an overall decrease in calcium transient amplitude with the GABA antagonist bicuculline at all developmental stages (Figure 6.3). Secondly, the exogenous application of GABA induces large calcium transients (though with a decreasing influence) until 21 DIV (Figure 6.12).

The overall excitatory effect of GABA in CC9-derived networks is evidently important for modulation of activity, as can be seen by the change in excitation of the network through the addition of bicuculline to the perfusate. Intriguingly, however, despite decreasing the amplitude of individual cellular calcium transients, bicuculline results in an increase in both rate of individual region/cell spontaneous transients and overall network activity (regions/cells active), and the variation of this activity at all stages of development (Figure 6.1). GABA therefore appears to have mixed excitatory and inhibitory effects at the network level. It was not seen as an absolute requirement for spontaneous activity (in contrast to findings on GDPs in immature hippocampus (Ben-Ari et al., 1989, Garaschuk et al., 1998), though it clearly modulated this activity in a developmental stage-dependent manner. Another example of such contrasting effects can be seen in the developing turtle retina where lower concentrations of bicuculline were found to stop the generation of spontaneous waves of activity, but with increasing concentrations the activity returned, with waves propagating significantly faster (Sernagor et al., 2003).

Blockade of GABA decreased transient amplitude, increased the activity and the number of active cells and increased the kurtosis of the ITI distribution. Exploring a link between these changes could point to intrinsic mechanisms and help clarify the apparent complexity and seemingly contradictory nature of the findings. Primarily, as transients are not all mediated by GABA (due to their persistence in the presence of bicuculline), the decrease in transient amplitude with bicuculline may be induced through the removal of a purely excitatory $GABA_A$ component in transient generation. If rate of transient occurrence is dependent on intrinsic neuronal properties related to the metabolic state of the cell, a decrease in transient amplitude would suggest reduced calcium entry per event and a reduced metabolic load. As a consequence, hyperpolarizing K_{ATP} conductances would not be so active (as they are inhibited by the presence of a high ATP to ADP ratio) and cells would be more excitable in general (Cunningham et al., 2006, Haller et al., 2001, Lorier et al., 2008), as is reflected in the higher levels of activity and number of cells activated with bicuculline.

This process is also likely to lead to a longer burst duration, and a shorter IBI, as was found in SWO in the cerebral cortex (Cunningham et al., 2006). If CC9 calcium activity pertained to bursts of action potentials within the cell, burst duration may relate to FWHM, though no significant changes were seen. Shorter ITIs were also not seen overall in CC9 cultures. However, there was a higher kurtosis for ITI distribution that, in the case of bursting, indicates a tighter control over the timing between bursts, and also a highly developmentally-dependent change in the relationship between amplitude and ITI (Figure 6.5). Longer bursts, but not an increase in the inter-burst interval, were found for in respiratory network dynamics, showing the variability in output affected by the K_{ATP} metabolic influence (Haller et al., 2001) in some preparations.

While little overall change in FWHM was seen there was a wider distribution of this measure seen with bicuculline than with controls. This tended towards a plateau in the region where a bimodal response is seen at 17 DIV. This bimodal response has also been shifted to be dominant earlier, in 17 DIV cultures, rather than the 18 DIV seen with controls. The earlier appearance suggests that the expression of briefer calcium transients is actively delayed during development by a mechanism involving GABA. As the expression of these additional, shorter events signalled the onset of synchronous discharges in control cultures, these data suggested that synchrony should also be modified in the presence of bicuculline (see Section 6.5.3 below).

As stated in the introduction to this chapter, $GABA_A$ receptor-mediated effects on individual neurons can be mixed. The chloride gradient is set predominantly by KCC2 (Rivera et al., 1999). However, KCC2 expression is still developing at this stage in development (Delpire, 2000, Li et al., 2002) and in mature neurons is highly compartment-specific (Báldi et al., 2010), with a gradient along the axo-somato-dendritic axis. Thus while axonal and somatic effects of GABA may be depolarising, effects out on dendrites may concurrently be hyperpolarising. It is not clear yet in these cultures where the majority of GABA receptors may be situated.

As was mentioned above, it is clear that not all of the calcium transients seen are mediated by GABA and thus, a blockade of all $GABA_A$-ergic effects may serve to decrease individual transient intensity directly by removing and excitatory GABA component – but not abolish

the events themselves. So where may the events in CC9 cultures originate from? The source of CC9 calcium transients may be ICCR from stores activated through either membrane potential fluctuations or CICR from calcium entry into the cell. By blocking GABA and reducing the amount of calcium entering the cell, there will be a lower probability of inducing further calcium release from stores via ryanodine receptors. Such a reduction in transient production is not seen with GABA blockade. However, if ICCR from stores is voltage activated (De Crescenzo et al., 2004) the reduced amplitude with GABA blockade may simply reflect the removal of the tonic GABA-induced calcium component of each transient. The exogenous application of GABA to the perfusate, inducing exaggerated calcium transients, could then cause the uncoupling of gap junctional connections that provide a path for activity propagation (Perez-Velazquez et al., 1994). This provides a further potential explanation for the quiescent period following these GABA-evoked calcium transients, and the gradual recruitment of cells back into synchronous events. This still does not account for the increase in transient activity seen with blockade of GABA with bicuculline.

In the case of CC9 cultures expressing active synapses, a further effect of the removal of the $GABA_A$ component could be to change sensitivity of neurons to excitatory glutamatergic inputs onto distal dendrites. In mature neuronal networks it is these distal dendritic compartments that form the target for the majority of glutamatergic excitatory synapses, whereas $GABA_A$ receptor subtypes are reduced in dendritic compartments (Andrásfalvy and Magee, 2001, Nusser et al., 1998). This scenario suggests that, during the early stages of development studied, the enhanced network excitability seen was dominated by excitatory GABA effects to the extent that underlying glutamatergic excitatory connections may be actively attenuated. However, it is also known that excitatory GABA effects also feed onto NMDA receptor-mediated glutamatergic excitatory events (Staley et al., 1995). Thus, a removal of GABA excitation during development in these CC9 cultures may also attenuate glutamatergic excitation. Such excitatory events are a major contributor to the calcium signals recorded in neurons (see General Introduction), perhaps explaining the reduced amplitude of events seen here.

In the developing turtle retina, where GABA modulates retinal waves throughout its shift from an excitatory to an inhibitory role. Bicuculline was nevertheless found to have

contrasting effects at different concentrations, as was discussed in the introduction (Sernagor et al., 2003). The results reported here show an increase in calcium transient activity with blockade of GABA using higher concentrations of bicuculline. This may be due to a similar effect seen in the turtle retina with higher concentrations of bicuculline, where it was suggested that the differential effects of low and high concentrations may relate to the fine balance between synaptic and extrasynaptic $GABA_A$ receptor dynamics, or between the depolarizing effects of GABA and shunting inhibition (Sernagor et al., 2003).

The observed lack of absolute requirement for GABA to generate spontaneous events is in contrast with data from immature hippocampal studies (Garaschuk et al., 1998). However, it is similar to the observed absence of GABA as an essential network driver in early development in tissue that will ultimately develop into neocortex (Wagner and Luhmann, 2006). In this immature neuronal system glutamatergic excitation dominated as a source of spontaneous activity in combination with network functionality via gap junctional communication.

Gap-junction coupling is present very early in development and a strong influence on activity propagation in developing neuronal circuits (Kandler and Katz, 1995). Gap-junctions are highly sensitive to intracellular calcium levels, therefore the reduction in intracellular calcium during transients through bicuculline application may perhaps increase the strength of gap-junction coupling, thus aiding signal propagation through the network and increasing overall network excitability as seen with GABA blockade in CC9 cultures here (Perez-Velazquez et al., 1994).

6.5.2 Developmental shift in the effects of GABA in CC9 cultures

A number of measures taken in this study suggested a change in the role of GABA during the developmental period examined. At early time points (15-17 DIV) blockade of GABA effects through $GABA_A$ receptors with bicuculline caused increases in transient rate and proportion of regions recruited in a developmental stage-dependent manner. The largest effects were seen at 17 DIV. After this these effects faded. However, further developmental changes in bicuculline's effects could be seen at later time points. A marked change in the effects of bicuculline on amplitude/ITI relationship was seen at 17-21 DIV, with the contrasting effects noted at 17 DIV compared to 18-19 DIV. These data suggest a change in the role of GABA in

controlling spontaneous activity at around 17 DIV. In addition, for synchronous discharges the regional recruitment rates into each network event were dramatically increased by GABA blockade at 17 DIV, but this effect was abolished at the later developmental time point (see next section for detailed discussion of this network property). Finally, at the latest stages examined (21 & 22 DIV) the ability of exogenously applied GABA to induce a calcium transient was also almost abolished. All these changes point to a varying role for GABA in the developing network. However, understanding whether these changes are purely down to a switch from depolarising to hyperpolarising effects was extremely difficult.

The decrease seen in the effects of exogenous GABA application over later DIV numbers could be attributed to the precedented shift in the chloride gradient with development, induced by the up-regulation of KCC2. More than 80% of mouse hippocampal neurons responded to GABA at P6, yet by P13 this figure had reduced to less than 20% of neurons. This change was correlated with KCC2 channel expression (Liu et al., 2006). NKCC1 and KCC2 channel expression are modulated in development by activation of $GABA_B$ receptors that facilitate calcium entry through L-type VGCCs and this effect becomes strong in the second postnatal week in rats (Bray and Mynlieff, 2009). KCC2 up-regulation has been linked to the termination of neuronal migration in mouse cortical interneurons by causing a decrease in the generation of intracellular calcium transients through the reversal of the chloride gradient with development, which allows a reduction in membrane potential following GABA receptor activation (Bortone and Polleux, 2009); and somatic translocation was seen to terminate in the present study around 17 DIV. The present data suggest neuronal migration, somatic translocation and enhanced rates of calcium transients all coincide with the beginning of a decrease in the strength of GABA's ability to excite CC9 cultured neurons.

In CC9 cultures between 17–20 DIV that display synchronous activity, the effect of GABA application is initially a large calcium transient, followed by a quiescent period. Activity then re-appears through the gradual re-introduction of cells into synchronous events. In other cultures of ESC-derived neurons, cultured on MEAs for 28 days (by which time the chloride gradient had become hyperpolarizing), the application of GABA induced a quiescent period in spike-burst activity, followed by the gradual recruitment of cells back into the event (Illes et al., 2007). This expected response from a system where GABA has an inhibitory effect is

the same as that seen in CC9 cultures, where GABA evokes calcium influx. It is possible that the large calcium transient initially evoked by GABA application does not result in a barrage of spikes, but indeed induces the quiescent period in the network; i.e. large exogenous GABA application induces an inhibitory response. Synaptic activity then resumes later, as with the ESC-derived cultures in the Illes study (Illes et al., 2007).

As discussed earlier, GABA is not required for calcium transient production at any developmental time point studied in CC9 networks here. Thus it is difficult to interpret the apparent excitatory effects of GABA application with the above cited work dealing with GDPs in hippocampus. It may be that, although tonic activation of GABA increases the overall membrane excitability, synaptic GABA may have an inhibitory role. Such an effect has been demonstrated in the neonatal hippocampus where GABA is still depolarizing (Lamsa et al., 2000). Recurrent connections in interneurons were excitatory, yet GABA inhibited activity in pyramidal cells (even though it produced a depolarization), reducing the size of the active population. This was found to be a frequency-dependent response with high-frequency activity from the interneuron population inducing large depolarizations in the pyramidal cells. Shunting inhibition may play an important role here, as increased chloride conductances would be very pronounced during such a sudden influx of GABA (Staley and Mody, 1992). In immature CC9 cultures, the sudden influx of GABA may cause massive membrane depolarizations initially (leading to the calcium transient seen), which then lead to shunting inhibition and a cessation of on-going spontaneous activity.

From the above it can be seen that the increase in activity seen with bicuculline in CC9 cultures fits with the idea that although GABA can be seen to be excitatory, its effect on network output appears to be inhibitory. This is confirmed by a mirrored response to bicuculline application in the Lamsa study (Lamsa et al., 2000).

Furthermore, the addition of bicuculline resulted in hypersynchrony across the pyramidal cell population (again demonstrating the inhibitory effect of GABA, regardless of it depolarizing nature) in the neonatal hippocampus, which matches with the high levels of synchrony and the loss of activity motifs seen with bicuculline-perfused CC9 cultures post 17 DIV in the present study.

Shunting inhibition from depolarizing GABAergic inputs is a common influence when combined with glutamatergic inputs if there is an appropriate temporal separation between the initiation of these two post-synaptic responses. A tonic form of shunting inhibition due to GABA has been shown in rat cerebellar slices due to the constant presence of low levels of GABA, likely due to spill over from synapses (Brickley et al., 1996). Such a constant drive could be present in CC9-derived neurons, leading to the constant generation of background spontaneous post-synaptic currents that contribute to shunting inhibition. Such a tonic effect could in principle be present in the absence of synapses. Blockade of these currents with bicuculline would remove this gain-dependent effect on post-synaptic action potential generation and result in higher levels of activity – as is seen in CC9 cultures. GDP generation in the immature hippocampus was not abolished by blockers of phasic GABA activity but instead reduced GDP frequency demonstrating the influence of tonic $GABA_A$ in GDP activity. In accordance with this, tonic GABA agonists increased GDP frequency (Sipilä et al., 2005). In CC9 cultures the opposite effect was seen, tonic application of GABA antagonist increased spontaneous transient frequency, with effects most marked at 17 DIV. This, again, confuses the issue, suggesting that the predominant effect of GABA on spontaneous event occurrence was an inhibitory one, even at these early time points.

Clearly no simple delineation between excitatory and inhibitory actions of GABA exist during the developmental period studied here. As discussed above, some observations point to excitation whereas others to inhibition. What is clear is that the spontaneous calcium transients themselves do not require GABA actions through $GABA_A$ receptors to manifest. In addition, the patterns of network activity constructed in CC9 cultures with these events were dramatically affected by GABA in a manner that pointed to an overall inhibitory influence of this neurotransmitter post 17DIV (see next section). With the data available it therefore appears that the apparent excitatory effects of exogenously applied GABA do not inform accurately on the role played by endogenously released GABA in the cultures themselves – though they do demonstrate the possibility of an excitatory GABAergic response up to 20 DIV.

6.5.3 The effect of GABA on network interactions in CC9 cultures

The probability of neurons acting as hubs during the initiation of synchronous events was increased 3-fold with the application of bicuculline. At the same time, overall correlations

between regions were higher and the rate of recruitment of regions into a synchronous event also increased. The pattern of activity propagation through the neuronal sub-clusters appeared to be in the same manner as in controls, with activity spreading through all sub-clusters within the same temporal time-frame. These observations also tied in well with the observed decrease in slope of neuronal avalanche size indicating the shift to an even more super-critical state in late development in the absence of GABA influences via $GABA_A$ receptors.

In the neonatal rat hippocampus, spontaneous generation of synchronous activity in CA3, and its transmission to CA1, were generated through glutamatergic synapses. Blockade of GABA (depolarizing as it still was at that stage) induced hypersynchrony (Lamsa et al., 2000). This is consistent with the supposition (see Section 6.5.1) that blockade of GABA in CC9 cultures increases glutamatergic sensitivity and ultimately leads to higher levels of synchrony. Alternatively, it may be that GABA's inhibitory effects on the network were serving to dampen down the generation of synchrony by these transient events, regardless of the mechanism of synchronization. Mature GABAergic synaptic transmission is associated with certain forms of network synchrony (Whittington et al., 1995). However, in networks that have prominent recurrent glutamatergic excitation (such as area CA3 of the hippocampus) lateral inhibition decreases percolation of excitatory events, spatially localizing transients and also temporally restricting them (Traub and Miles, 1991, Pouille and Scanziani, 2001). This pattern of spatial and temporal localisation of events originating from a single source would be expected to lead to subcritical avalanche behaviour.

This role of GABA in limiting percolation of activity through a network may also underlie another of the effects seen at later developmental stages. As discussed in Chapter 5, 18 DIV sees a transient period of hypersynchrony in CC9 cultures reach a peak. Later this synchrony drops for a few days, to reappear with cultures older than this adapting back to a state where activity motifs appear in the network. These motifs represent stereotyped but spatiotemporally limited network events – similar to those predicted for near-critical behaviour proposed as an ideal state for information processing (see introduction to this chapter). Abolishing the effects of GABA reverses this effect, keeping cultures in a state of over-correlated activity and preventing the development of more efficient information transfer mechanisms in the circuit. The gradual increase in transmembrane chemical

chloride ion gradient, could affect such a change by reducing GABA's excitatory, depolarizing, role in favour of its inhibitory effects typical in mature networks.

Finally, hubs found in neonatal hippocampal slices were reported to be exclusively GABAergic (Bonifazi et al., 2009, Lamsa et al., 2000). It appears that this is not the case in CC9 networks owing to the increase in hub appearance with the application of bicuculline. This suggests further that GABA is not the major excitatory transmitter in CC9 cultures. Rather, that the non-GABA generated spontaneous calcium transients seen were limited in their ability to act as hubs by GABA. While the amplitude of these events was boosted by the presence of active $GABA_A$ receptors in individual regions/neurons, it is clear that their network consequences were attenuated. Thus GABA may act as an excitatory influence on individual neurons but an inhibitory influence on network consequences of individual neuron outputs.

While it is unlikely that glial cells are responsible for the signals recorded here, glial cells can interact with neurons (see Chapter 4, section 4.2.3). $GABA_A$ receptors have been found on glial cells (MacVicar et al., 1989). Indeed, in Bergmann glia from the mouse cerebellum, they were developmentally regulated, expressing an increasing number of $GABA_A$ receptors up until P7-10, before showing a drop off with very few present by P20 (Muller et al., 1994). The morphology of these cells changed during this developmental period, and the differential expression of receptors on the surface was in line with changes in functional behaviour. Initially, Bergmann glia are involved in the migration of granule cells (up until P20), though in the mature cerebellum they are closely associated with Purkinje cells (Lordkipanidze and Dunaevsky, 2005). $GABA_A$ receptors were also found on cultured astrocytes (Bormann and Kettenmann, 1988). Potentially, with bicuculline in the perfusate, developing glia may be directly activated via $GABA_A$ receptors on the glial cell surface or indirectly activated through changes in the underlying neuronal activity. In the case of the former, a decrease in the effect of $GABA_A$ receptor activation would be expected with development, as the number of $GABA_A$ receptors decreases. Application of GABA directly onto the culture shows a decrease in effect (in terms of amplitude and FWHM of the evoked calcium transient) with development. However, such a reaction is not mirrored with the GABA antagonist, bicuculline.

6.5.4 Concluding Remarks

This chapter has described how the modulatory effect of GABA act to keep the network in an excitable state, while also maintaining an appropriate level of criticality for propagation of information through its inhibitory mechanisms. These dual excitatory and inhibitory components have been observed in mature and immature slice preparations. Here it can be seen that *de novo* self-organizing 2D networks of neurons, derived from CC9 stem cells, are far from 'random' in terms of their spontaneous behaviour. Their spatiotemporal organisation depended on GABAergic influences, but was not precipitated by these influences. Indeed, they were able to produce an architecture with intrinsic and network properties capable of reproducing activities that correlated with activity seen in fully developed brain architectures, and immature neocortex in particular.

CHAPTER 7: GENERAL DISCUSSION AND FUTURE DIRECTION

7.1 GENERAL FINDINGS IN CC9-DERIVED NEURONAL CULTURES

This study has explored the capacity for these ESCs to differentiate and self-organize into de novo functional networks on 2D substrates. It has fostered an understanding of how that network activity evolves and is influenced by both structural and intrinsic mechanisms. As such, the complex interaction between overt morphological changes and the development of intrinsic influences together shaping network properties have been revealed. By using a combination of calcium imaging and network dynamics analyses it has been possible to look at dynamic properties of functional development independently from quantification of unit activity. Although the source of this calcium activity is speculative, and possibly changes over the developmental period measured, the system could still be observed to mature towards typical critical dynamics when viewed at this hierarchical level, as has been shown with unit activity in primary cultures of dissociated neurons.

The existence of complex spatiotemporal patterning of activity and its modulation through mechanisms specific to early neuronal development have been confirmed in these novel ESC-derived preparations. This has provided a unique glimpse into how, even in highly abstracted, sparsely populated environments, neuronal cells are pre-programmed to self-assemble themselves into functional units capable of the percolation of partially stereotyped activity displaying temporal and spatial motifs with scale-free properties. All of the measurements of temporal and spatiotemporal properties recorded in this thesis pointed to a critical period around 17-18 DIV for emergence of patterned network activity (Figure 7.1). Coincident behaviour in neurons emerged around 17 DIV as the proportion of active cells increased and the amplitude of events peaked following early developmental decreases. Further increases in coincident behaviour led to the emergence of highly synchronous events at 18 DIV, an observation which also correlated with a peak in the number of cells active in a network.

While the switch to highly synchronous discharges was rather abrupt at 17-18 DIV, linear regression lines for the developmental profile of calcium transients fitted well (in the majority of cases) with the near-linear trend towards clustering in the network (Figure 7.1).

Transient rate, rate of recruitment across the network, correlation index and number of active cells all correlated with clustering as a measure of anatomical network development. FWHM values did not change and amplitude of the fluorescence transients actually negatively correlated with clustering. The latter may reflect the decrease in influence of excitatory GABAergic events (see chapter 6 discussion) rather than being an emergent property of network structure.

Thus, many functional properties changed in line with the emergence of a structural change in the network – the establishment of neuronal clusters separated by dense neuritic bundles. With opportunistic connectivity rules (i.e. neurons closer together are more likely to form connections) such a structural change would likely lead to small world connectivity profiles which would enhance, efficiently, the degree of intercommunication in the CC9 derived networks.

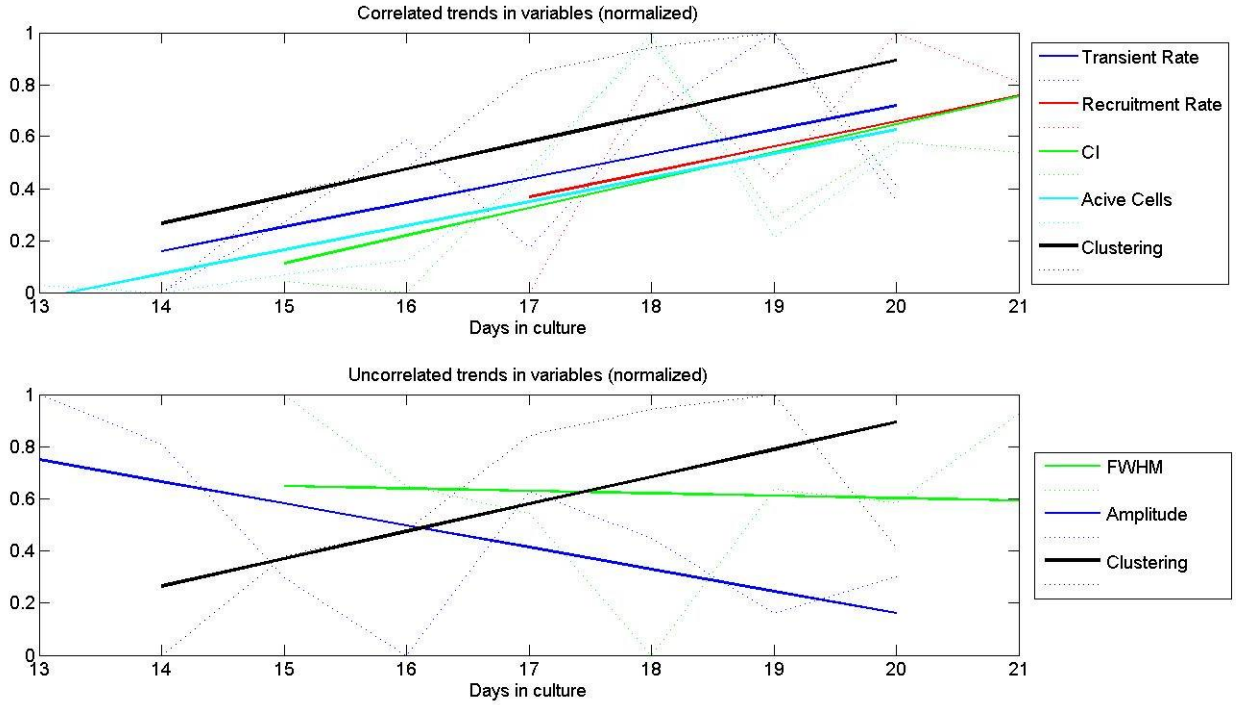

Figure 7.1 – Summary of developmental activity trends. All variables that correlated with the development of network architecture (Clustering, thick black line) are shown plotted together (**A**), and uncorrelated variables are similarly shown in **B**. The developmental trends are shown are dotted lines and their linear line of best fit.

GABA, an important neuromodulatory element in developing neuronal systems, is shown here to be critical to the regulation of activity as it evolves dynamically over a period of days, employing seemingly simultaneously excitatory and inhibitory effects, even before the migration of the chloride gradient. It is difficult to associate GABA with a purely excitatory

role in CC9 activity for a number of reasons. Firstly, the decrease in amplitude of calcium transients may simply be a consequence of the increased rate caused by GABA blockade. Figure 7.2 shows an almost mirror relationship between amplitude and rate of transients in control networks during development and the magnitude of the amplitude decrease with bicuculline is in line with what would be expected for the bicuculline-induced rate increase alone. Secondly, while exogenous GABA application was able to generate calcium transients, the magnitude and kinetics of these fell dramatically to spontaneous activity values by 20 DIV. This suggests that any excitatory role for GABA is on the wane during this developmental period and it is their developmental removal that is important to the development of more mature activity states.

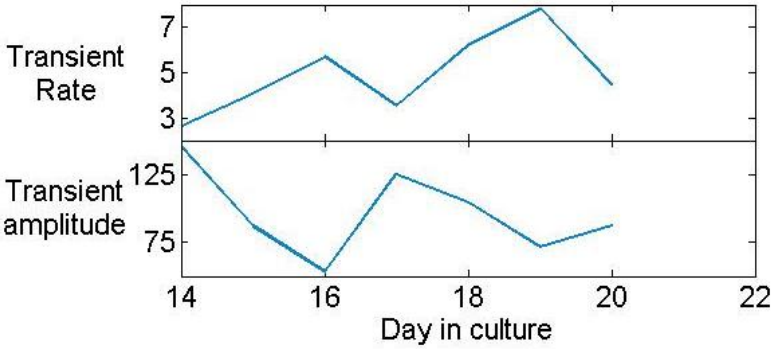

Figure 7.2– Mirror relationship between transient amplitude and rate of transient occurrence. The same trend is observed for both parameters, though opposingly.

This unique system has demonstrated how the general excitable state of nascent neuronal cells is influenced by GABAergic excitation, while the regulation of motifs of activity and the overall criticality of the network are concurrently mediated by GABAergic inhibition, all before mature aspects of network activity generation are fully developed. Interestingly, the pattern of effects of GABA seen in CC9 cultures here point more to developing neocortex than hippocampus or retina. In the developing neocortex spontaneous early discharges are not mediated by excitatory effects of GABA (Minlebaev et al., 2007). However, the spatial extent of their propagation was dependent on GABA – highly reminiscent of the supercritical, motif-less behaviour seen in this study with GABA receptor blockade. GABA is thus crucial to the maintenance of a CC9 derived system that moves towards generation of

more mature patterns of activity over a range of developmental stages, but appears not to be the underlying generator of that activity.

7.2 FUTURE DIRECTIONS

7.2.1 Key questions following these results

These intriguing finds, however, are surrounded by much speculation and many questions have been generated as a result of this work. Some of these are summarised as follows:

- Why was unit activity not detected using MEAs while previous patch-clamp studies suggested precedence for the capacity of these cells to generate sodium spikes?
- At what developmental day do key amino acid-based receptors migrate to form active synapses and what is their role in activity propagation?
- What role does gap-junctional coupling play in the propagation of activity through CC9 development?
- Which intrinsic mechanisms influence activity generation and does this change with development?
- What is the causal relationship, if any, between the coincident move to spatiotemporally organized activity and morphological restructuring of the network?
- What mechanisms lie behind the complex, seemingly dual role that GABA plays in the mediation of activity development?

7.2.1.1 Unit Activity

The lack of unit activity, as explained in Chapter 3, may be due technical, physiological or developmental reasons. Platinum black arrays that have nanotopographic roughness and increased cell-substrate contact density could provide a more effective electrode contact surface. In addition, smaller electrode diameters may further reduce current leakage and facilitate a stronger signal to noise ratio. If the cells can generate spike bursts, yet extracellular activity is not detectable due to physiological mechanisms (such as immature spiking in such small cells), this could be confirmed with concurrent patch-clamping and MEA experiments on the same culture. Alternatively, detectable network activity may be

restricted to localized areas of an array, becoming more robust with development, and its measurement may simply require a larger sample size at higher DIV numbers.

To add, the ability of these nascent cells to produce voltage-gated fast-acting sodium spikes (involved in mature action potential generation and subsequent calcium transient generation), could be confirmed with the application of tetrodotoxin (TTX) while observing any changes in calcium transient activity.

7.2.1.2 Synapse formation

The source of activity propagation could then be explored a number of ways. Immunocytochemistry could be employed post hoc to stain for synaptic vesicle proteins, such as by using synaptophysin, though this would not demonstrate the extent of synaptic influence on network output. Alternatively, a definitive, functional test for the presence of synaptic activity could be the blockade of synaptic vesicle release with, for instance, botulinum neurotoxin fragments (Antonucci et al., 2010).

The migration of different receptors to synapses, as described in the introduction to Chapter 4, each follows a different developmental profile. The number and distribution of integrous GABAergic and glutamatergic (involving NMDAR and AMPAR) synapses will affect network output and so it will be useful to explore this both functionally by using pharmacological techniques, and by employing post hoc immunostaining for $GABA_A$, NMDA and AMPA receptors.

7.2.1.3 Gap junctional connectivity

Network activity, however, may be propagated by gap junctions rather than synapses. Gap junctions are expressed before synapse development, and persist after synapses become functional, though the specific connexins that form these junctions are numerous and follow a complex developmental profile (e.g. Cx26 and Cx43 found in rat embryonic neocortex, with Cx 32 introduced shortly after birth). Various agents can be used to uncouple or block gap junctions, such as glycyrrhetinic acid and its derivatives (Juszczak and Swiergiel, 2009), thus it would be possible to map the functional influence of gap junctions throughout CC9 development. To add, western blots (or even immunostaining) could show the prevalence of specific connexins in these nascent neurons as they develop. This could be important as gap junctions are multifunctional structures influencing mechanical migration, cell-cell

communication and network propagation of activity. Considering the dramatic changes in somatic translocation, cell-cell positioning and activity patterns, all of these functions must vary through CC9 development within the window studied here and gap junctions may play a crucial role.

7.2.1.4 Intrinsic mechanisms of activity generation

As suggested in the discussion in Chapter 4, activity may be mediated by ICCR from stores, either activated through CICR or membrane voltage changes. Both IP3 and ryanodine receptors may influence calcium release from stores. 2-aminoethoxydimethyl borate (2-APB), an IP3 receptor antagonist could be employed to block ICCR, though its effect has been shown to vary by cell type. Ryanodine, which causes the release of calcium from stores in low (up to nanomolar) concentrations, blocks ryanodine receptors at large (micromolar) concentrations, preventing calcium release from stores and would be an effective way to observe the influence that this mechanism has on the generation of calcium activity in CC9s across all developmental stages.

Mechanisms that set the slow rhythms seen in this network may be due to metabolic processes, for instance K_{ATP} channel activity. This could be examined by altering glucose concentrations in the perfusate and observing changes in activity rates; or by blocking K_{ATP} channels directly. The functional purpose of such rhythms and how they change with development could be explored through the chronic alteration of available energy to the system and observing the difference in the development of temporal and spatial activity trends.

If intrinsic bursting is found to be a cause of calcium transient activity, it is interesting to note that, although spatiotemporal patterns of activity alter radically with time, the temporal characteristics of individual transients do not change dramatically. However, it is unconfirmed as to whether this was due to a stability in intrinsic neuronal properties, or counterbalancing changes that preserve basic calcium signalling properties, particularly considering the ubiquitous nature and universal importance of calcium signalling mechanisms in cell development and function.

7.2.1.5 Structure-function relationships

The link between the cessation of migration as cells form interconnected sub-clusters and the dramatic shift from sparse, uncorrelated activity to synchronized, spatiotemporally patterned activity has been discussed here, though any causal relationship between the two has not been determined. For instance, it may be that the structural changes in cellular organization and macro-architecture influence communication wiring strategies and ultimately network properties; or it may be that innate intrinsic cell properties that change with development to favour different wiring strategies consequently influence cell aggregation patterns. An interplay between the two is likely, but the extent of this influence could be further explored. The manipulation of network architecture using CNTs was successfully demonstrated in the results in Chapter 3. Other methods of network patterning (described in detail in the introduction to Chapter 3) could also be employed to dictate cell cluster size and positioning, and also potentially to encourage monolayered architectures where clustering is absent.

Ultimately it would be useful to quantify mean connectivity rates within and between clusters and relate this to conduction times in the nascent axons involved. The level of inter- to intra-cluster connectivity will affect functional network topologies. Interestingly, propagation of activity in these nascent, low-population clusters of cells did not show a difference in activation time during synchronous events – clusters were all activated within the same temporal window and acted as a single functional unit. This may be demonstrative of a limitation on the smallest cluster size amenable to spatial segregation of functional activity motifs; i.e. a limitation on the spatial distribution of discrete function units. However, it may also point to functional 'small worldness' in the network as it matures, with densely interconnected neurons within individual clusters being linked by a small number of longer range, inter-cluster, connections. This would be a fascinating aspect of neuronal topology to explore, for example, by using patterning techniques. Immunostaining to reveal the ratio of axonal and dendritic arbours (perhaps using tau-1 and MAP2 for axons and dendrites respectively), particularly along thick fasciculated bundles of neurites bridging cell clusters, could provide a method to explore the ratio intra- and inter-cluster connectivity.

7.2.1.6 The complex role of GABA

The presence of evidence for both excitatory and inhibitory GABAergic effects (at least up to 19 DIV) have been illuminated in these nascent networks to a degree through the use of GABA and bicuculline. Yet the assembly of $GABA_A$ receptors into synaptic complexes has not been confirmed. A more thorough exploration of the tonic and phasic effects of GABA would be useful to understand its modulatory effect on network activity with respect to neuronal development. The use of the general agonist, GABA, also activates $GABA_B$ receptors, present early in development. These metabotropic receptors are inhibitory, activating outward K^+ conductances and reducing Ca^{2+} entry. In order to delineate activation of $GABA_A$ and $GABA_B$ receptors, selective antagonists (such as gabazine and 2-OH saclofen for $GABA_A$ and $GABA_B$ receptors respectively) could be used, as could muscimol, a selective $GABA_A$ agonist. The development of critical network behaviours appears to be dependent on GABAergic influence; significantly, immature inhibitory mechanisms prior to the switch in chloride gradient from depolarising to hyperpolarising. A more in depth analysis of differing GABAergic mechanisms could isolate elements of this developmental profile.

7.2.2 Protocol improvements

7.2.2.1 Data gathering

Small sample sizes for a few developmental stages mean that rigorous statistical trends are difficult to produce and gathering more data sets would be necessary to confirm their significance. Also, a more thorough analysis of functional network properties would be possible with larger amounts of activity produced in a single dataset. This could be achieved by increasing the length of the recording period. Limitations inherent in the current system mean that this could only be achieved by reducing the sampling rate, though this may be altered by updating the system so that sampling rates could be maintained. Increases in the amount of activity gathered from a single data set would also open up the possibility of functional connectivity and causal relationship analyses. It was also noted that the duration of the developmental study could not be extended much beyond 20 DIV. This may have been a technical issue relating to the difficulty in preventing infection of live cultures. However, it may also have coincided with the trend towards hypersynchronous (supercritical) behaviour. In the absence of patterned inputs this behaviour has been shown

to dominate in a number of neuronal culture systems and, as it was enhanced by GABA receptor blockade (chapter 6), may have reflected a hyperexcitable network state. It would be interesting to repeat the study on larger cultures (where the criticality measures may have been more accurate) or with cultures receiving continual, patterned stimulation to mimic inputs from other brain regions during development.

7.2.2.2 Data analysis

The analysis tools developed in MATLAB for determining regions of interest were based on flat thresholding, and manual input from the user. This resulted in a slight lack of standardization (due to the user input) and the joining together of multiple, overlapping regions (through flat thresholding). This could be improved with a topographical map style of thresholding that separates out peaks within thresholded areas of region overlap and could compensate for the need for user input. The consequence of this would be that more regions of interest would relate to individual neurons rather than cell clusters (a problem that became increasingly evident with higher DIV numbers). Combined with removing the need for user input, this allows for a more robust separation of signals for analysis, increasing the number of neurons to be analysed and improving the efficacy of network analysis on sub-clusters of neurons at later stages of development.

7.3 FINAL SUMMARY

This body of work has lead to some unique finds as regards structure-function relationships and the developmental profile of GABAergic signalling. These experiments were performed using a novel system employing ESCs with distinctive migratory mechanisms, displaying very early onset synchronous activity. Network analyses could be applied to this system without the need for recording unit activity directly and the development of information-processing characteristics has been shown to be an innate property of self-organising de novo neuronal systems, even before the development of mature neuronal mechanisms. This has raised a number of questions regarding the origins of this early activity and specific causal mechanisms underlying system interactions. Further study, as outlined in this chapter, would be beneficial to understanding the intricacies of how function and form are inter-dependent in neuronal network development.

APPENDICES

Analysis of the data in this project was scripted almost exclusively in MATLAB. Only the scripts used in the final analyses displayed in the results sections of this report have been provided here, and the scripts themselves have been cut down for brevity (for instance, removing load- and save-paths, graphs created for later reference and data that was not specifically relevant to the programme). References are given at the start of each script if downloaded scripts have also been employed, although those scripts are not reproduced here (they can all be downloaded from the MATLAB Central file exchange).

APPENDIX A – IMAGE PREPROCESSING

The below macro describes each imaging process performed on all data in ImageJ before input into MATLAB for full analysis and involves subtracting background fluorescence intensities and smoothing the data.

```
open("file_location\\file.tif");
run("Subtract Background...", "rolling=25 stack");
run("Z Project...", "start=1 stop=5 projection=[Average Intensity]");
imageCalculator("Subtract create stack", "file.tif","AVG_file.tif");
//run("Image Calculator...", "image1=[file.tif] operation=Subtract
image2=[file.tif] create stack");
selectWindow("file.tif");
close();
selectWindow("file.tif");
close();
run("Kalman Stack Filter", "acquisition_noise=0.05 bias=0.80");
run("Remove Outliers...", "radius=1 threshold=50 which=Bright stack");
run("Remove Outliers...", "radius=1 threshold=50 which=Dark stack");
saveAs("Tiff", "file_location\\IJ file.tif");
close();
```

APPENDIX B – TEMPORAL ANALYSIS

The below function was used to identify regions of interest (ROI) from the ImageJ pre-processed data and create channel data from each of these regions (i.e. traces showing change in intensity with time for each ROI).

```
function [] = OriginalRoiAnalyse(filename,sq,fps,Num_hp,indices,savename)
% filename      = tiff stack
% image_file    = a brightfield image of the culture
% sq            = pixel size of tiffs (usually 256)
% fps           = frame rate (usually 10Hz)
% Num_hp        = highpass filter custom designed with the FDA tool to
%                 remove very low frequency wandering of the signal
% indices       = frames (usually 1:6000)
% savename      = output .mat filename
% maximize function downloaded from MATLAB Central file exchange.  Written
% by Yuval Cohen, Be4 Ltd.

% Read in file to 3D matrix.
D = zeros(sq,sq,length(indices));
c = 1;
for k = indices;
    D(:,:,c) = imread(filename,'tiff',k);
    c = c+1;
end

% Calculate a mask threshold based on a percentage of the data range.
Drange = range(D,3); Drangemean = mean(mean(Drange));
Dmax = max(max(Drange));
perc = %40;
thresh4mask = Dmax - ((Dmax/100)*(100-perc));
increment = Dmax - ((Dmax/100)*95);
choice = 'Yes';
while strcmp(choice, 'Yes')
    prompt2 = {'Higher or lower threshold? [h/l]'};
    dlg_title2 = 'Finding the number of regions';
    num_lines2 = 1;
    dlg_answer2 = inputdlg(prompt2,dlg_title2,num_lines2);
        if dlg_answer2{1} == 'h';
            thresh4mask = thresh4mask + increment;
        else thresh4mask = thresh4mask - increment;
        end
        clear Dr Dbw
        Dr = Drange; Dr(Dr<thresh4mask) = 0; Dr(Dr>=thresh4mask) = 1;
        Dbw = bwlabel(Dr); Ch_Info = regionprops(Dbw);
        for k = 1:length(Ch_Info);
             Area1(k) = Ch_Info(k).Area;
        end
        A = find(Area1<=9);
        for k = 1:length(A);
            Dbw(Dbw==A(1,k)) = 0;
        end
        Ch_Info = regionprops(Dbw);
        for k = 1:length(Ch_Info);
            Area2(k) = Ch_Info(k).Area;
        end
        Area2 = Area2./0; zero2remove = isnan(Area2);
        c = 1;
```

```
        for k = 1:length(zero2remove);
            if zero2remove(k)==0;
                Area3(:,c) = Area1(:,k);
                c = c+1;
            end
        end
    figure; I1 = imagesc(Dbw); colorbar;
    choice = questdlg('Do you want to re-iterate?');
end

% Separate regions that cover multiple cells and recreate mask.
a = xlsread('a.xls');
for k = 1:size(a,1);
    Dbw(a(k,1),a(k,2)) = 0;
end
Dr = Dbw; Dr(Dr<1) = 0; Dr(Dr>=1) = 1;
Dbw = bwlabel(Dr); Ch_Info = regionprops(Dbw);

% Create channel data and plot.
for k = 1:size(D,3);
    DMeanInt = regionprops(Dbw,D(:,:,k),'MeanIntensity');
    for r = 1:length(Ch_Info);
        Dx(k,r) = DMeanInt(r).MeanIntensity;
    end
end
clear D
dDx = diff(Dx);
Dxf = filtfilt(Num_hp,1,Dx);

% Time vectors.
sep = 1/fps;
len = sep*(length(indices));
Dxt = [sep:sep:len];
dDxt = [sep:sep:len-sep];

% Normalize and plot the distribution for reference (user input next).
for j = 1:length(indices);
    Dx_n(j,:) = (Dx(j,:) - min(Dx(j,:)))/range(Dx(j,:));
end
hhDx_n = hist(reshape(Dx_n,1,[]),100);
Figures of Dx and Dxf vs time created for viewing

% Re-threshold based on dDx to rid wandering regions with no activity.
Dxf_thresh = 4*(mean(std(Dxf)));
choice = 'Yes';
while strcmp(choice, 'Yes')
    prompt2 = {'Higher or lower threshold? [h/l]'};
    dlg_title2 = 'Finding the number of regions';
    num_lines2 = 1;
    dlg_answer2 = inputdlg(prompt2,dlg_title2,num_lines2);
        if dlg_answer2{1} == 'h';
            Dxf_thresh = Dxf_thresh + mean(std(Dxf));
        else Dxf_thresh = Dxf_thresh - mean(std(Dxf));
        end
    Dxf_td = Dxf;
    dDx_td = dDx;
    Dx_td = Dx;
    Dbw_td = Dbw;
    for k = 1:size(dDx,2);
        if all(Dxf_td(10:length(indices),k)<=Dxf_thresh);
```

```
            trash(k) = 1;
            Dbw_td(Dbw_td==k) = 0;
        else trash(k) = 0;
        end
    end
    trash_ind = find(trash==1);
    Dxf_td(:,trash_ind) = [];
    dDx_td(:,trash_ind) = [];
    Dx_td(:,trash_ind) = [];
        for r = 1:size(Dx_td,2);
            for j = 1:size(Dx,1);
                Dx_td_n(j,r)=(Dx_td(j,r)-min(Dx_td(:,r)))/range(Dx_td(:,r));
            end
        end
        hh = hist(Dx_td_n,100);
        qwand = find(sum(hh(51:100,:))>=2000);
        Dxf_td(:,qwand) = [];
        dDx_td(:,qwand) = [];
        Dx_td(:,qwand) = [];
        for q = 1:length(qwand);
            Dbw_td(Dbw_td==qwand(q)) = 0;
        End
    Figures of Dx_td and Dx_td created for user viewing
    choice = questdlg('Do you want to re-iterate?');
end

% Re-create mask.
Dbw2 = bwlabel(Dbw_td);
Ch_Info_td = regionprops(Dbw2);
for k = 1:length(Ch_Info);
    Ch_Info(k).Centroid = round(Ch_Info(k).Centroid);
end
for r = 1:size(Dx_td,2);
    for j = 1:length(indices);
        Dx_td_n(j,r) = (Dx_td(j,r) - min(Dx_td(:,r)))/range(Dx_td(:,r));
    end
end
hhDx_td_n = hist(reshape(Dx_td_n,1,[]),100);
Dx_td_activity_level = sum(hhDx_td_n(50:99));
end
```

The function below takes the channel data (i.e. traces for each ROI) created in the programme above and finds all information on each detectable calcium transient within those regions, including temporal information and transient characteristics.

```
function [Region_Info,Peak_Info] = fwhm_pref(pref,fps)
% pref = m*6 cell array containing file location information
% fps = frame rate (usually 10Hz)
% maximize function downloaded from MATLAB Central file exchange.  Written
% by Yuval Cohen, Be4 Ltd.
for pr = 1:size(pref,1);
load Dx_td data

    Dx_td(1,:) = [];
    n = size(Dx_td,1);
    m = size(Dx_td,2);
```

```
for k = 1:m,
    Region_Info(k).Dx_td = Dx_td(:,k);
end

for r = 1:m;
    for j = 1:n;
        Region_Info(r).Dx_td_dFoverF(j) = ((Dx_td(j,r) - ...
            min(Dx_td(:,r)))/range(Dx_td(:,r))).*100;
        Region_Info(r).Dx_td_n(j) = Dx_td(j,r) - min(Dx_td(:,r));
    end
end

% Smooth (mean moving window) and hp filter each region (for peaks)
load('Num_hp400_23Hz_0p2');
for k = 1:m;
    c = 1;
    for i = 10:n-10;
      Region_Info(k).Dxs_td(c) = mean(Region_Info(k).Dx_td_n(i-9:i+9));
      c = c+1;
    end
    Region_Info(k).Dxsf_td = filtfilt(Num_hp400_23Hz_0p2,1,...
        Region_Info(k).Dxs_td);
    d = 1;
end

% Determine threshold on the filtered data for each region individually
for k = 1:m;
    Region_Info(k).Dxsf_thresh = 2.5*((std(Region_Info(k).Dxsf_td)));
end
thr = ones(n,m);
for k = 1:m;
    thr(:,k) = thr(:,k).*Region_Info(k).Dxsf_thresh;
end

% Locate peaks.
for k = 1:m;
    [pks,locs] = findpeaks(Region_Info(k).Dxsf_td,'minpeakheight',...
        Region_Info(k).Dxsf_thresh);
    Peak_Info(k).locs(1:length(locs)) = locs;
end
for k = 1:length(Peak_Info);
    c = 1;
    for i = 1:length(Peak_Info(k).locs)-1;
        dist2pk = Peak_Info(k).locs(i+1) - Peak_Info(k).locs(i);
        if dist2pk>=50;
            if Peak_Info(k).locs(i)>=1;
                Peak_Info(k).burstend(c) = Peak_Info(k).locs(i);
                    if length(find(Peak_Info(k).locs==...
                         Peak_Info(k).burstend(c)))>=2;
                        Peak_Info(k).burstend_locindex(c) = 0;
                    else Peak_Info(k).burstend_locindex(c) = find...
                         (Peak_Info(k).locs==Peak_Info(k).burstend(c));
                    end
                c = c+1;
            end
        elseif i==length(Peak_Info(k).locs)-1;
            Peak_Info(k).burstend(c) = Peak_Info(k).locs(i+1);
                if length(find(Peak_Info(k).locs==...
                        Peak_Info(k).burstend(c)))>=2;
                    Peak_Info(k).burstend_locindex(c) = 0;
```

```
                else Peak_Info(k).burstend_locindex(c) = find...
                        (Peak_Info(k).locs==Peak_Info(k).burstend(c));
                end
            c = c+1;
        end
    end
    if length(Peak_Info(k).locs)==1;
        Peak_Info(k).burstend = Peak_Info(k).locs;
        Peak_Info(k).burstend_locindex = 1;
    else
        for i = length(Peak_Info(k).locs);
            if Peak_Info(k).locs(i)~=Peak_Info(k).burstend(length...
                    (Peak_Info(k).burstend));
                Peak_Info(k).burstend(c) = Peak_Info(k).locs(i);
            if length(find(Peak_Info(k).locs==...
                    Peak_Info(k).burstend(c)))>=2;
                Peak_Info(k).burstend_locindex(c) = 0;
            else Peak_Info(k).burstend_locindex(c) = find...
                    (Peak_Info(k).locs==Peak_Info(k).burstend(c));
            end
            c = c+1;
            end
        end
    end
end

% Figure out the peak value and its location in the datastream.
for k = 1:length(Peak_Info);
    c = 1;
    for i = 1:length(Peak_Info(k).burstend);
        if i==1;
            if Peak_Info(k).burstend_locindex(i)>=1;
                burst_indices = 1:Peak_Info(k).burstend_locindex(i);
            end
        else
            if Peak_Info(k).burstend_locindex(i)>=1;
                burst_indices = Peak_Info(k).burstend_locindex(i-1)...
                    +1:Peak_Info(k).burstend_locindex(i);
            end
        end
        if Peak_Info(k).burstend(i)>=1;
            Peak_Info(k).maxpk(c) = max(Region_Info(k).Dxs_td...
                (Peak_Info(k).locs(burst_indices)));
            Peak_Info(k).finloc(c) = Peak_Info(k).locs...
                (burst_indices(Region_Info(k).Dxs_td(Peak_Info...
                (k).locs(burst_indices))==Peak_Info(k).maxpk(c)));
            c = c+1;
            clear burst_indices
        end
    end
end

% Search in the specified area for the onset of each peak.
for k = 1:m;
    for i = 1:length(Peak_Info(k).finloc);
     LookInY = fliplr(Region_Info(k).Dxs_td(1:Peak_Info(k).finloc(i)));
     TRI = delaunay([1:length(LookInY)],LookInY);
     Loc1 = dsearch([1:length(LookInY)]',LookInY,TRI,1,((Peak_Info...
         (k).maxpk(i))/100)*20);
     if Peak_Info(k).finloc(i) - Loc1 ~= 0;
         Peak_Info(k).Onset(1,i) = Peak_Info(k).finloc(i) - Loc1;
```

```
            Peak_Info(k).Onset(2,i) = Region_Info(k).Dxs_td(Peak_Info...
                (k).finloc(i) - Loc1);
            Peak_Info(k).TimeOnset(i) = (Peak_Info(k).Onset(1,i))*sep;
         end
        end
    end

    % Search for half-max pt at start and end of each peak for each region.
    for k = 1:m;
        for i = 1:length(Peak_Info(k).finloc);
            Peak_Info(k).StartEnd(1,1,i) = ((Peak_Info(k).finloc(i) - ...
                Peak_Info(k).Onset(1,i))/2) + Peak_Info(k).Onset(1,i);
            Peak_Info(k).StartEnd(2,1,i) = ((Peak_Info(k).maxpk(i) - ...
                Peak_Info(k).Onset(2,i))/2) + Peak_Info(k).Onset(2,i);
            Peak_Info(k).TimeStartEnd(1,i) = (Peak_Info(k).StartEnd...
                (1,1,i))*sep;
            LookInY = Region_Info(k).Dxs_td(Peak_Info(k).finloc(i):n-19);
            TRI = delaunay([Peak_Info(k).finloc(i):n-19],LookInY);
            Loc1 = dsearch([Peak_Info(k).finloc(i):n-19]',LookInY,TRI,...
                Peak_Info(k).finloc(i)+50,(Peak_Info(k).maxpk(i))*0.5);
            Peak_Info(k).StartEnd(1,2,i) = Loc1 + Peak_Info(k).finloc(i)-1;
            Peak_Info(k).StartEnd(2,2,i) = Region_Info(k).Dxs_td(Loc1 +...
                Peak_Info(k).finloc(i) - 1);
            Peak_Info(k).TimeStartEnd(2,i) = (Peak_Info(k).StartEnd...
                (1,2,i))*sep;
            Peak_Info(k).FWHM(i) = Peak_Info(k).TimeStartEnd(2,i) - ...
                Peak_Info(k).TimeStartEnd(1,i);

        end
    end

    % kick out xls of FWHMs for manipulating in, eg GraphPad.
    for k = 1:m;
        FWHMs(1:length(Peak_Info(k).FWHM),k) = Peak_Info(k).FWHM;
    end

      for k = 1:length(Peak_Info);
          for i = 1:length(Peak_Info(k).finloc)-1;
              if length(Peak_Info(k).finloc)~=1;
                  Peak_Info(k).ISI(i) = (Peak_Info(k).finloc(i+1)...
                      - Peak_Info(k).finloc(i))/fps;
              end
          end
      end
      ITI_hist = cat(2,Peak_Info.ISI);
      ITI_hist(ITI_hist>=265) = 0;

    for r = 1:length(Peak_Info);
        amp_temp = Peak_Info(r).maxpk - Peak_Info(r).Onset(2,:);
        amp(1:length(amp_temp),r) = amp_temp;
        amp_max(r) = max(amp_temp);
        amp_min(r) = min(amp_temp);
    end
    amp(amp==0) = NaN;
    amp_hist = hist(amp,20);
    amp_hist_all = hist(reshape(amp,[],1),50);
end
end
```

The below function is designed to look at the relationship between transient amplitude and ITI.

```
function [] = AmpITI2(pref)
for pr = 1:size(pref,1);
load Peak_Info and Amp data
    % get ITIs into matrix format
    for r = 1:length(Peak_Info);
        eval(['Z' pref{pr,6} pref{pr,1}...
            'ITI(1:length(Peak_Info(r).ISI),r) = Peak_Info(r).ISI;']);
    end
    eval(['Z' pref{pr,6} pref{pr,1} 'ITI(Z' pref{pr,6}...
        (5:9) pref{pr,1} 'ITI==0) = nan;']);

    % ITI/Amp relation (and forward relation) with linear fit & delta error
    c = 1;
    for r = 1:length(Peak_Info);
 eval(['n = find(isnan(Z' pref{pr,6} pref{pr,1} 'ITI(:,r)),1,''first'');']);
 tf = isempty(n);
 if tf==1;
eval(['[p1 S1] = polyfit(Z' pref{pr,6} pref{pr,1} 'ITI(:,r),Z' pref{pr,6}
pref{pr,1} 'Amp(2:end,r),1);']);
eval(['[y1 delta1] = polyval(p1,Z' pref{pr,6} pref{pr,1} 'ITI(:,r),S1);']);
if length(Peak_Info(r).ISI)<2;
    rs1 = [];
else eval(['rs1 = regstats(Z' pref{pr,6} pref {pr,1} 'ITI(:,r),Z' pref{pr,6}
pref{pr,1} 'Amp(2:end,r));']);
end
eval(['[p2 S2] = polyfit(Z' pref{pr,6} pref{pr,1} 'ITI(:,r),Z' pref{pr,6}
pref{pr,1} 'Amp(1:end-1,r),1);']);
eval(['[y2 delta2] = polyval(p2,Z' pref{pr,6} pref{pr,1} 'ITI(:,r),S2);']);
if length(Peak_Info(r).ISI)<2;
    rs1 = [];
else eval(['rs2 = regstats(Z' pref{pr,6} pref {pr,1} 'ITI(:,r),Z' pref{pr,6}
pref {pr,1} 'Amp(1:end-1,r));']);
end
else
eval(['[p1 S1] = polyfit(Z' pref{pr,6} pref{pr,1} 'ITI(1:n-1,r),Z'
pref{pr,6} pref{pr,1} 'Amp(2:n,r),1);']);
eval(['[y1 delta1] = polyval(p1,Z' pref{pr,6} pref{pr,1} 'ITI(1:n-
1,r),S1);']);
if length(Peak_Info(r).ISI)<2;
    rs1 = [];
else eval(['rs1 = regstats(Z' pref{pr,6} pref{pr,1} 'ITI(1:n-1,r),Z'
pref{pr,6} pref{pr,1} 'Amp(2:n,r));']);
end
eval(['[p2 S2] = polyfit(Z' pref{pr,6} pref{pr,1} 'ITI(1:n-1,r),Z'
pref{pr,6} pref{pr,1} 'Amp(1:n-1,r),1);']);
eval(['[y2 delta2] = polyval(p2,Z' pref{pr,6} pref{pr,1} 'ITI(1:n-
1,r),S2);']);
if length(Peak_Info(r).ISI)<2;
rs1 = [];
else eval(['rs2 = regstats(Z' pref{pr,6} pref{pr,1} 'ITI(1:n-1,r),Z'
pref{pr,6} pref{pr,1} 'Amp(1:n-1,r));']);
end
end
eval(['Z' pref{pr,6} pref{pr,1} 'y.r' num2str(r)' = y1;']);
if tf==1;
```

```
eval(['Z' pref{pr,6} pref{pr,1} 'y.rx' num2str(r) ' = Z' pref{pr,6}
pref{pr,1} 'ITI(:,r);']);
else eval(['Z' pref{pr,6} pref{pr,1} 'y.rx' num2str(r) ' = Z' pref{pr,6}
pref{pr,1} 'ITI(1:n-1,r);']);
end
eval(['Z' pref{pr,6} pref{pr,1} 'y.r_delta' num2str(r) ' = delta1;']);
if ~isempty(rs1);
eval(['Z' pref{pr,6} pref{pr,1} 'y.r_rs'num2str(r) ' = rs1.rsquare;']);
rs_count(c) = r;
c = c+1;
end
eval(['Z' pref{pr,6} pref{pr,1} 'y.r' num2str(r)'f = y2;']);
eval(['Z' pref{pr,6} pref{pr,1} 'y.r_delta' num2str(r) 'f = delta2;']);
if ~isempty(rs1);
eval(['Z' pref{pr,6} pref{pr,1} 'y.r_rs'num2str(r) 'f = rs2.rsquare;']);
end
end

    % start creating R-squared for regions with 5 or more ITIs
    c2 = 1;
if exist('rs_count');
for r = rs_count;
if length(Peak_Info(r).ISI)>=5;
eval(['Z' pref{pr,6} pref{pr,1} 'R2Regs{c2,1} = strcat(pref{pr,6},
pref{pr,1});']);
eval(['Z' pref{pr,6} pref{pr,1}'R2Regs{c2,2} = Z' pref{pr,6} pref
{pr,1} 'y.r_rs' num2str(r) ';']);
eval(['Z' pref{pr,6} pref{pr,1} 'R2Regs{c2,3} = r;']);
c2 = c2+1;
end
end
end
end
end
```

APPENDIX C – SPATIOTEMPORAL ANALYSIS

The below programme describes the process used to analyse each synchronous event in cultures that displayed them. This included looking at the synchronicity, acceleration of recruitment in each event and the order of region recruitment.

```
function [] = BurstAnalysisPlus(pref,region1)
% pref = m*6 cell array containing file location information
% region1  = user-selected region involved in all events
for pr = 1:size(pref,1);
load Peak_Info and Dbw2 data

% CREATE MATRICES FROM WHICH TO WORK
for o = 1:length(Peak_Info(region1).TimeOnset);
    Onset1 = Peak_Info(region1).TimeOnset(o);
    Onset1min = Onset1 - 10; Onset1max = Onset1 + 10;
    Bursts(o).Patt(1,1) = 1;
    Bursts(o).Patt(1,2) = Onset1 - Onset1min;
    for k = 2:length(Peak_Info);
        Bursts(o).Patt(k,1) = k;
        ta = Peak_Info(k).TimeOnset(find(Onset1max>=Peak_Info...
            (k).TimeOnset & Peak_Info(k).TimeOnset>=Onset1min,1,'first'));
        TF = isempty(ta);
        if TF==1;
            Bursts(o).Patt(k,2) = 0;
        else Bursts(o).Patt(k,2) = ta-Onset1min;
        end
    end
    Bursts(o).PattSort = sortrows(Bursts(o).Patt,2);
    Bursts(o).PattSort(:,4) = Bursts(o).PattSort(:,2);
    en = find(Bursts(o).PattSort(:,2)==0,1,'last');
    TF = isempty(en);
    if TF~=1;
        Bursts(o).PattSort(1:en,:) = [];
    end
    mino = min(Bursts(o).PattSort(:,2));
    Bursts(o).PattSort(:,2) = Bursts(o).PattSort(:,2) - mino;
end
reg = length(Peak_Info); bur = length(Bursts);

% SYNCHRONICITY
    for k = 1:length(Bursts);
    hist1(k,:) = hist(Bursts(k).Patt(:,2),[1:20]);
    end
    hist1b = sum(hist1,1);

% number of regions preceding the firing of specific region:
for o = 1:bur;
    c = 1;
    Bursts(o).PattSort(1,3) = c;
    for r = 2:size(Bursts(o).PattSort,1);
        l = Bursts(o).PattSort(r-1,2);
        if l==Bursts(o).PattSort(r,2);
            Bursts(o).PattSort(r,3) = c;
        else c = c+1;
            Bursts(o).PattSort(r,3) = c;
        end
```

```
    end
end

% ORDER OF EVENTS THROUGHOUT EACH BURST
BurstsPatt = Bursts(1).Patt(:,2);
for o = 2:bur;
    BurstsPatt = cat(2,BurstsPatt,Bursts(o).Patt(:,2));
end
BurstsPatt(BurstsPatt==0) = NaN;
BurstsPatt_min = min(BurstsPatt,[],2);
for o = 1:size(BurstsPatt,1);
    BurstsPatt(o,:) = BurstsPatt(o,:) - BurstsPatt_min(o);
end
BurstsPatt = permute(BurstsPatt,[2 1]);
[BurstsPatt_mod BurstsPatt_freq BurstsPatt_modAll] = mode(BurstsPatt);
for k = 1:reg;
    if length(BurstsPatt_modAll{k})>2;
        BurstsPatt_mod(k) = round(mean(BurstsPatt_modAll{k}(~isnan...
            (BurstsPatt_modAll{k})))*10)/10;
    end
    if length(BurstsPatt_modAll{k})==2;
        if BurstsPatt_modAll{k}(2)-BurstsPatt_modAll{k}(1)==0.1;
            BurstsPatt_mod(k) = Bursts_modAll{k}(2);
        else BurstsPatt_mod(k) = NaN;
        end
    end
end
[BurstsPatt_sort BurstsPatt_sortI] = sort(BurstsPatt_mod);
BurstsPatt_freq_sort = zeros(size(BurstsPatt_sortI));
BurstPatt_modAll_sort = zeros(size(BurstsPatt_sortI));
for k = 1:length(BurstsPatt_sortI);
    BurstsPatt_freq_sort(k) = BurstsPatt_freq(BurstsPatt_sortI(k));
    BurstsPatt_modAll_sort(k) = BurstsPatt_modAll(BurstsPatt_sortI(k));
end
i = find(isnan(BurstsPatt_sort));
BurstsPatt_freq_sort(i) = [];
BurstsPatt_modAll_sort(i) = [];
BurstsPatt_sort(i) = [];
BurstsPatt_sortI(i) = [];
for o = 1:bur;
    m(o) = max(Bursts(o).PattSort(:,3));
end
m_tot = max(m);
for g = 1:m_tot;
    for o = 1:bur;
        vl = find(Bursts(o).PattSort(:,3)==g);
        PattSort(g).Bursts(1:length(vl),o) = Bursts(o).PattSort(vl,1);
    end
end
for o = 1:bur;
    c = 1;
    for k = 1:length(BurstsPatt_sortI);
        for g = 1:m_tot;
            loc = find(PattSort(g).Bursts(:,o)==BurstsPatt_sortI(k));
            TF = isempty(loc);
            if TF~=1;
                R(c,1,o) = loc;
                R(c,2,o) = g;
                R(c,3,o) = k;
                c = c+1;
            end
```

```
        end
    end
end
end
end
```

The script below split the ROI map into clusters of regions, based on their spatial distribution.

```
function [] = cluster2(pref,num_clus)
% pref      = m*6 cell array containing file location information
% num_clus  = user defined number of clusters
for pr = 1:size(pref,1);
load Hubprob, Hubn01, Hubfin, Ch_Info_td and Bursts data
    for r = 1:length(Ch_Info);
        C(r,:) = round(Ch_Info(r).Centroid);
    end
    if length(Bursts)>12;
        subl = 12;
    else subl = length(Bursts);
    end
    for b = 1:subl;
        eval(['event' num2str(b) ' = zeros(length(Ch_Info),200);']);
        for r = 1:length(Bursts(b).Patt);
            eval(['event' num2str(b)...
                '(r,round((Bursts(b).Patt(r,2)*10)+1)) = 1;']);
        end
        inds = find(Bursts(b).PattSort(:,2)==0);
        stpix(1:length(inds),b) = Bursts(b).PattSort(inds,1);
    end
    C1 = zeros(length(C)+1,2);
    for k = 1:length(C);
        C1(k,:) = C(k,:);
    end
    T = clusterdata(C1,num_clus);
    for k = 1:7;
        eval(['C' num2str(k+1) ' = C1(T==k,:);']);
    end
    Euc1 = squareform(pdist(C1));
    for so = 1:size(Hubn01,1);
     for k = 1:num_clus-1;
     for b = 1:subl;
       if Hubn01(so,b)~=0;
       eval(['sortvector' num2str(k) num2str(b)...
         ' = transpose(cat(1,Euc1(Hubn01(so,b),T==k),find(T==k)''));']);
         %length(C)+1 %Hubfin %stpix(so,b)
       eval(['sortvector' num2str(k) num2str(b) ' = cat(2,sortvector'...
           num2str(k) num2str(b) ',event' num2str(b) '(T==k,:));']);
       eval(['sortvector' num2str(k) num2str(b) ' = sortrows(sortvector'...
           num2str(k) num2str(b) ');']);
       end
     end
     end
        for b = 1:subl;
            if Hubn01(so,b)~=0;
            eval(['SORT' num2str(b) ' = [];']);
            eval(['SORTreg' num2str(b) ' = [];']);
            for k = 1:num_clus-1;
```

```
                eval(['SORT' num2str(b) ' = cat(1,SORT' num2str(b) ...
                  ',(sortvector' num2str(k) num2str(b) '(:,3:202)).*k);']);
                eval(['SORTreg' num2str(b) ' = cat(1,SORTreg' num2str(b)...
                    ',sortvector' num2str(k) num2str(b) '(:,2));']);
            end
            eval(['strow(so,b) = find(SORTreg' num2str(b)...
                '==Hubn01(so,b));']);
            end
        end
    end
end
end
```

The below function calculates the probabilities of a regions acting as a hub for a synchronous event.

```
function [] = HUBBINESS2(pref)
% pref = m*6 cell array containing file location information
for pr = 1:size(pref,1);
load Bursts, Peak_Info and Dbw2 data
    xt = [0:0.1:20];
    for b = 1:length(Bursts);
        c = 1;
        for dt = 0:0.1:20;
            hubtemp = find((dt-0.05)<Bursts(b).PattSort(:,2)...
                & Bursts(b).PattSort(:,2)<(dt+0.05));
            hubdesc(c,b) = length(hubtemp); c = c+1;
        end
    end
    [hubdesc_max hubdesc_max_i] = max(hubdesc);
    for b = 1:length(Bursts);
  hubtime1 = xt(hubdesc_max_i(b)); rbps = round(Bursts(b).PattSort(:,2)*10);
    while ~isempty(Bursts(b).PattSort(rbps==round((hubtime1-0.1)*10),1))...
         | ~isempty(Bursts(b).PattSort(rbps==round((hubtime1-0.2)*10),1));
     if ~isempty(Bursts(b).PattSort(rbps==round((hubtime1-0.1)*10),1));
       hubtime1 = hubtime1 - 0.1;
     else hubtime1 = hubtime1 - 0.2;
     end
    end
        hubtemp = Bursts(b).PattSort(rbps==round((hubtime1)*10),1);
        Hubn01(1:length(hubtemp),b) = hubtemp;
        Hubn01(1:length(hubtemp),b) = hubtemp;
        if b==1;
            TF = isempty(Hubn01(:,b));
            if TF==1;
              hubtemp1 = find(Bursts(b).PattSort(:,2)>=hubtime1,1,'first');
              hubtemp2 = Bursts(b).PattSort(hubtemp1,1);
              Hubn01(1:length(hubtemp2),b) = hubtemp2;
            end
        else
            if Hubn01(:,b)==0;
              hubtemp1 = find(Bursts(b).PattSort(:,2)>=hubtime1,1,'first');
              hubtemp2 = Bursts(b).PattSort(hubtemp1,1);
              Hubn01(1:length(hubtemp2),b) = hubtemp2;
            end
        end
        if hubtime1-0.1<0;
            HubStartEnd01(b,1) = 0;
```

```
        else HubStartEnd01(b,1) = hubtime1-0.1;
        end
        HubStartEnd01(b,2) = hubtime1;
    end
    for o = 1:length(Bursts);
        hist1(o,:) = histc(Bursts(o).PattSort(:,2),[0:20]);
    end
    [Hubfin Hubnum] = mode(zero2nan(reshape(Hubn01,[],1)));
    Hubprob = Hubnum/length(Bursts);
end
end
```

The below function looks at the probability distributions for 'hub' regions and performs a z-test to determine the significance levels of those probabilities.

```
function [] = hubprob(pref)
for pr = 1:size(pref,1);
    load Bursts, Peak_Info and Hubn01 data
    ble(pr) = length(Bursts);
    rle(pr) = length(Peak_Info);
    for r = 1:rle(pr);
        reg_n(r) = length(find(Hubn01==r));
    end
    reg_n(reg_n==0) = nan;
    reg_P = reg_n./ble(pr); % prob each region is a hub
    hubr_P(pr) = max(reg_P);
end
hubr_Zb = (hubr_P-(1/rle'))./(std(hubr_P)./sqrt(ble));
hubr_Zr = (hubr_P-(1/rle'))./(std(hubr_P)./sqrt(rle));
hubr_Zstd = (hubr_P-(1/rle'))./std(hubr_P);
figure, bar([-1:0.5:6],histc(hubr_Zstd,[-
1:0.5:6]),'BarWidth',1,'FaceColor',[0 0 0]); axis tight;
end
```

The below function calculates avalanche size and lifetime distributions.

```
function [] = AVAL_SL_half(pref)
% pref = m*6 cell array containing file location information
for pr = 1:size(pref,1);
load Peak_Info data

% Avalanche Size
Bins1 = zeros(1200,1);
for r = 1:(length(Peak_Info));
    c = 1;
    for dt = 0.5:0.5:600;
        tempbin1 = find(dt-1<=Peak_Info(r).TimeOnset & Peak_Info...
            (r).TimeOnset<dt);
        Bins1(c,1) = Bins1(c,1) + length(tempbin1);
        c = c+1;
    end
end
Bins1(1) = 0;
c = 1;
for dt = 2:1199;
    if Bins1(dt,1)~=0;
```

```
        Av1_StartEnd(c,1) = (find(Bins1(1:dt,1)==0,1,'last'));
        Av1_StartEnd(c,2) = dt-1 + (find(Bins1(dt:end,1)==0,1,'first'));
        c = c+1;
    end
end
Av1_StartEndU = unique(Av1_StartEnd,'rows');
for a = 1:size(Av1_StartEndU,1);
 eval(['Z' pref{pr,6} pref{pr,1}...
  'A.Av1_Size(a) = sum(Bins1(Av1_StartEndU(a,1):Av1_StartEndU(a,2),1));']);
end
eval(['Z' pref{pr,6} pref{pr,1} 'A.Av1_distr20 = histc(Z' ...
    pref{pr,6} pref{pr,1} 'A.Av1_Size,[0:5:100]);']);
eval(['Z' pref{pr,6} pref{pr,1} 'A.Av1_distr100 = histc(Z' ...
    pref{pr,6} pref{pr,1} 'A.Av1_Size,[0:100]);']);
eval(['Z' pref{pr,6} pref{pr,1} 'A.Av1_distr20_prob = Z' ...
    pref{pr,6} pref{pr,1} 'A.Av1_distr20./max(Z'...
    pref{pr,6} pref{pr,1} 'A.Av1_distr20);']);
eval(['Z' pref{pr,6} pref{pr,1} 'A.Av1_distr100_prob = Z' ...
    pref{pr,6} pref{pr,1} 'A.Av1_distr100./max(Z'...
    pref{pr,6} pref{pr,1} 'A.Av1_distr100);']);

% Avalanche Lifetime
for k = 1:size(Av1_StartEndU,1);
    eval(['Z' pref{pr,6} pref{pr,1} ...
        'A.Av1_life(k) = (Av1_StartEndU(k,2) - Av1_StartEndU(k,1))./2;']);
end
eval(['Z' pref{pr,6} pref{pr,1} 'A.maxAv1l = max(Z' ...
    pref{pr,6} pref{pr,1} 'A.Av1_life);']);
eval(['Z' pref{pr,6} pref{pr,1} 'A.Av1_life_distr = hist(Z'...
    pref{pr,6} pref{pr,1} 'A.Av1_life,(Z' pref{pr,6}...
    (5:9) pref{pr,1} 'A.maxAv1l)*2);']);
eval(['Z' pref{pr,6} pref{pr,1} 'A.Av1_life_distr_prob = Z'...
    pref{pr,6} pref{pr,1} 'A.Av1_life_distr./max(Z'...
    pref{pr,6} pref{pr,1} 'A.Av1_life_distr);']);
end
for k = 1:size(pref,1);
    Ns1(k) = str2num(pref{k,4});
end
Ns = unique(Ns1); N = length(Ns); clear Ns
n = size(pref,1);

% Finish avalanches overall
Av1_Size_all = [];
for pr = 1:size(pref,1);
    eval(['Av1_Size_all = cat(2,Av1_Size_all,Z' pref{pr,6} ...
        pref{pr,1} 'A.Av1_Size);']);
end
eval(['Z' pref{pr,6} 'Av1_distr20_all = hist(Av1_Size_all,20);']);
eval(['Z' pref{pr,6} 'Av1_distr100_all=hist(Av1_Size_all,100);']);

% Finish lifetimes overall
Av1_life_all = [];
for pr = 1:size(pref,1);
    eval(['Av1_life_all = cat(2,Av1_life_all,Z' pref{pr,6}...
        pref{pr,1} 'A.Av1_life);']);
end
eval(['Z'  pref{pr,6} 'Av1_life_distr_all= hist(Av1_life_all,Z'...
    pref{pr,6} pref{pr,1} 'A.maxAv1l);']);
end
```

APPENDIX 4 – DOWNLOADED SCRIPTS

Downloaded functions (all downloaded from MATLAB Central file exchange) used during this project have been listed below (and referenced in the scripts reproduced above when used:

- 'tiffread' written by Francois Nedelec, EMBL, 1999-2008.
- 'jbfill' written by John A. Bockstege, November 2006.
- 'rasterplot' written by Rajiv Narayan, Boston University, November 2006.
- 'logfit' written by Jonathan Lansey, posted November 2010.
- 'maximize' written by Yuval Cohen, Be4 Ltd.

REFERENCES

AGMON, A. & WELLS, J. E. 2003. The Role of the Hyperpolarization-Activated Cationic CurrentI h in the Timing of Interictal Bursts in the Neonatal Hippocampus. *The Journal of Neuroscience,* 23**,** 3658-3668.

AGUADO, F., ESPINOSA-PARRILLA, J. F., CARMONA, M. A. A. & SORIANO, E. 2002. Neuronal Activity Regulates Correlated Network Properties of Spontaneous Calcium Transients in Astrocytes In Situ. *The Journal of Neuroscience,* 22**,** 9430-9444.

ALGER, B. E. & NICOLL, R. A. 1979. GABA-mediated biphasic inhibitory responses in hippocampus. *Nature,* 281**,** 315-317.

ALSINA, B., VU, T. & COHEN-CORY, S. 2001. Visualizing synapse formation in arborizing optic axons in vivo: dynamics and modulation by BDNF. *Nat Neurosci,* 4**,** 1093-1101.

ANAVA, S., GREENBAUM, A., JACOB, E. B., HANEIN, Y. & AYALI, A. 2009. The Regulative Role of Neurite Mechanical Tension in Network Development. *Biophysical Journal,* 96**,** 1661-1670.

ANDERSON, T. R., SHAH, P. A. & BENSON, D. L. 2004. Maturation of glutamatergic and GABAergic synapse composition in hippocampal neurons. *Neuropharmacology,* 47**,** 694-705.

ANDRÁSFALVY, B. K. & MAGEE, J. C. 2001. Distance-Dependent Increase in AMPA Receptor Number in the Dendrites of Adult Hippocampal CA1 Pyramidal Neurons. *The Journal of Neuroscience,* 21**,** 9151-9159.

ANTONUCCI, F., CERRI, C., VETENCOURT, J. F. M. & CALEO, M. 2010. Acute neuroprotection by the synaptic blocker botulinum neurotoxin E in a rat model of focal cerebral ischaemia. *Neuroscience,* 169**,** 395-401.

ARNOLD, F. J. L., HOFMANN, F., BENGTSON, C. P., WITTMANN, M., VANHOUTTE, P. & BADING, H. 2005. Microelectrode array recordings of cultured hippocampal

networks reveal a simple model for transcription and protein synthesis-dependent plasticity. *The Journal of Physiology,* 564**,** 3-19.

ARTAVANIS-TSAKONAS, S., RAND, M. D. & LAKE, R. J. 1999. Notch Signaling: Cell Fate Control and Signal Integration in Development. *Science,* 284**,** 770-776.

AUGUSTINE, G. J., SANTAMARIA, F. & TANAKA, K. 2003. Local Calcium Signaling in Neurons. 40**,** 331-346.

AYALI, A., SHEFI, O. & BEN-JACOB, E. Self Organization of Two-dimensional Insect Neural Networks. Experimental Chaos: 6th Experimental Chaos Conference, 2002 Potsdam (Germany). AIP, 465-475.

BACCI, A., VERDERIO, C., PRAVETTONI, E. & MATTEOLI, M. 1999. Synaptic and intrinsic mechanisms shape synchronous oscillations in hippocampal neurons in culture. *European Journal of Neuroscience,* 11**,** 389-397.

BAHINSKI, A., YATANI, A., MIKALA, G., TANG, S., YAMAMOTO, S. & SCHWARTZ, A. 1997. Charged amino acids near the pore entrance influence ion-conduction of a human L-type cardiac calcium channel. *Molecular and Cellular Biochemistry,* 166**,** 125-134.

BAIMBRIDGE, K. G., CELIO, M. R. & ROGERS, J. H. 1992. Calcium-binding proteins in the nervous system. *Trends in Neurosciences,* 15**,** 303-308.

BAIN, G., KITCHENS, D., YAO, M., HUETTNER, J. E. & GOTTLIEB, D. I. 1995. Embryonic Stem Cells Express Neuronal Properties in Vitro. *Developmental Biology,* 168**,** 342-357.

BAIN, G., RAY, W. J., YAO, M. & GOTTLIEB, D. I. 1996. Retinoic Acid Promotes Neural and Represses Mesodermal Gene Expression in Mouse Embryonic Stem Cells in Culture. *Biochemical and Biophysical Research Communications,* 223**,** 691-694.

BAKEINE, G. J., BAN, J., GRENCI, G., POZZATO, A., ZILIO, S. D., PRASCIOLU, M., BUSINARO, L., TORMEN, M. & RUARO, M. E. 2000. Design, fabrication and evaluation of nanoscale surface topography as a tool in directing differentiation and organisation of embryonic stem-cell-derived neural precursors. *Microelectronic Engineering,* 86**,** 1435-1438.

BAKER, S. N., KILNER, J. M., PINCHES, E. M. & LEMON, R. N. 1999. The role of synchrony and oscillations in the motor output. *Experimental Brain Research,* 128**,** 109-117.

BÁLDI, R., VARGA, C. & TAMÁS, G. 2010. Differential distribution of KCC2 along the axo-somato-dendritic axis of hippocampal principal cells. *European Journal of Neuroscience,* 32**,** 1319-1325.

BAN, J., BONIFAZI, P., PINATO, G., BROCCARD, F. D., STUDER, L., TORRE, V. & RUARO, M. E. 2007. Embryonic Stem Cell-Derived Neurons Form Functional Networks In Vitro. *Stem Cells,* 25**,** 738-749.

BANI-YAGHOUB, M., TREMBLAY, R., VOICU, R., MEALING, G., MONETTE, R., PY, C., FAID, K. & SIKORSKA, M. 2005. Neurogenesis and neuronal communication on micropatterned neurochips. *Biotechnology & Bioengineering,* 92**,** 336-345.

BANKER, G. A. & COWAN, W. M. 1977. Rat hippocampal neurons in dispersed cell culture. *Brain Research,* 126**,** 397-425.

BANSAL, A., SINGER, J. H., HWANG, B. J., XU, W., BEAUDET, A. & FELLER, M. B. 2000. Mice Lacking Specific Nicotinic Acetylcholine Receptor Subunits Exhibit Dramatically Altered Spontaneous Activity Patterns and Reveal a Limited Role for Retinal Waves in Forming ON and OFF Circuits in the Inner Retina. *The Journal of Neuroscience,* 20**,** 7672-7681.

BARBIN, G., POLLARD, H., GAÏARSA, J. L. & BEN-ARI, Y. 1993. Involvement of GABAA receptors in the outgrowth of cultured hippocampal neurons. *Neuroscience Letters,* 152**,** 150-154.

BARBOUR, B., BREW, H. & ATTWELL, D. 1991. Electrogenic uptake of glutamate and aspartate into glial cells isolated from the salamander (Ambystoma) retina. *The Journal of Physiology,* 436**,** 169-193.

BARTLETT, P. F., REID, H. H., BAILEY, K. A. & BERNARD, O. 1988. Immortalization of mouse neural precursor cells by the c-myc oncogene. *Proceedings of the National Academy of Sciences,* 85**,** 3255-3259.

BARUCHI, I., VOLMAN, V., RAICHMAN, N., SHEIN, M. & BEN-JACOB, E. 2008. The emergence and properties of mutual synchronization in in vitro coupled cortical networks. *European Journal of Neuroscience,* 28**,** 1825-1835.

BAZHENOV, M., TIMOFEEV, I., STERIADE, M. & SEJNOWSKI, T. J. 1999. Self-sustained rhythmic activity in the thalamic reticular nucleus mediated by depolarizing GABAA receptor potentials. *Nat Neurosci,* 2**,** 168-74.

BEGGS, J. M. & PLENZ, D. 2003. Neuronal Avalanches in Neocortical Circuits. *The Journal of Neuroscience,* 23**,** 11167-11177.

BEGGS, J. M. & PLENZ, D. 2004. Neuronal Avalanches Are Diverse and Precise Activity Patterns That Are Stable for Many Hours in Cortical Slice Cultures. *The Journal of Neuroscience,* 24**,** 5216-5229.

BEHAR, T., LI, Y., TRAN, H., MA, W., DUNLAP, V., SCOTT, C. & BARKER, J. 1996. GABA stimulates chemotaxis and chemokinesis of embryonic cortical neurons via calcium-dependent mechanisms. *The Journal of Neuroscience,* 16**,** 1808-1818.

BEHAR, T. N., SCHAFFNER, A. E., SCOTT, C. A., O'CONNELL, C. & BARKER, J. L. 1998. Differential Response of Cortical Plate and Ventricular Zone Cells to GABA as a Migration Stimulus. *The Journal of Neuroscience,* 18**,** 6378-6387.

BEHREND, M. R., AHUJA, A. K., HUMAYUN, M. S., WEILAND, J. D. & CHOW, R. H. 2009. Selective labeling of retinal ganglion cells with calcium indicators by retrograde loading in vitro. *Journal of Neuroscience Methods,* 179**,** 166-172.

BEN-ARI, Y., CHERUBINI, E., CORRADETTI, R. & GAIARSA, J. L. 1989. Giant synaptic potentials in immature rat CA3 hippocampal neurones. *The Journal of Physiology,* 416**,** 303-325.

BENDER, R. A. & BARAM, T. Z. 2008. Hyperpolarization activated cyclic-nucleotide gated (HCN) channels in developing neuronal networks. *Progress in Neurobiology,* 86**,** 129-140.

BENDER, R. A., GALINDO, R., MAMELI, M., GONZALEZ-VEGA, R., VALENZUELA, C. F. & BARAM, T. Z. 2005. Synchronized network activity in developing rat hippocampus involves

regional hyperpolarization-activated cyclic nucleotide-gated (HCN) channel function. *European Journal of Neuroscience,* 22**,** 2669-2674.

BERGLÖF, E., BJERKÉN, S. A. & STRÖMBERG, I. 2007. Glial influence on nerve fiber formation from rat ventral mesencephalic organotypic tissue cultures. *The Journal of Comparative Neurology,* 501**,** 431-442.

BEURG, M., FETTIPLACE, R., NAM, J.-H. & RICCI, A. J. 2009. Localization of inner hair cell mechanotransducer channels using high-speed calcium imaging. *Nat Neurosci,* 12**,** 553-558.

BHATT, H., BRUNET, L. J. & STEWART, C. L. 1991. Uterine expression of leukemia inhibitory factor coincides with the onset of blastocyst implantation. *Proceedings of the National Academy of Sciences,* 88**,** 11408-11412.

BIEBERICH, E. & GUISEPPI-ELIE, A. 2004. Neuronal differentiation and synapse formation of PC12 and embryonic stem cells on interdigitated microelectrode arrays:: Contact structures for neuron-to-electrode signal transmission (NEST). *Biosensors and Bioelectronics,* 19**,** 923-931.

BOLEA, S., AVIGNONE, E., BERRETTA, N., SANCHEZ-ANDRES, J. V. & CHERUBINI, E. 1999. Glutamate Controls the Induction of GABA-Mediated Giant Depolarizing Potentials Through AMPA Receptors in Neonatal Rat Hippocampal Slices. *Journal of Neurophysiology,* 81**,** 2095-2102.

BOLEA, S., SANCHEZ-ANDRES, J. V., HUANG, X. & WU, J.-Y. 2006. Initiation and Propagation of Neuronal Coactivation in the Developing Hippocampus. *Journal of Neurophysiology,* 95**,** 552-561.

BONGSO, A. & RICHARDS, M. 2004. History and perspective of stem cell research. *Best Practice & Research Clinical Obstetrics & Gynaecology,* 18**,** 827-842.

BONIFAZI, P., GOLDIN, M., PICARDO, M. A., JORQUERA, I., CATTANI, A., BIANCONI, G., REPRESA, A., BEN-ARI, Y. & COSSART, R. 2009. GABAergic Hub Neurons Orchestrate Synchrony in Developing Hippocampal Networks. *Science,* 326**,** 1419-1424.

BONNEFONT, X., FIEKERS, J., CREFF, A. & MOLLARD, P. 2000. Rhythmic Bursts of Calcium Transients in Acute Anterior Pituitary Slices. *Endocrinology,* 141**,** 868-875.

BORMANN, J. & KETTENMANN, H. 1988. Patch-clamp study of gamma-aminobutyric acid receptor Cl- channels in cultured astrocytes. *Proceedings of the National Academy of Sciences,* 85**,** 9336-9340.

BORODINSKY, L. N., O'LEARY, D., NEALE, J. H., VICINI, S., COSO, O. A. & FISZMAN, M. L. 2003. GABA-induced neurite outgrowth of cerebellar granule cells is mediated by GABA(A) receptor activation, calcium influx and CaMKII and erk1/2 pathways. *J Neurochem,* 84**,** 1411-20.

BORTONE, D. & POLLEUX, F. 2009. KCC2 Expression Promotes the Termination of Cortical Interneuron Migration in a Voltage-Sensitive Calcium-Dependent Manner. *Neuron,* 62**,** 53-71.

BRANCO, T. & HÄUSSER, M. 2010. The single dendritic branch as a fundamental functional unit in the nervous system. *Current Opinion in Neurobiology,* 20**,** 494-502.

BRAY, J. G. & MYNLIEFF, M. 2009. Influx of calcium through L-type calcium channels in early postnatal regulation of chloride transporters in the rat hippocampus. *Developmental Neurobiology,* 69**,** 885-896.

BREWER, G. J., BOEHLER, M. D., IDE, A. N. & WHEELER, B. C. 2009. Chronic electrical stimulation of cultured hippocampal networks increases spontaneous spike rates. *Journal of Neuroscience Methods,* 184**,** 104-109.

BRICKLEY, S. G., CULL-CANDY, S. G. & FARRANT, M. 1996. Development of a tonic form of synaptic inhibition in rat cerebellar granule cells resulting from persistent activation of GABAA receptors. *The Journal of Physiology,* 497**,** 753-759.

BRITLAND, S., PERRIDGE, C., DENYER, M., MORGAN, H., CURTIS, A. & WILKINSON, C. 1997. Morphogenetic guidance cues can interact synergistically and hierarchically in steering nerve cell growth. *Experimental Biology Online,* 1**,** 1-15.

BRUNET, I., DI NARDO, A. A., SONNIER, L., BEURDELEY, M. & PROCHIANTZ, A. 2007. The topological role of homeoproteins in the developing central nervous system. *Trends in Neurosciences,* 30**,** 260-267.

BULL, N. D. & BARTLETT, P. F. 2005. The Adult Mouse Hippocampal Progenitor Is Neurogenic But Not a Stem Cell. *The Journal of Neuroscience,* 25**,** 10815-10821.

BURDON, T., SMITH, A. & SAVATIER, P. 2002. Signalling, cell cycle and pluripotency in embryonic stem cells. *Trends in Cell Biology,* 12**,** 432-438.

CAREY, M. B. & MATSUMOTO, S. G. 1999. Spontaneous Calcium Transients Are Required for Neuronal Differentiation of Murine Neural Crest. *Developmental Biology,* 215**,** 298-313.

CATHALA, L., BRICKLEY, S., CULL-CANDY, S. & FARRANT, M. 2003. Maturation of EPSCs and Intrinsic Membrane Properties Enhances Precision at a Cerebellar Synapse. *The Journal of Neuroscience,* 23**,** 6074-6085.

CATSICAS, M., BONNESS, V., BECKER, D. & MOBBS, P. 1998. Spontaneous Ca2+ transients and their transmission in the developing chick retina. *Current Biology,* 8**,** 283-288.

CAVAZZINI, M., BLISS, T. & EMPTAGE, N. Ca2+ and synaptic plasticity. *Cell Calcium,* 38**,** 355-367.

CELLOT, G., CILIA, E., CIPOLLONE, S., RANCIC, V., SUCAPANE, A., GIORDANI, S., GAMBAZZI, L., MARKRAM, H., GRANDOLFO, M., SCAINI, D., GELAIN, F., CASALIS, L., PRATO, M., GIUGLIANO, M. & BALLERINI, L. 2009. Carbon nanotubes might improve neuronal performance by favouring electrical shortcuts. *Nat Nano,* 4**,** 126-133.

CHADA, S., LAMOUREUX, P., BUXBAUM, R. E. & HEIDEMANN, S. R. 1997. Cytomechanics of neurite outgrowth from chick brain neurons. *Journal of Cell Science,* 110**,** 1179-1186.

CHAO, T.-I., XIANG, S., CHEN, C.-S., CHIN, W.-C., NELSON, A. J., WANG, C. & LU, J. 2009. Carbon nanotubes promote neuron differentiation from human embryonic stem cells. *Biochemical and Biophysical Research Communications,* 384**,** 426-430.

CHARLES, A. C., KODALI, S. K. & TYNDALE, R. F. 1996. Intercellular Calcium Waves in Neurons. *Molecular and Cellular Neuroscience,* 7**,** 337-353.

CHEN, C. & SCHOFIELD, G. G. 1993. Differential neuromodulation of calcium currents by norepinephrine in rat sympathetic neurons. *Journal of Neurophysiology,* 70**,** 1440-1450.

CHEN, G., TROMBLEY, P. Q. & VAN DEN POL, A. N. 1996. Excitatory actions of GABA in developing rat hypothalamic neurones. *The Journal of Physiology,* 494**,** 451-464.

CHEN, L., CHATTERJEE, M. & LI, J. Y. H. 2010. The Mouse Homeobox Gene Gbx2 Is Required for the Development of Cholinergic Interneurons in the Striatum. *The Journal of Neuroscience,* 30**,** 14824-14834.

CHEUNG, K. 2007. Implantable microscale neural interfaces. *Biomedical Microdevices,* 9**,** 923-938.

CHIANG, E. & STROWBRIDGE, B. W. 2007. Diversity of Neural Signals Mediated by Multiple, Burst-Firing Mechanisms in Rat Olfactory Tubercle Neurons. *Journal of Neurophysiology,* 98**,** 2716-2728.

CHIAPPALONE, M., BOVE, M., VATO, A., TEDESCO, M. & MARTINOIA, S. 2006. Dissociated cortical networks show spontaneously correlated activity patterns during in vitro development. *Brain Research,* 1093**,** 41-53.

CHIQUET, M. 1999. Regulation of extracellular matrix gene expression by mechanical stress. *Matrix Biology,* 18**,** 417-426.

COHEN, A., SHAPPIR, J., YITZCHAIK, S. & SPIRA, M. E. 2006. Experimental and theoretical analysis of neuron-transistor hybrid electrical coupling: The relationships between the electro-anatomy of cultured Aplysia neurons and the recorded field potentials. *Biosensors and Bioelectronics,* 22**,** 656-663.

CONBOY, I. M. & RANDO, T. A. 2002. The Regulation of Notch Signaling Controls Satellite Cell Activation and Cell Fate Determination in Postnatal Myogenesis. *Developmental cell,* 3**,** 397-409.

CONNORS, B. W. & GUTNICK, M. J. 1990. Intrinsic firing patterns of diverse neocortical neurons. *Trends in Neurosciences,* 13**,** 99-104.

CONTRERAS, D. 2004. Electrophysiological classes of neocortical neurons. *Neural Networks,* 17**,** 633-646.

COSSART, R., IKEGAYA, Y. & YUSTE, R. 2005. Calcium imaging of cortical networks dynamics. *Cell Calcium,* 37**,** 451-457.

CUNNINGHAM, M. O., PERVOUCHINE, D. D., RACCA, C., KOPELL, N. J., DAVIES, C. H., JONES, R. S. G., TRAUB, R. D. & WHITTINGTON, M. A. 2006. Neuronal metabolism governs cortical network response state. *Proceedings of the National Academy of Sciences,* 103**,** 5597-5601.

CURTIS, A. S. G. & WILKINSON, C. D. W. 1998. Reactions of cells to topography. *Journal of Biomaterials Science. Polymer Edition,* 9**,** 1313-1329.

DALBY, M. J., RIEHLE, M. O., JOHNSTONE, H., AFFROSSMAN, S. & CURTIS, A. S. G. 2002. In vitro reaction of endothelial cells to polymer demixed nanotopography. *Biomaterials,* 23**,** 2945-2954.

DAMMERMAN, R. S., FLINT, A. C., NOCTOR, S. & KRIEGSTEIN, A. R. 2000. An Excitatory GABAergic Plexus in Developing Neocortical Layer 1. *Journal of Neurophysiology,* 84**,** 428-434.

DANI, J. W., CHERNJAVSKY, A. & SMITH, S. J. 1992. Neuronal activity triggers calcium waves in hippocampal astrocyte networks. 8**,** 429-440.

DE BARTOLO, L., RENDE, M., MORELLI, S., GIUSI, G., SALERNO, S., PISCIONERI, A., GORDANO, A., DI VITO, A., CANONACO, M. & DRIOLI, E. 2008. Influence of membrane surface properties on the growth of neuronal cells isolated from hippocampus. *Journal of Membrane Science,* 325**,** 139-149.

DE CRESCENZO, V., ZHUGE, R., VELÁZQUEZ-MARRERO, C., LIFSHITZ, L. M., CUSTER, E., CARMICHAEL, J., LAI, F. A., TUFT, R. A., FOGARTY, K. E., LEMOS, J. R. & WALSH, J. V. 2004. Ca2+ Syntillas, Miniature Ca2+ Release Events in Terminals of Hypothalamic

Neurons, Are Increased in Frequency by Depolarization in the Absence of Ca2+ Influx. *The Journal of Neuroscience,* 24**,** 1226-1235.

DELPIRE, E. 2000. Cation-Chloride Cotransporters in Neuronal Communication. *News Physiol Sci,* 15**,** 309-312.

DENCKER, L., ANNERWALL, E., BUSCH, C. & ERIKSSON, U. 1990. Localization of specific retinoid-binding sites and expression of cellular retinoic-acid-binding protein (CRABP) in the early mouse embryo. *Development,* 110**,** 343-352.

DENT, M. A., RAISMAN, G. & LAI, F. A. 1996. Expression of type 1 inositol 1,4,5-trisphosphate receptor during axogenesis and synaptic contact in the central and peripheral nervous system of developing rat. *Development,* 122**,** 1029-1039.

DERTINGER, S. K. W., CHIU, D. T., JEON, N. L. & WHITESIDES, G. M. 2001. Generation of Gradients Having Complex Shapes Using Microfluidic Networks. *Analytical Chemistry,* 73**,** 1240-1246.

DESARMENIEN, M. G. & SPITZER, N. C. 1991. Role of calcium and protein kinase C in development of the delayed rectifier potassium current in xenopus spinal neurons. *Neuron,* 7**,** 797-805.

DISTASI, C., ARIANO, P., ZAMBURLIN, P. & FERRARO, M. 2002. In vitro analysis of neuron-glial cell interactions during cellular migration. *European Biophysics Journal,* 31**,** 81-88.

DOETSCH, F., CAILLÉ, I., LIM, D. A., GARCÍA-VERDUGO, J. M. & ALVAREZ-BUYLLA, A. 1999. Subventricular Zone Astrocytes Are Neural Stem Cells in the Adult Mammalian Brain. *Cell,* 97**,** 703-716.

DOTTI, C., SULLIVAN, C. & BANKER, G. 1988. The establishment of polarity by hippocampal neurons in culture. *The Journal of Neuroscience,* 8**,** 1454-1468.

DRAVID, S. M. & MURRAY, T. F. 2004. Spontaneous synchronized calcium oscillations in neocortical neurons in the presence of physiological [Mg2+]: involvement of AMPA/kainate and metabotropic glutamate receptors. *Brain Research,* 1006**,** 8-17.

DUCHEN, M. R. 1990. Effects of metabolic inhibition on the membrane properties of isolated mouse primary sensory neurones. *The Journal of Physiology,* 424**,** 387-409.

DUMOLLARD, R., MCDOUGALL, A., ROUVIÈRE, C. & SARDET, C. 2004. Fertilisation calcium signals in the ascidian egg. *Biology of the Cell,* 96**,** 29-36.

ECHEVARRIA, W., LEITE, M. F., GUERRA, M. T., ZIPFEL, W. R. & NATHANSON, M. H. 2003. Regulation of calcium signals in the nucleus by a nucleoplasmic reticulum. *Nat Cell Biol,* 5**,** 440-446.

ELIAS, L. A. B., WANG, D. D. & KRIEGSTEIN, A. R. 2007. Gap junction adhesion is necessary for radial migration in the neocortex. *Nature,* 448**,** 901-907.

FAN, Y., SHI, F., SMITH, J. K., LIN, W., GILMORE, J. H. & SHEN, D. 2011. Brain anatomical networks in early human brain development. *NeuroImage,* 54**,** 1862-1871.

FANELLI, A., TITAPICCOLO, J. I., ESPOSTI, F., RIPAMONTI, M., MALGAROLI, A. & SIGNORINI, M. G. 2011. Novel image processing methods for the analysis of calcium dynamics in glial cells. *IEEE Trans Biomed Eng,* 58**,** 2640-7.

FELDT, S., BONIFAZI, P. & COSSART, R. 2011. Dissecting functional connectivity of neuronal microcircuits: experimental and theoretical insights. *Trends in Neurosciences,* 34**,** 225-236.

FELLER, M. B. 1999. Spontaneous correlated activity in developing neural circuits. *Neuron,* 22**,** 653-6.

FÉNELON, V. S., KILMAN, V., MEYRAND, P. & MARDER, E. 1999. Sequential developmental acquisition of neuromodulatory inputs to a central pattern-generating network. *The Journal of Comparative Neurology,* 408**,** 335-351.

FINLEY, M. F., KULKARNI, N. & HUETTNER, J. E. 1996. Synapse formation and establishment of neuronal polarity by P19 embryonic carcinoma cells and embryonic stem cells. *The Journal of Neuroscience,* 16**,** 1056-1065.

FISCHER, K. F., LUKASIEWICZ, P. D. & WONG, R. O. L. 1998. Age-Dependent and Cell Class-Specific Modulation of Retinal Ganglion Cell Bursting Activity by GABA. *The Journal of Neuroscience,* 18**,** 3767-3778.

FISZMAN, M. L., BORODINSKY, L. N. & NEALE, J. H. 1999. GABA induces proliferation of immature cerebellar granule cells grown in vitro. *Developmental Brain Research,* 115**,** 1-8.

FRAICHARD, A., CHASSANDE, O., BILBAUT, G., DEHAY, C., SAVATIER, P. & SAMARUT, J. 1995. In vitro differentiation of embryonic stem cells into glial cells and functional neurons. *Journal of Cell Science,* 108**,** 3181-3188.

FRANZE, K., GERDELMANN, J., WEICK, M., BETZ, T., PAWLIZAK, S., LAKADAMYALI, M., BAYER, J., RILLICH, K., GÖGLER, M., LU, Y.-B., REICHENBACH, A., JANMEY, P. & KÄS, J. 2009. Neurite Branch Retraction Is Caused by a Threshold-Dependent Mechanical Impact. *Biophysical Journal,* 97**,** 1883-1890.

FREEDMAN, D., PISANI, R. & PURVES, R. (eds.) 1998. *Statistics,* New York: Norton.

FUENTEALBA, P. & STERIADE, M. 2005. Thalamic oscillations modulate membrane properties of cat thalamic reticular neurons. *Thalamus & Related Systems,* 3**,** 53-62.

FUKUDA, T., KOSAKA, T., SINGER, W. & GALUSKE, R. A. W. 2006. Gap Junctions among Dendrites of Cortical GABAergic Neurons Establish a Dense and Widespread Intercolumnar Network. *The Journal of Neuroscience,* 26**,** 3434-3443.

GABAY, T., BEN-DAVID, M., KALIFA, I., ABRAMS, Z. R., SORKIN, R., BEN-JACOB, E. & HANEIN, Y. 2007a. Carbon Nanotube Micro-electrode array. *Transducers and Neurosensors - The 14th International Conference on Solid-State Sensors, Actuators and Microsystems, Lyon, France, June 10-14, 2007*.

GABAY, T., BEN-DAVID, M., KALIFA, I., SORKIN, R., ABRAMS, Z. E. R., BEN-JACOB, E. & HANEIN, Y. 2007b. Electro-chemical and biological properties of carbon nanotube based multi-electrode arrays. *Nanotechnology,* 18.

GABAY, T., JAKOBS, E., BEN-JACOB, E. & HANEIN, Y. 2005a. Engineered self-organization of neural networks using carbon nanotube clusters. *Physica A: Statistical Mechanics and its Applications,* 350**,** 611-621.

GABAY, T., KALIFA, I., EZRA, L., JAKOBS, E., BEN-JACOB, E. & HANEIN, Y. 2005b. Carbon Nanotube Based Neuro-Chip for Engineering, Recording and Stimulation of Cultured Networks. ***Solid-State Sensors, Actuators and Microsystems****,* 2**,** 1226- 1229.

GABI, M., LARMAGNAC, A., SCHULTE, P. & VÖRÖS, J. 2010. Electrically controlling cell adhesion, growth and migration. *Colloids and Surfaces B: Biointerfaces,* 79**,** 365-371.

GAIANO, N. & FISHELL, G. 2002. THE ROLE OF NOTCH IN PROMOTING GLIAL AND NEURAL STEM CELL FATES. *Annual Review of Neuroscience,* 25**,** 471-490.

GAILLARD, C., CELLOT, G., LI, S., TOMA, F. M., DUMORTIER, H., SPALLUTO, G., CACCIARI, B., PRATO, M., BALLERINI, L. & BIANCO, A. 2009. Carbon Nanotubes Carrying Cell-Adhesion Peptides do not Interfere with Neuronal Functionality. *Advanced Materials,* 21**,** 2903-2908.

GANGULY, K., SCHINDER, A. F., WONG, S. T. & POO, M.-M. 2001. GABA Itself Promotes the Developmental Switch of Neuronal GABAergic Responses from Excitation to Inhibition. *Cell,* 105**,** 521-532.

GARASCHUK, O., HANSE, E. & KONNERTH, A. 1998. Developmental profile and synaptic origin of early network oscillations in the CA1 region of rat neonatal hippocampus. *The Journal of Physiology,* 507**,** 219-236.

GARASCHUK, O., LINN, J., EILERS, J. & KONNERTH, A. 2000. Large-scale oscillatory calcium waves in the immature cortex. *Nat Neurosci,* 3**,** 452-9.

GEIGER, B., BERSHADSKY, A., PANKOV, R. & YAMADA, K. M. 2001. Transmembrane crosstalk between the extracellular matrix and the cytoskeleton. *Nat Rev Mol Cell Biol,* 2**,** 793-805.

GELLER, H. M., GELLER, N. L., KRESPAN, B. & COOPERSTEIN, R. 1985. Statistical analysis of temperature-dependent neuronal activity. *Journal of Neuroscience Methods,* 14**,** 127-136.

GERECHT, S., BETTINGER, C. J., ZHANG, Z., BORENSTEIN, J. T., VUNJAK-NOVAKOVIC, G. & LANGER, R. 2007. The effect of actin disrupting agents on contact guidance of human embryonic stem cells. *Biomaterials,* 28**,** 4068-4077.

GIUGLIANO, M., PRATO, M. & BALLERINI, L. 2008. Nanomaterial/neuronal hybrid system for functional recovery of the CNS. *Drug Discovery Today: Disease Models,* 5**,** 37-43.

GRACE, A. & BUNNEY, B. 1984. The control of firing pattern in nigral dopamine neurons: burst firing. *The Journal of Neuroscience,* 4**,** 2877-2890.

GREENE, L. A. & TISCHLER, A. S. 1976. Establishment of a noradrenergic clonal line of rat adrenal pheochromocytoma cells which respond to nerve growth factor. *Proceedings of the National Academy of Sciences,* 73**,** 2424-2428.

GRISCOM, L., DEGENAAR, P., LEPIOUFLE, B., TAMIYA, E. & FUJITA, H. 2002. Techniques for patterning and guidance of primary culture neurons on micro-electrode arrays. *Sensors and Actuators B: Chemical,* 83**,** 15-21.

GROSS, P. G., KARTALOV, E. P., SCHERER, A. & WEINER, L. P. 2007. Applications of microfluidics for neuronal studies. *Journal of the Neurological Sciences,* 252**,** 135-143.

GRZYWACZ, N. M. & SERNAGOR, E. 2000. Spontaneous activity in developing turtle retinal ganglion cells: Statistical analysis. *Visual Neuroscience,* 17**,** 229-241.

GU, X., OLSON, E. & SPITZER, N. 1994. Spontaneous neuronal calcium spikes and waves during early differentiation. *J. Neurosci.,* 14**,** 6325-6335.

HALDEMAN, C. & BEGGS, J. M. 2005. Critical Branching Captures Activity in Living Neural Networks and Maximizes the Number of Metastable States. *Physical Review Letters,* 94**,** 058101.

HALLER, M., MIRONOV, S. L., KARSCHIN, A. & RICHTER, D. W. 2001. Dynamic activation of KATP channels in rhythmically active neurons. *The Journal of Physiology,* 537**,** 69-81.

HARDINGHAM, G. E., CRUZALEGUI, F. H., CHAWLA, S. & BADING, H. 1998. Mechanisms controlling gene expression by nuclear calcium signals. *Cell Calcium,* 23**,** 131-134.

HE, B. J., ZEMPEL, J. M., SNYDER, A. Z. & RAICHLE, M. E. 2010a. The Temporal Structures and Functional Significance of Scale-free Brain Activity. *Neuron,* 66**,** 353-369.

HE, M., ZHANG, Z.-H., GUAN, C.-B., XIA, D. & YUAN, X.-B. 2010b. Leading Tip Drives Soma Translocation via Forward F-Actin Flow during Neuronal Migration. *The Journal of Neuroscience,* 30**,** 10885-10898.

HEIKKILÄ, T. J., YLÄ-OUTINEN, L., TANSKANEN, J. M. A., LAPPALAINEN, R. S., SKOTTMAN, H., SUURONEN, R., MIKKONEN, J. E., HYTTINEN, J. A. K. & NARKILAHTI, S. 2009. Human embryonic stem cell-derived neuronal cells form spontaneously active neuronal networks in vitro. *Experimental Neurology,* 218**,** 109-116.

HEINEMANN, U. & GUTNICK, M. J. 1979. Relation between extracellular potassium concentration and neuronal activities in cat thalamus (VPL) during projection of cortical epileptiform discharge. *Electroencephalography and Clinical Neurophysiology,* 47**,** 345-357.

HELLER, D. A., GARGA, V., KELLEHER, K. J., LEE, T.-C., MAHBUBANI, S., SIGWORTH, L. A., LEE, T. R. & REA, M. A. 2005. Patterned networks of mouse hippocampal neurons on peptide-coated gold surfaces. *Biomaterials,* 26**,** 883-889.

HENČEK, M. & ZACHAR, J. 1977. Calcium currents and conductances in the muscle membrane of the crayfish. *The Journal of Physiology,* 268**,** 51-71.

HENNIG, M. H., GRADY, J., VAN COPPENHAGEN, J. & SERNAGOR, E. 2011. Age-dependent homeostatic plasticity of GABAergic signaling in developing retinal networks. *J Neurosci,* 31**,** 12159-64.

HEPLER, P. K. 1989. Calcium transients during mitosis: observations in flux. *J Cell Biol,* 109**,** 2567-73.

HILLE, B., WOODHULL, A. M. & SHAPIRO, B. I. 1975. Negative Surface Charge Near Sodium Channels of Nerve: Divalent Ions, Monovalent Ions, and pH [and Discussion]. *Philosophical Transactions of the Royal Society of London. B, Biological Sciences,* 270**,** 301-318.

HIRASE, H., QIAN, L., BARTHÓ, P. & BUZSÁKI, G. 2004. Calcium Dynamics of Cortical Astrocytic Networks In Vivo. *PLoS Biol,* 2**,** e96.

HOLLIDAY, J., ADAMS, R. J., SEJNOWSKI, T. J. & SPITZER, N. C. 1991. Calcium-induced release of calcium regulates differentiation of cultured spinal neurons. *Neuron,* 7**,** 787-796.

HOOGLAND, T. M., KUHN, B., GOBEL, W., HUANG, W., NAKAI, J., HELMCHEN, F., FLINT, J. & WANG, S. S. 2009. Radially expanding transglial calcium waves in the intact cerebellum. *Proc Natl Acad Sci U S A,* 106**,** 3496-501.

HOSAKA, R., ARAKI, O. & IKEGUCHI, T. 2008. STDP Provides the Substrate for Igniting Synfire Chains by Spatiotemporal Input Patterns. *Neural Computation,* 20**,** 415-435.

HUA, J. Y., SMEAR, M. C., BAIER, H. & SMITH, S. J. 2005. Regulation of axon growth in vivo by activity-based competition. *Letters to Nature,* 434**,** 1022-1026.

HUTCHEON, B. & YAROM, Y. 2000. Resonance, oscillation and the intrinsic frequency preferences of neurons. *Trends in Neurosciences,* 23**,** 216-222.

ICHIKAWA, M., MURAMOTO, K., KOBAYASHI, K., KAWAHARA, M. & KURODA, Y. 1993. Formation and maturation of synapses in primary cultures of rat cerebral cortical cells: an electron microscopic study. *Neuroscience Research,* 16**,** 95-103.

IIJIMA, S. 1991. Helical Microtubules of Graphitic Carbon. *Nature,* 354**,** 56-58.

ILLES, S., FLEISCHER, W., SIEBLER, M., HARTUNG, H.-P. & DIHNÉ, M. 2007. Development and pharmacological modulation of embryonic stem cell-derived neuronal network activity. *Experimental Neurology,* 207**,** 171-176.

ILLES, S., THEISS, S., HARTUNG, H.-P., SIEBLER, M. & DIHNE, M. 2009. Niche-dependent development of functional neuronal networks from embryonic stem cell-derived neural populations. *BMC Neuroscience,* 10**,** 93.

ITO, D., TAMATE, H., NAGAYAMA, M., UCHIDA, T., KUDOH, S. N. & GOHARA, K. 2010. Minimum neuron density for synchronized bursts in a rat cortical culture on multi-electrode arrays. *Neuroscience,* 171**,** 50-61.

IVANNIKOV, M. V., SUGIMORI, M. & LLINÁS, R. R. 2010. Calcium clearance and its energy requirements in cerebellar neurons. *Cell Calcium,* 47**,** 507-513.

JABLONSKA, B., AGUIRRE, A., RAYMOND, M., SZABO, G., KITABATAKE, Y., SAILOR, K. A., MING, G.-L., SONG, H. & GALLO, V. 2010. Chordin-induced lineage plasticity of adult SVZ neuroblasts after demyelination. *Nat Neurosci,* 13**,** 541-550.

JACKSON, M. F., ESPLIN, B. & ČAPEK, R. 1999. Inhibitory Nature of Tiagabine-Augmented GABAAReceptor–Mediated Depolarizing Responses in Hippocampal Pyramidal Cells. *Journal of Neurophysiology,* 81**,** 1192-1198.

JAHR, C. & STEVENS, C. 1990. Voltage dependence of NMDA-activated macroscopic conductances predicted by single-channel kinetics. *The Journal of Neuroscience,* 10**,** 3178-3182.

JAHR, C. E. & STEVENS, C. F. 1987. Glutamate activates multiple single channel conductances in hippocampal neurons. *Nature,* 325**,** 522-525.

JAMES, C. D., DAVIS, R., MEYER, M., TURNER, A., TURNER, S., WITHERS, G., KAM, L., BANKER, G., CRAIGHEAD, H., ISSACSON, M., TURNER, J. & SHAIN, W. 2000. Aligned microcontact printing of micrometer-scale poly-L-Lysine structures for controlled growth of cultured neurons on planar microelectrode arrays. *Biomedical Engineering, IEEE Transactions on,* 47**,** 17-21.

JAMES, C. D., SPENCE, A. J. H., DOWELL-MESFIN, N. M., HUSSAIN, R. J., SMITH, K. L., CRAIGHEAD, H. G., ISAACSON, M. S., SHAIN, W. & TURNER, J. N. 2004. Extracellular

recordings from patterned neuronal networks using planar microelectrode arrays *IEEE Transactions on Biomedical Engineering,* 51**,** 1640-1648.

JAN, E. & KOTOV, N. A. 2007. Successful Differentiation of Mouse Neural Stem Cells on Layer-by-Layer Assembled Single-Walled Carbon Nanotube Composite. *Nano Letters,* 7**,** 1123-1128.

JEDLICKA, P., DELLER, T., GUTKIN, B. S. & BACKUS, K. H. 2010. Activity-dependent intracellular chloride accumulation and diffusion controls GABAA receptor-mediated synaptic transmission. *Hippocampus***,** n/a-n/a.

JIMBO, Y., ROBINSON, H. P. & KAWANA, A. 1998. Strengthening of synchronized activity by tetanic stimulation in cortical cultures: application of planar electrode arrays. *IEEE Trans Biomed Eng,* 45**,** 1297-304.

JONAS, P., RACCA, C., SAKMANN, B., SEEBURG, P. H. & MONYER, H. 1994. Differences in Ca2+ permeability of AMPA-type glutamate receptor channels in neocortical neurons caused by differential GluR-B subunit expression. *Neuron,* 12**,** 1281-1289.

JORGENSEN, N. R., GEIST, S. T., CIVITELLI, R. & STEINBERG, T. H. 1997. ATP- and gap junction-dependent intercellular calcium signaling in osteoblastic cells. *J Cell Biol,* 139**,** 497-506.

JUN, S. B., HYND, M. R., DOWELL-MESFIN, N., SMITH, K. L., TURNER, J. N., SHAIN, W. & KIM, S. J. 2007. Low-density neuronal networks cultured using patterned poly-l-lysine on microelectrode arrays. *Journal of Neuroscience Methods,* 160**,** 317-326.

JUSZCZAK, G. R. & SWIERGIEL, A. H. 2009. Properties of gap junction blockers and their behavioural, cognitive and electrophysiological effects: Animal and human studies. *Progress in Neuro-Psychopharmacology and Biological Psychiatry,* 33**,** 181-198.

KANDLER, K. & KATZ, L. C. 1995. Neuronal coupling and uncoupling in the developing nervous system. *Current Opinion in Neurobiology,* 5**,** 98-105.

KATZ, P. S. & FROST, W. N. 1996. Intrinsic neuromodulation: altering neuronal circuits from within. *Trends in Neurosciences,* 19**,** 54-61.

KAWAGUCHI, H. & FUKUNISHI, K. 1998. Dendrite classification in rat hippocampal neurons according to signal propagation properties Observation by multichannel optical recording in cultured neuronal networks. *Experimental Brain Research,* 122**,** 378-392.

KAWAJI, K., UMESHIMA, H., EIRAKU, M., HIRANO, T. & KENGAKU, M. 2004. Dual phases of migration of cerebellar granule cells guided by axonal and dendritic leading processes. *Molecular and Cellular Neuroscience,* 25**,** 228-240.

KEEFER, E. W., BOTTERMAN, B. R., ROMERO, M. I., ROSSI, A. F. & GROSS, G. W. 2008. Carbon nanotube coating improves neuronal recordings. *Nat Nano,* 3**,** 434-439.

KERR, R., LEV-RAM, V., BAIRD, G., VINCENT, P., TSIEN, R. Y. & SCHAFER, W. R. 2000. Optical Imaging of Calcium Transients in Neurons and Pharyngeal Muscle of C. elegans. *Neuron,* 26**,** 583-594.

KIRBY, D. M., RENNIE, K. J., SMULDERS-SRINIVASAN, T. K., ACIN-PEREZ, R., WHITTINGTON, M., ENRIQUEZ, J. A., TREVELYAN, A. J., TURNBULL, D. M. & LIGHTOWLERS, R. N. 2009. Transmitochondrial embryonic stem cells containing pathogenic mtDNA mutations are compromised in neuronal differentiation. *Cell Proliferation,* 42**,** 413-424.

KIRMSE, K. & KIRISCHUK, S. 2006. Ambient GABA Constrains the Strength of GABAergic Synapses at Cajal-Retzius Cells in the Developing Visual Cortex. *The Journal of Neuroscience,* 26**,** 4216-4227.

KLEIN, M., HOCHNER, B. & KANDEL, E. R. 1986. Facilitatory transmitters and cAMP can modulate accommodation as well as transmitter release in Aplysia sensory neurons: Evidence for parallel processing in a single cell. *Proceedings of the National Academy of Sciences,* 83**,** 7994-7998.

KLEINFELD, D., KAHLER, K. H. & HOCKBERGER, P. E. 1988. Controlled outgrowth of dissociated neurons on patterned substrates. *Journal of Neuroscience,* 8**,** 4098-4120.

KOLAJ, M., CERNE, R., CHENG, G., BRICKEY, D. A. & RANDIC, M. 1994. Alpha subunit of calcium/calmodulin-dependent protein kinase enhances excitatory amino acid and

synaptic responses of rat spinal dorsal horn neurons. *Journal of Neurophysiology,* 72**,** 2525-2531.

KOMURO, H. & RAKIC, P. 1996. Intracellular Ca2+ Fluctuations Modulate the Rate of Neuronal Migration. 17**,** 275-285.

KOMURO, H. & RAKIC, P. 1998. Orchestration of neuronal migration by activity of ion channels, neurotransmitter receptors, and intracellular Ca2+ fluctuations. *Journal of Neurobiology,* 37**,** 110-130.

KRAMER, R. H. & LEVITAN, I. B. 1990. Activity-dependent neuromodulation in Aplysia neuron R15: intracellular calcium antagonizes neurotransmitter responses mediated by cAMP. *Journal of Neurophysiology,* 63**,** 1075-1088.

KRAUSE, D. S., THEISE, N. D., COLLECTOR, M. I., HENEGARIU, O., HWANG, S., GARDNER, R., NEUTZEL, S. & SHARKIS, S. J. 2001. Multi-Organ, Multi-Lineage Engraftment by a Single Bone Marrow-Derived Stem Cell. *Cell,* 105**,** 369-377.

KRETSINGER, R. H. 1976. Calcium-binding proteins. *Annu Rev Biochem,* 45**,** 239-66.

KRUGER, G. M., MOSHER, J. T., BIXBY, S., JOSEPH, N., IWASHITA, T. & MORRISON, S. J. 2002. Neural Crest Stem Cells Persist in the Adult Gut but Undergo Changes in Self-Renewal, Neuronal Subtype Potential, and Factor Responsiveness. *Neuron,* 35**,** 657-669.

KYROZIS, A., CHUDOMEL, O., MOSHÉ, S. L. & GALANOPOULOU, A. S. 2006. Sex-dependent maturation of GABAA receptor-mediated synaptic events in rat substantia nigra reticulata. *Neuroscience Letters,* 398**,** 1-5.

LAMBERTZ, M. & LANGHORST, P. 1998. Simultaneous changes of rhythmic organization in brainstem neurons, respiration, cardiovascular system and EEG between 0.05 Hz and 0.5 Hz. *Journal of the Autonomic Nervous System,* 68**,** 58-77.

LAMSA, K., PALVA, J. M., RUUSUVUORI, E., KAILA, K. & TAIRA, T. 2000. Synaptic GABAA Activation Inhibits AMPA-Kainate Receptor–Mediated Bursting in the Newborn (P0–P2) Rat Hippocampus. *Journal of Neurophysiology,* 83**,** 359-366.

LANNER, J. T., GEORGIOU, D. K., JOSHI, A. D. & HAMILTON, S. L. 2010. Ryanodine Receptors: Structure, Expression, Molecular Details, and Function in Calcium Release. *Cold Spring Harbor Perspectives in Biology,* 2.

LARSEN, M., ARTYM, V. V., GREEN, J. A. & YAMADA, K. M. 2006. The matrix reorganized: extracellular matrix remodeling and integrin signaling. *Current Opinion in Cell Biology,* 18**,** 463-471.

LAUFFENBURGER, D. A. & HORWITZ, A. F. 1996. Cell migration: a physically integrated molecular process. *Cell,* 84**,** 359-69.

LAUTERMILCH, N. J. & SPITZER, N. C. 2000. Regulation of Calcineurin by Growth Cone Calcium Waves Controls Neurite Extension. *The Journal of Neuroscience,* 20**,** 315-325.

LEE, C. W., EGLEN, S. J. & WONG, R. O. L. 2002. Segregation of on and offRetinogeniculate Connectivity Directed by Patterned Spontaneous Activity. *Journal of Neurophysiology,* 88**,** 2311-2321.

LEINEKUGEL, X., KHAZIPOV, R., CANNON, R., HIRASE, H., BEN-ARI, Y. & BUZSÁKI, G. 2002. Correlated Bursts of Activity in the Neonatal Hippocampus in Vivo. *Science,* 296**,** 2049-2052.

LEINEKUGEL, X., MEDINA, I., KHALILOV, I., BEN-ARI, Y. & KHAZIPOV, R. 1997. Ca2+ Oscillations Mediated by the Synergistic Excitatory Actions of GABAA and NMDA Receptors in the Neonatal Hippocampus. *Neuron,* 18**,** 243-255.

LEITCH, E., COAKER, J., YOUNG, C., MEHTA, V. & SERNAGOR, E. 2005. GABA Type-A Activity Controls Its Own Developmental Polarity Switch in the Maturing Retina. *The Journal of Neuroscience,* 25**,** 4801-4805.

LEVITAN, I. B. 1994. Modulation of ion channels by protein phosphorylation and dephosphorylation. *Annu Rev Physiol,* 56**,** 193-212.

LI, B., MA, Y., WANG, S. & MORAN, P. M. 2005a. Influence of carboxyl group density on neuron cell attachment and differentiation behavior: Gradient-guided neurite outgrowth. *Biomaterials,* 26**,** 4956-4963.

LI, B., MA, Y., WANG, S. & MORAN, P. M. 2005b. A technique for preparing protein gradients on polymeric surfaces:: effects on PC12 pheochromocytoma cells. *Biomaterials,* 26**,** 1487-1495.

LI, H., TORNBERG, J., KAILA, K., AIRAKSINEN, M. S. & RIVERA, C. 2002. Patterns of cation-chloride cotransporter expression during embryonic rodent CNS development. *European Journal of Neuroscience,* 16**,** 2358-2370.

LI, Y., ZHOU, W., LI, X., ZENG, S., LIU, M. & LUO, Q. 2007. Characterization of synchronized bursts in cultured hippocampal neuronal networks with learning training on microelectrode arrays. *Biosensors and Bioelectronics,* 22**,** 2976-2982.

LIESI, P. 1985. Do neurons in the vertebrate CNS migrate on laminin? *EMBO J,* 4**,** 1163-70.

LIU, Q. S., XU, Q., KANG, J. & NEDERGAARD, M. 2004. Astrocyte activation of presynaptic metabotropic glutamate receptors modulates hippocampal inhibitory synaptic transmission. *Neuron Glia Biol,* 1**,** 307-316.

LIU, Z., NEFF, R. A. & BERG, D. K. 2006. Sequential Interplay of Nicotinic and GABAergic Signaling Guides Neuronal Development. *Science,* 314**,** 1610-1613.

LO TURCO, J. & KRIEGSTEIN, A. 1991. Clusters of coupled neuroblasts in embryonic neocortex. *Science,* 252**,** 563-566.

LOHR, C. 2003. Monitoring neuronal calcium signalling using a new method for ratiometric confocal calcium imaging. *Cell Calcium,* 34**,** 295-303.

LOM, B. & HOCKBERGER, P. E. 1997. Is laminin-1 a guidance cue for cerebellar granule cell migration? *Journal of Neurobiology,* 33**,** 72-84.

LORDKIPANIDZE, T. & DUNAEVSKY, A. 2005. Purkinje cell dendrites grow in alignment with Bergmann glia. *Glia,* 51**,** 229-234.

LORIER, A. R., LIPSKI, J., HOUSLEY, G. D., GREER, J. J. & FUNK, G. D. 2008. ATP sensitivity of preBötzinger complex neurones in neonatal rat in vitro: mechanism underlying a P2

receptor-mediated increase in inspiratory frequency. *The Journal of Physiology,* 586**,** 1429-1446.

LOTURCO, J. J., OWENS, D. F., HEATH, M. J. S., DAVIS, M. B. E. & KRIEGSTEIN, A. R. 1995. GABA and glutamate depolarize cortical progenitor cells and inhibit DNA synthesis. *Neuron,* 15**,** 1287-1298.

LOVAT, V., PANTAROTTO, D., LAGOSTENA, L., CACCIARI, B., GRANDOLFO, M., RIGHI, M., SPALLUTO, G., PRATO, M. & BALLERINI, L. 2005. Carbon Nanotube Substrates Boost Neuronal Electrical Signaling. *Nano Letters,* 5**,** 1107-1110.

LUCKENBILL-EDDS, L. 1997. Laminin and the mechanism of neuronal outgrowth. *Brain Research Reviews,* 23**,** 1-27.

MACHACA, K. & HAUN, S. 2000. Store-operated Calcium Entry Inactivates at the Germinal Vesicle Breakdown Stage of Xenopus Meiosis. *Journal of Biological Chemistry,* 275**,** 38710-38715.

MACIS, E., TEDESCO, M., MASSOBRIO, P., RAITERI, R. & MARTINOIA, S. 2007. An automated microdrop delivery system for neuronal network patterning on microelectrode arrays. *Journal of Neuroscience Methods,* 161**,** 88-95.

MACKENZIE, P. J., UMEMIYA, M. & MURPHY, T. H. 1996. Ca2+ Imaging of CNS Axons in Culture Indicates Reliable Coupling between Single Action Potentials and Distal Functional Release Sites. *Neuron,* 16**,** 783-795.

MACLAREN, E. J., CHARLESWORTH, P., COBA, M. P. & GRANT, S. G. N. 2011. Knockdown of mental disorder susceptibility genes disrupts neuronal network physiology in vitro. *Molecular and Cellular Neuroscience,* In Press, Corrected Proof.

MACVICAR, B., TSE, F., CRICHTON, S. & KETTENMANN, H. 1989. GABA-activated Cl- channels in astrocytes of hippocampal slices. *The Journal of Neuroscience,* 9**,** 3577-3583.

MARCUM, J. M., DEDMAN, J. R., BRINKLEY, B. R. & MEANS, A. R. 1978. Control of microtubule assembly-disassembly by calcium-dependent regulator protein. *Proceedings of the National Academy of Sciences,* 75**,** 3771-3775.

MARDER, E., BUCHER, D., SCHULZ, D. J. & TAYLOR, A. L. 2005. Invertebrate Central Pattern Generation Moves along. *Current biology : CB,* 15**,** R685-R699.

MARDER, E. & THIRUMALAI, V. 2002. Cellular, synaptic and network effects of neuromodulation. *Neural Networks,* 15**,** 479-493.

MARTIN, G. R. 1981. Isolation of a pluripotent cell line from early mouse embryos cultured in medium conditioned by teratocarcinoma stem cells. *Proceedings of the National Academy of Sciences,* 78**,** 7634-7638.

MARTINOIA, S., BONZANO, L., CHIAPPALONE, M., TEDESCO, M., MARCOLI, M. & MAURA, G. 2005. In vitro cortical neuronal networks as a new high-sensitive system for biosensing applications. *Biosensors and Bioelectronics,* 20**,** 2071-2078.

MARTINOIA, S., BOVE, M., TEDESCO, M., MARGESIN, B. & GRATTAROLA, M. 1999. A simple microfluidic system for patterning populations of neurons on silicon micromachined substrates. *Journal of Neuroscience Methods,* 87**,** 35-44.

MASLAND, R. H. 1977. Maturation of function in the developing rabbit retina. *The Journal of Comparative Neurology,* 175**,** 275-286.

MASLAND, R. H. & TAUCHI, M. 1986. The cholinergic amacrine cell. *Trends in Neurosciences,* 9**,** 218-223.

MATTHEWS, G. & WICKELGREN, W. O. 1977. On the effect of calcium on the frequency of miniature end-plate potentials at the frog neuromuscular junction. *The Journal of Physiology,* 266**,** 91-101.

MAZZATENTA, A., GIUGLIANO, M., CAMPIDELLI, S., GAMBAZZI, L., BUSINARO, L., MARKRAM, H., PRATO, M. & BALLERINI, L. 2007. Interfacing Neurons with Carbon Nanotubes: Electrical Signal Transfer and Synaptic Stimulation in Cultured Brain Circuits. *Journal of Neuroscience,* 27**,** 6931-6936.

MCDONALD, B. J. & MOSS, S. J. 1994. Differential phosphorylation of intracellular domains of gamma-aminobutyric acid type A receptor subunits by calcium/calmodulin type 2-

dependent protein kinase and cGMP-dependent protein kinase. *Journal of Biological Chemistry,* 269**,** 18111-18117.

MCKENZIE, J. L., WAID, M. C., SHI, R. & WEBSTER, T. J. 2004. Decreased functions of astrocytes on carbon nanofiber materials. *Biomaterials,* 25**,** 1309-1317.

MCKINSEY, T. A., ZHANG, C. L. & OLSON, E. N. 2002. MEF2: a calcium-dependent regulator of cell division, differentiation and death. *Trends in Biochemical Sciences,* 27**,** 40-47.

MCLAUGHLIN, T., TORBORG, C. L., FELLER, M. B. & O'LEARY, D. D. M. 2003. Retinotopic Map Refinement Requires Spontaneous Retinal Waves during a Brief Critical Period of Development. *Neuron,* 40**,** 1147-1160.

MIENVILLE, J.-M. 1998. Persistent depolarizing action of GABA in rat Cajal-Retzius cells. *The Journal of Physiology,* 512**,** 809-817.

MINAMI, Y., EMORI, Y., KAWASAKI, H. & SUZUKI, K. 1987. E-F Hand Structure-Domain of Calcium-Activated Neutral Protease (CANP) Can Bind Ca2+ Ions. *Journal of Biochemistry,* 101**,** 889-895.

MINLEBAEV, M., BEN-ARI, Y. & KHAZIPOV, R. 2007. Network Mechanisms of Spindle-Burst Oscillations in the Neonatal Rat Barrel Cortex In Vivo. *Journal of Neurophysiology,* 97**,** 692-700.

MINTZ, I. M. & BEAN, B. P. 1993. GABAB Receptor Inhibition of P-type Ca2+ Channels in Central Neurons. *Neuron,* 10**,** 889-898.

MOGAMI, H., NAKANO, K., TEPIKIN, A. V. & PETERSEN, O. H. 1997. Ca2+ Flow via Tunnels in Polarized Cells: Recharging of Apical Ca2+ Stores by Focal Ca2+ Entry through Basal Membrane Patch. *Cell,* 88**,** 49-55.

MORENO, A., SAEZ, J., FISHMAN, G. & SPRAY, D. 1994. Human connexin43 gap junction channels. Regulation of unitary conductances by phosphorylation. *Circ Res,* 74**,** 1050-1057.

MORIN, F., NISHIMURA, N., GRISCOM, L., LEPIOUFLE, B., FUJITA, H., TAKAMURA, Y. & TAMIYA, E. 2006. Constraining the connectivity of neuronal networks cultured on microelectrode arrays with microfluidic techniques: A step towards neuron-based functional chips. *Biosensors and Bioelectronics,* 21**,** 1093-1100.

MORITA, K., NORTH, R. A. & TOKIMASA, T. 1982. The calcium-activated potassium conductance in guinea-pig myenteric neurones. *The Journal of Physiology,* 329**,** 341-354.

MORRIS, R. J., LIU, Y., MARLES, L., YANG, Z., TREMPUS, C., LI, S., LIN, J. S., SAWICKI, J. A. & COTSARELIS, G. 2004. Capturing and profiling adult hair follicle stem cells. *Nat Biotech,* 22**,** 411-417.

MORSHEAD, C. M., CRAIG, C. G. & VAN DER KOOY, D. 1998. In vivo clonal analyses reveal the properties of endogenous neural stem cell proliferation in the adult mammalian forebrain. *Development,* 125**,** 2251-2261.

MRKSICH, M., CHEN, C. S., XIA, Y., DIKE, L. E., INGBER, D. E. & WHITESIDES, G. M. 1996. Controlling Cell Attachment on Contoured Surfaces with Self-Assembled Monolayers of Alkanethiolates on Gold. *Proceedings of the National Academy of Sciences of the United States of America,* 93**,** 10775-10778.

MRKSICH, M., DIKE, L. E., TIEN, J., INGBER, D. E. & WHITESIDES, G. M. 1997. Using Microcontact Printing to Pattern the Attachment of Mammalian Cells to Self-Assembled Monolayers of Alkanethiolates on Transparent Films of Gold and Silver. *Experimental Cell Research,* 235**,** 305-313.

MRKSICH, M. & WHITESIDES, G. M. 1995. Patterning self-assembled monolayers using microcontact printing: A new technology for biosensors? *Trends in Biotechnology,* 13**,** 228-235.

MULLER, T., FRITSCHY, J., GROSCHE, J., PRATT, G., MOHLER, H. & KETTENMANN, H. 1994. Developmental regulation of voltage-gated K+ channel and GABAA receptor expression in Bergmann glial cells. *The Journal of Neuroscience,* 14**,** 2503-2514.

MURAMOTO, K., ICHIKAWA, M., KAWAHARA, M., KOBAYASHI, K. & KURODA, Y. 1993. Frequency of synchronous oscillations of neuronal activity increases during development and is correlated to the number of synapses in cultured cortical neuron networks. *Neuroscience Letters,* 163**,** 163-165.

MURPHY, T. H., BARABAN, J. M. & WIER, W. G. 1995. Mapping miniature synaptic currents to single synapses using calcium imaging reveals heterogeneity in postsynaptic output. *Neuron,* 15**,** 159-168.

MWENIFUMBO, S., SHAFFER, M. S. & STEVENS, M. M. 2007. Exploring cellular behaviour with multi-walled carbon nanotube constructs. *Journal of Materials Chemistry,* 17**,** 1894 - 1902.

NADARAJAH, B., JONES, A. M., EVANS, W. H. & PARNAVELAS, J. G. 1997. Differential Expression of Connexins during Neocortical Development and Neuronal Circuit Formation. *The Journal of Neuroscience,* 17**,** 3096-3111.

NAM, Y., BRANCH, D. W. & WHEELER, B. C. 2006. Epoxy-silane linking of biomolecules is simple and effective for patterning neuronal cultures. *Biosensors and Bioelectronics,* 22**,** 589-597.

NERBONNE, J. & GURNEY, A. 1989. Development of excitable membrane properties in mammalian sympathetic neurons. *J. Neurosci.,* 9**,** 3272-3286.

NEWMAN, E. A. 2001. Propagation of Intercellular Calcium Waves in Retinal Astrocytes and Müller Cells. *The Journal of Neuroscience,* 21**,** 2215-2223.

NEWMAN, E. A. & ZAHS, K. R. 1997. Calcium waves in retinal glial cells. *Science,* 275**,** 844-7.

NOWICKA, A., GRABOWSKA, A. & FERSTEN, E. 1996. Interhemispheric transmission of information and functional asymmetry of the human brain. *Neuropsychologia,* 34**,** 147-151.

NUSSER, Z., SIEGHART, W. & SOMOGYI, P. 1998. Segregation of Different GABAA Receptors to Synaptic and Extrasynaptic Membranes of Cerebellar Granule Cells. *The Journal of Neuroscience,* 18**,** 1693-1703.

O'DONOVAN, M. & LANDMESSER, L. 1987. The development of hindlimb motor activity studied in the isolated spinal cord of the chick embryo. *The Journal of Neuroscience,* 7**,** 3256-3264.

O'DONOVAN, M. J., CHUB, N. & WENNER, P. 1998. Mechanisms of spontaneous activity in developing spinal networks. *Journal of Neurobiology,* 37**,** 131-145.

O'DOWD, D., RIBERA, A. & SPITZER, N. 1988. Development of voltage-dependent calcium, sodium, and potassium currents in Xenopus spinal neurons. *The Journal of Neuroscience,* 8**,** 792-805.

OAKLEY, C., JAEGER, N. A. F. & BRUNETTE, D. M. 1997. Sensitivity of Fibroblasts and Their Cytoskeletons to Substratum Topographies: Topographic Guidance and Topographic Compensation by Micromachined Grooves of Different Dimensions. *Experimental Cell Research,* 234**,** 413-424.

OBRIETAN, K. & VAN DEN POL, A. N. 1998. GABAB Receptor-Mediated Inhibition of GABAA Receptor Calcium Elevations in Developing Hypothalamic Neurons. *Journal of Neurophysiology,* 79**,** 1360-1370.

OERTNER, T. G., SABATINI, B. L., NIMCHINSKY, E. A. & SVOBODA, K. 2002. Facilitation at single synapses probed with optical quantal analysis. *Nat Neurosci,* 5**,** 657-664.

OKADA, Y., SHIMAZAKI, T., SOBUE, G. & OKANO, H. 2004. Retinoic-acid-concentration-dependent acquisition of neural cell identity during in vitro differentiation of mouse embryonic stem cells. *Developmental Biology,* 275**,** 124-142.

OLSSON, R. H., III & WISE, K. D. 2005. A three-dimensional neural recording microsystem with implantable data compression circuitry. *Solid-State Circuits, IEEE Journal of,* 40**,** 2796-2804.

OMI, T., KANTER, I. & SHINOMOTO, S. 2011. Optimal observation time window for forecasting the next earthquake. *Physical Review E,* 83**,** 026101.

OPITZ, T., DE LIMA, A. D. & VOIGT, T. 2002. Spontaneous Development of Synchronous Oscillatory Activity During Maturation of Cortical Networks In Vitro. *Journal of Neurophysiology,* 88**,** 2196-2206.

ORR-URTREGER, A., GIVOL, D., YAYON, A., YARDEN, Y. & LONAI, P. 1991. Developmental expression of two murine fibroblast growth factor receptors, flg and bek. *Development,* 113**,** 1419-1434.

OWEN, G. R., MEREDITH, D., AP GWYNN, I. & RICHARDS, R. 2005. Focal Adhesion Quantification - A New Assay fo Material Biocompatibility?: Review. *European Cels and Materials,* 9**,** 85-96.

PACZUSKI, M., MASLOV, S. & BAK, P. 1996. Avalanche dynamics in evolution, growth, and depinning models. *Physical Review E,* 53**,** 414.

PAINA, S., GARZOTTO, D., DEMARCHIS, S., MARINO, M., MOIANA, A., CONTI, L., CATTANEO, E., PERERA, M., CORTE, G., CALAUTTI, E. & MERLO, G. R. 2011. Wnt5a Is a Transcriptional Target of Dlx Homeogenes and Promotes Differentiation of Interneuron Progenitors In Vitro and In Vivo. *The Journal of Neuroscience,* 31**,** 2675-2687.

PALMER, T. D., RAY, J. & GAGE, F. H. 1995. FGF-2-Responsive Neuronal Progenitors Reside in Proliferative and Quiescent Regions of the Adult Rodent Brain. *Molecular and Cellular Neuroscience,* 6**,** 474-486.

PALMER, T. D., TAKAHASHI, J. & GAGE, F. H. 1997. The Adult Rat Hippocampus Contains Primordial Neural Stem Cells. *Molecular and Cellular Neuroscience,* 8**,** 389-404.

PANZERI, S., PETRONI, F. & BRACCI, E. 2004. Exploring structure–function relationships in neocortical networks by means of neuromodelling techniques. *Medical engineering & physics,* 26**,** 699-710.

PARNAS, I. & PARNAS, H. 2010. Control of neurotransmitter release: From Ca²⁺ to voltage dependent G-protein coupled receptors. *Pflügers Archiv European Journal of Physiology,* 460**,** 975-990.

PARPURA, V. & HAYDON, P. G. 2000. Physiological astrocytic calcium levels stimulate glutamate release to modulate adjacent neurons. *Proceedings of the National Academy of Sciences,* 97**,** 8629-8634.

PASQUALE, V., MASSOBRIO, P., BOLOGNA, L. L., CHIAPPALONE, M. & MARTINOIA, S. 2008. Self-organization and neuronal avalanches in networks of dissociated cortical neurons. *Neuroscience,* 153**,** 1354-1369.

PATTERSON, P. H. 1994. Leukemia inhibitory factor, a cytokine at the interface between neurobiology and immunology. *Proc Natl Acad Sci U S A,* 91**,** 7833-5.

PEINADO, A. 2000. Traveling slow waves of neural activity: a novel form of network activity in developing neocortex. *J Neurosci,* 20**,** RC54.

PEREA, G. & ARAQUE, A. 2005. Properties of Synaptically Evoked Astrocyte Calcium Signal Reveal Synaptic Information Processing by Astrocytes. *The Journal of Neuroscience,* 25**,** 2192-2203.

PEREZ-VELAZQUEZ, J., VALIANTE, T. & CARLEN, P. 1994. Modulation of gap junctional mechanisms during calcium-free induced field burst activity: a possible role for electrotonic coupling in epileptogenesis. *The Journal of Neuroscience,* 14**,** 4308-4317.

PERRIS, R. & PERISSINOTTO, D. 2000. Role of the extracellular matrix during neural crest cell migration. *Mechanisms of Development,* 95**,** 3-21.

PICKERING, M., PICKERING, B. W., MURPHY, K. J. & O'CONNOR, J. J. 2008. Discrimination of cell types in mixed cortical culture using calcium imaging: A comparison to immunocytochemical labeling. *Journal of Neuroscience Methods,* 173**,** 27-33.

PIZZI, R., CINO, G., GELAIN, F., ROSSETTI, D. & VESCOVI, A. 2007. Learning in human neural networks on microelectrode arrays. *Biosystems,* 88**,** 1-15.

POENIE, M., ALDERTON, J., STEINHARDT, R. & TSIEN, R. 1986. Calcium rises abruptly and briefly throughout the cell at the onset of anaphase. *Science,* 233**,** 886-889.

POUILLE, F. & SCANZIANI, M. 2001. Enforcement of Temporal Fidelity in Pyramidal Cells by Somatic Feed-Forward Inhibition. *Science,* 293**,** 1159-1163.

POWER, J. M. & SAH, P. 2002. Nuclear Calcium Signaling Evoked by Cholinergic Stimulation in Hippocampal CA1 Pyramidal Neurons. *The Journal of Neuroscience,* 22**,** 3454-3462.

PUJOL, J., LÓPEZ-SALA, A., DEUS, J., CARDONER, N., SEBASTIÁN-GALLÉS, N., CONESA, G. & CAPDEVILA, A. 2002. The Lateral Asymmetry of the Human Brain Studied by Volumetric Magnetic Resonance Imaging. *NeuroImage,* 17**,** 670-679.

PUMAIN, R., KURCEWICZ, I. & LOUVEL, J. 1987. Ionic changes induced by excitatory amino acids in the rat cerebral cortex. *Can J Physiol Pharmacol,* 65**,** 1067-77.

PUTNEY, J. W. 2003. Capacitative calcium entry in the nervous system. *Cell Calcium,* 34**,** 339-344.

RAICHMAN, N. & BEN-JACOB, E. 2008. Identifying repeating motifs in the activation of synchronized bursts in cultured neuronal networks. *Journal of Neuroscience Methods,* 170**,** 96-110.

RAKIC, P., CAMERON, R. S. & KOMURO, H. 1994. Recognition, adhesion, transmembrane signaling and cell motility in guided neuronal migration. *Current Opinion in Neurobiology,* 4**,** 63-69.

RECKNOR, J. B., SAKAGUCHI, D. S. & MALLAPRAGADA, S. K. 2006. Directed growth and selective differentiation of neural progenitor cells on micropatterned polymer substrates. *Biomaterials,* 27**,** 4098-4108.

REEVES, A. M. B., SHIGETOMI, E. & KHAKH, B. S. 2011. Bulk Loading of Calcium Indicator Dyes to Study Astrocyte Physiology: Key Limitations and Improvements Using Morphological Maps. *The Journal of Neuroscience,* 31**,** 9353-9358.

RENONCOURT, Y., CARROLL, P., FILIPPI, P., ARCE, V. & ALONSO, S. 1998. Neurons derived in vitro from ES cells express homeoproteins characteristic of motoneurons and interneurons. *Mechanisms of Development,* 79**,** 185-198.

REPRESA, A. & BEN-ARI, Y. 2005. Trophic actions of GABA on neuronal development. *Trends in Neurosciences,* 28**,** 278-283.

REYES, A. D. 2003. Synchrony-dependent propagation of firing rate in iteratively constructed networks in vitro. *Nat Neurosci,* 6**,** 593-9.

RICE, D. S. & CURRAN, T. 2001. ROLE OF THE REELIN SIGNALING PATHWAY IN CENTRAL NERVOUS SYSTEM DEVELOPMENT. *Annual Review of Neuroscience,* 24**,** 1005-1039.

RICH, A. & HARRIS, A. K. 1981. Anomalous preferences of cultured macrophages for hydrophobic and roughened substrata. *Journal of Cell Science,* 50**,** 1-7.

RIVERA, C., VOIPIO, J., PAYNE, J. A., RUUSUVUORI, E., LAHTINEN, H., LAMSA, K., PIRVOLA, U., SAARMA, M. & KAILA, K. 1999. The K+/Cl- co-transporter KCC2 renders GABA hyperpolarizing during neuronal maturation. *Nature,* 397**,** 251-255.

ROBINSON, H. P., KAWAHARA, M., JIMBO, Y., TORIMITSU, K., KURODA, Y. & KAWANA, A. 1993. Periodic synchronized bursting and intracellular calcium transients elicited by low magnesium in cultured cortical neurons. *Journal of Neurophysiology,* 70**,** 1606-1616.

ROHRBOUGH, J. & SPITZER, N. 1996. Regulation of intracellular Cl- levels by Na(+)-dependent Cl- cotransport distinguishes depolarizing from hyperpolarizing GABAA receptor-mediated responses in spinal neurons. *The Journal of Neuroscience,* 16**,** 82-91.

ROHWEDEL, J., KLEPPISCH, T., PICH, U., GUAN, K., JIN, S., ZUSCHRATTER, W., HOPF, C., HOCH, W., HESCHELER, J., WITZEMANN, V. & WOBUS, A. M. 1998. Formation of Postsynaptic-Like Membranes during Differentiation of Embryonic Stem Cellsin Vitro. *Experimental Cell Research,* 239**,** 214-225.

ROZENTAL, R., MORALES, M., MEHLER, M. F., URBAN, M., KREMER, M., DERMIETZEL, R., KESSLER, J. A. & SPRAY, D. C. 1998. Changes in the Properties of Gap Junctions during Neuronal Differentiation of Hippocampal Progenitor Cells. *The Journal of Neuroscience,* 18**,** 1753-1762.

RUBIN, J. E., HAYES, J. A., MENDENHALL, J. L. & DEL NEGRO, C. A. 2009. Calcium-activated nonspecific cation current and synaptic depression promote network-dependent burst oscillations. *Proceedings of the National Academy of Sciences,* 106**,** 2939-2944.

RUTISHAUSER, U., GALL, W. E. & EDELMAN, G. M. 1978. Adhesion among neural cells of the chick embryo. IV. Role of the cell surface molecule CAM in the formation of neurite bundles in cultures of spinal ganglia. *Journal of Cell Biology,* 79**,** 382-393.

RUTISHAUSER, U. & JESSELL, T. M. 1988. Cell Adhesion Molecules in Vertebrate Neural Development. *Physiological Reviews,* 68**,** 819-857.

SAFIULINA, V. F., KASYANOV, A. M., SOKOLOVA, E., CHERUBINI, E. & GINIATULLIN, R. 2005. ATP contributes to the generation of network-driven giant depolarizing potentials in the neonatal rat hippocampus. *The Journal of Physiology,* 565**,** 981-992.

SAHA, K., KEUNG, A. J., IRWIN, E. F., LI, Y., LITTLE, L., SCHAFFER, D. V. & HEALY, K. E. 2008. Substrate Modulus Directs Neural Stem Cell Behavior. *Biophysical Journal,* 95**,** 4426-4438.

SANAI, N., TRAMONTIN, A. D., QUINONES-HINOJOSA, A., BARBARO, N. M., GUPTA, N., KUNWAR, S., LAWTON, M. T., MCDERMOTT, M. W., PARSA, A. T., MANUEL-GARCIA VERDUGO, J., BERGER, M. S. & ALVAREZ-BUYLLA, A. 2004. Unique astrocyte ribbon in adult human brain contains neural stem cells but lacks chain migration. *Nature,* 427**,** 740-744.

SANCHEZ-VIVES, M. V. & MCCORMICK, D. A. 2000. Cellular and network mechanisms of rhythmic recurrent activity in neocortex. *Nature neuroscience,* 3**,** 1027-34.

SANDOVAL, I. V. & WEBER, K. 1978. Calcium-Induced Inactivation of Microtubule Formation in Brain Extracts. *European Journal of Biochemistry,* 92**,** 463-470.

SASAKI, T., TAKAHASHI, N., MATSUKI, N. & IKEGAYA, Y. 2008. Fast and Accurate Detection of Action Potentials From Somatic Calcium Fluctuations. *J Neurophysiol,* 100**,** 1668-1676.

SCHLAUG, G., JANCKE, L., HUANG, Y. & STEINMETZ, H. 1995. In vivo evidence of structural brain asymmetry in musicians. *Science,* 267**,** 699-701.

SCHOLL, M., SPRÖSSLER, C., DENYER, M., KRAUSE, M., NAKAJIMA, K., MAELICKE, A., KNOLL, W. & OFFENHÄUSSER, A. 2000. Ordered networks of rat hippocampal neurons attached to silicon oxide surfaces. *Journal of Neuroscience Methods,* 104**,** 65-75.

SCHONER, G. & KELSO, J. 1988. Dynamic pattern generation in behavioral and neural systems. *Science,* 239**,** 1513-1520.

SCHWIENING, C. J. & WILLOUGHBY, D. 2002. Depolarization-induced pH microdomains and their relationship to calcium transients in isolated snail neurones. *The Journal of Physiology,* 538**,** 371-382.

SEGEV, R., BENVENISTE, M., SHAPIRA, Y. & BEN-JACOB, E. 2003. Formation of Electrically Active Clusterized Neural Networks. *Physical Review Letters,* 90**,** 168101.

SERNAGOR, E., CHABROL, F., BONY, G. & CANCEDDA, L. 2010. GABAergic control of neurite outgrowth and remodeling during development and adult neurogenesis: general rules and differences in diverse systems. *Front Cell Neurosci,* 4**,** 11.

SERNAGOR, E. & GRZYWACZ, N. M. 1999. Spontaneous Activity in Developing Turtle Retinal Ganglion Cells: Pharmacological Studies. *The Journal of Neuroscience,* 19**,** 3874-3887.

SERNAGOR, E. & MEHTA, V. 2001. The role of early neural activity in the maturation of turtle retinal function. *Journal of Anatomy,* 199**,** 375-383.

SERNAGOR, E., YOUNG, C. & EGLEN, S. J. 2003. Developmental Modulation of Retinal Wave Dynamics: Shedding Light on the GABA Saga. *The Journal of Neuroscience,* 23**,** 7621-7629.

ŠESTAN, N., ARTAVANIS-TSAKONAS, S. & RAKIC, P. 1999. Contact-Dependent Inhibition of Cortical Neurite Growth Mediated by Notch Signaling. *Science,* 286**,** 741-746.

SHEFI, O., HAREL, A., B. CHKLOVSKII, D., BEN-JACOB, E. & AYALI, A. 2004. Biophysical constraints on neuronal branching. *Neurocomputing,* 58-60**,** 487-495.

SHEFI, O., SHARON, G., ESHEL, B.-J. & AMIR, A. 2005. A two-phase growth strategy in cultured neuronal networks as reflected by the distribution of neurite branching angles. *Journal of Neurobiology,* 62**,** 361-368.

SHEIN, M., GREENBAUM, A., GABAY, T., SORKIN, R., DAVID-PUR, M., BEN-JACOB, E. & HANEIN, Y. 2009. Engineered neuronal circuits shaped and interfaced with carbon nanotube microelectrode arrays. *Biomedical Microdevices,* 11**,** 495-501.

SHOVAL, A., ADAMS, C., DAVID-PUR, M., SHEIN, M., HANEIN, Y. & SERNAGOR, E. 2009. Carbon nanotube electrodes for effective interfacing with retinal tissue. *Front Neuroengineering,* 2**,** 4.

SILBERBERG, G., GUPTA, A. & MARKRAM, H. 2002. Stereotypy in neocortical microcircuits. *Trends in Neurosciences,* 25**,** 227-230.

SIPILÄ, S. T., HUTTU, K., SOLTESZ, I., VOIPIO, J. & KAILA, K. 2005. Depolarizing GABA Acts on Intrinsically Bursting Pyramidal Neurons to Drive Giant Depolarizing Potentials in the Immature Hippocampus. *The Journal of Neuroscience,* 25**,** 5280-5289.

SMART, T. G. 1997. Regulation of excitatory and inhibitory neurotransmitter-gated ion channels by protein phosphorylation. *Current Opinion in Neurobiology,* 7**,** 358-367.

SNYDER, D., ATLAN, H., MARKUS, M. & PANET, R. 1991. Na+/K+/Cl- cotransport is stimulated by a Ca(++)-calmodulin-mediated pathway in BALB/c 3T3 fibroblasts. *J Cell Physiol,* 149**,** 497-502.

SORKIN, R., GABAY, T., BLINDER, P., BARANES, D., BEN-JACOB, E. & HANEIN, Y. 2006. Compact self-wiring in cultured neural networks. *Journal of Neural Engineering,* 3**,** 95-101.

SORKIN, R., GREENBAUM, A., DAVID-PUR, M., ANAVA, S., AYALI, A., BEN-JACOB, E. & HANEIN, Y. 2009. Process entanglement as a neuronal anchorage mechanism to rough surfaces. *Nanotechnology,* 20**,** 015101.

SPITZER, N. C. 2006. Electrical activity in early neuronal development. *Nature,* 444**,** 707-712.

SPITZER, N. C., DEBACA, R. C., ALLEN, K. A. & HOLLIDAY, J. 1993. Calcium dependence of differentiation of GABA immunoreactivity in spinal neurons. *The Journal of Comparative Neurology,* 337**,** 168-175.

SPITZER, N. C. & GU, X. 1997. Purposeful patterns of spontaneous calcium transients in embryonic spinal neurons. *Seminars in Cell and Developmental Biology,* 8**,** 13-19.

SPITZER, N. C., GU, X. & OLSON, E. 1994. Action potentials, calcium transients and the control of differentiation of excitable cells. *Current Opinion in Neurobiology,* 4**,** 70-77.

SPITZER, N. C. & LAMBORGHINI, J. E. 1976. The development of the action potential mechanism of amphibian neurons isolated in culture. *Proceedings of the National Academy of Sciences,* 73**,** 1641-1645.

SPITZER, N. C., ROOT, C. M. & BORODINSKY, L. N. 2004. Orchestrating neuronal differentiation: patterns of Ca2+ spikes specify transmitter choice. *Trends in Neurosciences,* 27**,** 415-421.

SPORNS, O., CHIALVO, D. R., KAISER, M. & HILGETAG, C. C. 2004. Organization, development and function of complex brain networks. *Trends in Cognitive Sciences,* 8**,** 418-425.

SPORS, H. & GRINVALD, A. 2002. Spatio-Temporal Dynamics of Odor Representations in the Mammalian Olfactory Bulb. *Neuron,* 34**,** 301-315.

STALEY, K., SOLDO, B. & PROCTOR, W. 1995. Ionic mechanisms of neuronal excitation by inhibitory GABAA receptors. *Science,* 269**,** 977-981.

STALEY, K. J. & MODY, I. 1992. Shunting of excitatory input to dentate gyrus granule cells by a depolarizing GABAA receptor-mediated postsynaptic conductance. *Journal of Neurophysiology,* 68**,** 197-212.

STELLWAGEN, D. & SHATZ, C. J. 2002. An Instructive Role for Retinal Waves in the Development of Retinogeniculate Connectivity. *Neuron,* 33**,** 357-367.

STORCK, T., SCHULTE, S., HOFMANN, K. & STOFFEL, W. 1992. Structure, expression, and functional analysis of a Na(+)-dependent glutamate/aspartate transporter from rat brain. *Proceedings of the National Academy of Sciences,* 89**,** 10955-10959.

STRATA, F., ATZORI, M., MOLNAR, M., UGOLINI, G., TEMPIA, F. & CHERUBINI, E. 1997. A Pacemaker Current in Dye-Coupled Hilar Interneurons Contributes to the Generation of Giant GABAergic Potentials in Developing Hippocampus. *The Journal of Neuroscience,* 17**,** 1435-1446.

STRÜBING, C., AHNERT-HILGER, G., SHAN, J., WIEDENMANN, B., HESCHELER, J. & WOBUS, A. M. 1995. Differentiation of pluripotent embryonic stem cells into the neuronal lineage in vitro gives rise to mature inhibitory and excitatory neurons. *Mechanisms of Development,* 53**,** 275-287.

SUN, Y.-M., COOPER, M., FINCH, S., LIN, H.-H., CHEN, Z.-F., WILLIAMS, B. P. & BUCKLEY, N. J. 2008. Rest-Mediated Regulation of Extracellular Matrix Is Crucial for Neural Development. *PLoS ONE,* 3**,** e3656.

TABAK, J., RINZEL, J. & O'DONOVAN, M. J. 2001. The Role of Activity-Dependent Network Depression in the Expression and Self-Regulation of Spontaneous Activity in the Developing Spinal Cord. *The Journal of Neuroscience,* 21**,** 8966-8978.

TAKAHASHI, K.-I. & COPENHAGEN, D. R. 1996. Modulation of neuronal function by intracellular pH. *Neuroscience Research,* 24**,** 109-116.

TAKAHASHI, N., SASAKI, T., USAMI, A., MATSUKI, N. & IKEGAYA, Y. 2007. Watching neuronal circuit dynamics through functional multineuron calcium imaging (fMCI). *Neuroscience Research,* 58**,** 219-225.

TAKEUCHI, A., HAMASAKI, T., LITWACK, E. D. & O'LEARY, D. D. M. 2007. Novel IgCAM, MDGA1, Expressed in Unique Cortical Area- and Layer-Specific Patterns and Transiently by Distinct Forebrain Populations of Cajal–Retzius Neurons. *Cerebral Cortex,* 17**,** 1531-1541.

TAYLOR, A., RHEE, S., TU, C., CRIBBS, D., COTMAN, C. & JEON, N. 2003. Microfluidic multicompartment device for neuroscience research. *Langmuir,* 19**,** 1551-1556.

TAYLOR, C. W. & TOVEY, S. C. 2010. IP3 Receptors: Toward Understanding Their Activation. *Cold Spring Harbor Perspectives in Biology,* 2.

TEIXIDOR, G. T., III, R. A. G., TRIPATHI, P. P., BISHT, G. S., KULKARNI, M., MAITI, T. K., BATTACHARYYA, T. K., SUBRAMANIAM, J. R., SHARMA, A., PARK, B. Y. & MADOU, M. 2008. Carbon microelectromechanical systems as a substratum for cell growth. *Biomedical Materials,* 3**,** 1-8.

THOMPSON, W. J. 1985. Activity and synapse elimination at the neuromuscular junction. *Cellular and Molecular Neurobiology,* 5**,** 167-182.

THOMSON, A. M. & DEUCHARS, J. 1994. Temporal and spatial properties of local circuits in neocortex. *Trends in Neurosciences,* 17**,** 119-126.

TRAUB, R. D. 1979. Neocortical pyramidal cells: a model with dendritic calcium conductance reproduces repetitive firing and epileptic behavior. *Brain Research,* 173**,** 243-257.

TRAUB, R. D., CUNNINGHAM, M. O., GLOVELI, T., LEBEAU, F. E. N., BIBBIG, A., BUHL, E. H. & WHITTINGTON, M. A. 2003. GABA-enhanced collective behavior in neuronal axons underlies persistent gamma-frequency oscillations. *Proceedings of the National Academy of Sciences,* 100**,** 11047-11052.

TRAUB, R. D., KNOWLES, W. D., MILES, R. & WONG, R. K. S. 1984. Synchronized afterdischarges in the hippocampus: Simulation studies of the cellular mechanism. *Neuroscience,* 12**,** 1191-1200.

TRAUB, R. D. & MILES, R. 1991. Multiple Modes of Neuronal Population Activity Emerge after Modifying Specific Synapses in a Model of the CA3 Region of the Hippocampus. *Annals of the New York Academy of Sciences,* 627**,** 277-290.

TREVELYAN, A. J., KIRBY, D. M., SMULDERS-SRINIVASAN, T. K., NOOTEBOOM, M., ACIN-PEREZ, R., ENRIQUEZ, J. A., WHITTINGTON, M. A., LIGHTOWLERS, R. N. & TURNBULL,

D. M. 2010. Mitochondrial DNA mutations affect calcium handling in differentiated neurons. *Brain***,** awq023.

TSUJI, H., SOMMANI, P., HATTORI, M., YAMADA, T., SATO, H., GOTOH, Y. & ISHIKAWA, J. 2009. Negative ion implantation for pattering mesenchymal-stem cell adhesion on silicone rubber and differentiation into nerve cells with keeping their adhesion pattern. *Surface and Coatings Technology,* 203**,** 2562-2565.

TURRIGIANO, G. G. 1999. Homeostatic plasticity in neuronal networks: the more things change, the more they stay the same. *Trends in Neurosciences,* 22**,** 221-227.

TYZIO, R., COSSART, R., KHALILOV, I., MINLEBAEV, M., HÜBNER, C. A., REPRESA, A., BEN-ARI, Y. & KHAZIPOV, R. 2006. Maternal Oxytocin Triggers a Transient Inhibitory Switch in GABA Signaling in the Fetal Brain During Delivery. *Science,* 314**,** 1788-1792.

UKHANOV, K., BOBKOV, Y. & ACHE, B. W. 2011. Imaging ensemble activity in arthropod olfactory receptor neurons in situ. *Cell Calcium,* 49**,** 100-107.

ULLIAN, E. M., CHRISTOPHERSON, K. S. & BARRES, B. A. 2004. Role for glia in synaptogenesis. *Glia,* 47**,** 209-216.

ULLIAN, E. M., SAPPERSTEIN, S. K., CHRISTOPHERSON, K. S. & BARRES, B. A. 2001. Control of Synapse Number by Glia. *Science,* 291**,** 657-661.

VALIANTE, T. A., PEREZ VELAZQUEZ, J. L., JAHROMI, S. S. & CARLEN, P. L. 1995. Coupling potentials in CA1 neurons during calcium-free-induced field burst activity. *J Neurosci,* 15**,** 6946-56.

VALOR, L. M., CHARLESWORTH, P., HUMPHREYS, L., ANDERSON, C. N. G. & GRANT, S. G. N. 2007. Network activity-independent coordinated gene expression program for synapse assembly. *Proceedings of the National Academy of Sciences,* 104**,** 4658-4663.

VAN PELT, J., WOLTERS, P. S., CORNER, M. A., RUTTEN, W. L. & RAMAKERS, G. J. 2004. Long-term characterization of firing dynamics of spontaneous bursts in cultured neural networks. *IEEE Trans Biomed Eng,* 51**,** 2051-62.

VERKHRATSKY, A. J. & PETERSEN, O. H. 1998. Neuronal calcium stores. *Cell Calcium,* 24**,** 333-343.

VOGEL, R. & WEINGART, R. 2002. The electrophysiology of gap junctions and gap junction channels and their mathematical modelling. *Biology of the Cell,* 94**,** 501-510.

VOIGT, T., OPITZ, T. & DE LIMA, A. D. 2005. Activation of Early Silent Synapses by Spontaneous Synchronous Network Activity Limits the Range of Neocortical Connections. *The Journal of Neuroscience,* 25**,** 4605-4615.

VOLMAN, V., BARUCHI, I. & BEN-JACOB, E. 2005. Manifestation of function-follow-form in cultured neuronal networks. *Physical Biology,* 2**,** 1-13.

WAGENAAR, D., PINE, J. & POTTER, S. 2006. An extremely rich repertoire of bursting patterns during the development of cortical cultures. *BMC Neuroscience,* 7**,** 11.

WAGENAAR, D. A., PINE, J. & POTTER, S. M. 2004. Effective parameters for stimulation of dissociated cultures using multi-electrode arrays. *Journal of Neuroscience Methods,* 138**,** 27-37.

WAGNER, J. & LUHMANN, H. J. 2006. Activation of metabotropic glutamate receptors induces propagating network oscillations in the intact cerebral cortex of the newborn mouse. *Neuropharmacology,* 51**,** 848-857.

WALICKE, P., COWAN, W. M., UENO, N., BAIRD, A. & GUILLEMIN, R. 1986. Fibroblast growth factor promotes survival of dissociated hippocampal neurons and enhances neurite extension. *Proceedings of the National Academy of Sciences,* 83**,** 3012-3016.

WANG, L.-Y., FEDCHYSHYN, M. & YANG, Y.-M. 2009. Action potential evoked transmitter release in central synapses: insights from the developing calyx of Held. *Molecular Brain,* 2**,** 1-11.

WEBB, S. E. & MILLER, A. L. 2000. Calcium signalling during zebrafish embryonic development. *BioEssays,* 22**,** 113-123.

WEBSTER, T. J., SIEGEL, R. W. & BIZIOS, R. 1999. Osteoblast adhesion on nanophase ceramics. *Biomaterials,* 20**,** 1221-1227.

WEIMANN, J. M. & MARDER, E. 1994. Switching neurons are integral members of multiple oscillatory networks. *Current biology : CB,* 4**,** 896-902.

WEISS, S., DUNNE, C., HEWSON, J., WOHL, C., WHEATLEY, M., PETERSON, A. C. & REYNOLDS, B. A. 1996. Multipotent CNS Stem Cells Are Present in the Adult Mammalian Spinal Cord and Ventricular Neuroaxis. *The Journal of Neuroscience,* 16**,** 7599-7609.

WEISSMAN, T. A., RIQUELME, P. A., IVIC, L., FLINT, A. C. & KRIEGSTEIN, A. R. 2004. Calcium Waves Propagate through Radial Glial Cells and Modulate Proliferation in the Developing Neocortex. *Neuron,* 43**,** 647-661.

WHITTINGTON, M. A., TRAUB, R. D. & JEFFERYS, J. G. R. 1995. Synchronized oscillations in interneuron networks driven by metabotropic glutamate receptor activation. *Nature,* 373**,** 612-615.

WONG, J. Y., LEACH, J. B. & BROWN, X. Q. 2004. Balance of chemistry, topography, and mechanics at the cell-biomaterial interface: Issues and challenges for assessing the role of substrate mechanics on cell response. *Surface Science,* 570**,** 119-133.

WONG, R. O. L. & GHOSH, A. 2002. Activity-dependent regulation of dendritic growth and patterning. *Nat Rev Neurosci,* 3**,** 803-812.

WONG, R. O. L., MEISTER, M. & SHATZ, C. J. 1993. Transient period of correlated bursting activity during development of the mammalian retina. *Neuron,* 11**,** 923-938.

WONG, W. T., SANES, J. R. & WONG, R. O. L. 1998. Developmentally Regulated Spontaneous Activity in the Embryonic Chick Retina. *The Journal of Neuroscience,* 18**,** 8839-8852.

WU, K. D., LEE, W. S., WEY, J., BUNGARD, D. & LYTTON, J. 1995. Localization and quantification of endoplasmic reticulum Ca(2+)-ATPase isoform transcripts. *American Journal of Physiology - Cell Physiology,* 269**,** C775-C784.

XIE, J., CHEN, L., AATRE, K. R., SRIVATSAN, M. & VARADAN, V. K. 2006. Somatosensory neurons grown on functionalized carbon nanotube mats. *Smart Materials and Structures,* 15**,** N85-N88.

YING, Q., STAVRIDIS, M., GRIFFITHS, D., LI, M. & SMITH, A. 2003. Conversion of embryonic stem cells into neuroectodermal precursors in adherent monoculture. *Nat Biotechnol,* 21**,** 183-186.

YUSTE, R. & KATZ, L. C. 1991. Control of postsynaptic Ca2+ influx in developing neocortex by excitatory and inhibitory neurotransmitters. *Neuron,* 6**,** 333-344.

YUSTE, R., MAJEWSKA, A. & HOLTHOFF, K. 2000. From form to function: calcium compartmentalization in dendritic spines. *Nat Neurosci,* 3**,** 653-659.

YUSTE, R., NELSON, D. A., RUBIN, W. W. & KATZ, L. C. 1995. Neuronal domains in developing neocortex: Mechanisms of coactivation. *Neuron,* 14**,** 7-17.

ZAPPERI, S., LAURITSEN, K. B., AELIG, KGAARD & STANLEY, H. E. 1995. Self-Organized Branching Processes: Mean-Field Theory for Avalanches. *Physical Review Letters,* 75**,** 4071.

ZHANG, J., NIU, C., YE, L., HUANG, H., HE, X., TONG, W.-G., ROSS, J., HAUG, J., JOHNSON, T., FENG, J. Q., HARRIS, S., WIEDEMANN, L. M., MISHINA, Y. & LI, L. 2003. Identification of the haematopoietic stem cell niche and control of the niche size. *Nature,* 425**,** 836-841.

ZHANG, S., YAN, L., ALTMAN, M., LASSLE, M., NUGENT, H., FRANKEL, F., LAUFFENBURGER, D. A., WHITESIDES, G. M. & RICH, A. 1999. Biological surface engineering: a simple system for cell pattern formation. *Biomaterials,* 20**,** 1213-1220.

ZHENG, J., LEE, S. & ZHOU, Z. J. 2006. A transient network of intrinsically bursting starburst cells underlies the generation of retinal waves. *Nat Neurosci,* 9**,** 363-371.

ZHOU, C., WEN, Z.-X., SHI, D.-M. & XIE, Z.-P. 2004. Muscarinic acetylcholine receptors involved in the regulation of neural stem cell proliferation and differentiation in vitro. *Cell Biology International,* 28**,** 63-67.